

**Numerical Investigation on Thermal-Hydraulic  
Characteristics of Pillow Plate Heat Exchanger for Low  
Temperature Applications**

**THESIS**

Submitted in partial fulfillment  
of the requirements for the degree of  
**DOCTOR OF PHILOSOPHY**

by

**RAMESH KUMAR**

**2019PHXF0049P**

Under the Supervision of

**Prof. ANEESH A.M.**

and

Co-supervision of

**Prof. ANIRUDH SINGH RANA**



**BITS Pilani**  
Pilani | Dubai | Goa | Hyderabad

**BIRLA INSTITUTE OF TECHNOLOGY & SCIENCE, PILANI  
2024**

*..... Dedicated to my  
parents.....*



**BIRLA INSTITUTE OF TECHNOLOGY AND SCIENCE,  
PILANI, PILANI CAMPUS**

---

**CERTIFICATE**

This is to certify that the thesis entitled **Numerical Investigation on Thermal-Hydraulic Characteristics of Pillow Plate Heat Exchanger for Low Temperature Applications** and submitted by **RAMESH KUMAR** ID No **2019PHXF0049P** for award of Ph.D. of the Institute embodies original work done by him/her under my supervision.

Signature of Supervisor

Signature of Co-Supervisor

Name: - **Prof. ANEESH A.M.**

Name: - **Prof. ANIRUDH SINGH RANA**

Designation: - Assistant Professor

Designation: - Associate Professor

Date: -

Date: -

# Acknowledgement

---

I extend my heartfelt gratitude to Prof. Aneesh A.M. (Mechanical Engineering Department, BITS Pilani) and Prof. Anirudh Singh Rana (Mathematics Department, BITS Pilani), my esteemed Ph.D. supervisor and Co-supervisor, respectively, whose inspiring leadership and unwavering encouragement have been instrumental in shaping the current state of both the presentation and content of my research. This milestone would not have been achieved without their enthusiastic involvement, guidance, and assistance. I owe a profound debt of gratitude to these mentors, who served as excellent guides and consistently supported me in overcoming obstacles throughout the study project.

I would also like to thank Prof. V. Ramgopal, Vice-Chancellor, BITS Pilani, and Prof. Sudhir Kumar Barai, Director, BITS Pilani, Pilani campus, for their invaluable support and blessings. My appreciation extends to Prof. S.K. Verma (Dean, Administration, BITS Pilani, Pilani Campus), Prof. Raj Kumar Gupta (Present Associate Dean, Grants, Consultancy and Industrial Research Division, GCIRD), Prof. Navneet Gupta (Ex Associate Dean, GCIRD), and others who provided essential facilities and unwavering support for my research. Special thanks to Prof. M.B. Srinivas, Dean, Academic-Graduate Studies & Research Division (AGSRD), BITS Pilani, Hyderabad Campus, Prof. Shamik Chakraborty, Present Associate Dean, BITS Pilani, Pilani campus, and Prof. Jitendra Panwar, Ex AGSRD, BITS Pilani, Pilani Campus, for their motivation, constant support, and encouragement. I am also indebted to Prof. Navin Singh, Associate Dean, Student Welfare Division (SWD), BITS Pilani Campus, for his encouragement and valuable suggestions.

Furthermore, I express my gratitude to Prof. Ashish Tiwari of the Department of Mathematics and Prof. Shyam Sunder Yadav of the Department of Mechanical Engineering at BITS Pilani, Pilani Campus, for their insightful comments and dedicated time in reviewing my thesis outline, significantly contributing to the improvement of my Ph.D. thesis report. Special thanks to Prof. Arun Kumar Jalan, Convener, DRC, Department of Mechanical Engineering, for essential assistance in my research.

I thank Prof. Srikanta Routroy, Head of the Mechanical Engineering Department, for valuable support and guidance and to the entire faculty and staff of the Mechanical Engineering Department, BITS Pilani, Pilani Campus, for their moral support and assistance. Special

appreciation goes to Prof. M.S. Dasgupta and Prof. Chennu Ranganayakulu of the Mechanical Engineering Department at BITS Pilani for their unwavering support and encouragement.

My elder brother, Mr. Brajesh Kumar, IIT Patna, Bihar. I am deeply grateful for his continuous moral support throughout my PhD journey. His timely encouragement played a crucial role in the completion of my Ph.D.

I also thank my colleague, Dr. Rishi Parvanda, for providing moral support whenever needed. While it's impossible to name everyone who has assisted me, whether directly or indirectly, I want to acknowledge each of them for their support.

Finally, my sincere thanks go to my parents, Mr. Ramchandra Prasad and Mrs. Kamla Devi. I am profoundly grateful for their dedicated efforts to realize my dreams. Their unwavering support and encouragement have instilled in me the confidence and courage to make choices, complete my thesis, and embrace additional challenges in my life.

Ramesh Kumar

# Abstract

---

In recent decades, there has been a heightened focus on sustainability in product and process design, aiming to balance resource use with improving human society's quality of life. A key aspect of sustainable design in processing plants is minimizing energy consumption, leading to reduced environmental impacts and costs. Heat recovery systems, including heat exchangers, are vital in achieving this goal by facilitating efficient thermal energy exchange between different mediums.

The study emphasizes the crucial role of minimizing energy consumption in processing plants' sustainable design and operation. Industrial heat recovery, achieved through specialized systems like heat exchangers, is essential for meeting thermal demands and optimizing thermal energy exchange. Pillow-plate heat exchangers (PPHEs), known for their superior compactness, find wide application across diverse industries. They are commonly used as reboilers, condensers, and thermal storage units, and play a vital role in HVAC systems. In the food industry, they are particularly favored for processing dairy products, chocolate, and wine. These exchangers are also integral to operations in the pulp and paper sector. The design involves laser-welded stainless-steel sheets with a custom circle weld pattern, ensuring a pressure-tight structure. The reliability and functionality of PPHEs make them a preferred choice in diverse industrial settings.

Computational Fluid Dynamics (CFD) analysis, conducted using ANSYS Fluent software, investigated the performance of PPHEs, which are known for their compact design, flexibility, and cost-effectiveness. The study delves into the geometric parameters of PPHEs, optimizing the PPHE design and exploring heat transfer enhancement techniques. Over 60 plate patterns for PPHEs have been developed globally, emphasizing their significant role in heat exchanger performance. Geometrical configuration emerges as a critical factor in enhancing PPHEs' overall efficiency, with research focusing on experimental and numerical studies to optimize these parameters.

The literature review reveals the potential of these techniques in improving thermal-hydraulic performance, offering benefits such as reduced equipment size, increased capacity, and lower temperature differences. The comprehensive overview combines two critical aspects: optimization of geometrical parameters and heat transfer enhancement techniques in PPHEs.

While numerous review papers exist, this study bridges the gap by considering a more comprehensive range of relevant studies in both aspects. The review emphasizes the need for a holistic understanding of the interaction between the pillow-plate surface and other enhancement techniques.

The study was predominantly focused on developing a detailed numerical model for predicting the performance of PPHE, and using this model, the geometric parameters of the pillow-plate heat exchanger were optimized through entropy and exergy minimization techniques. It investigated the uniform velocity distribution within the pillow-plate structure channels.

The work explores the inverse relationship between Reynolds number ( $Re$ ) variation and overall entropy generation (EG) fluctuation. Low  $Re$  ( $<2000$ ) primarily affects EG through heat transfer. Increased  $Re$  improves heat transmission while decreasing irreversibility and lowering EG. Evaluating exergy efficiency ( $\eta_{ex}\%$ ) is vital for analyzing the effectiveness of transforming energy into work. Higher  $\eta_{ex}\%$  indicates improved energy quality and sustainability, affected by reduced heat dissipation and increased heat transfer rates. In addition, exergy efficiency ( $\eta_{ex}\%$ ) variation total length of Pillow-plate channel ( $L_{(A,1-E,25)}$ ) with decreasing streamwise pitch ( $X_L$ ) and rising  $Re$ . Staggered Circular Welding Spot Patterns (SCWSPs) induce periodic profile formations and 'elliptical vortices,' which benefit exergy efficiency, especially at shorter streamwise lengths and channel diameters ( $d_{cws} = 9\text{mm}, 10\text{mm}$ ).

Moreover, the study also examined the effects of Staggered Circular Welding Spot Pattern-Vortex Generators (SCWSP-VGs), where Staggered Circular Welding Spot Pattern (SCWSP) acts as a vortex generator, on enhancing the thermal performance of the heat exchanger. The numerical results showed that at lower Reynolds numbers ( $Re = 1,000$  and  $2,000$ ), flow velocity profiles remain low until encountering central SCWSP-VGs. Their presence causes flow intensity to increase, redirecting flow inward and outward inducing convergent and divergent behavior. This leads to periodic velocity profiles and enhances turbulent mixing, boosting convective heat transfer. Comparison at  $Re = 2,000$  shows significant wake regions and opposing recirculation flow behind SCWSP-VGs. SCWSP-VGs induce secondary flow, which is crucial for improving flow characteristics and heat transfer. High-speed (Opposite Elliptical Recirculation Vortex/vortices) 'OERV' growth reduces backflow, enhancing mixing and turbulence, fostering improved heat transfer efficiency across all Reynolds numbers.

These comprehensive analyses aimed to uncover strategies for improving the efficiency and effectiveness of the pillow-plate heat exchanger, thereby contributing to advancements in heat transfer technology and sustainable design practices in processing plants.



# Table of Contents

---

<i>CERTIFICATE</i> .....	(i)
<i>Acknowledgement</i> .....	(ii)
<i>Abstract</i> .....	(iv)
<i>Table of Contents</i> .....	(vii)
<i>List of Tables</i> .....	(xi)
<i>List of Figures</i> .....	(xii)
<i>Nomenclature, symbols, and abbreviation</i> .....	(xv)
<b>Chapter -1: Introduction</b> .....	<b>1</b>
1.1 Introduction.....	1
1.2 Motivation for research.....	4
1.3 History of Pillow-plate heat exchanger.....	6
1.4 Construction and material of PPHE.....	7
1.5 Classification of Pillow-plate heat exchanger (PPHE) .....	9
1.6 Advantages and disadvantages of PPHE .....	12
1.6.1 Advantages of PPHEs .....	12
1.6.2 Disadvantages of PPHEs.....	13
1.7 Solution methodology.....	13
1.7.1 CFD as solution methodology .....	15
1.7.2 Overview of ANSYS Fluent Package.....	17
1.7.3 Problem-solving steps.....	17
1.7.4 Flow of numerical simulation methodology .....	18
1.8 Significance of study, thesis structure and organization.....	19
<b>Chapter - 2: Literature review</b> .....	<b>24</b>
2.1 Introduction.....	24
2.2 Numerical work on PPHEs .....	25
2.3 Experimental work on PPHE .....	34
2.4 Optimization of PPHE .....	43
2.5 Heat transfer enhancement in PPHE.....	45

2.6	Summary of literature survey and Gaps in the literature .....	51
2.7	Needs of the work .....	52
2.8	Thesis objectives .....	53
<b>Chapter - 3: PPHE Modelling and Verification.....</b>		<b>55</b>
3.1	Introduction.....	55
3.2	Geometry modelling (Solid geometry) .....	55
3.3	Mathematical and numerical method.....	59
3.4	Meshing.....	62
3.4.1	Tetrahedral mesh .....	62
3.4.2	Hexahedral mesh .....	62
3.4.3	Polyhedral mesh .....	63
3.4.4	Justification for selecting tetrahedral mesh.....	63
3.5	Boundary conditions .....	65
3.6	Numerical methodology.....	66
3.6.1	SIMPLE scheme.....	66
3.6.2	SIMPLEC scheme .....	67
3.6.3	Justification for usage: .....	67
3.7	Solver setting .....	67
3.8	Data reduction.....	68
3.9	Grid independence study.....	69
3.10	Operating conditions and parameters.....	70
3.11	Validation and results .....	72
3.12	Comparison of different pillow-plate section/channel unit .....	74
3.13	Summary of chapter.....	76
<b>Chapter - 4: Heat Transfer Enhancement in Pillow-Plate Type Heat Exchangers (PPHE) with SCWSCs: An Entropy and Exergy Generation Optimization Approach .</b>		<b>77</b>
4.1	Introduction.....	77
4.2	Objectives .....	79
4.3	Problem formulation .....	81
4.3.1	The assumptions.....	82
4.3.2	Boundary conditions .....	82
4.4	Grid independence test and validation of numerical models .....	83
4.5	Thermodynamic analysis .....	86
4.5.1	Entropy analysis .....	86

4.5.2	Exergy efficiency ( $\eta_{ex}$ ) and entropy generation number ( $NS$ ).....	87
4.6	Results and discussion .....	88
4.6.1	Velocity and temperature field distribution .....	89
4.6.2	The energy balance analysis.....	91
4.6.3	Nusselt number and friction factor.....	94
4.6.4	Thermal and frictional entropy generation.....	97
4.6.5	Thermal and frictional exergy destruction .....	100
4.6.6	Bejan number and entropy generation number .....	102
4.6.7	Exergy efficiency and thermal evaluation factor .....	104
<b>Chapter - 5: Effect of SCWSP-VGs on Thermal-Hydraulic Performance of Pillow-Plate Heat Exchanger (PPHE).....</b>		<b>109</b>
5.1	Introduction.....	109
5.2	Objectives .....	113
5.3	Description of the numerical Method .....	114
5.3.1	Computational simulation .....	114
5.3.2	The assumptions for the solution domain .....	114
5.3.3	Boundary conditions and solver setting .....	114
5.3.4	Grid independence test.....	116
5.4	Computational results and discussion.....	118
5.4.1	Effect of SCWSP-VGs and $XL$ on velocity and temperature distribution.....	118
5.4.2	Effect of SCWSP-VGs and $L_{A-E}$ on Nusselt number, and friction factor .....	122
5.4.3	Standard correlation of Nusselt number and Friction factor .....	128
5.4.4	Influence of SCWSP-VGs and $XL$ on Colburn j-factor .....	129
5.4.5	Calculation of normalized drag coefficient and RAF (Reynolds analogy factor)...	131
5.4.6	Performance evaluation criteria of PPHE with SCWSP-VGs .....	134
5.4.7	Comparison of the effect of SCWSP-VGs with some previous VGs .....	136
<b>Chapter - 6: Summary, Conclusion, and Future scope .....</b>		<b>137</b>
6.1	Summary and conclusion.....	137
6.2	Future scope.....	141
References.....		142
<b>Appendix 1.....</b>		<b>155</b>
The cost estimation and analysis of PPHE .....		155
<b>List of Publication .....</b>		<b>158</b>
SCI Journal.....		158

International and National conference proceedings..... 158  
**Biography.....160**

# List of Tables

---

Table No.	Page no.
<b>Table. 2.1.</b> Overview of experimental and numerical research on heat transfer enhancement in PPHEs.	47
<b>Table. 3.1</b> Physical properties of water as working fluid and value used for simulations.....	66
<b>Table. 3.2</b> Effect of different mesh sizes on $Nu$ at $Re = 1200$ .....	70
<b>Table. 3.3</b> Parameters of the pillow plates investigated by Tran et al.[51,75,76] and Present study.	71
<b>Table. 3.4</b> Operating conditions for the current computational study	71
<b>Table. 3.5</b> Nusselt number and pressure drop value obtained in numerical simulation.....	72
<b>Table. 4.1</b> Geometrical parameters considered in the present computational work (all dimensions in mm).....	83
<b>Table. 4.2</b> Effect of different mesh sizes on $Nu$ at $Re = 7,800$ .....	84
<b>Table. 5.1</b> Currently used numerical parameters in computational investigations (all dimensions in mm) .....	113
<b>Table. 5.2</b> The impact of various mesh Sizes on $Nu$ .....	116

# List of Figures

Figures serial number	Page no.
<b>Fig. 1.1</b> The pillow plate heat exchanger channel's geometry and shape.....	3
<b>Fig. 1.2</b> Fabricated or constructed Pillow-plate channel .....	7
<b>Fig. 1.3</b> Manufacturing of Pillow-plate heat exchanger by Laser welding operation	9
<b>Fig. 1.4</b> Different types of pillow plates.....	11
<b>Fig. 1.5</b> Pillow-plates as heating jacket for tanks and piping lines .....	11
<b>Fig. 1.6</b> Flow chart of numerical methodology.....	19
<b>Fig. 3.1</b> A schematic representation of the computational domain of a Pillow-Plate channel type heat exchanger.....	58
<b>Fig. 3.2</b> Schematic diagram of Pillow-Plate type heat exchanger channel.....	59
<b>Fig. 3.3</b> A schematic diagram of a pillow plate heat exchanger with SCWSP, and boundary conditions. ....	65
<b>Fig. 3.4</b> A fine grid view of Pillow-plate computational domain.....	70
<b>Fig. 3.5</b> Validation of Nusselt number ( $Nu$ ) of numerical results against experimental results.....	73
<b>Fig. 3.6</b> Validation of pressure drop ( $\Delta p/L$ ) of numerical results against experimental results.....	74
<b>Fig. 3.7</b> Comparison of velocity profile in different pillow-plate channel unit /section.....	75
<b>Fig. 3.8</b> Comparison of temperature distribution profile in different pillow-plate channel units/sections.....	75
<b>Fig. 4.1</b> Schematic diagram of the pillow plate heat exchanger with SCWSPs.....	81
<b>Fig. 4.2</b> A schematic representation of a pillow plate heat exchanger with SCWSPs and fluid flow condition.....	82
<b>Fig. 4.3</b> Close grid view of Pillow plate domain.....	84
<b>Fig. 4.4</b> Comparison of $Nu$ obtained in the numerical simulation with experimental results for $Re = 1200, 2800, 4200, 6500,$ and $7800$ .....	85
<b>Fig. 4.5</b> Comparison of pressure drop obtained in the numerical simulation with experimental results for $Re = 1200, 2800, 4200, 6500,$ and $7800$ .....	86

<b>Fig. 4.6</b> Representative domains used for thermal modeling, Case (A-E) temperature velocity and Case (A-E) velocity contour of five different streamwise arrangements $L_{A,11-E,15}$ = (256-384 mm (Case 11 to 15)) of the PPC at $Re = 2000$ .....	90
<b>Fig. 4.7</b> Static Pressure contour of different pillow-plate channel configurations $L_{A,11-E,15}$ = 256-384 mm (Case 11 to 15)) of the PPC at $Re = 2000$ .....	91
<b>Fig. 4.8</b> Representative domain of fluid flow inside the pillow-plate channel with two distinct zones at $d_h/X_L = 0.076$ & Case (A) at $Re = 2000$ .....	92
<b>Fig. 4.9</b> Energy contour of different pillow-plate channel arrangement $L_{A,11-E,15}$ = (256-384 mm (Case 11 to 15)) of the PPC at $Re = 2000$ .....	93
<b>Fig. 4.10</b> Surface Nusselt number contour of different pillow-plate channel configurations $L_{A,11-E,15}$ = (256-384 mm (Case 11 to 15)) of the PPC at $Re = 2000$ .	94
<b>Fig. 4.11</b> Variation of Nusselt number vs. Reynolds number.....	96
<b>Fig. 4.12</b> Variation of Friction factor vs. Reynolds number.....	96
<b>Fig. 4.13</b> Entropy generation contour of different pillow-plate channels..... configuration $L_{A,11-E,15}$ = (256-384 mm (Case 11 to 15)) of the PPC at $Re = 2,000$	97
<b>Fig. 4.14</b> Thermal entropy generation vs. Reynolds number.....	99
<b>Fig. 4.15</b> Frictional entropy generation vs. Reynolds number.....	100
<b>Fig. 4.16</b> Thermal exergy destruction vs. Reynolds number.....	101
<b>Fig. 4.17</b> Frictional exergy destruction vs. Reynolds number.....	102
<b>Fig. 4.18</b> Bejan number vs. Reynolds number.....	103
<b>Fig. 4.19</b> Entropy generation number ( $N_s$ ) vs. Reynolds number ( $Re$ ).....	104
<b>Fig. 4.20</b> Exergy efficiency vs. Reynolds number.....	106
<b>Fig. 4.21</b> Thermal evaluation factor ( $\eta_{eff}$ ) variation with Reynolds number ( $Re$ )...	107
<b>Fig. 5.1</b> Schematic diagram of PP (a) Isometric view (b) Top view (vertical cut) (c) PPC.....	112
<b>Fig. 5.2</b> Schematic diagram of one PPC (a) Isometric view (b) Side view.....	115
<b>Fig. 5.3</b> (a) Meshing and (b) close mesh view of PP domain.....	117
<b>Fig. 5.4</b> Streamline profile and longitudinal vortex formation at $d_h/X_L = 0.076$ and $Re = 2000$ .....	119

<b>Fig. 5.5</b> Velocity contour and Temperature contour case (A-E) inside the PPHX with a computational domain at $Re = 2,000$ .....	121
<b>Fig. 5.6</b> Surface Nusselt number variation inside PPC with SCWSP-VGs for case A-E at $Re = 2000$ .....	122
<b>Fig. 5.7</b> Nusselt number for different Reynolds numbers ( $Re$ ) through the PPC with SCWSP-VGs for $d_h/X_L = 0.076-0.043$ and $X_L = 64-96$ mm.....	123
<b>Fig. 5.8</b> Nusselt number ratio for different Reynolds numbers ( $Re$ ) through the PPC with SCWSPs for $d_h/X_L = 0.076-0.043$ and $X_L = 64-96$ mm.....	124
<b>Fig. 5.9</b> Variation of Friction factor against different $Re$ through the PPC with SCWSPs for $r = 0.076-0.043$ and $X_L = 64-96$ mm.....	126
<b>Fig. 5.10</b> Friction factor ratio for different $Re$ through the PPC with SCWSP-VGs for $r = 0.076-0.043$ and $X_L = 64-96$ mm.....	127
<b>Fig. 5.11</b> Static Pressure profile inside the PPC domain with SCWSP-VGs for case A-E at $Re = 2000$ .....	128
<b>Fig. 5.12</b> Variation of calculated Colburn $j$ -factor against $Re$ for $r = 0.076-0.043$ and $X_L = 64-96$ mm.....	130
<b>Fig. 5.13</b> Variation of Numerical Colburn $j$ -factor against $Re$ for $r = 0.076-0.043$ and $X_L = 64-96$ mm.....	131
<b>Fig. 5.14</b> Variation of $C_x/C_{x0}^{0.33}$ against different $Re$ for $r = 0.076-0.043$ and $X_L = 64-96$ mm.....	132
<b>Fig. 5.15</b> Variation of $RAF$ against different $Re$ for $r = 0.076-0.043$ and $X_L = 64-96$ mm.....	133
<b>Fig. 5.16</b> The variation of $(Nu/Nu_0)/(f/f_0)^{1/3}$ against different $Re$ for $r = 0.076-0.043$ and $X_L = 64-96$ mm.....	135



# Nomenclature, symbols, and abbreviations

---

## Nomenclature

$A$	Area (m <sup>2</sup> )
$A_{cs}$	Cross section area (m <sup>2</sup> )
$A_{ht}$	Heat transfer area (m <sup>2</sup> )
$C_x$	Drag coefficient of PPHE (-)
$C_{x0}$	Drag coefficient of straight elliptical channel (-)
$d_{cws}$	Welding spot diameter (mm)
$d_h$	Hydraulic diameter of PPHE (mm)
$f$	Friction factor of PPHE, (-)
$f_0$	Friction factor of a without SCWSPs (straight elliptical) channel (-)
$f_d$	Total Drag (-)
$h_i$	Internal channel height (mm)
$h_{conv}$	Convective heat transfer coefficient (W/m <sup>2</sup> K)
$j$	Colburn $j$ factor $Sr/Pr^{2/3}$ (-)
$k$	Thermal conductivity (W/m. K)
$Nu$	Nusselt number (-)
$Nu_0$	Nusselt number of straight elliptical (without SCWSPs) channel (-)
$Nu/Nu_0/(f/f_0)^{0.33}$	Thermal performance factor/Thermal evaluation criterion (-)
$PEC$	$Nu/Nu_0/(f/f_0)^{0.33}$ (-)
$r = d_h/X_L$	Hydraulic diameter to streamwise length ratio (-)

$RAF$	$(St/St_0/C_x/C_{x0})^{0.33}$ (-)
$Re$	Reynolds number, $\rho v_m d_h / \mu$ (-)
$s_r$	Dimension less factor (-)
$St$	Stanton Number (-)
$St_0$	Stanton Number straight elliptical channel (-)
$v_m$	Mean velocity (m/s)
$X_L$	Streamwise length/pitch in $x$ direction (mm)
$Y_L$	Spanwise length/pitch in $y$ direction (mm)

## Greek Symbol

$\mu$	Dynamic viscosity (Pa-s)
$\rho$	Density of water (kg/m <sup>3</sup> )
$\Delta p$	Pressure resistance (Pa)
$\varphi$	Dimensionless “two-zone” factors (-)

## Superscripts

$0$	Predefined value
$q$	Heat
$tot$	Total
$w$	wall
$z1$	Zone 1

## Abbreviations

CFHE	Cross-Flow Heat Exchanger
CHE	Circular Heat Exchanger
CPHE	Chevron- Plate heat exchanger
CPE	Criterion for Performance Evaluation
CWS	Circular Welding Spot
DPHE	Dimple plate heat exchanger
DPPHE	Dimple pillow plate heat exchanger
EA	Exergy Analysis
EG	Entropy Generation
EGM	Entropy Generation Minimization
EGN	Entropy Generation Number
EVs	Elliptical Vortices
HEs/HXs	Heat Exchangers
OERV	Opposite Elliptical Recirculating Vortex/vortices
PEC	Performance evaluation criterion
PES	Periodic Enhanced Surface
PHE	Plate Heat Exchanger
PP	Pillow-plate

PPC(C)	Pillow-Plate Channel (Configuration)
PPHE/PPHX	Pillow-plate heat exchanger
QUICK	Quadratic Upstream Interpolation for Convective Kinematics
RAF	Reynolds Analogy Factor
SCWSPs(Cs)	Staggered Circular Welding Spot Patterns/configurations
SCWSP-VGs	Staggered Circular Welding Spot Pattern-Vortex Generators
SF	Secondary flow
SIMPLE	Semi-Implicit Method for Pressure-Linked Equations
SIMPLEC	Semi-Implicit Method for Pressure Linked Equations-Consistent
SLOT	Second Law of Thermodynamics
STHE	Shell and Tube Heat Exchanger
TE	Thermo-Economics
TEF	Thermal Evaluation Factor
TEP	Thermal Evaluation Parameters
VG	Vortex Generator
WVG	Winglet Vortex Generator

# **Chapter -1: Introduction**

---

This chapter introduces pillow-plate heat exchangers (PPHE), including their research motivation, historical background, classification, and potential applications. In this chapter, we discuss solution methodologies encompassing numerical and experimental approaches, outline the objectives and scope of the CFD study, and present the methodology and significance of the research. Finally, it delineates the organization of the thesis.

## **1.1 Introduction**

The pillow-plate heat exchanger is a versatile and efficient solution in thermal management, offering a distinct design tailored to optimize heat transfer across various industries. Comprising two thin sheets welded together to form interconnected channels, its unique construction allows for enhanced heat exchange between two fluids for cooling, heating, or thermal storage. This introduction sets the stage to delve deeper into its mechanics, applications, and advantages, highlighting its pivotal role in modern engineering and industrial processes as shown in Fig. 1.1. With its versatility and efficacy, the pillow-plate heat exchanger has become indispensable in industries ranging from food and beverage processing to pharmaceuticals, refrigeration, and beyond.

At the heart of the pillow-plate heat exchanger lies its unique construction. Thin plates, typically made of stainless steel, are welded together at regular intervals, forming a pattern of interconnected channels referring to Fig. 1.1 (a). This pillow-like structure enhances the surface area for heat transfer and ensures uniform fluid flow distribution, maximizing thermal efficiency. The design flexibility allows customization according to specific requirements, whether varying plate thicknesses, shapes, or sizes, catering to various applications.

One of the key advantages of the pillow-plate heat exchanger is its exceptional heat transfer capabilities. The convoluted surface created by the interconnected channels promotes turbulent flow, significantly enhancing heat exchange rates compared to conventional heat exchangers. This efficiency translates into reduced energy consumption, lower operating costs, and enhanced process control, making it an attractive choice for industries striving for optimal performance and sustainability.

The compactness of a heat exchanger is specified by its surface area density, which is the ratio of the heat transfer surface area to the volume of the heat exchanger. For Pillow-Plate Heat Exchangers (PPHE), the surface area density is typically in the range of 50-200  $\text{m}^2/\text{m}^3$  [1] (square meters of surface area per cubic meter of volume) [2]. This high surface area density means PPHEs offer a large surface area for heat transfer relative to their size, making them compact compared to traditional shell-and-tube or plate heat exchangers.

PPHEs are typically constructed using materials that offer excellent corrosion resistance, mechanical strength, and durability, and such robust construction reduces the frequency of failures, leaks, or material degradation, making them relatively low maintenance. The common cleaning methods include chemical cleaning, which is generally inexpensive and easy to implement and can be conducted without disassembling the unit. However, if mechanical issues such as leakage occur between the welded pillow plates, the maintenance costs can be higher because specialized welding or replacement may be required.

In the food and beverage industry, where precise temperature control is paramount, pillow-plate heat exchangers play a crucial role in pasteurization, fermentation, and chilling [3]. Whether it's heating milk for dairy products, cooling wort in beer brewing, or maintaining the ideal temperature for chocolate couching, these heat exchangers ensure product quality and safety while maximizing production throughput (refer to Fig. 1.1 (b) and (c)).

Moreover, pillow-plate heat exchangers offer hygienic and reliable thermal solutions in pharmaceutical and chemical processing, where stringent regulations govern product integrity and purity. Their smooth, crevice-free surfaces minimize the risk of contamination and facilitate thorough cleaning and sterilization, meeting the strict standards of good manufacturing practices (GMP) and ensuring product integrity throughout the manufacturing process.

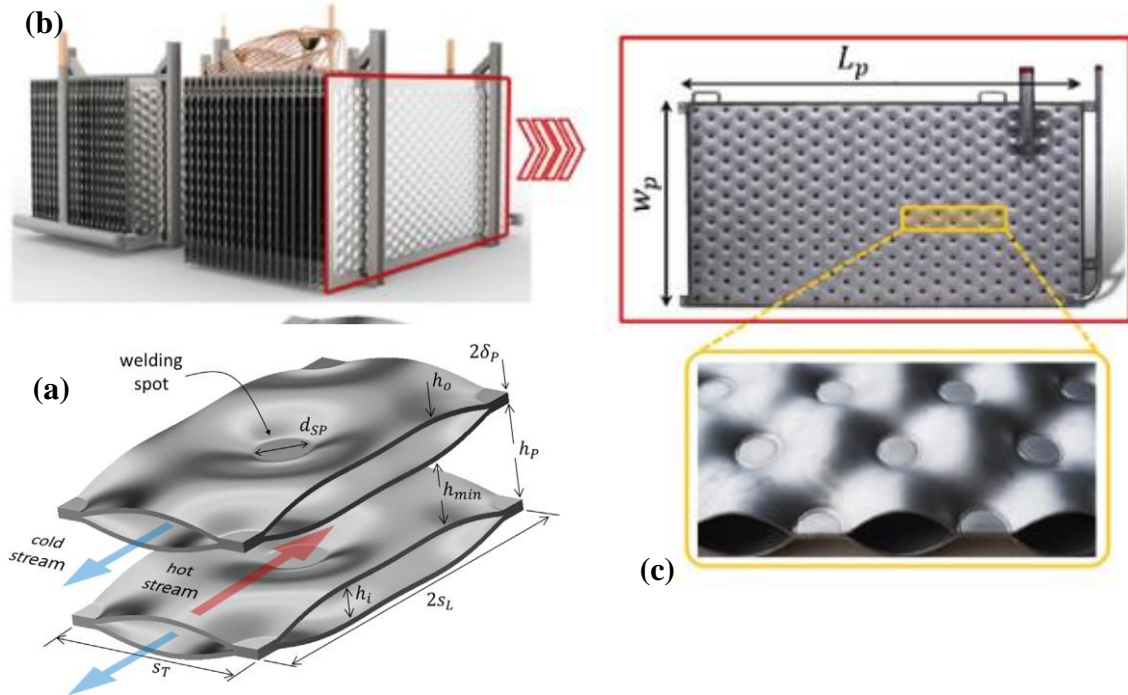


**Fig. 1.1** The pillow plate heat exchanger channel's geometry and shape [4].

**Note:** Circular Welding Spot ( $d_{sp}$ ), Streamwise length ( $2S_L$ ), Spanwise length ( $S_T$ ), Outer channel height ( $h_o$ ), inner channel height ( $h_i$ )

In refrigeration and HVAC systems, pillow-plate heat exchangers find application in evaporators, condensers, and heat recovery units. Their compact design, high thermal efficiency, and resistance to fouling make them ideal for demanding cooling and heating applications, ranging from commercial refrigeration to industrial air conditioning systems. Furthermore, the versatility of pillow-plate heat exchangers extends to renewable energy applications, including solar thermal systems and heat pumps. By harnessing the sun's energy or utilizing waste heat from industrial processes, these heat exchangers contribute to energy conservation and carbon footprint reduction, aligning with global efforts towards sustainable development.

The pillow-plate heat exchanger is a testament to ingenuity and innovation in thermal engineering. Its unique design, exceptional heat transfer performance, and broad applicability make it a cornerstone of modern industrial processes across various sectors. As industries prioritize efficiency, sustainability, and product quality, the pillow-plate heat exchanger remains indispensable for achieving these objectives while driving technological advancement.

## 1.2 Motivation for research

The motivation behind research on pillow-plate heat exchangers lies in the quest for continuous improvement and innovation in thermal engineering, specifically optimizing design parameters and enhancing heat transfer performance across diverse practical applications. This drive stems from the pressing need to address evolving industrial requirements, improve energy efficiency, and meet stringent regulatory standards while ensuring cost-effectiveness and sustainability.

One of the primary motivations for researching the optimization of design parameters is to maximize the thermal efficiency and operational performance of pillow-plate heat exchangers. By systematically studying and fine-tuning key design variables such as plate thickness, channel geometry, welding techniques, and fluid flow patterns, researchers aim to identify optimal configurations that minimize pressure drop, reduce fouling tendencies, and maximize heat transfer rates. Researchers seek to uncover the intricate interplay between these parameters and their impact on overall heat exchanger performance through computational modeling, experimental validation, and advanced optimization algorithms.

Furthermore, the drive to enhance heat transfer in pillow-plate heat exchangers is fueled by the growing demand for increased energy efficiency and reduced environmental impact across various industries. By developing innovative heat transfer enhancement techniques such as surface texturing, passive augmentation structures, and advanced heat transfer fluids, researchers strive to elevate the thermal performance of these heat exchangers to new heights. The goal is to achieve higher heat transfer coefficients, lower overall thermal resistance, and improved thermal homogeneity, enabling more efficient heat exchange processes while minimizing energy consumption and greenhouse gas emissions.

Practical applications across diverse industries serve as compelling drivers for research in this field. In the food and beverage industry, for instance, optimizing heat exchanger design parameters arises from meeting stringent food safety regulations, enhancing product quality, and improving production efficiency. By tailoring pillow-plate heat exchangers to specific food processing applications such as pasteurization, sterilization, and chilling, researchers aim to ensure optimal thermal performance while preserving food products' sensory attributes and nutritional integrity.

Similarly, in the pharmaceutical and chemical sectors, the optimization of pillow-plate heat exchangers is driven by the imperative to maintain product purity, consistency, and



efficacy. Researchers focus on refining design parameters to minimize the risk of contamination, mitigate fouling and scaling issues, and enhance heat transfer uniformity, thereby safeguarding the integrity of sensitive pharmaceutical formulations and chemical processes.

Moreover, the quest for optimized pillow-plate heat exchanger designs extends to renewable energy applications such as solar thermal systems and waste heat recovery. By harnessing advanced optimization techniques and innovative heat transfer enhancement strategies, researchers aim to maximize the efficiency of these systems, increase their overall energy yield, and accelerate the transition to sustainable energy sources.

In conclusion, research on the optimization of design parameters and heat transfer enhancement in pillow-plate heat exchangers is driven by the imperative to meet evolving industrial demands, enhance energy efficiency, and promote sustainability across various practical applications. By leveraging advanced computational tools, experimental techniques, and interdisciplinary collaborations, researchers strive to unlock new frontiers in thermal engineering, paving the way for more efficient, reliable, and environmentally friendly heat exchange solutions.

Research efforts have explored multi-layer and multi-channel configurations with different flowing fluids mini-layers, and micro-channels to enhance PPHE performance. Surface improvements, including wavy patterns, have been investigated to increase turbulence, provide self-cleaning mechanisms, and reduce fouling propensity.

Traditional plate heat exchangers are recognized for their excellent thermal efficiency. The novel Pillow-plate heat exchanger has been studied mathematically and experimentally, considering geometric parameters' impact on thermal performance. Advances in PPHE design and fabrication have occurred, but ongoing research focuses on optimizing geometries and surfaces for improved thermal performance.

The current proposal explores the applicability of pillow plates or heat exchangers for typical low and medium-temperature applications. PPHEs offer advantages like fully welded construction, high leak tightness, lightweight design, wide operating ranges, adaptability, and high overall heat transfer coefficients. Despite their potential applications in various industries, comprehensive design principles and uncertainties in dimensioning hinder the commercial penetration of PPHEs.

The current research aims to provide more efficient solutions with lower pressure drop and production costs, leading to innovative designs such as Pillow-plate Heat Exchangers (PPHEs). With pillow-like surfaces and fully welded constructions, these structures

achieve comparable heat transfer performance to existing systems while using less material and occupying smaller volumes. For example, pillow plates' compactness makes them excellent for applications like condensers in distillation processes, contributing to energy savings and reduced environmental impact compared to other heat exchangers.

### **1.3 History of Pillow-plate heat exchanger**

The pillow-plate heat exchanger's (PPHE) evolution can be traced back to the mid-20th century when advancements in welding technology, particularly laser and resistance welding, laid the foundation for its development. In the 1950s and 1960s, engineers harnessed these improved welding techniques to create flat, double-walled plates with dimples, designating channels for the flow of one fluid and allowing space between dimples for the flow of another.

The concept of the Pillow-plate heat exchanger emerged in the early 1970s, [3,5,6] marked by the overlay of two identically thick metallic sheets, often made of stainless steel. After seam-welding along specific edges, the assembled structure undergoes hydroforming within a pressure vessel equipped with strategically positioned fixtures. The hydraulic inflation during hydroforming imparts a uniform geometry to the plates, followed by spot-welding at fixture points to complete the construction as shown in Fig. 1.1 (c). Behrend's 1993 [1] overview explored various types and applications of PPHE, with Mitrovic and Peterson [7] presenting preliminary experimental findings and Mitrovic and Maletic [8] utilizing Computational Fluid Dynamics (CFD) for detailed flow analysis. In recent years, extensive experimental and numerical studies have been conducted on PPHE, covering single-phase, condensing, and evaporating media. Research has extended to film flow over wavy plates, and methodologies for determining key geometrical parameters have been established.

An alternative to the traditional plate heat exchanger is the wavy pillow-plate heat exchanger, where a stack of wavy plates is welded together to induce fluid flow passageways, promoting turbulence and wall shear stress for enhanced thermal performance. Notably, the construction characteristics of pillow-plate heat exchanger enable higher working temperatures and pressures, making it suitable for multi-stream applications. Research on pillow-plate heat exchangers also emphasizes its superior overall thermal performance in reducing fouling, positioning it as a compelling choice for

heavy-duty applications. Critical considerations in design include the number of passes and the specific type of wavy enhanced surface.

Pillow-plate heat exchangers are integral to various sectors such as dairy, brewing, pharmaceuticals, and chemicals due to their efficiency, flexibility, and maintenance. Ongoing advancements in materials and manufacturing processes suggest a promising future for the continued evolution and application of pillow-plate heat exchangers.

#### 1.4 Construction and material of PPHE

The versatility of pillow-plate design extends beyond traditional heat exchanger applications, as showcased in Fig. 1.2, where they serve as heating or cooling jackets for various industrial equipment. This adaptability underscores their potential across different industrial settings, signaling a shift in heat exchange technology paradigms.

According to Arsenyeva et al. [9,10], a pillow plate comprises two metal sheets, typically stainless steel, spot-welded in a specific pattern. Hydroforming expands the sheets internally using water or a similar medium, creating the characteristic pillow structure. This process, facilitated by inlet and outlet nozzles, can yield "double-embossed" pillow plates with symmetrical waves, which is ideal for PPHEs.

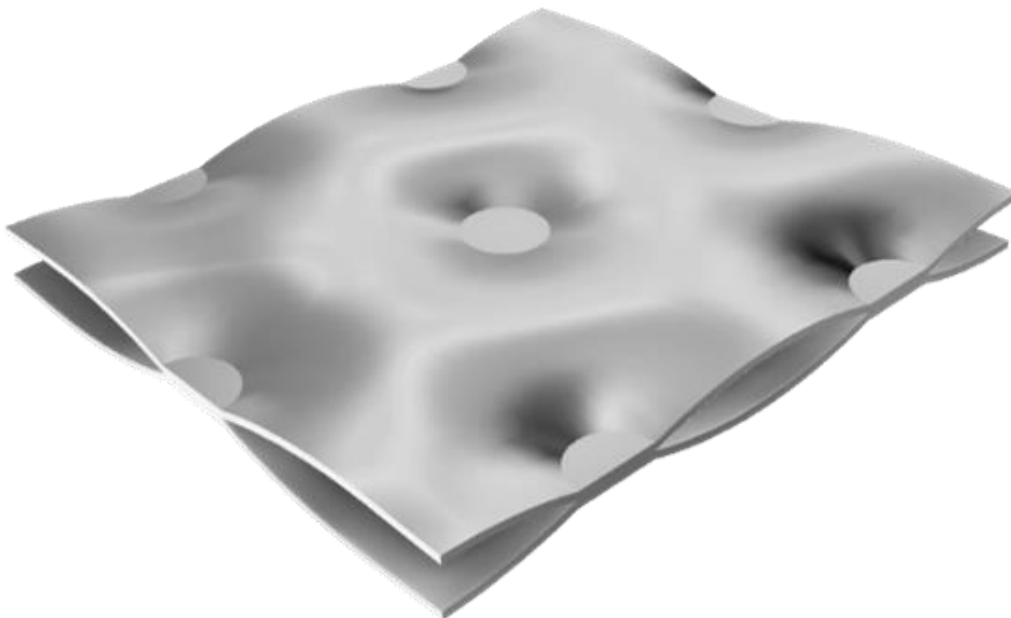


**Fig. 1.2** Fabricated or constructed Pillow-plate channel [11].

The turbulent flow generated by the pillow-like structure enhances heat transfer efficiency, self-cleaning properties, and resistance to fouling. Fully welded construction

ensures hermetic sealing, contributing to operational reliability and enabling lightweight construction without additional support structures.

Materials like stainless steel variants 1.4541 (X6 CrNiTi 18-10, AISI/SAE321) and 1.4571 (X6 CrNiMoTi 17-12-2, AISI/SAE 316Ti) are commonly used [9,10], with welding technologies such as laser or resistance welding ensuring precise assembly. Hydroforming, a critical step, pressurizes the plates to surpass design operating pressures, creating hermetic channels without external gaskets.

While double-embossed plates are standard, single-embossed plates can be achieved using one thin and one thick sheet. As Djakow et al. [12] suggested surface modifications can further enhance performance. In addition, the construction of pillow-plates integrates advanced materials and welding technologies with meticulous hydroforming processes, ensuring airtight integrity and meeting stringent design specifications. This innovative approach enhances reliability and underscores the transformative potential of pillow-plate technology in heat exchange systems.

Three main welding methods are employed for joining metal sheets: laser welding, resistance welding, and tungsten inert gas (TIG) welding without filler metal [13–16]. Of these, laser welding is the most economical and allows for manufacturing various shapes, including precise pillow-plate channels (PPCs) and dimple-plate channels (DPCs) [16]. The type of welding commonly used to develop a spot between two thin sheets in Pillow-Plate Heat Exchangers (PPHE) is typically resistance spot welding or laser welding [17].

**1. Resistance Spot Welding (RSW):** - In resistance spot welding, an electrical current is passed through the two thin metal sheets while two copper electrodes apply pressure. The electrical resistance at the contact points between the sheets generates heat, causing the metal to melt and form a weld nugget. Once the current is stopped, the molten material solidifies, creating a strong spot weld [17,18].

**Advantages:**

- Suitable for thin materials (like the sheets used in PPHE).
- Provides strong mechanical joints that can withstand pressure.
- Efficient and widely used in industrial applications.

**Typical Application:** Commonly used in PPHE manufacturing due to its high-speed, low-cost, and reliable joining method for metals like stainless steel, which is often used in PPHEs.

**2. Laser Welding:** - In laser welding, a highly focused laser beam is used to melt the material at the spot where the two sheets are joined. The heat generated by the laser forms a small molten pool, and upon cooling, the sheets are fused together [14], Fig. 1.5.

**Advantages:**

- Provides precise control over the weld size and shape.
- Minimal heat-affected zone (HAZ), which reduces thermal distortion, making it ideal for thin materials.
- It can be automated for high-precision manufacturing.

**Typical Application:** Used when higher precision is required or when smaller weld spots and minimal material deformation are necessary for specific designs; refer to Fig. 1.3.



**Fig. 1.3** Manufacturing of Pillow-plate heat exchanger by Laser welding operation [18]

## 1.5 Classification of Pillow-plate heat exchanger (PPHE)

Two fundamental types of heat exchangers (HEs) delineate their working principles: 1) Direct heat exchangers, facilitating direct contact between exchanging mediums, exemplified by cooling towers, and 2) Indirect heat exchangers, employing thin conducting walls to prevent mixing between mediums. Diverse technical solutions, such as shell-and-tube, plate (gasketed, welded), and micro heat exchangers, have emerged to

cater to varied applications [17]. Recently, a notable shift towards sustainability has fueled advancements, seeking a harmonious equilibrium between resource utilization and the enhancement of human society's quality of life. This evolving landscape in heat exchanger technology reflects a conscientious effort to address environmental concerns while optimizing efficiency and functionality.

Pillow plate heat exchangers represent a fascinating engineering advancement achieved through an inflation process. In this innovative method, using laser or resistance techniques, two thin metal sheets undergo seamless welding across the entire surface [3,14]. The sealed plates, leaving only connecting ports, are then pressurized with hydraulic fluid (water and air) [14,16], forming the distinctive wavy surface characteristic of PPHEs. This process not only exemplifies the capabilities of modern technology but also highlights the ingenuity of engineering minds. As industries increasingly prioritize maximum efficiency, the popularity of PPHEs has surged. These heat exchangers boast innovative "pillow" seam welding, providing targeted flow guidance in their channels. This welding is an ideal solution in scenarios where fluid velocity or distribution is a concern. Recent developments introducing flow guidance by cushions between adjacent pillow plates have the potential to further enhance heat exchanger performance, enabling industries to operate more efficiently and cost-effectively.

Within the field of pillow plate heat exchangers, two main types are noteworthy: single-embossed and double-embossed. Single-embossed PPHEs, with a thicker base plate and a thinner top plate, are commonly used as the double walls of jacketed vessels. This design allows the top plate to deform while the base plate remains unaffected, providing versatility in manufacturing specialized PPHEs [19].

The design of a pillow plate is always customized to order, particularly in applications involving sanitary products that employ single-embossed heat exchangers. With its flat product side, the single-embossed design ensures no heat tint after welding due to precise welding procedures. Due to their flat interior surface, single-embossed pillow plates are commonly integrated into cooling tables, conveyor structures, bulk or pressure vessels, and process tanks [1,14].

On the other hand, double-embossed pillow plates consist of two sheets of material with comparable thicknesses, represented in Fig. 1.4. The absence of a flat side in this design allows the product to flex on both sides following inflation. Double-embossed PPHEs find applications in refrigeration, heat recovery banks, immersion, and clamp-on equipment, among other process applications. These plates are processed in immersion

chillers, ice banks, falling film chillers, and ice machines, showcasing their versatility in various industrial [3] settings illustrated in Fig. 1.5.

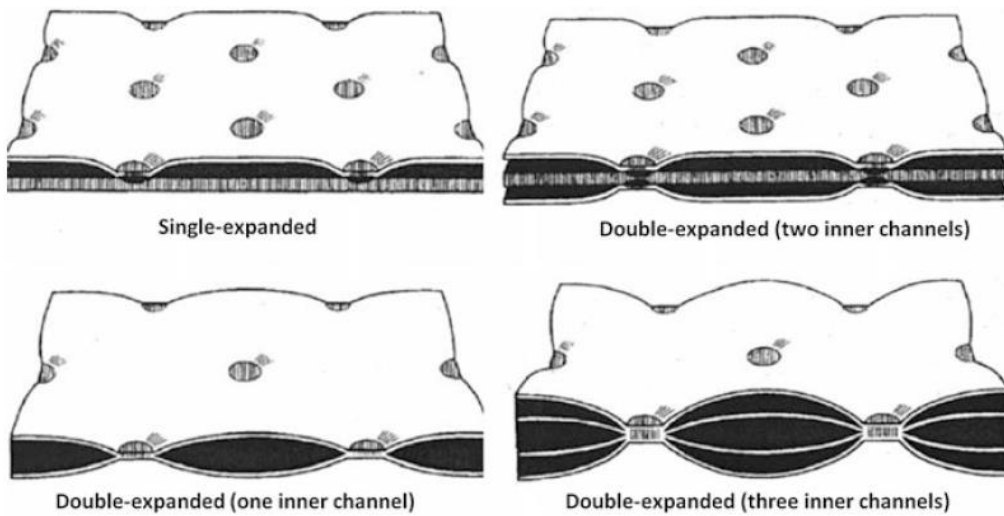


**Fig. 1.4** Different types of pillow-plates (Behrend 1993) [1]



**Fig. 1.5** Pillow-plates as heating jacket for tanks (left, © [www.buco-international.com](http://www.buco-international.com)) and piping lines (right, © [www.lob-gmbh.de](http://www.lob-gmbh.de)) [1]

## 1.6 Advantages and disadvantages of PPHE

Pillow plate heat exchangers (PPHEs), also known as laser-welded heat exchangers [14], offer a range of advantages that make them a compelling choice in various industries. These advantages stem from their unique design and manufacturing process. However, it's essential to consider the potential drawbacks associated with PPHEs. An overview of both the advantages and disadvantages:

### 1.6.1 Advantages of PPHEs

1. Pillow Plate Heat Exchangers seamlessly blends the robust temperature and pressure resistance inherent in shell-and-tube heat exchangers (STHE) with the cost-effectiveness and compact nature of plate heat exchangers (PHE).
2. With an emphasis on ease of maintenance, the inner channels of pillow plates can undergo chemical cleaning or be efficiently cleaned using a return flow method. This contrasts the more cumbersome and costly mechanical cleaning procedures for other heat exchangers like STHE.
3. Enhanced welding reliability is a standout feature of PPHEs. The small diameter of welding points contributes to mechanical stability, optimizes heat transfer, diminishes pressure loss, and excels in thermal performance, particularly at elevated Reynolds numbers.
4. With their wavy configuration, the plates' ingenious design actively promotes turbulent movement within the heat exchanger. This allows for a versatile design strategy with varying cross-sectional areas for both the cold and hot sides.
5. PPHEs boast a high heat exchange coefficient thanks to the continuous redirection of the medium within the pillow plates. This results in thin boundary layers, outstanding heat transfer efficiency, and a reduced need for surface area, translating to lower investment costs.
6. Eliminating gaskets in PPHEs permits operation at high temperatures and pressures and reduces production costs. Additionally, concerns about gasket material compatibility become obsolete.
7. The adaptable design of pillow plates makes them suitable for many applications, serving as heating or cooling jackets for reactors, vessels, and tubing in storage tanks, among other uses.



8. Simplicity in the manufacturing process is a hallmark of PPHEs, requiring less physical space, minimizing transportation and installation costs, and utilizing fewer materials compared to the more complex manufacturing process of STHes.

### **1.6.2 Disadvantages of PPHEs**

2. Limited Applications: Not suitable for all applications, primarily used in industries like food processing, pharmaceuticals, and HVAC, but may not be the best choice for high-pressure or corrosive environments.
3. Complex Manufacturing Process: The manufacturing process, especially laser welding, can be complex and may require specialized equipment, leading to potentially higher production costs compared to traditional heat exchangers.
4. Limited Thermal Performance: In some cases, traditional heat exchangers may offer better thermal performance due to limitations in the design and geometry of pillow plates.
5. Cleaning Challenges: The design may pose challenges for thorough cleaning, especially in the presence of deposits or fouling, crucial for maintaining optimal heat transfer efficiency.
6. High Initial Cost: While long-term operational costs may be lower, initial purchasing and installation costs can be higher than other heat exchangers.
7. Sensitivity to Pressure and Temperature: PPHEs may have operating pressure and temperature limitations, requiring careful consideration of design and material selection.
8. Material Compatibility: Material selection for pillow plates must be carefully chosen to ensure compatibility with processed substances, particularly in industries dealing with aggressive or corrosive materials.
9. Size Limitations: Depending on manufacturing capabilities and application requirements, there may be size limitations, potentially necessitating multiple units or alternative heat exchanger designs for large-scale applications.

## **1.7 Solution methodology**

Solution methodology for pillow-plate heat exchangers involves analytical, numerical, and experimental approaches:

### **1. Analytical Approach**

- Analytical methods use mathematical formulations to understand fundamental heat transfer principles and predict overall performance.
- Equations governing heat conduction, fluid flow, and energy conservation are utilized to develop analytical models.
- These models provide quick insights into heat transfer behavior and can aid in preliminary design and feasibility studies.

## **2. Numerical Simulation**

- Numerical simulations offer detailed insights into pillow-plate heat exchangers' complex fluid dynamics and heat transfer phenomena.
- Model development involves discretizing governing equations using finite difference, finite volume, or finite element methods.
- Heat transfer enhancement techniques, such as adding fins or modifying flow paths, are incorporated into the numerical model to optimize heat transfer efficiency.
- Optimization algorithms, such as genetic or gradient-based methods, are employed to optimize design parameters such as plate geometry, fluid flow rates, and operating conditions.
- Computational Fluid Dynamics simulations allow for the visualization of flow patterns, temperature distributions, and pressure gradients, aiding in the design optimization.

## **3. Experimental Studies**

- Experimental investigations validate numerical simulations and provide real-world performance data.
- Prototype pillow-plate heat exchangers are constructed and tested under controlled laboratory conditions or in actual operating environments.
- Performance metrics such as heat transfer coefficients, pressure drops, and temperature distributions are measured and compared with numerical predictions.
- Heat transfer enhancement techniques are validated experimentally to assess their effectiveness in improving heat exchanger performance.
- Insights gained from experimental studies help refine numerical models and optimize the design of pillow-plate heat exchangers for specific applications.

### 1.7.1 CFD as solution methodology

Computational Fluid Dynamics stands at the forefront of cutting-edge analysis, employing computer-based simulations to unravel the intricacies of fluid flow, heat transfer, and associated phenomena, including chemical reactions. This powerful technique finds applications across a diverse spectrum of industrial and non-industrial domains, showcasing its versatility [20,21]:

1. Aerodynamics of aircraft and vehicles: Unraveling lift and drag dynamics [22].
2. Hydrodynamics of ships: Understanding water-based fluid behaviors.
3. Power plants: Analyzing combustion processes in internal combustion engines and gas turbines [23].
4. Turbomachinery: Examining flow within rotating passages and diffusers.
5. Electrical and electronics engineering: Evaluating cooling mechanisms for equipment, including microcircuits.
6. Chemical process engineering: Assessing loads on offshore structures [23].
7. Environmental considerations: Investigating mixing, separation, and polymer molding
8. Building design: Exploring wind loading and heating/ventilation aspects [24].
9. Marine engineering: Understanding loads on offshore structures.
10. Environmental engineering: Studying the distribution of pollutants and effluents.
11. Hydrology and oceanography: Analyzing flows in rivers, estuaries, and oceans.
12. Meteorology: Enhancing weather prediction capabilities.
13. Biomedical engineering: Simulating blood flows through arteries and veins.

Since the 1960s, the aerospace industry has seamlessly integrated CFD techniques into aircraft and jet engine design, research and development, and manufacturing. Recent applications extend to internal combustion engines, gas turbine combustion chambers, and even predicting drag forces and airflow under the bonnet in the automotive industry. This powerful tool has become integral in designing various industrial products and processes.

The evolving landscape of CFD aims to synergize with other Computer-Aided Engineering (CAE) tools like stress analysis codes. Despite historical challenges due to fluid flow behavior complexity, recent decades have seen a surge of interest. Affordable high-performance computing hardware and user-friendly interfaces have propelled CFD into mainstream industrial applications since the 1990s, marking a transformative era in the understanding and optimizing fluid dynamics.

The evolution of affordable high-performance computing hardware, coupled with user-friendly interfaces, has catalyzed the advancement of commercial Computational Fluid Dynamics packages. In the past, custom code creation for CFD analyses was the norm, leading to many programs for distinct problems and often questionable reliability of results due to inadequate testing. However, the landscape has transformed with well-tested commercial CFD packages, making CFD analysis a routine design tool in the industry. These packages streamline the process and empower research engineers to focus more effectively on the physical system. A typical formal CFD software encompasses three crucial elements: a pre-processor, the main solver, and a post-processor, fostering an integrated approach that enhances efficiency and reliability across diverse applications.

The pre-processing stage in Computational Fluid Dynamics involves transforming user-input flow problem data into a format suitable for the solver. Key activities encompass defining the geometry of the computational domain, generating a grid (mesh), selecting physical and chemical phenomena for modeling, defining fluid properties, and specifying boundary conditions. Grid generation, a significant pre-processing task, consumes a substantial amount of time, with optimization efforts focusing on developing CFD codes with adaptive meshing capabilities.

At the core of CFD software, the solver undertakes tasks such as selecting appropriate physical models, defining material properties, prescribing boundary conditions, providing initial solutions, setting up solver controls, establishing convergence criteria, solving the equation set, and saving results. Real-time monitoring of intermediate results, displayed in residuals indicating the satisfaction level of governing equations, adds to the solver's capabilities. Current research emphasizes the development of adaptive meshing capabilities to enhance computation time and solution accuracy.

The post-processor, the final component of CFD software, facilitates the examination and extraction of useful data from results. Visualization options include vector plots, contour plots, streamlines, and animations. Global parameters like drag coefficient, lift coefficient, Nusselt number, and friction factor can be computed. Post-processor data can be exported to visualization software for enhanced display, contributing to a comprehensive analysis of simulation outcomes.

Several general-purpose CFD packages cater to diverse applications, including PHOENICS, FLUENT, STAT-CD, CFX, CFD-ACE, ANSWER, CFD++, FLOW-3D, and COMPACT. Specialized packages address specific industry needs, like FLOTHERM and ICEPAK for electronics cooling or CFX-TASCFLOW and FINE/TURBO for

turbomachinery. Complementing these packages are visualization software tools such as RECPlot and FIELDVIEW.

## 1.7.2 Overview of ANSYS Fluent Package

ANSYS Fluent is a state-of-the-art CFD program that models fluid flow and heat transfer in complex geometries. Its complete mesh flexibility, supporting unstructured meshes for intricate geometries, sets it apart. Mesh types include 2D triangular/quadrilateral and 3D structures, and users can refine or coarsen grids based on flow solutions. FLUENT, written in the C computer language, employs dynamic memory allocation, efficient data structures, and flexible solver control. Its client/server architecture allows simultaneous processes on client workstations and powerful servers. The interactive, menu-driven interface, written in Scheme, offers customization options through menu macros and functions, making FLUENT a versatile and powerful tool in CFD.

### 1.7.3 Problem-solving steps

- **Problem Identification:** Determine the critical features of the problem at hand.
- **Model Geometry and Grid Creation:** Develop the geometric representation of the model. Generate a grid (mesh) subdividing the domain into smaller, non-overlapping sub-domains.
- **Solver Initialization:** Launch the appropriate solver based on the problem's dimensionality (2D or 3D).
- **Grid Integration:** Import the generated grid into the solver.
- **Grid Validation:** Perform checks on the grid to ensure its integrity and suitability for the simulation
- **Solver Formulation:** Select the appropriate solver formulation based on the nature of the problem.
- **Equation Specification:** Choose the fundamental equations to be solved, considering aspects like laminar or turbulent flow, chemical reactions, and heat transfer models. Identify and incorporate additional models for components such as fans, heat exchangers, and porous media.
- **Material Properties Definition:** Specify material properties essential for accurate simulation.

- **Boundary Condition Specification:** Define boundary conditions to establish the environmental constraints for the simulation.
- **Solution Control Parameters Adjustment:** Fine-tune solution control parameters to optimize convergence and accuracy.
- **Flow Field Initialization:** Set initial conditions for the flow field.
- **Solution Calculation:** Execute the solver to compute the flow field and associated phenomena.
- **Results Examination:** Analyze and interpret the simulation results for insights into the system's behavior.
- **Results Preservation:** Save the obtained results for future reference or further analysis.
- **Interphase Coupling (if applicable):** Incorporate interphase coupling by updating source terms in continuous phase equations through discrete phase trajectory calculations.
- **Convergence Check:** Verify the convergence of the equation set, ensuring that the simulation has reached a stable solution.

#### 1.7.4 Flow of numerical simulation methodology

The flow chart Fig. 1.5 for the geometrical design of a pillow-plate heat exchanger and its numerical simulation begins with the preliminary study, where fundamental factors such as heat transfer requirements and geometric constraints are analyzed. Next, appropriate methods or models for simulation are selected based on the complexity of the pillow-plate heat exchanger design and the desired accuracy of results. Following this, the geometry is parameterized, allowing for variations in dimensions and configurations to be easily explored. Once the geometry is parameterized, the meshing process begins, where the computational domain is discretized into more minor elements to facilitate numerical analysis. Subsequently, a computational fluid dynamics model is developed, incorporating the meshed geometry and appropriate boundary conditions. The numerical model is then validated against previous articles by comparing Nusselt numbers and pressure drop per streamwise length, ensuring its accuracy and reliability. Finally, the design process concludes upon achieving satisfactory results, and the optimized pillow-plate heat exchanger design is ready for further development and implementation.

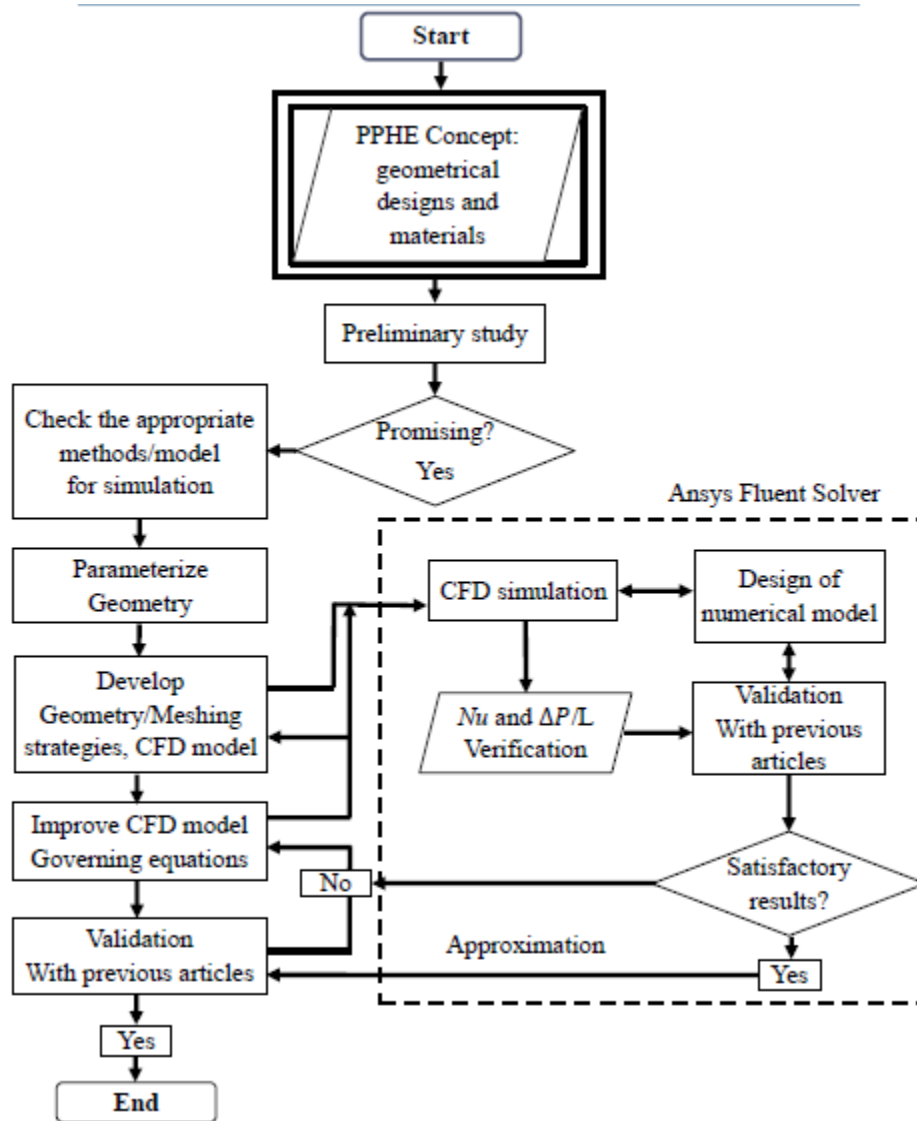


Fig. 1.6 Flow chart of numerical methodology.

## 1.8 Significance of study, thesis structure and organization

The study of pillow-plate heat exchangers holds significant importance, particularly concerning the development of models, numerical investigation of heat transfer enhancement, and optimization techniques. These aspects collectively contribute to advancing the understanding and performance of pillow-plate heat exchangers across various industries, improving efficiency, cost-effectiveness, and sustainability.

Firstly, developing accurate and comprehensive models for pillow-plate heat exchangers enables researchers and engineers to gain insights into the underlying physics governing heat transfer within these devices. By capturing complex fluid flow patterns, heat

conduction mechanisms, and thermal boundary conditions, these models serve as valuable tools for predicting and analyzing the performance of pillow-plate heat exchangers under different operating conditions. They facilitate the exploration of various design parameters and their impact on heat transfer characteristics, aiding in optimizing these devices for specific applications.

Numerical investigation is crucial in enhancing our understanding of heat transfer processes within pillow-plate heat exchangers. Researchers can visualize and quantify heat transfer phenomena with high spatial and temporal resolution through computational fluid dynamics (CFD) simulations and finite element analysis (FEA). This allows for identifying heat transfer enhancement opportunities, such as optimizing channel geometries, enhancing fluid mixing, or implementing passive augmentation techniques. By iteratively refining numerical models and validating them against experimental data, researchers can develop robust predictive tools for optimizing pillow-plate heat exchanger performance across various operating conditions.

Furthermore, optimizing pillow-plate heat exchanger models represents a key area of research aimed at maximizing thermal efficiency, minimizing pressure drop, and reducing overall system costs. Optimization techniques, including genetic algorithms, gradient-based methods, and machine learning approaches, enable researchers to systematically explore the design space and identify optimal configurations that meet specific performance objectives. By leveraging advanced optimization algorithms in conjunction with numerical simulations and experimental validation, researchers can develop innovative pillow-plate heat exchanger designs tailored to the needs of various industries, resulting in enhanced energy efficiency, reduced environmental impact, and improved competitiveness in the marketplace.

The study of pillow-plate heat exchangers, focusing on model development, numerical investigation of heat transfer enhancement, and optimization techniques, holds immense significance in advancing the state-of-the-art in thermal engineering. By elucidating the underlying physics, optimizing design parameters, and developing predictive tools, researchers can drive innovation and optimize the performance of pillow-plate heat exchangers across a wide range of practical applications, ultimately leading to more efficient, sustainable, and cost-effective thermal management solutions for industries worldwide.



The following is the thesis structure and organization.

- Chapter 1 works as an introduction to pillow-plate heat exchangers, covering research motivation, historical background, classification, and potential applications. In this chapter we discussed solution methodologies, including numerical and experimental approaches, outlining the objectives and scope of the CFD study. The chapter also highlights the research's methodology and significance and outlines the thesis's organization. Additionally, it categorizes PPHEs, discussing their various types and examining the advantages and disadvantages of their application. Furthermore, the chapter provides a concise overview of simulation and numerical methodology, focusing on computational fluid dynamics (CFD) and using Ansys Fluent. Finally, it offers a clear organizational roadmap for subsequent chapters, setting the stage for a detailed examination of PPHE modeling.
- The literature review chapter 2 on pillow-plate heat exchangers encompasses numerical and experimental studies, examining both laminar and turbulent models and various variable studies to evaluate performance. It covers different pillow-type channels and their applications with diverse working fluids. Optimization techniques like genetic algorithms, artificial neural networks (ANN), and particle swarm optimization algorithms (PSOA) have been utilized to improve efficiency. Additionally, research explores heat transfer enhancement techniques. Key objectives are synthesizing existing knowledge, identifying gaps, and guiding future research directions. Understanding advancements and limitations in heat exchangers and optimization methods is pivotal for enhancing their design, performance, and industrial relevance.
- Modeling and verification chapter 3 has presented a detailed exploration of the numerical modeling of pillow-plate heat exchangers, employing the transition SST  $k-\omega$  (omega) turbulence model. The chapter began by outlining the motivation behind utilizing computational fluid dynamics (CFD) simulations for PPHE analysis, emphasizing the significance of accurate modeling in optimizing heat exchanger performance. The transition SST  $k-\omega$  turbulence model was chosen for its ability to effectively capture both laminar and turbulent flow regimes, making it suitable for simulating the complex flow phenomena within PPHEs. Through a comprehensive methodology section, the chapter detailed the setup and implementation of the CFD simulations using ANSYS Fluent. Key parameters such as mesh generation, boundary

conditions, and solver settings were carefully defined to ensure accurate and reliable results. Additionally, the chapter discussed the validation process, where simulation results were compared against experimental data to assess the model's predictive capability. This validation step is crucial for establishing confidence in the numerical simulations and verifying their accuracy in representing real-world phenomena. Furthermore, the transition SST  $k-\omega$  turbulence model demonstrated its effectiveness in capturing the flow behavior within PPHEs, providing insights into flow patterns, heat transfer rates, and pressure losses. By validating the simulation results against experimental data, the chapter confirmed the model's ability to accurately predict the thermal-hydraulic performance of PPHEs under various operating conditions.

- Chapter 4 examines into a detailed analysis of heat transfer and friction factor parameters across 25 different pillow-plate heat exchanger designs. By considering a wide range of dimensional and non-dimensional thermodynamic and thermal-hydraulic influencers, the chapter aims to optimize exergy efficiency and thermal evaluation factors. Employing the SST transition  $k-\omega$  method and entropy/exergy approximation techniques, the analysis provides comprehensive insights into thermodynamic and thermal-hydraulic performance. These findings contribute valuable insights into optimizing exergy efficiency and thermal evaluation within diverse operating conditions and geometrical configurations.
- In chapter 5, the additional upper-lower Staggered Circular Welding Spot Patterns (SCWSP) are considered vortex generator (VGs) in a periodic enhanced Pillow-plate type heat exchanger. This chapter reveals the impact of SCWSP-VGs on thermal performance of PPHX. Numerical analysis using ANSYS Fluent 18.1 demonstrates significant improvements in thermo-hydrodynamics, inducing periodic velocity profiles and opposite elliptical recirculation vortex (OERV) turbulence. Graphical representation of PPHX performance showcases enhancements in Colburn  $j$ -factor,  $Nu/Nu_0$ ,  $f/f_0^{1/3}$ , Reynolds analogy factor, normalized drag coefficient ratio  $(C_x/C_{x0})^{0.33}$ , and  $(Nu/Nu_0)/(f/f_0)^{1/3}$ .
- Chapter 6 presents the numerical findings of the pillow plate heat exchanger alongside potential future avenues for exploration. The numerical results offer insights into the performance and behavior of the pillow plate configuration under various conditions, contributing to the understanding of its thermal characteristics. Additionally, the chapter outlines promising directions for further research and development,

suggesting areas such as optimization of geometric parameters, exploration of novel materials, and refinement of numerical models. These future scopes aim to advance the efficacy, adaptability, and sustainability of pillow plate heat exchangers, paving the way for continued innovation in thermal engineering.

## **Chapter - 2: Literature review**

---

A literature survey on pillow-plate heat exchangers reveals a tripartite categorization, each segment delineated by distinct parameters: model development, heat transfer enhancement, and applications. In model development, researchers have extensively explored various mathematical frameworks to elucidate the intricacies of pillow-plate heat exchangers. From empirical correlations to CFD simulations, these models aim to accurately predict temperature distributions, flow patterns, and pressure drops within the exchanger. Through iterative refinement, these models evolve to encapsulate the complex fluid dynamics and thermal behavior inherent in pillow-plate designs. Heat transfer enhancement constitutes another pivotal facet of research in pillow-plate heat exchangers. Innovations such as surface modifications, fluid additives, and geometric optimizations have been investigated to augment heat transfer rates. These enhancements seek to maximize the efficiency and effectiveness of heat exchange processes, thereby improving overall system performance.

### **2.1 Introduction**

A literature survey on pillow-plate heat exchangers reveals a tripartite categorization, each segment delineated by distinct parameters: model development, heat transfer enhancement, and applications.

In model development, researchers have extensively explored various mathematical frameworks to elucidate the intricacies of pillow-plate heat exchangers. From empirical correlations to computational fluid dynamics simulations, these models aim to accurately predict temperature distributions, flow patterns, and pressure drops within the exchanger. Through iterative refinement, these models evolve to encapsulate the complex fluid dynamics and thermal behavior inherent in pillow-plate designs.

Heat transfer enhancement constitutes another pivotal facet of research in pillow-plate heat exchangers. Innovations such as surface modifications, fluid additives, and geometric optimizations have been investigated to augment heat transfer rates. These enhancements seek to maximize the efficiency and effectiveness of heat exchange processes, thereby improving overall system performance.

Furthermore, the applications of pillow-plate heat exchangers span diverse industries including food and beverage processing, pharmaceuticals, renewable energy, and HVAC

systems. Each application necessitates tailored designs and operational parameters to meet specific requirements, driving continuous innovation and adaptation within the field.

In summary, the literature on pillow-plate heat exchangers is characterized by a multifaceted exploration encompassing model development, heat transfer enhancement, and diverse applications, each contributing to the advancement of this critical thermal technology.

## 2.2 Numerical work on PPHEs

Pillow-plate heat exchangers are widely employed in heating, ventilation, air conditioning, and refrigeration (HVAC&R) applications due to their compact design and high heat transfer efficiency. Extensive research has been conducted on both single-phase [25] and two-phase [26] flows in PHXs since their introduction in the late 20th century. Pillow-plate heat exchangers find common use in the chemical and processing industry for both single-phase and two-phase applications. However, there is limited research on the application of PPHXs in HVAC&R.

In 2011, Mitrovic and Maletic [8] established a universal relationship, expressed by Eqn. (1) and (2) below, correlating heat transfer and pressure drop for single-phase fluid flow and heat transmission through a CFD based analysis. Their findings suggested welding spots in the pillow plate channel enhance thermal performance compared to conventional designs, particularly in high Reynolds number ( $Re$ ) conditions. These studies employed a laminar model, despite the potential for turbulent flow at  $Re \sim 1000$ . Furthermore, using an approximate trigonometric function to describe the wavy surface led to notable inaccuracies, as pointed out by Piper et al. in 2015, [9].

$$Nu_m = C_1 \left(\frac{S_L}{L}\right)^{n_1} \left(\frac{S_T}{L}\right)^{n_2} \left(\frac{d_h}{L}\right)^{n_3} Re^{n_4} Pr^{n_5} \quad (2.1)$$

$$Nu_m = C_2 \left(\frac{S_L}{L}\right)^{n_1} \left(\frac{S_T}{L}\right)^{n_2} \left(\frac{d_h}{L}\right)^{n_3} Re^{n_4}, \quad (2.2)$$

Where the constant considers the influence of the Prandtl number,  $C_2 = C_1 Pr^{n_5}$ .

$$C_2 = 0.102; n_1 = 0; n_2 = -0.69; n_3 = 0.66; n_4 = 0.6$$

$S_L$  = Streamwise length (mm),  $S_T$  = Spanwise length (mm),  $d_h$  = Hydraulic diameter (mm),  $d_p$  = Plate length (mm)

Piper et al. [9] recently implemented a novel design approach involving numerical simulations to determine the geometric characteristics of Plate Heat Exchangers using

Finite Element Analysis (FEA). The simulations focused on austenitic stainless steels (1.4301, 1.4404, 1.4541, and 1.4571) as plate materials. The study also incorporated empirical Dittus-Boelter Nusselt correlations, encompassing parameters such as hydraulic diameter, wetted heat transfer area, channel cross-section area, and channel volume of PPHEs. Piper et al. [8,14] also conducted a numerical investigation into the fundamental geometric constraints of pillow plates in I-channel configurations, proposing correlations between hydraulic diameters and convective heat transfer coefficients. They provided a comprehensive analysis of PPHE geometry for both I-channel and E-channel configurations in [9], utilizing CFD simulations to explore surface area expansion and its impact on thermo-hydraulic characteristics in PPHEs. The suggested correlations offer precise assessments of hydraulic diameter and cross-sectional area, enhancing the applicability of pillow plates.

In 2015, Piper et al. [9] introduced a numerical forming simulation-based approach for determining the geometric characteristics of Pillow Plate Heat Exchangers. Although this method was deemed flexible and capable of predicting the hydroforming process during PPHX manufacture, inaccuracies were observed in the correlations developed for calculating various parameters, including volumetric mean hydraulic diameter, wetted heat transfer area, channel cross-section area, and channel volume. Another numerical study conducted by Eldeeb and co-authors in 2016 [27], employing a similar approach to Piper et al. [9], demonstrated good agreement with volume calculations for some geometries. However, agreements for heat transfer areas were only within 20%. It was concluded that more accurate design methods are needed to reduce uncertainties in PPHX design.

In recent work, Piper et al. [13] extended their numerical investigation to explore the fundamental geometric constraints of pillow plates in I-channel configurations. They proposed basic correlations between hydraulic diameters and convective heat transfer coefficients. Furthermore, their comprehensive study in [9] delved into I-channel and E-channel configurations using CFD simulations, examining surface area expansion and its impact on thermo-hydraulic characteristics in Plate Heat Exchangers (PPHEs). The suggested correlations were designed for precise assessments of hydraulic diameter and cross-sectional area, contributing to the broad application of pillow-plate technology. In a related study, Piper et al. [21] employed numerical simulations to investigate turbulent forced convection in single-phase water flow within PPHEs, exploring Reynolds numbers ranging from 1,000 to 8,000. The results highlighted a two-zone fluid flow pattern consisting of a meandering core and a symmetrical recirculation region.

In 2017, Piper et al. [11] extended a design methodology focusing on pressure loss and heat transfer in turbulent forced convection within Pillow-plate channels for the range  $1,000 \leq Re \leq 8,000$  and  $1 \leq Pr \leq 150$ . The study involved characterizing geometrical parameters, including welding configuration and inflation height. Two approaches for calculating the heat transfer coefficient were employed: the first based on the Dittus-Boelter type power law function for Nusselt number [21], and the second relying on characteristic flow patterns (meandering core flow and recirculation) within the pillow plates, as suggested in Ref. [21].

In 2016, Piper et al. [21] conducted a Computational Fluid Dynamics (CFD) study on the turbulent single-water flow in Pillow Plate Heat Exchangers with Reynolds numbers ranging from 1000 to 8000. The PPHX surface was derived through forming simulations. They introduced an efficiency metric, calculated as the total heat transfer divided by the total pumping power, revealing that lower Reynolds numbers, larger pillow heights, and a transverse weld pattern resulted in improved performance. Additionally, smaller weld diameters and oval weld shapes were identified as factors that could significantly reduce pumping power, although with a reduced heat transfer area. In a subsequent work in 2017, Piper and colleagues [11] utilized these simulations to formulate and validate heat transfer coefficient and pressure drop correlations for over 20 different geometries. While the correlations demonstrated agreement with their numerical simulations within  $\pm 15\%$  and covered a wide range of Prandtl numbers (1-150), they did not consider lower Reynolds numbers, and the influence of pillow height on performance was not addressed, providing opportunities for future validation.

In 2017, Tran et al. [28] conducted a study indicating that the heat transfer coefficient values in Pillow Plate Heat Exchangers were superior compared to vertical tubes in applications involving coupled condensation-evaporation. Furthermore, Eldeeb and colleagues [27] performed a preliminary optimization study on PPHX, exploring 32 different geometries and illustrating potential enhancements for PPHX despite the study's limitation in the number of geometries considered.

Piper et al. [29] employed a numerical study using the realizable k- $\epsilon$  model to investigate turbulent single-phase water flow and heat transfer in Pillow-plate channels, considering Reynolds numbers ranging from 1,000 to 8,000. Their findings revealed boundary layer separation upstream of welding spots, forming large, flat-shaped recirculation zones. These recirculation zones were identified as the primary contributors to form drag, accounting for nearly 50% of the Darcy friction factor. The surface area

occupied by these recirculation zones was less effective for heat transfer. To enhance heat transfer rates, it was emphasized that minimizing the size and shape of these regions and reducing the contribution of form drag to the total pressure drop could be achieved by increasing turbulent mixing near the wall and delaying boundary layer separation.

Vocciante et al. [30] examined various turbulence methods for single-phase flow ( $3,000 \leq Re \leq 8,000$ ) in the outer channel using OpenFOAM simulation software. The primary objective of their study was to compare pressure loss measurements. Their results indicated that Detached Eddy Simulation (DES) with the  $k-\omega$  Shear-Stress Transport (SST) model provided the best agreement with experimental results, offering a lower computational cost and greater ease of configuration compared to Large Eddy Simulation (LES).

In another study, Kumar et al. [31] delved into a numerical exploration of the heat transfer and fluid flow dynamics within a pillow-plate channel. Their investigation spanned various geometric parameters, encompassing longitudinal and transverse pitch, channel height, and weld spot diameter, across a broad spectrum of Reynolds numbers. Water served as the cooling medium in their simulations. Notably, the study unveiled the influence of flow development on the formation of hot recirculating zones within the pillow-plate channel. As the flow progressed, smaller hot recirculating zones were observed in developing regions, growing with flow advancement. The study further identified increased longitudinal pitch correlated with higher specific pressure drop, bulk mean velocity, and wall shear stress. This was attributed to the reduced hydraulic diameter with increased longitudinal pitch, causing elevated bulk mean velocity for a constant Reynolds number. Conversely, a decrease in transverse pitch resulted in a substantial reduction in channel cross-section, leading to an increase in bulk mean velocity and specific pressure drop, reaching up to 2.5 bar/m for a specific channel configuration. Channels with a pitch ratio of  $2X_L/Y_L = 1$  exhibited the lowest normalized thermo-hydraulic efficiency. The non-dimensional pillow-plate channel height and weld spot diameter influence heat transfer and pressure loss, with larger weld spot diameters decreasing thermo-hydraulic efficiency. The study provided a power law correlation accurately predicting the Nusselt number and emphasized the significant influence of the Reynolds number on heat transfer. In an additional study, Kumar et al. [32] concentrated on the numerical analysis of fluid flow and heat transfer characteristics in a pillow plate channel using Large Eddy Simulation (LES) at a Reynolds number of 7800, employing water as the working fluid.



Zibart and Kenig [33] numerically assessed the heat resistance of the pillow plate through conjugate heat transfer modeling and CFD-based simulation. Their investigation involved the simultaneous simulation of internal and outer channel flows, considering thermal coupling through the sheet metal. Using aluminum as a material demonstrated significant potential due to its higher thermal conductivity than stainless steel, leading to a 10-25% reduction in the overall thermal resistance of a Pillow-Plate Heat Exchanger. The study delved into the partial thermal resistance of the inner channel flow, metal sheet, and outer channel, highlighting the notable impact of welding spots on enhancing the active heat transfer surface for the outer channel over the inner channel. Shirzad et al. [34] conducted a numerical analysis, identifying optimal geometrical parameters for Pillow-Plate Heat Exchangers and revealing that configurations with longer longitudinal or transversal distances in the channel exhibited higher efficiency, particularly lower friction coefficients.

In [35], Arsenyeva et al. introduced an innovative approach for designing Pillow Plate Heat Exchangers (PPHEs) tailored to diverse process conditions. The research focused on evaluating the impact of the distance between pillow-plate panels on the unit's thermal and hydraulic parameters. They developed a mathematical model to characterize the thermal and hydraulic behavior of PPHEs, highlighting overall heat transfer coefficients and pressure drops concerning fluid velocity. The proposed approach relied on a mathematical model that considered predefined allowable pressure drops, and case studies involved scenarios such as water heating and crude oil preheat train conditions. The study compared PPHE designs with minimal heat transfer area against Chevron-type Plate Heat Exchangers (CPHEs) under similar operating conditions, illustrating the effective utilization of PPHEs in situations with significantly different flow rates for hot and cold fluids.

Goedecke and Scholl [36] devised a comprehensive model for simulating a pillow plate thermosiphon reboiler's fluid dynamics and thermal performance, considering evaporation between the plates. Experimental axial temperature profiles were utilized to analyze heat transfer, discerning between heating and evaporation zones. Extracted overall heat transfer coefficients were then used to formulate correlations for single and two-phase heat transfer, demonstrating favorable agreement with experimental data within  $\pm 30\%$ . The study incorporated a model of convective boiling to describe heat transfer in the evaporation zone. It quantified single-phase pressure drop and integrated this information into a simulation program. Calculated heat fluxes for water closely matched experimental

values within  $\pm 30\%$ . Although qualitative agreement was achieved for fluid dynamic performance, the absolute values were slightly underestimated, possibly due to a slight underestimation of the two-phase pressure drop. The authors suggested that future work should delve deeper into heat transfer and pressure drop mechanisms to enhance correlation accuracy.

Tran et al. [37] recently validated numerical results against experimental findings. Their observations underscored a consistent increase in spanwise Reynolds shear stress compared to streamwise and wall-normal stress. This occurrence was ascribed to the dynamic displacement of the recirculation zone within the channel, as unveiled through the examination of instantaneous flow characteristics. Furthermore, the study identified that the predominant factor contributing to heat transfer enhancement in the pillow plate channel is the elevated velocity within the primary core flow zone.

Djakow et al. [38] introduced a surface structuring method involving dimples on pillow plates and explored its influence on fluid dynamics and heat transfer through Computational Fluid Dynamics (CFD) simulations. The study revealed a significant 24% increase in the heat transfer coefficient compared to a smooth-surface pillow plate channel within a Plate Heat Exchanger. The findings highlighted that the impact of the dimpled surface on thermo-hydraulic characteristics is expected to be more pronounced in the outer channel than in the inner one.

In 2021, Toghari et al. [39] numerically explored the fluid flow and heat transfer characteristics of  $\text{Al}_2\text{O}_3$ -based nanofluids in a Pillow-plate heat exchanger using a two-phase model. The study covered Reynolds numbers of 250, 500, 750, and 1,000 and varying volume concentrations ( $\phi$ ) ranging from 0% to 3%. Additionally, three modes of welding spots, including elliptical welding spots, were investigated. The findings indicated that welding points significantly enhanced fluid momentum and mixing, increasing heat transfer with rising Reynolds numbers.

In 2021, Zibart et al. [40] employed conjugate heat transfer techniques and CFD-based simulations in a counter-current mode to conduct a detailed analysis of thermal resistance for Aluminum and Stainless Steel with thicknesses of  $\delta_r = 1$  and 2 mm each. The numerical simulations demonstrated that aluminum is a better substitute for stainless steel due to higher thermal conductivity. The results indicated that aluminum could reduce the overall thermal resistance of a PPHE by 10 to 25%. Furthermore, the study highlighted the substantial enlargement of the active heat transfer surface for the outer channel due to welding spots compared to the inner channel.

Zibert and Kenig [41] conducted a numerical investigation into falling-film behaviour using the volume of fluid (VOF) method in STAR-CCM+. While there was reasonable agreement between numerical and experimental results, disparities were noted, including a delayed numerical film disturbance compared to experiments. Unrealistic capillary waves were identified in the numerical results, prompting a recommendation for utilizing a piecewise linear interface calculation method in ANSYS Fluent. Despite qualitative analyses, no correlation has been established. Further studies are needed to explore diverse pitch patterns and investigate two-phase heat transfer phenomena.

Selven et al. [42] engineered a cold thermal energy storage (CTES) unit utilizing a Plate Heat Exchanger (PPHX) for their project, detailed in references [42]. This CTES unit was integrated into the secondary circuit of a large-scale cascade refrigeration system tailored for industrial applications, with ammonia (R717) and CO<sub>2</sub> (R744) employed in the primary and secondary circuits. The primary goal was to fulfil cooling and freezing requirements at -5°C and -40°C, respectively. The CTES was strategically incorporated to facilitate peak load shifting by acknowledging the substantial temperature difference between these operational points. The researchers developed a lab-scale prototype for experimental validations, selecting water as the phase change material (PCM). In these experiments, the refrigerant (R744) circulated through the Pillow Plate Heat Exchanger for either condensation or evaporation, while the PCM underwent melting or solidification processes. Selven et al.'s inventive design and experimental setup demonstrate a practical implementation of a CTES unit within a cascade refrigeration system, highlighting its potential for effective peak load management in industrial settings. Selven et al. examined two 2D sections of the Cold Thermal Energy Storage (CTES) unit in their numerical analysis by transversally and longitudinally cutting it. The initial investigation [20] evaluated the impact of pillow-plate waviness, comparing it with a flat plate heat exchanger. The pillow-plate heat exchanger exhibited more vigorous natural convection, particularly in the initial stages. Despite this, the phase change duration was similar between the PPHX and the flat plate heat exchanger, simplifying subsequent investigations.

In a subsequent investigation [24], Selven et al. chose to exclude the consideration of pillow-plate waviness and instead examined a flat plate configuration. The study focused on analyzing the mushy zone constant, which gauges the rate of reaching zero velocity during melting and solidification. The results indicated that higher values of the mushy zone constant led to a prolonged phase change duration. Selven et al.'s numerical

examinations [24] offered valuable insights into how pillow-plate waviness influences natural convection and the duration of phase change within the Cold Thermal Energy Storage (CTES) unit. The comparison with a flat plate heat exchanger and the investigation of mushy zone constants contribute to a comprehensive understanding of the system's thermal performance under various configurations.

In 2020, Sevault and Naess [20] developed a thermal storage unit integrated into the central heating system of an office building to address peak heating demand. The design incorporated an organic phase change material (PCM) with a phase change temperature ranging from 35 to 37°C situated in the outer container (OC). At the same time, water circulated within the inner container (IC) through two passes. The selection of a pillow-plate heat exchanger over fin-and-tube alternatives was driven by the PPHX's compactness, higher heat output, and durability. The storage capacity was established at 200 kWh with 3 tons of PCM, presenting a more efficient solution than employing a water tank, which would have necessitated approximately four times more volume. Previous dynamic simulations validated the unit's ability to achieve heat input/output surpassing 12 kW for over 6 hours, relying on a 3-6°C temperature difference between the PCM phase change and heat transfer fluid (HTF) temperatures [43].

Continuing from this, Sevault et al. [44] proceeded to fabricate and operate the PCM-PPHX unit, providing practical insights. They underscored that in Plate Heat Exchangers (PPHXs), the primary cost driver in the manufacturing process is the number of plates rather than their dimensions. Consequently, it is more cost-effective to maximize the size of each plate within production constraints and minimize the overall number of plates.

Also in 2020, Lin et al. [45] innovated a novel heat exchanger for heat storage, rooted in the pillow-plate concept. In this configuration, the inner container (IC) was partitioned into distinct sections, facilitating the utilization of different heat transfer fluids (HTFs) for the charging and discharging processes. A decline in average power and effectiveness was noted throughout the phase change material (PCM) and HTF processes. Moreover, an increase in HTF flow rate resulted in enhanced power, attributed to intensified turbulence, while diminishing effectiveness. However, beyond a specific flow rate, the impact on power and effectiveness became negligible.

Al-Turki et al. [46] examined  $Al_2O_3$  nanoparticles at concentrations ranging from 0 to 3 vol% (Reynolds 250-1000), consistently observing a PEC exceeding one. The optimum performance was noted at the highest nanoparticle concentration. Meanwhile, Shirzad et al. [47] investigated CuO and  $TiO_2$  nanoparticles at concentrations of 0-5 vol%

(Reynolds 1000-8000). Due to CuO's elevated friction factor, it was excluded from consideration. At 2 vol%, Al<sub>2</sub>O<sub>3</sub> demonstrated the best performance for Reynolds values above 2000, striking a balance between an enhanced heat transfer coefficient and an increased friction factor. It's noteworthy that Al-Turki considered a 2Y<sub>L</sub> pillow-plate length, while Shirzad contemplated what appears to be a 10X<sub>L</sub> length with a fully developed flow. Drawing comparisons between these studies is challenging, and it's emphasized that nanofluids are yet to be explored in outer containers (OC). It's crucial to highlight that Al-Turki et al. [46] investigated a pillow-plate length of only 2Y<sub>L</sub>, encompassing the hydrodynamically developing region. In contrast, Shirzad et al. [47] considered what seems to be 10X<sub>L</sub>, indicating fully-developed flow. Consequently, the findings may not be directly comparable. Additionally, it is noteworthy that nanofluids have not been investigated in outer containers (OC) thus far.

In 2022, Yao et al. [48] introduced an innovative design for a pillow-plate heat exchanger to improve heat transfer between molten salt (MS) and supercritical carbon dioxide (SCO<sub>2</sub>). The novel PPHE incorporated periodically staggered convex and concave spots, impacting flow dynamics and thermal performance. The simulation results revealed distinctive variations in temperature and heat transfer coefficients, attributed to the interplay of fluid scouring effects and vortices generated by the periodically convex/concave spots flow pattern. In regions downstream of convex spots or upstream of concave spots, the simulations depicted rapid changes in fluid temperature and reduced thermal boundary layers, resulting in relatively higher heat transfer coefficients. Conversely, vortices were observed in the upstream region of convex spots or downstream of concave spots, leading to thicker thermal boundary layers and lower heat transfer coefficients. The heat transfer coefficient within the flat plate region was lower than in the convex spot region but higher than in the concave spot region. Notably, the flat plate region contributed to over 50% of the heat flow percentage in the total system, primarily due to its large surface area ratio. The study underscored the significant impact of PPHE structures on heat transfer coefficients, indicating a 28.1% increase with channel height rising from 2.4 mm to 4.8 mm and a 40.4% increase with spot longitudinal distance decreasing from 42 mm to 18 mm. Additionally, the research provided predictions for flow friction factors and heat transfer correlations of heat transfer fluids (HTFs) in the PPHE across laminar to turbulent flow, considering different channel heights and spot longitudinal distances.

## 2.3 Experimental work on PPHE

In the literature, PPHEs are often called thermo-plates, pillow-plates, embossed plate heat exchangers, and welded plate heat exchangers. However, it should be noted that a PPHE is not always meant when the term "thermo-plate" is used [7,49]. One of the pioneering work on PPHE is by Mitrovic and Peterson [7] published in 2007. In this work, the authors investigated the influence of geometric parameters on forced convection in the three-dimensional configuration of PPHE. They also visualized the flow and heat transfer characteristics inside a typical PPHE and determined the  $Nu$  (Nusselt number) and  $f$  (Friction factor) for  $50 \leq Re \leq 4000$ . It was noted that the recirculation developed behind the circular welding spot and the size and shape of recirculation zone change with  $Re$ . They also observed that this recirculation zone adds extra pressure drop and does not contribute much to the heat transfer. The combined effect of the welding spot and recirculation zone is the formed meandering zone core flow, which serves the purpose of heat transfer inside the channel.

In 2007, Mitrovic and Peterson [7] were the first to experimentally studied the single-phase based on forced convective flow in the three-dimensional geometrical configuration of the Pillow plate surface using mathematical modelling. They showed that the recirculation zone increases with the Reynolds number, and thermo-plate provided better results than vertical or smooth tube and overall pressure drop increase across the thermo-plate channel. The experimental study conducted by Mitrovic and Peterson [49] focused on the performance of a thermoplate heat exchanger operating as a condenser. The study is divided into two sections, each addressing different aspects of the heat exchanger operation. In Section 1, the emphasis is on single-phase forced convection heat transfer and pressure drop in the thermoplate. Marlotherm oil and distilled water are used as working fluids. The findings revealed that the thermoplate demonstrated enhanced heat transfer compared to condensation on a vertical tube or plane plate. This improvement was attributed to the 3-D surface structure of the thermoplate. The study also investigated pressure drop in the thermoplate and observed that it decreased in the condensation channel due to phase change. However, the total pressure drop increased with higher vapour velocity. Correlation equations were developed based on experimental data to predict heat transfer and pressure drop for the cooling fluid and condensing vapour. In Section 2, the study investigated vapour condensation occurring in channels between neighbouring thermoplates. Saturated isopropanol vapour was utilized at pressures below

atmospheric pressure. The results indicated that the thermoplate's 3-D surface structure offered improved heat transfer during vapor condensation. Correlation expressions were proposed for the heat transfer and pressure drop of the inside (cooling) fluid and the outside condensation. These correlations aimed to provide a more reliable foundation for practical calculations. Essentially, these expressions include dimensionless quantities crucial for condensation kinetics. However, the study acknowledged that the reliable application of these correlations is constrained to the specific parameter ranges covered by the experiments. Overall, the study contributes valuable insights into the performance of the thermoplate heat exchanger, offering correlations that can be applied within the defined experimental conditions for practical calculations related to heat transfer and pressure drop in condensation processes.

Mitrovic and Maletic [8] conducted a numerical investigation to comprehend the flow of single-phase fluids and heat transfer in channels of thermo-plates. Their goal is to improve understanding and optimize the geometry of thermo-plate channels. The outcome of their study is the development of a general correlation between heat transfer and pressure drop. In [50], Arsenyeva and colleagues conducted experiments on Plate Heat Exchangers (PPHE), focusing on fluid flow resistance and heat transfer. They suggested correlations for predicting the friction factor and heat transfer in PPHEs. They observed deviations of around  $\pm 10\%$  in fully developed turbulent flows within the specified Reynolds number range. However, they noticed deviations of approximately 20% lower friction at high Reynolds numbers and different temperatures.

Tran et al. [1] conducted a detailed investigation into the manufacturing process, basic design, and geometric application of pillow-plate heat exchangers. Their paper encompasses complex plate geometry, including calculating internal and external heat transfer surface areas, cross-sectional areas, and characteristic lengths. The study highlighted the significance of welding spot diameters, emphasizing the importance of keeping them as small as possible (8-12 mm) for significant mechanical stability during hydroforming and subsequent long-term usage. Additionally, smaller welding spot diameters enhanced the heat transfer rate and decreased pressure loss. The researchers introduced a categorization of pillow plates into staggered (longitudinal) grids or in-line (transversal) grids, akin to the tube layout of Shell and Tube heat exchangers. The experimental findings revealed that staggered grids exhibited excellent thermal efficiency due to the arrangement of welding spots, leading to intensified mixing of the liquid.

In 2015, to further investigate the effect of  $Re$  and  $Pr$ , Tran et al. [51] conducted experiments of single plane forced convection in the pillow plate channel. The channel height ( $h_i$ ) was measured at 3.4 mm, the transverse pitch ( $Y_L$ ) was measured at 72 mm, the longitudinal pitch ( $X_L$ ) was measured at 42 mm, and the spot-welding diameter ( $d_{cws}$ ) was measured at 10 mm. The studies' ranges were conducted at  $2 < Re < 80$  and  $300 < Re < 10,000$ . With a lower  $Re$ , the increase in heat transmission overcomes the rise in pressure drop. Numerical simulations were also used to obtain the flow field and temperature profiles.

In another study by Tran et al. [28], the investigation focuses on the two innovative operational modes of a pillow-plate heat exchanger (PPHE). These modes involve two phases: process medium condensation between neighbouring pillow plates and medium cooling evaporation in the plates. The researchers set up an experiment to evaluate several theories on analyzing natural circulation and forced convection evaporation (thermo-siphon). To simulate the (virtual) enthalpy of condensation, an electric current was conducted through the walls of a single pillow plate. This approach allowed for the reproduction of the enthalpy of condensation in a controlled experimental environment. The study aimed to determine the optimal methods for studying forced convection evaporation and natural circulation evaporation (thermo-siphon) in PPHEs. The experimental setup and simulations were designed to provide insights into the intricate processes involved in these operational modes.

In [52], Piper et al. conducted an experimental investigation concentrating on the flow characteristics of a descending liquid film over a distinct three-dimensional surface represented by a vertical pillow plate. The research revealed new insights, highlighting a unique two-zone film pattern. Notably, the observations showed a tendency for the liquid film to descend along the rows of vertically aligned welding spots, leading to a faster and thicker film in this specific region (zone 1). In contrast, the region between these zones displayed a thinner, slower-moving film (zone 2). The pillow-plate surface played a stabilizing role in maintaining this two-zone distribution, achieving stability across all tested irrigation densities. However, the extent of separation, particularly the ratio of film Reynolds numbers between zone 1 and zone 2, showed variability with irrigation density, reaching a maximum and then decreasing. Further exploration is necessary to fully understand these phenomena. Additionally, the study highlighted distinct features such as rapidly moving V-shaped waves observed exclusively in zone 1 and quasi-two-dimensional slowly moving wavefronts in zone 2. The latter originated from strong



interference between two adjacent V-shaped waves in zone 1. These V-shaped surface waves were wide enough to partially cover zone 2, causing liquid displacement alternately over zone 2 into an adjacent zone 1, preventing drying out after a certain length. The study recognized the need to investigate different geometries to determine whether this effect and the two-zone pattern occur in configurations with larger dimensions, especially larger  $Y_L$ .

Guo et al. [15] conducted an experimental investigation to assess the leakage failure of a pillow-plate heat exchanger after 80,000 hours of operation. The study identified a crack at the edge joints of corrugated 316L steel plates using dye permeability detection. The investigation thoroughly examined the failure of welding joints through optical microscopy, scanning electron microscopy (SEM), electron backscatter diffraction (EBSD), and X-ray diffraction (XRD). Corrosion products were exclusively observed on the inside of the edge joints. The morphology of the mud pattern and analysis using energy-dispersive X-ray spectroscopy (EDS) revealed a stress corrosion cracking mechanism, primarily attributed to a high chloride ion concentration (2.87 wt.%) on the fracture surface. The study found that chloride and hydrogen ions accumulated through an occluded cell mechanism in the narrow gap between plates. Additionally, carbide precipitation on the grain boundary of the heat-affected zone during the welding process was identified as a factor initiating cracking under crevice corrosion conditions. Based on these findings, recommendations were made for structural modification welding without a narrow gap, considering using duplex or finite stainless steel as alternatives to replace 316L stainless steel. The study also suggested implementing periodic inspections and stringent deionization of cooling water as preventive measures to mitigate such failures.

In [12], Geodecke et al. conducted experiments to evaluate the effectiveness of pillow-plate thermosiphon and tubular-type boilers using water and a water-glycerol mixture. The study employed the pillow plate apparatus E1, which included two single-embossed and one double-embossed pillow plate, with dimensions of  $800 \times 1.5 \times 220$  mm (height  $\times$  plate wall thickness  $\times$  width) and an overall heat transfer area ( $A$ ) of  $0.704 \text{ m}^2$ . The hydraulic diameter of a single duct between two pillow plates was 17.5 mm, decreasing to 8.5 mm inside a pillow plate. The overall cross-sectional area between the pillow plates was  $A_C = 3.85 \times 10^{-3} \text{ m}^2$ . The experiment covered a temperature difference range of  $5 \text{ K} \leq \Delta T_{OV} \leq 20 \text{ K}$ . The results indicated an increase in the heat transfer coefficient and a decrease in total pressure.

Selvnes and colleagues [53] conducted an experimental assessment of a cold thermal storage unit utilizing a pillow-plate heat exchanger design. The study focused on the design's evolution and the performance evaluation for a plates-in-tank Cold Thermal Energy Storage (CTES) unit designed to integrate into pump-circulated CO<sub>2</sub> industrial refrigeration systems. The CTES unit comprised a stainless-steel container filled with water as the latent storage medium and a pillow-plate heat exchanger facilitating heat transfer with the refrigerant (CO<sub>2</sub>). The research demonstrated the practicality of directly integrating a latent CTES unit into the main refrigerant circuit to manage peak loads in refrigeration. The findings highlighted the significant influence of refrigerant evaporation and condensation temperatures on the performance of the charging and discharging cycles. The unit exhibited an average discharge rate of 7.90 kW during a 4.5-hour discharge cycle, with a calculated maximum discharged energy of 35.29 kWh.

Lin et al. [45] experimented on an innovative latent thermal energy storage system. The newly devised energy storage unit incorporates a pillow-plate heat exchanger with multiple flowing channels, utilizing sodium acetate trihydrate (SAT) as the energy storage phase change material (PCM). Water is the working fluid circulating through the distributed channels inside the plates to charge or discharge the system. The assessment of the thermal performance of this latent heat thermal energy storage system considered parameters such as the outlet temperature of water, thermal power, energy, effectiveness, and heat transfer coefficient. The experimental outcomes revealed that the system could release up to 6.3 MJ of energy with an average power of 4 kW. The overall heat transfer coefficient and heat transfer area varied from approximately 25 to 70 W/k for flow rates between 100 and 500 L/h. The researchers concluded that the pillow-plate heat exchanger demonstrated outstanding thermal performance, delivering a high heat transfer rate within a compact structure. The innovative design with multiple flowing channels enhances flexibility and adaptability for practical applications. It holds promise for applications such as solar water energy storage, heat pump water heater systems, and waste heat recovery systems.

In [10], Arsenyeva et al. conducted an experimental investigation on a small-scale pillow plate heat exchanger, using water as the working fluid. The study details the heat transfer and hydraulic resistance within and between two channels. Additionally, numerical simulations were carried out for the single-phase fluid outside the channel to understand the local heat transfer behaviour and shear stress over the surface of the pillow plate channel. The observed deviation between the experimental and numerical results was

17%. Moreover, it was observed that the surface area of the Pillow-plate heat exchanger was 30% less than that of the Chevron plate heat exchanger.

Lin et al. [45] experimented on an innovative latent thermal energy storage system that utilized a pillow-plate heat exchanger with multiple flowing channels. The system utilized sodium acetate trihydrate (SAT) as the phase change material (PCM) and water as the working fluid. Parameters evaluated for thermal performance included the outlet temperature of water, thermal power, energy, effectiveness, and heat transfer coefficient. The findings revealed that the system could release up to 6.3 MJ of energy with an average power of 4 kW. The pillow-plate heat exchanger demonstrated exceptional thermal performance, providing a high heat transfer rate within a compact structure. It is suitable for applications such as solar water energy storage, heat pump water heaters, and waste heat recovery systems.

Arsenyeva et al. [10] performed an experimental study on a small-scale pillow-plate heat exchanger using water as the working fluid. The investigation analyzed heat transfer and hydraulic resistance within and between two channels. Furthermore, numerical simulations were conducted to understand local heat transfer and shear stress over the surface of the pillow plate channel. The results demonstrated a 17% deviation between the experimental and numerical data. Additionally, it was noted that the surface area of the pillow-plate heat exchanger was 30% less than that of a Chevron plate heat exchanger. In another work, Arsenyeva et al. [54] conducted an experimental investigation to explore the heat transfer between air and water in a small-scale pillow-plate heat exchanger (PPHE) composed of two assembled pillow plates within a single unit. The experimental configuration involved the circulation of cooling water in two inner channels (inside welded pillow plates), while air was directed to the outer channel between the plates. The primary objective of the research was to analyze heat transfer and hydraulic resistance in both the inner and outer PPHE channels based on experimental data. Correlations for pressure loss and heat transfer coefficients in both inner and outer channels were established using the collected measurements. To further investigate pressure loss and wall shear stress in the outer channel between pillow plates, Computational Fluid Dynamics (CFD) simulations were employed, ensuring a Reynolds number of 5,173 for fully developed turbulent flow. The derived correlations from experimental data were compared with results from numerical simulations, offering dependable predictions for the thermal and hydraulic performance of small-scale PPHEs. The experimental data for the small-scale PPHE were compared with CFD simulations, and correlations for friction factor and

heat transfer in the PPHE's outer channel were developed, demonstrating deviations from experimental results within  $\pm 10\%$ . These correlations were deemed reliable for Reynolds numbers ranging from 3000 to 20000. The CFD simulations, conducted for a Reynolds number of 5,173 corresponding to fully developed turbulent flow in the outer PPHE channels, exhibited satisfactory agreement with experimental values, with deviations in the heat transfer coefficient not exceeding 15%. Additionally, the CFD simulations enabled the prediction of the shear stress distribution on the surface of the pillow plates.

In 2018, Scholl [55] investigated the potential application of Pillow-plate heat exchangers in falling film or thermosiphon reboilers. The experimental approach utilized the density difference between the single-phase liquid feed and the two-phase vapor/liquid mixture in the reboilers. The results suggested that Pillow-plate heat exchangers could serve as a notable alternative in falling film evaporators and reboilers, particularly when compared to Shell and Tube equipment, under specific operating conditions with a pressure difference of  $\Delta p = 100$  mbar and a minimum temperature difference of  $\Delta T_{ov,min} = 4$  K.

Siebeneck et al. [56] conducted an experimental exploration involving the isothermal flow of deionized water mixed with a fluorescent dye, analyzing flat and pillow plates. The findings indicated that, under identical film Reynolds numbers, the film thickness was notably greater on pillow plates, and this distinction was amplified with higher film Reynolds numbers. The increased film thickness on pillow plates was ascribed to the deceleration of flow over the pillow surfaces, leading to an elevated film thickness. The authors formulated a correlation for the mean film thickness over pillow plates, expressed as:

$$\delta_f = 0.573 \left( \frac{v_f^2}{g} \right) Re_f^{0.5175} \quad 0 \leq Re_f \leq 620 \quad (2.3)$$

$\delta_f$  = Film thickness [mm],  $v_f$  = kinematic viscosity [ $\text{m}^2\text{s}^{-1}$ ],  $g$  = gravity acceleration [ $\text{ms}^{-2}$ ],  $Re_f$  = Reynolds number [-]

Distinct flow patterns were observed over pillow plates, characterized by a V-shaped pattern towards each weld spot and an inverse V-shaped pattern after the weld spot (over the inflation). Piper et al. [52] reported similar observations, categorizing the flow into Zone 1 featuring a faster, thicker film along the longitudinally aligned weld spots, and Zone 2 encompassing the remaining space with reduced speed and thickness.

Vocciante et al. [17] show a comprehensive overview of pillow-plate heat exchangers (PPHEs), highlighting their structural distinctions from other heat exchangers (HEs), unique features, flow arrangements, and potential applications. The authors explore limitations and recent advancements while outlining prospects, including strategies for enhancing equipment performance. PPHEs amalgamate advantages from commonly used conventional heat exchanger types, showcasing pressure and temperature resistance like shell-and-tube heat exchangers and the cost-effectiveness and compactness characteristic of plate heat exchangers. Significantly, PPHEs possess peculiarities that enable a reduction in heat transfer surface area compared to other plate heat exchangers under similar conditions, providing additional benefits for process sustainability. However, the design and optimization of PPHEs necessitate reliable estimates of overall heat transfer coefficients and friction factors. The available literature currently offers such information for only a limited number of pillow-plate panels, underscoring the imperative for further investigation into PPHEs.

In a recent investigation conducted by Wang et al. [57] in 2023, a two-layer multi-objective optimization approach was employed to examine the heat transfer rate and flow characteristics of a convex plate heat exchanger. The primary goals were to maximize the performance evaluation criterion (PEC) and the field synergy number (Fe). The study encompassed both experimental and numerical analyses. The optimization results underwent a comprehensive analysis, including single-factor analysis, response surface analysis, and sensitivity analysis. Across various objective functions, the study determined the optimal structural parameters as follows: a welding hole radius (R) of 5.81 mm, an ellipse radius (L) of 5.02 mm, and a welding hole spacing (P) of 64.00 mm. Comparative analysis with the pre-optimized structure revealed substantial enhancements. The size-optimized structure demonstrated a reduced temperature difference between the inlet and outflow of the cooling water by less than 8.27%. Additionally, there was a noteworthy increase in heat transfer performance by 20.43%. The overall improvement ranged from 2.3% to 19.59%. These findings underscore the effectiveness of the two-layer multi-objective optimization in improving the structural parameters of convex plate heat exchangers, resulting in enhanced heat transfer performance.

Djakow and collaborators [16] introduced a pioneering method for creating dimples on the surface of pillow plates. They utilized numerical simulations to understand the impact of the pillow-plate structure on heat transfer rates and fluid flow. Their results revealed a 24% increase in the convective heat transfer coefficient on a dimpled surface compared to

a plane-surface pillow plate channel in a Pillow-Plate Heat Exchanger (PPHE). The expectation was that the dimpled surface would significantly influence the thermal performance of the outer channel in comparison to the inner channel.

Sunderneier et al. [22] investigated the overall system behavior and high-speed flow characteristics within pillow plate channels. In their study, a pillow plate channel was positioned in the test section of a blow-down wind tunnel operating with dry air. The ensuing gas dynamics were analyzed using both conventional and focusing schlieren optics, in addition to static and total pressure measurements. The qualitative findings of this study demonstrated a robust agreement with theoretical predictions for compressible flow through pillow plate channels. The researchers concluded that the compressible flow within pillow-plate heat exchangers can be interpreted as a form of Fanno-Rayleigh flow. This interpretation implies the necessity to consider choking behavior at the end of the channel, influencing the exit conditions of the turbomachine. Despite the relatively low pressure drop due to friction in the pillow plate channel, the study anticipated high convective heat transfer coefficients attributed to substantial mixing and vortex structures. These observed flow phenomena were noted to be rather similar to incompressible flow.

While edge welding joints are commonly used for the main structure of PPHEs due to their cost-effectiveness, the study highlighted potential issues such as warping and cracking under specific conditions, resulting in premature welding failure and fluid leakage. The causes for such problems were attributed to stress concentration positions or misalignment of plates during installations. Another probable cause discussed was chemical attack by specific ions, to which the constituent material of heat exchangers (HE) is susceptible [58]. In the specific case of PPHEs manufacturing, the study noted the widespread use of AISI 316L austenitic stainless steel. This choice was based on its favorable characteristics, including good weldability and malleability, and corrosion resistance guaranteed by the high concentration of Ni and Cr in the alloy. However, it was also acknowledged that the austenitic alloy may be susceptible to environmental weaknesses in the presence of certain ions [59].

Subsequently, an experimental arrangement was established to investigate the effects of heat transfer fluid (HTF) inlet temperature, HTF mass flow rate, and phase distance on the charging and discharging performance of a Thermal Energy Storage (TES) unit within a CO<sub>2</sub> refrigeration system [20,60]. The observations revealed that a reduced plate distance was necessary to address short yet significant peaks in the system. Moreover, in contrast to the HTF mass flow rate, the HTF temperature had a more pronounced impact

on the average discharge rate of the phase change material (PCM), especially at greater plate distances. This underscored the potential use of HTF temperature to achieve a specific discharge rate tailored to meet the cooling load profile for a given application. Similar outcomes were reported when employing a commercial organic PCM with a phase change temperature of around  $-9^{\circ}\text{C}$  [23,60]. Additionally, it was determined that maintaining a temperature difference of approximately  $5^{\circ}\text{C}$  between the PCM phase change temperature and HTF charging temperature represented an optimal balance between heat transfer efficiency and energy consumption.

## 2.4 Optimization of PPHE

Tavallaei et al. [4] conducted a numerical study focusing on the thermo-hydraulic performance of pillow-plate heat exchangers (PPHE), considering various geometrical parameters and flow specifications. The study integrated fluid flow, heat transfer, and thermodynamics principles using the entropy generation minimization (EGM) approach. A comprehensive parametric analysis investigated the impact of dimensionless channel height, dimensionless plate width, number of pillow plates, Reynolds number, and Prandtl number on PPHE performance. A multi-objective optimization approach employing the non-dominated sorting genetic algorithm (NSGA-II) aimed to identify the optimal PPHE design. The study revealed a trade-off between thermal and frictional non-dimensional entropy generation, represented by the Pareto-optimal front. An optimum Reynolds number was identified to minimize total entropy generation for geometric parameters. The multi-objective optimization underscored a conflict between maximizing the performance evaluation criterion (PEC) and minimizing total entropy generation. The final optimum values for PEC and total entropy generation occurred at Reynolds number 3265, emphasizing the nuanced interplay of geometric and flow parameters in optimizing PPHE performance.

Yao et al. [61] conducted a numerical investigation to optimize Pillow-Plate Heat Exchangers (PPHE) by studying the correlation between the friction factor ( $f$ ), Nusselt number ( $Nu$ ), and the dimensionless number  $\Psi$ , defined as the ratio of weld spot length ( $D_L$ ) to weld spot width ( $D_W$ ). They explored three weld spot geometries: circular weld spots ( $\Psi = 1$ ), elliptical weld spots aligned with the flow ( $\Psi > 1$ ), and elliptical weld spots perpendicular to the flow ( $\Psi < 1$ ). The study examined both convex and concave elliptical weld spots. Their research examined the turbulent flow and heat transfer characteristics of

supercritical carbon dioxide within the PPHE channel. The findings indicated that the convex weld spot demonstrated higher flow velocity, lower flow fraction, and a greater heat transfer coefficient than the concave counterpart. Significantly, the study emphasized the enhanced thermal performance of the PPHE when contrasted with the Printed Circuit Heat Exchanger (PCHE) and Ultra Compact Plate Heat Exchanger (UCPHE). This superiority was attributed to the robust secondary flow effect generated by alternating weld spots, ultimately improving the overall efficiency of heat transfer.

Tong et al. [62] introduced a two-stage thermal-hydraulic optimization approach utilizing RZ parameterization. The initial stage involved the creation of a genetic particle swarm optimization algorithm, which combined genetic and particle swarm optimization techniques to maximize the thermal-hydraulic performance of the Pillow-plate heat exchanger. The subsequent stage aimed at refining the optimization objective to further enhance heat transfer characteristics based on the geometrical parameters of RZ. Assessment of the Computational Fluid Dynamics (CFD) model against experimental data demonstrated satisfactory agreement for hydraulic diameter, Nusselt coefficient, and pressure drop. Compared to the baseline design, the two-stage optimized PPHE exhibited a notable 29.3% improvement in average PEC over a Reynolds number range of approximately 4000 to 8000, simultaneously reducing the heat transfer area of RZ by an average of 25.3%. The outcomes underscored that a reduced welding spot pitch ratio fosters improved flow mixing between mainstream and stagnant fluid downstream of RZ. In contrast, smaller welding spots contribute significantly to enhanced turbulent energy dissipation, improving overall heat transfer.

In a series of investigations by Eldeeb et al. [63,64], the optimization of weld spot (WS) shapes was conducted using approximation-assisted optimization to achieve maximum thermo-hydraulic performance. The entire process, encompassing geometry generation, Computational Fluid Dynamics (CFD) analysis, metamodel development, and optimization, was automated, as depicted in Fig. 13a. The initial step involved a design of experiments based on Latin hypercube sampling, generating parameterized designs with WS shapes derived from fourth-order non-uniform rational B-splines. Following the CFD analysis, a metamodel was developed using the Kriging method with quadratic global mean and spherical correlation. Subsequently, optimization was carried out using a multi-objective genetic algorithm. The findings suggested that more streamlined and compact WS shapes led to lower pressure drops, attributed to the formation of smaller recirculation zones behind the WSs. As a result, optimal shapes were identified to be more streamlined,



with width-to-height ratio (WHR) values within the range of 1.6-2 (i.e., almond and eye-shaped, as illustrated in Fig. 13b). The optimization considered pitch ratio ( $s_{ratio}$ ) values ranging from 0.58 to 1.73, covering transversal to longitudinal pitch patterns, with optimal pitch ratio values falling within the range of 0.58-1.36. It's crucial to note that no optimal condition was found beyond a certain value ( $s_{ratio} = 1.36$ ). However, the manufacturability and structural stability of these optimum shapes require attention. It's important to emphasize that these studies focused on optimizing and investigating shapes solely based on inner container (IC) fluid flow and heat transfer, with the impact of WS shape on thermo-hydraulic behavior in the outer container (OC) yet to be explored.

In 2022, Kumar et al. [65] conducted a numerical investigation to assess the performance of a pillow-plate channel utilizing an artificial neural network (ANN) model. The training dataset for the ANN model encompassed four geometric parameters, Reynolds number, heat transfer coefficient, and specific pressure drop for each pillow-plate channel configuration. The ANN model underwent optimization to attain a configuration that minimized the mean square error. The resultant ANN demonstrated robust predictive capabilities, achieving R2 values of 0.987 and 0.9953 for the heat transfer coefficient and specific pressure drop, respectively. Employing the trained ANN model, the researchers derived values for the heat transfer coefficient and specific pressure drop across various pillow-plate channel configurations. The parameter range utilized during the training phase was retained for the performance analysis, with finer parameter increments applied in the prediction process. Subsequently, a numerically simulated random geometric configuration of the channel was utilized to validate the predictions of the ANN model. The findings indicated that the ANN model's predicted heat transfer coefficient and specific pressure drop deviated by less than 5% from the values obtained through the study.

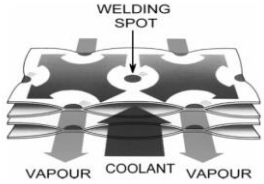
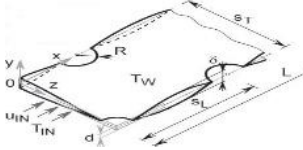
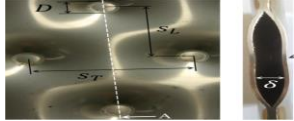
## **2.5 Heat transfer enhancement in PPHE**

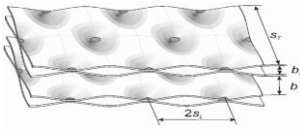
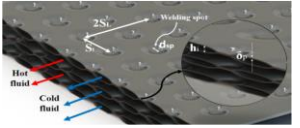
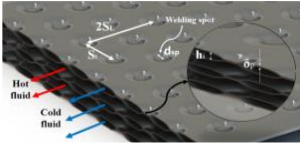
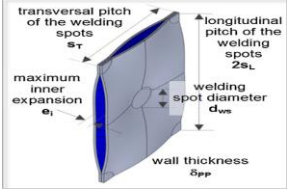
Piper et al. [66] performed a numerical computational fluid dynamics (CFD) simulation focused on the combined impact of a dimpled surface and a pillow plate. The simulation utilized STAR CCM+ based on the Finite Volume Method (FVM). The numerical results revealed that dimples led to a minor increase in recirculation regions, with reduced activity. Notably, the Nusselt number, representing convective heat transfer, exhibited a 2.2% increase, while the pressure drop decreased by 8.7% concurrently.

Kumar et al. [67] recently conducted a numerical investigation focusing on enhancing heat transfer within wavy pillow-plate channels utilized in pillow plate heat exchangers, using water as the cooling medium. They observed that the recirculation zone, particularly in the thermally developing region, significantly contributes to the overall heat transfer, primarily due to the lower average temperature of the hot recirculating zones. A parametric study was conducted by varying geometric parameters within the transversal and equal pitch pillow-plate configuration, specifically longitudinal and transverse pitches, maximum inner channel height, and welding spot diameter. Their results highlighted that the size of hot recirculating zones depends on flow development, with smaller zones observed in developing regions. Additionally, an increase in longitudinal pitch or a decrease in transverse pitch resulted in a rise in specific pressure drop within the channel. Notably, channels with a pitch ratio of 1 exhibited the lowest normalized thermo-hydraulic efficiency. The study identified "type E" geometry as having minimum thermo-hydraulic efficiency, where an increase in longitudinal and transverse pitch led to decreased heat transfer and pressure loss, albeit with a higher rate of decrease in pressure loss compared to heat transfer, thereby increasing thermo-hydraulic efficiency. Moreover, non-dimensional pillow plate channel height variations showed a trade-off between heat transfer rate and efficiency. The diameter of the weld spot exhibited a negligible effect on heat transfer but directly influenced pressure loss and thermo-hydraulic efficiency, decreasing with larger spot diameters. A power law correlation derived from numerical simulations predicted Nusselt numbers within  $\pm 10\%$  of simulated values, with sensitivity analysis revealing strong dependence of Nusselt number on Reynolds number and moderate to weak dependence on non-dimensional geometric parameters.

Table 2.1 provides an overview of the experimental and numerical studies conducted on Pillow-Plate Heat Exchangers (PPHE). This summary covers various flow regimes, including laminar and turbulent flows, the types of working fluids employed for different applications, the range of Reynolds numbers and velocities explored, as well as the parameters investigated. Additionally, the key findings from these experimental and numerical investigations are highlighted.

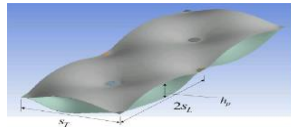
**Table. 2.1** Overview of experimental and numerical research on heat transfer enhancement in PPHEs [68].

Authors	Study	Design of PPHEs	$Re$ /working medium	Variable studied	Results/Remarks
Mitrovic et al. [7]	Experimental Laminar/ Turbulent.  Single-phase		$1,000 \leq Re \leq 8000$  Marlotherm oil, distilled water	<ul style="list-style-type: none"> <li>Examined the pressure resistance and transfer of heat</li> <li>Correlation developed for <math>Nu</math> and <math>f</math>.</li> </ul>	<ul style="list-style-type: none"> <li>Compared to vertical tubes or plain tubes, the thermo-plate produced significant results.</li> <li>Due to phase change, the pressure drop is reduced while the total pressure drop is enhanced with vapor velocity.</li> </ul>
Mitrovic et al. [8]	Computational  Single-phase		$50 \leq Re \leq 3,800$  Water	<ul style="list-style-type: none"> <li>Investigated the geometrical parameter.</li> <li>Correlation for heat transfer.</li> </ul>	<ul style="list-style-type: none"> <li>The enhancement of heat transfer is approximately 4.</li> <li>The recirculation zone affects the heat transfer and pressure drop.</li> </ul>
Piper et al. [13]	Computational Turbulent flow		$1,080 \leq Re \leq 8,680$  Water	<ul style="list-style-type: none"> <li>Investigated the thermal performance factor of elliptical and Circular welding spots.</li> </ul>	<ul style="list-style-type: none"> <li>EWS reduces heat transfer coefficient by 4% and pressure loss by 18% when compared to the CWS.</li> </ul>

Arsenyeva et al. [35]	Single phase Theoretical Single-phase		Water and crude oil	-	<ul style="list-style-type: none"> <li>• A new design approach for PPHX.</li> <li>• PPHX compared with CPHX.</li> </ul>	<ul style="list-style-type: none"> <li>• The heat transfer area of the PPHE should be less than that of the CPHX.</li> </ul>
Shirzad et al. [34]	Computational		Water $1,000 \leq Re \leq 8,000$	<ul style="list-style-type: none"> <li>• Geometrical Performance of PPHX and effect of <math>Re</math>.</li> </ul>	<ul style="list-style-type: none"> <li>• <math>Nu</math> and <math>Re</math> enhanced with channel height and reduced with a streamwise length, while <math>f</math> reduces with transverse distance.</li> </ul>	
Shirzad et al. [47]	Computational		Water $1,000 \leq Re \leq 8,000$ $Al_2O_3$ , $CuO$ , and $TiO_2$	<ul style="list-style-type: none"> <li>• Examined the heat transfer and pressure drop by increasing the nanofluid volume concentration by 2-5% in PPHX.</li> </ul>	<ul style="list-style-type: none"> <li>• Compared to other nanofluids, <math>Al_2O_3</math>-water and <math>TiO_2</math>-water with vol. con., 2% and 5% produced significantly greater results at lower and higher <math>Re</math>.</li> </ul>	
Tran et al. [51]	Computational / Experimental		Water $300 \leq Re \leq 10,000$	<ul style="list-style-type: none"> <li>• Investigation of the condensation performance of three different PPHXs.</li> <li>• Calculation of pressure</li> </ul>	<ul style="list-style-type: none"> <li>• PPHX provided more significant heat transfer results.</li> <li>• The correlations of <math>Nu</math> and <math>f</math> are in good agreement</li> </ul>	

Aute et al.  
[64]

Theoretical



Vel:  $1.6-2\text{ms}^{-1}$

Water

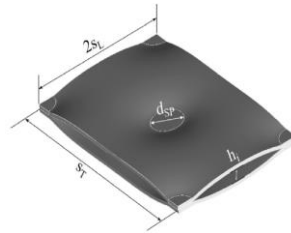
drop and convective heat transfer coefficient.

with experimental values.

- PPHX's thermal efficiency was examined using a circular weld and a non-uniform B-splines weld.
- Pressure drop is reduced by about 67% on the PPHX with innovative weld, and heat transfer is increased by up to 36%.

Kumar et al.  
[31]

Computational  
Turbulent/  
single-phase



$1200 \leq Re \leq 7800$

Water

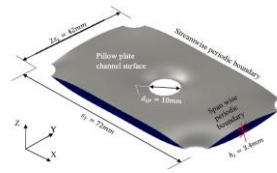
- Studied the spanwise and equal pitch configuration.
- Influence of geometrical factors on thermal performance.

• Thermal performance of "E-type" PPHX less efficient. In this case, pressure drop was decreased while longitudinal and transverse lengths increased heat transmission.

- CWS impacts the pressure drop and thermal efficiency but has no effect on heat transmission.

Kumar et al.  
[32]

Numerical  
Single-phase

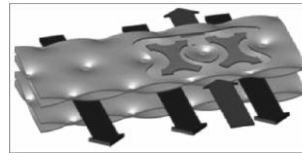


Water

- Studied the longitudinal and transverse configuration's heat transfer and flow characteristics using the Large eddy simulation method.
- The main factor enhancing heat transfer is the primary flow's high velocity.
- In longitudinal and transverse, spanwise Reynolds stress is higher than streamwise and wall-normal stress.

Scholl et al.  
[56]

Experimenta/  
Theoretical  
Single-phase



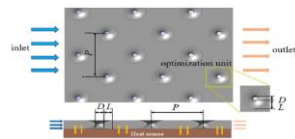
$400 \leq Re \leq 600$   
Deionized water  
fluorescing

- Examined the flow structure configuration and arrangement of the film thickness on the vertical PPHX.
- Pillow-plate channel developed more turbulence and significant heat and mass transfer.

- Mean film thickness dependent function of film  $Re$  for pillow-plate

Wang et al.  
[57]

Experimental  
Numerical  
Single-phase



Water flow rate  
= 400 L/h  
water

- Thermal performance evaluation and field synergy number.
- Thermal and overall performance is enhanced by 20.43% and 2.3~19.59%.

## 2.6 Summary of literature survey and Gaps in the literature

The numerical work on pillow-plate heat exchanger provides valuable insights into their thermal behavior and fluid dynamics. The findings can optimize design parameters for specific applications, improve energy efficiency, and guide the development of more advanced heat exchanger technologies. Future research may explore new materials and innovative plate designs and further enhance numerical models to better understand pillow plate heat exchangers and their applications in diverse industries.

- **Comparison with experimental data:** Numerical results are validated with experimental data obtained from real-world pillow plate heat exchangers. This ensures the accuracy and reliability of the numerical simulations.
- **Sensitivity Analysis:** sensitivity studies are conducted to understand how variations in parameters such as flow rates, temperatures, and plate geometries affect the performance of the heat exchanger.

The experimental studies collectively contribute valuable insights into the thermo-hydrodynamics, heat transfer, and operational considerations of PPHEs, shedding light on their efficiency, limitations, and potential areas for improvement. Experimental studies on pillow plate heat exchangers focus on optimizing their performance and understanding thermal characteristics. The unique pillow-like structure, formed through laser-welded plates, enhances heat transfer efficiency in industrial applications. Researchers conduct experiments investigating factors like fluid flow, heat transfer rates, and pressure drops by varying parameters such as plate thickness, welding patterns, and fluid properties. Temperature profile measurements across pillow plates help analyze heat distribution, facilitating design fine-tuning for specific applications. The goal is to ensure optimal thermal performance. Additionally, experiments explore the applicability of pillow plate heat exchangers in diverse industries like food processing and pharmaceuticals, validating their versatility and effectiveness under different operating conditions. Overall, the experimental work aims to make pillow plate heat exchangers more efficient and adaptable for various industrial settings.

The gaps in literature based on the presented literature survey are the following:

1. Existing numerical models have been reported in the literature. For their work, to optimize the pillow-plate heat exchanger by examining various heat transfer enhancement techniques, an economical computational model must be developed and validated for an extensive range of Reynolds numbers.
2. Entropy generation minimization/ energy distribution-based algorithms are increasingly popular in optimizing heat exchangers. However, such a detail around pillow-plate is missing in the literature.
3. Vortex generators have been used extensively for heat transfer enhancement in various heat exchangers. However, its application in pillow-plate heat exchangers has been explored less.

## **2.7 Needs of the work**

The increasing demands on companies for more efficient and adaptive heat exchange technology have led to a search for innovative solutions beyond traditional heat exchangers. Pillow plates (PP) have gained popularity due to their advantages, addressing limitations in size efficiency and maintenance associated with traditional counterparts. However, there is a lack of comprehensive knowledge and design experience in pillow plate thermo-hydraulic performance, prompting the development of commercial software tools to bridge this gap.

Current research on pillow plates is categorized into three main areas: geometrical analysis, fluid flow and heat transfer within pillow plates, and fluid flow and heat transfer between adjacent pillow plates. Thermo-hydraulic computations, including surface area, fluid hold-up volume, cross-sectional area, and hydraulic diameter, are crucial in determining pillow plate burst pressure. Finite Element Analysis (FEM) is a widely utilized method for accurately simulating the inflation process during manufacture and estimating burst pressures confidently.

Optimizing the flow arrangement within the pressure drop range is crucial for the efficient functioning of the pillow-plate heat exchanger. Seam welds and welding spot patterns direct fluid through the pillow plate, reducing dead zones and promoting optimal flow distribution. The three-dimensional pillow profile induces turbulent flows even at low Reynolds numbers, leading to higher internal heat transfer coefficients and increased overall heat transfer efficiency compared to tube-based alternatives.



Pillow plates offer sustainability benefits as they require less steel than tube-based alternatives, making them resource-efficient. Their flexibility in design surpasses solutions containing tubes or coils, particularly in applications where rigidity is a drawback. Despite these advantages, further research is needed to characterize liquid flow through pillow plates under external convection conditions such as natural, forced, or mixed convection. The performance of pillow plate heat exchangers for room heating purposes also requires accurate assessment, focusing on their potential applications in HVAC systems.

## **2.8 Thesis objectives**

The objectives of the study are as follows:

1. Based on the literature survey, we need to formulate a numerical model that can be used to validate the geometrical parameters of the pillow-plate heat exchangers.
2. This validated model is used to optimize the geometry of the pillow-plate heat exchanger for heat transfer enhancement for the specified operating conditions such as length, welding spot, and Reynolds number.
3. This numerical model is used to study the thermal performance enhancement of pillow-plate heat exchangers.

The final phase will involve the representation of suitable conclusions and recommendations based on the analysis, culminating in the completion and submission of the thesis.

In summary, this chapter addresses the challenge of fluid flow resistance and pressure loss associated with pillow plates, emphasizing the need for effective heat transfer enhancement methods. The study focuses on using pillow plate channels as a passive heat transfer augmentation technique, leveraging their wavy surface to promote lateral mixing and turbulence. The chapter concisely reviews heat transfer augmentation in Pillow-Plate Heat Exchangers (PPHEs) supported by experimental and numerical investigations.

The literature review highlights the direct dependence of the hot recirculating region on flow dynamics and recirculation zones. Additionally, the research indicates that the diameter of welded spots in PPHEs minimally impacts heat transfer but influences pressure drop. An increase in welding spot diameter is found to decrease the thermal performance of the channel.

Previous studies underscore the importance of an efficient channel height, showing a significant positive effect on thermal performance, particularly at lower Reynolds

numbers. Overall, the paper emphasizes the potential of pillow plate channels for passive heat transfer enrichment and underscores key factors influencing their thermal performance and pressure drop characteristics.

# Chapter - 3: PPHE Modelling and Verification

---

This chapter covers the geometry modeling of pillow-plate heat exchangers, numerical modeling, various meshing techniques and their selection, boundary conditions, solver settings, data reduction, validation procedures, and presentation of results.

## 3.1 Introduction

In this chapter, the focus shifts to the numerical modeling and geometric structure of pillow-plate heat exchangers (PPHE), a critical exploration building upon the introductory and historical insights presented in Chapters 1 and 2. Chapter 3 meticulously details the geometric intricacies inherent in PPHE, which are crucial for accurately representing and simulating heat transfer phenomena within these exchangers. A comprehensive understanding of the fundamental governing equations, encompassing continuity, momentum, and energy equations, is provided. These equations lay the theoretical groundwork for the numerical modeling approach, shaping the methodology employed in predicting and optimizing the performance of PPHE. The transition Shear Stress Transport  $k-\omega$  turbulence model is introduced within this numerical framework to capture the complexities of turbulent fluid flow. Furthermore, the chapter elucidates essential numerical methodology, different meshing types, including tetrahedral, hexahedral, and polyhedral, and its selection criteria and justification, boundary conditions, symmetry wall, and periodic boundaries, delineating the limits and constraints necessary for a precise simulation.

## 3.2 Geometry modelling (Solid geometry)

The production of the PPC involves a somewhat intricate process due to its unique single closed-unit design, featuring only one inlet-outlet section. To create the PP, the ends and sides of the plate's surface are sealed through seam welding, while the central section of the plates is spot-welded in a staggered pattern. Subsequently, the welded plates undergo an expansion process known as hydroforming, forming an internal fluid flow channel. It's important to note that the specific configurations of these SCWS notably influence the thermo-hydraulic performance of the PPHE.

The manufacturing process of pillow plates is relatively straightforward compared to other heat exchangers. After welding, the plates undergo a hydroforming process where

they are inflated with pressures typically ranging from 60 to 80 bar, significantly higher than the operating pressures. The channels formed through this process are hermetically separated and secured without gaskets. Typically, plates are manufactured with uniform thickness, causing both plates to deform and resulting in one-sided expansion during hydroforming. Various models can be obtained based on the thickness of the plates.

For PPHEs, maintaining structural integrity is crucial, especially because these heat exchangers operate under various thermal stresses and fluid pressures. The welding spots, plate thickness, and geometrical parameters all influence the mechanical strength, pressure-handling capacity, and overall efficiency of the system [35]. The thickness of the plates used in PPHEs is typically selected based on a balance between strength, thermal conductivity, and manufacturing feasibility. Thinner plates promote better heat transfer, but they must be thick enough to handle the mechanical stresses during operation. Typical plate thickness ranges from 0.5 mm to 2.0 mm for most applications [16] however, a thickness ranging from 0.6 mm to 1.0 mm is commonly used in industries where heat transfer efficiency is a priority and the pressures are moderate. However, thicker plates (up to 2.0 mm) are used for applications requiring higher pressure tolerance or in corrosive environments. The structural integrity of PPHEs largely depends on the strength of the welding spots that join the two plates together. These spots are the critical areas where mechanical stress is concentrated. PPHEs can typically withstand pressures ranging from 10 to 60 bar [11,14]. Spot welds need to be uniformly distributed to avoid stress concentration, and the weld diameter influences the pressure tolerance. Larger weld spots provide better resistance to pressure but may reduce heat transfer efficiency due to reduced flow area. Smaller pitches (distance between weld spots) enhance mechanical stability but reduce fluid flow and heat transfer.

Following the complete welding of the pillow-plate heat exchanger, the volume of the pressure chamber is defined through pneumatic cold deformation of the inner space under high pressure. This parameter, determined by engineers, complements the previously mentioned variables. The "press-on height," the maximum clear distance between both inner surface sides of the plate, defines the flow cross-sections in the pre-welded spot pattern and contributes to the distinctive visual surface design of a pillow-plate heat exchanger. Additionally, strain hardening during the pneumatic deformation process enhances the stability of the predominantly stainless-steel laser pillow plates.

Fig. 3.1 and Fig. 3.2 visually represent the three-dimensional periodic section of the Plate Heat Exchanger (PPC). Key geometric factors influencing the design of the Heat

Exchanger (HE) include the diameter of the welding spots ( $d_{cws}$ ), the longitudinal pitch ( $X_L$ ), the transverse pitch ( $Y_L$ ) of the welding spots, the internal channel height ( $h_i$ ), and the outer channel height ( $h_o$ ), as detailed in Fig. 3.2. The selection of these parameters is based on the operating conditions and the intended service of the PPHE to ensure cost efficiency. Standard PPHE dimensions range from 300 to 2000 mm in width, 700 to 8000 mm in length (or height), and weld spot diameters typically range from 8 to 12 mm. However, a higher number of weld spots per plate is recommended for applications involving high operating pressures. These variations in geometric design and flow patterns within the PPCs lead to the development of PPHEs with diverse structural characteristics. The design employs a three-dimensional wavy channel to enhance flow separation and mixing and intensify heat transfer.

The study classifies PP geometries into three configurations [21]:

1. Spanwise Configuration ( $s_r < 1$ ):  $Y_L$  is smaller than  $X_L$ , resulting in a rectangular arrangement with more excellent elongation in the streamwise direction.
2. Streamwise Configuration ( $s_r > 1$ ):  $X_L$  is more significant than  $Y_L$ , leading to a rectangular arrangement with more excellent elongation in the spanwise direction.
3. Equal-Length ( $s_r = 1$ ):  $X_L$  and  $Y_L$  are equal, resulting in a square-like arrangement.

$$s_r = \frac{X_L - d_{cws}}{Y_L - d_{cws}} \quad (3.1)$$

These configurations significantly impact the PPC's heat transfer and fluid flow characteristics, playing a crucial role in its design and performance optimization.

Fig. 3.1 and Fig. 3.2 illustrate the Pillow-plate heat exchanger's physical model and internal fluid flow. A simplified domain is employed for computational simulations, assuming uniform flow distribution inside the channel. Effects of potential maldistribution, arising from improper configuration and the complex geometry of the PPHE, are disregarded in this simulation.

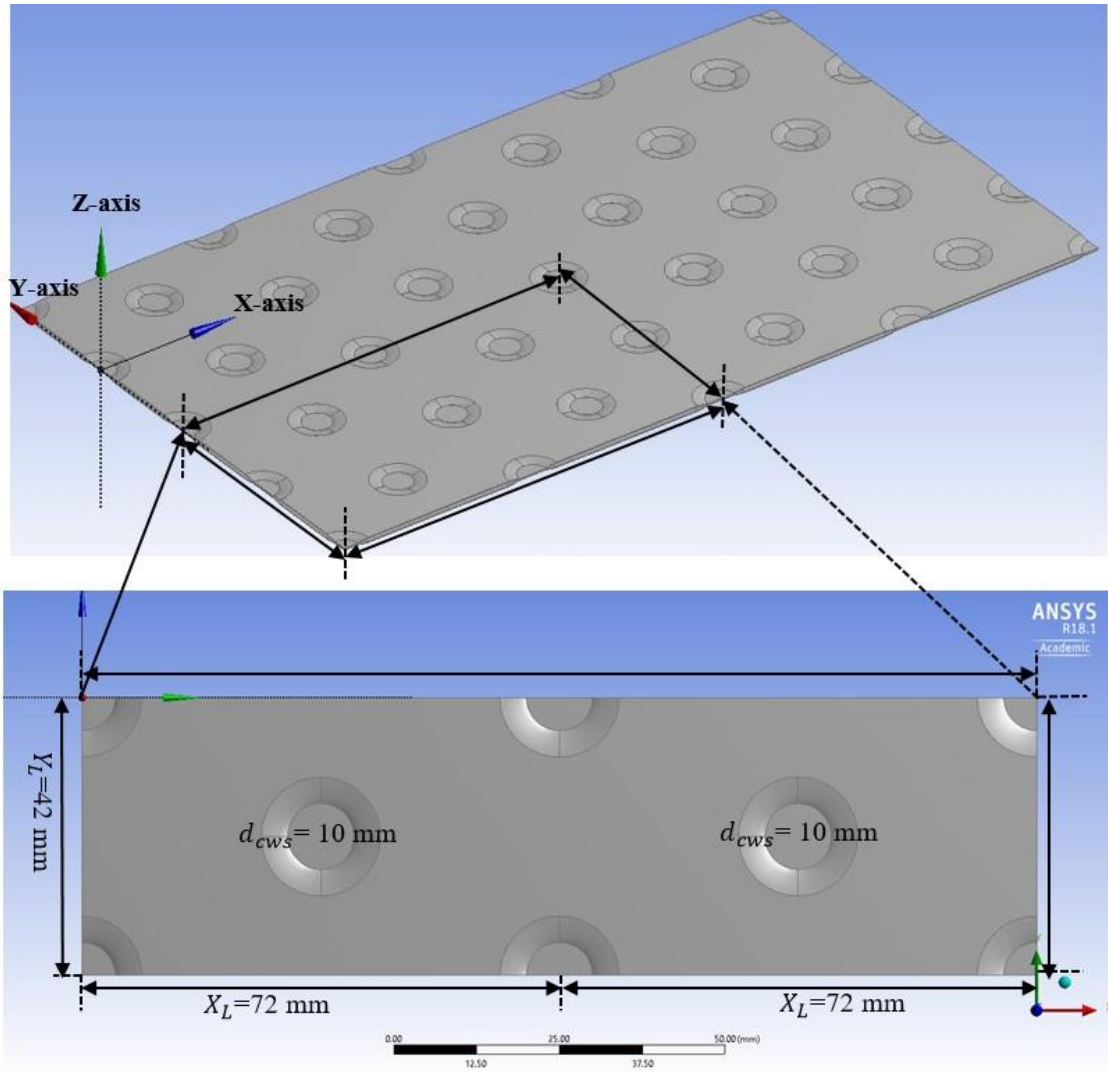


**Fig. 3.1** A schematic representation of the computational domain of a Pillow-Plate channel-type heat exchanger.

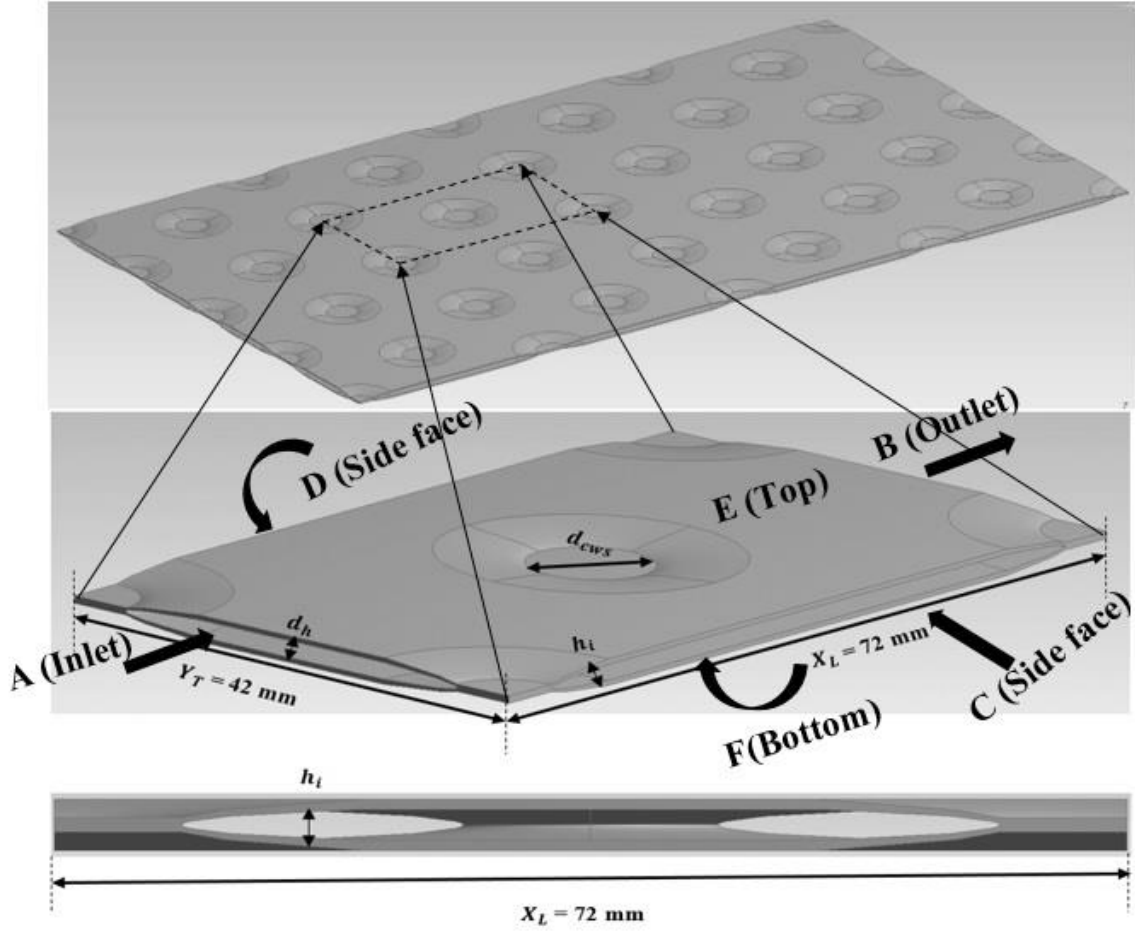


**Fig. 3.2** Schematic diagram of Pillow-Plate type heat exchanger channel.

### 3.3 Mathematical and numerical method

The governing equation is presented as follows [34]:

Continuity equation: which is signify the conservation of mass in fluid flow.

$$\nabla \cdot \vec{V} = 0 \quad (3.2)$$

Momentum equation states that the rate of change of momentum of a fluid element is equal to the net force acting on it. This equation helps describe fluid motion, where gravity and body forces are ignored.

$$\vec{V} \cdot \nabla \vec{V} = -\frac{1}{\rho} \nabla \bar{p} + \nu \nabla^2 \vec{V} - \frac{\partial}{\partial x_j} (\overline{u'_i u'_j}) \quad (3.3)$$

Energy equation: The energy equation describes the transfer and transformation of energy through a fluid flow, considering pressure, velocity, and internal energy changes. It

measures the balance of energy input, dissipation, and transfer, allowing for the investigation of heat transfer and fluid dynamics while generally ignoring gravitational and body forces.

$$\vec{V} \cdot \nabla \bar{T} = \alpha \nabla^2 \bar{T} - \frac{\partial}{\partial x_i} (\overline{u_i' T'}) \quad (3.4)$$

The transition SST (Shear-Stress Transport)  $k$ - $\omega$  (omega) model stands as a cornerstone in computational fluid dynamics (CFD) simulations, renowned for its ability to accurately capture turbulent flow phenomena across a wide array of flow conditions and geometries. Widely favored in software packages like ANSYS Fluent, its versatility and precision are owed to the unique amalgamation of two seminal turbulence models: the  $k$ - $\epsilon$  (epsilon) model, introduced by Launder and Spalding in 1974 [69], and the transition SST  $k$ - $\omega$  (omega) model, pioneered by Wilcox in 1998 [70].

At the heart of its efficacy lies the model's adeptness at addressing near-wall and free-stream turbulence characteristics. In regions proximal to solid boundaries, where viscosity and boundary layers exert significant influence, the model seamlessly integrates the  $k$ -epsilon formulation. This facet allows for the accurate resolution of boundary layer phenomena, including boundary layer separation and the transition to turbulence. Conversely, in the outer flow regions distant from solid boundaries where turbulence holds away, the model seamlessly transitions to the transition SST  $k$ - $\omega$  formulation. This strategic switching mechanism ensures the holistic representation of flow dynamics, effectively capturing the effects of turbulence generated by shear stresses and other turbulent sources.

One of the most distinguishing strengths of the transition SST  $k$ - $\omega$  model is its robustness in handling adverse pressure gradients. This attribute renders it particularly adept at simulating flows characterized by complex geometries, flow separation, and the formation of recirculation zones. Its robust performance in adverse pressure gradient scenarios is instrumental in achieving accurate predictions of flow behavior, even in challenging environments where flow separation and reattachment occur.



The turbulence model equations proposed by Menter [67] are outlined below.

Turbulence kinetic energy [71]:

$$u_j \frac{\partial(k)}{\partial x_j} = P_k - \beta_1 k \omega + \frac{\partial}{\partial x_j} \left[ (v + \sigma_k v_{turb}) \frac{\partial k}{\partial x_j} \right] \quad (3.5)$$

Specific dissipation rate:

$$u_j \frac{\partial(\omega)}{\partial x_j} = \alpha S^2 - \beta_2 \omega^2 + \frac{\partial}{\partial x_j} \left[ (v + \sigma_\omega v_{turb}) \frac{\partial \omega}{\partial x_j} \right] + 2(1 - F_1) \sigma_\omega \omega^2 \frac{1}{\omega} \frac{\partial k}{\partial x_i} \frac{\partial \omega}{\partial x_i} \quad (3.6)$$

Where,  $\sigma_k$  and  $\sigma_\omega$  are the turbulent Prandtl number for  $k$  and  $\omega$ , respectively.  $S$  is the strain rate.

The transport equation for the intermittency  $\gamma$  is defined as:

$$\frac{\partial(\rho U_j \gamma)}{\partial x_j} = P_{\gamma 1} - E_{\gamma 1} + P_{\gamma 2} - E_{\gamma 2} + \frac{\partial}{\partial x_j} \left[ \left( \mu + \frac{\mu_t}{\sigma_\gamma} \right) \frac{\partial \gamma}{\partial x_j} \right] \quad (3.7)$$

The transport equation for the transition momentum thickness Reynolds number  $\widetilde{Re}_{\theta t}$  is

$$\frac{\partial(\rho U_j \widetilde{Re}_{\theta t})}{\partial x_j} = P_{\theta t} + \frac{\partial}{\partial x_j} \left[ \sigma_{\theta t} \left( \mu + \frac{\mu_t}{\sigma_\gamma} \right) \frac{\partial \widetilde{Re}_{\theta t}}{\partial x_j} \right] \quad (3.8)$$

F1 (Blending Function):

$$F_1 = \tanh \left\{ \left\{ \min \left[ \max \left( \frac{\sqrt{k}}{\beta^* \omega \gamma}, \frac{500v}{\gamma^2 \omega} \right), \frac{4\sigma_\omega k}{CD_{k\omega} \gamma^2} \right] \right\} \right\} \quad (3.9)$$

$$CD_{k\omega} = \max \left( 2\rho \sigma_\omega^2 \frac{1}{\omega} \frac{\partial k}{\partial x_i} \frac{\partial \omega}{\partial x_i}, 10^{-10} \right) \quad (3.10)$$

F2 (Second blending Function):

$$F_2 = \tanh \left[ \left[ \max \left( \frac{2\sqrt{k}}{\beta^* \omega \gamma}, \frac{500v}{\gamma^2 \omega} \right) \right]^2 \right] \quad (3.11)$$

Kinematic eddy viscosity:

$$v_T = \frac{\alpha_1 k}{\max(\alpha_1 \omega, S F_2)} \quad (3.12)$$

Production limiter:

$$P_k = \min\left(\tau_{ij} \frac{\partial U_i}{\partial x_j}, 10\beta^* k\omega\right) \quad (3.13)$$

$$\Phi = \Phi_1 F_1 + \Phi_2 (1 - F_1) \quad (3.14)$$

Where  $\omega$ ,  $k$ ,  $S$ ,  $\beta$ ,  $\gamma$ ,  $F_1$ ,  $F_2$ ,  $v_T$ ,  $\Phi$  and  $P_k$  are represented by the specific dissipation, turbulent kinetic energy, the positive value of shear strain rate, the model constant, intermittency factor, first and second blending, kinetic viscosity, turbulent dissipation, and production term, respectively.

### 3.4 Meshing

Meshing methods, such as tetrahedral, hexahedral, and polyhedral meshes, each have their characteristics and significance in computational fluid dynamics (CFD) simulations using software like ANSYS Fluent. The comparison of these mesh types and their suitability for CFD simulations:

#### 3.4.1 Tetrahedral mesh

- Tetrahedral meshes consist of tetrahedral elements, which are simple to generate and adapt to complex geometries.
- They are versatile and well-suited for simulations involving irregular shapes and intricate geometries.
- Tetrahedral meshes are easy to generate and require less computational resources than other meshes.
- However, they may not accurately capture flow features in regions with high gradients or complex flow patterns, leading to numerical inaccuracies.

#### 3.4.2 Hexahedral mesh

- Hexahedral meshes are composed of hexahedral (or brick) elements, which provide better accuracy and stability for certain types of flow simulations.
- They are particularly advantageous for simulations involving regular geometries and structured flow domains.

- Hexahedral meshes often yield more accurate results with fewer elements than tetrahedral meshes, reducing computational cost.
- However, generating hexahedral meshes can be challenging for complex geometries and may require more manual intervention.

### 3.4.3 Polyhedral mesh

- Polyhedral meshes consist of polyhedral elements, combining the advantages of tetrahedral and hexahedral meshes.
- They offer improved accuracy compared to tetrahedral meshes in capturing flow features, especially in regions with complex flow patterns or high gradients.
- Polyhedral meshes can be more computationally efficient than hexahedral meshes, requiring fewer elements to achieve similar levels of accuracy.
- However, generating polyhedral meshes may involve more sophisticated meshing techniques and software capabilities compared to tetrahedral or hexahedral meshes.

In ANSYS Fluent, the optimal of mesh type depends on various factors such as the geometry of the problem, the desired level of accuracy, computational resources, and the specific flow phenomena being simulated. Polyhedral meshes are often preferred for many cases involving complex geometries and turbulent flows due to their ability to provide accurate results with reasonable computational cost. However, hexahedral meshes may be more suitable for simpler geometries or cases where structured grids are advantageous. Tetrahedral meshes are still commonly used for their simplicity and versatility, especially in cases where computational resources are limited or when dealing with highly irregular geometries. Ultimately, selecting the most appropriate mesh type involves a trade-off between accuracy, computational cost, and ease of mesh generation.

### 3.4.4 Justification for selecting tetrahedral mesh

In ANSYS Fluent, the selection between tetrahedral, hexahedral, and polyhedral mesh depends on factors such as geometry complexity, simulation accuracy, computational resources, and solver capabilities. The justification of why tetrahedral mesh might be preferred over hexahedral and polyhedral meshes in certain scenarios:

- **Flexibility and Adaptability:** Tetrahedral meshes are highly flexible and can conform well to complex geometries like PPHE with irregular shapes, holes, and

sharp features. This adaptability is especially beneficial when dealing with intricate geometries where creating a structured hexahedral mesh might be challenging or impractical.

- **Ease of Generation:** Tetrahedral meshes are generally easier and quicker to generate than hexahedral meshes, especially for complex geometries. This can save significant pre-processing time, particularly when dealing with difficult CAD models to mesh with structured elements.
- **Better Capture of Geometry Details:** Tetrahedral elements provide better resolution and capture more intricate geometry details, particularly around curved surfaces and sharp corners. This can lead to more accurate simulation results where capturing boundary layer effects, flow separation, or complex fluid dynamics phenomena is crucial.
- **Adaptive Mesh Refinement:** Tetrahedral meshes are well-suited for adaptive mesh refinement techniques, where the mesh density is dynamically adjusted based on solution gradients or specific regions of interest. This adaptively allows for better resolution in critical areas while maintaining a coarser mesh in less significant regions, optimizing computational resources and simulation accuracy.
- **Compatibility with Certain Solver Features:** Some solver features in ANSYS Fluent, such as certain turbulence models or specific boundary conditions, may work more efficiently or accurately with tetrahedral meshes. Therefore, using tetrahedral elements might be advantageous when employing these features in simulations.
- **Parallel Processing Efficiency:** In certain cases, tetrahedral meshes can offer better parallel processing efficiency than hexahedral meshes, especially for large-scale simulations involving distributed computing resources. This can result in faster solution convergence and reduced computational time for simulations.

While tetrahedral meshes offer several advantages, it's important to note that the mesh type selection should always be based on the specific requirements of the simulation problem, including accuracy, computational resources, solver capabilities, and user expertise in meshing techniques. Sometimes, hexahedral or polyhedral meshes may be more suitable depending on the application and simulation objectives.

### 3.5 Boundary conditions

Due to the symmetry of the Pillow-plate Heat Exchanger (PPHE) geometry around the horizontal cutting-edge planes, a symmetry boundary condition is applied to these planes as L1, L2, R1, and R2 (here “L” and “R” is represented as left and Right side of Pillow-plate channel) as shown in Fig. 3.3, implying zero flux for all scalar and vector quantities across them. For the staggered circular welded spot patterns (SCWSP) arranged in a regular array, focus is confined to the region between these planes. Utilizing the repetitive geometry, the symmetry boundaries significantly reduce the computational domain while preserving essential components such as the pillow-plate channel wall, circular welding spot, and internal channel area.

The working medium utilized is normal water, with a density of  $997.2 \text{ kg/m}^3$ , a viscosity of  $0.89 \times 10^{-5} \text{ kg/m}\cdot\text{s}$  at standard atmospheric pressure, and a temperature of  $298.15 \text{ K}$  (all the physical properties of water is mentioned in Table 3.1). The inlet surface is assigned a uniform velocity profile with a magnitude of  $0.1875 \text{ m/s}$  and  $0.242 \text{ m/s}$  in the normal direction of the face, corresponding to a Reynolds number ( $Re$ ) of  $1,000$  and  $1,200$ . The pressure outflow boundary condition is applied at the outlet plane. The temperature at the pillow-plate channel wall is maintained at  $323.15 \text{ K}$ . Conjugate heat transfer is facilitated by coupling the fluid and walls to closely resemble actual flow conditions. The no-slip condition is imposed at the pillow-plate channel walls.

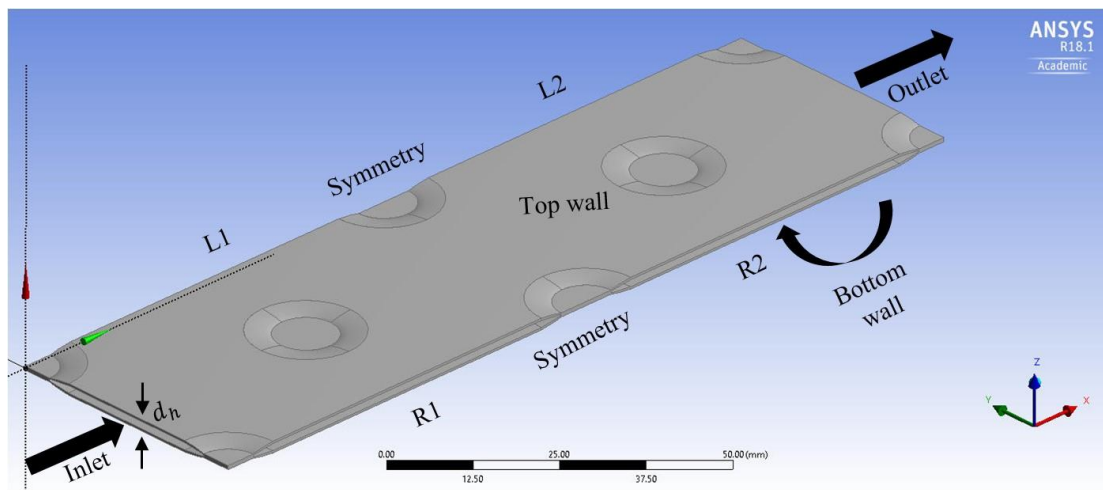


**Fig. 3.3** A schematic diagram of a pillow plate channel with SCWSP, and boundary conditions.

**Table. 3.1** Physical properties of water as working fluid and value used for simulations.

Parameters (units)	Values
Temperature (K)	298.15
Pressure (bar)	1.0132
Density (kg/m <sup>3</sup> )	997.2
Volume (m <sup>3</sup> /kg)	0.001
Internal Energy (kJ/kg)	104.86
Enthalpy (kJ/kg)	104.86
Entropy (J/g*K)	0.36734
C <sub>v</sub> (J/g*K)	4.1375
C <sub>p</sub> (J/g*K)	4.1813
Viscosity (Pa*s)	0.00089
Therm. Cond. (W/m*K)	0.60653
Phase	liquid

### 3.6 Numerical methodology

In ANSYS Fluent, the SIMPLE [72] (Semi-Implicit Method for Pressure-Linked Equations) and SIMPLEC [73] (Semi-Implicit Method for Pressure-Linked Equations-Consistent) algorithms are fundamental approaches for solving the pressure-velocity coupling in computational fluid dynamics (CFD) simulations. On the other hand, the QUICK [70] (Quadratic Upstream Interpolation for Convective Kinematics) scheme is a convection scheme used for discretizing convective terms in the governing equations. The explanation of each, along with their differences and justifications for their usage:

#### 3.6.1 SIMPLE scheme

- The SIMPLE algorithm is a classical and widely used pressure-correction method in CFD simulations.
- It iteratively solves the Navier-Stokes equations by decoupling the pressure and velocity fields, making it computationally efficient.
- In each iteration, the momentum equations are solved implicitly, while the pressure equation is solved explicitly.
- The pressure equation is typically solved using a pressure-correction method such as the SIMPLE algorithm to ensure mass conservation.

- However, decoupling pressure and velocity may lead to numerical oscillations or instability, particularly in highly transient or turbulent flows.

### 3.6.2 SIMPLEC scheme

- The SIMPLEC algorithm is an extension of the SIMPLE scheme (algorithm), providing consistent coupling between pressure and velocity fields.
- It addresses some of the limitations of the SIMPLE scheme algorithm by implicitly solving both momentum and pressure equations in each iteration.
- This consistent treatment of pressure-velocity coupling enhances stability and convergence properties, especially for challenging flow conditions.
- While computationally more expensive than SIMPLE, SIMPLEC offers improved accuracy and robustness, making it suitable for turbulent or highly transient flows.

### 3.6.3 Justification for usage:

- **SIMPLE vs. SIMPLEC:** The selection between SIMPLE and SIMPLEC depends on the flow characteristics and computational requirements. SIMPLE is suitable for steady or mildly transient flows where computational efficiency is crucial. On the other hand, SIMPLEC is preferred for turbulent or highly transient flows where stability and accuracy are paramount. SIMPLEC's consistent coupling between pressure and velocity fields enhances convergence and robustness, justifying its usage in challenging flow conditions.

## 3.7 Solver setting

The analysis of fluid flow and heat transfer characteristics incorporates the following key assumptions:

1. **Flow Characteristics:** The flow is assumed to be three-dimensional (3-D), incompressible, turbulent, and steady.
2. **Gravity and Body Force:** The influence of gravity and other body forces is considered negligible in the analysis.
3. **Thermo-physical Properties:** Thermo-physical properties, except viscosity, are treated as constants throughout the simulation (refer to Table 3.1).

4. **Channel Wall Characteristics:** The channel wall is assumed to be hydrodynamically smooth, focusing the study on the effects of various structural parameters.
5. **Phase Model:** A single-phase model is employed for the simulation, simplifying the analysis to a single fluid phase.
6. **Viscous Dissipation:** Viscous dissipation effects are neglected in the analysis, streamlining the focus on key heat transfer and fluid flow characteristics.

These assumptions provide a foundational framework for the analysis, allowing for a targeted exploration of the specific fluid flow and heat transfer aspects under consideration.

The study employed ANSYS Fluent, a commercial finite-volume solver, to solve Navier-Stokes and energy equations with second-order spatial accuracy. Momentum equations were solved implicitly using an estimated pressure field, and a pressure-velocity correction via the SIMPLE and SIMPLER algorithm ensured a divergence-free velocity field. Using Menter's [69,70] transition SST  $k-\omega$  4-equation turbulence model, CFD simulations predicted thermo-fluid performance in Pillow-plate heat exchangers (PPHEs). FLUENT 18.1, unstructured tetrahedral meshing, the SIMPLE and SIMPLER algorithm were utilized, and the convergence criteria were set for residuals. The transition model included additional equations for intermittency and laminar-turbulent transition. Mesh refinement focused on the circular welding spot. Under relaxation factors facilitated convergence. The study considered the complexity of the computational domain and achieved convergence when residuals fell below-specified thresholds. Velocity and pressure were coupled using the SIMPLE and SIMPLER algorithm with under relaxation factors (0.3 for pressure, 0.7 for momentum, and 0.9 for energy) facilitating convergence, declared when residuals fell below  $10^{-5}$  for all variables except the energy equation, where a threshold of  $10^{-5}$  was set. Although flow variables reach a quasi-steady state of around 1500 iterations, simulations are performed over 5000 to ensure comprehensive analysis.

### 3.8 Data reduction

$$\text{Convective heat transfer coefficient, [66]} \quad h_{conv} = (\dot{q}_m / T_w - T_m) \quad (3.15)$$

Where,  $T_m \approx T_{in}$



$$\text{Nusselt number, [66]} \quad Nu = h_{conv} d_h / k \quad (3.16)$$

$$\text{Friction factor, [66]} \quad f = 2d_h \Delta p / \rho X_L v_m^2 \quad (3.17)$$

$$\text{Reynolds number, [66]} \quad Re = \rho v_m d_h / \mu \quad (3.18)$$

$$\text{The drag coefficient, [74]} \quad C_x = F_d / 0.5 \rho v_m^2 d_h \quad (3.19)$$

### 3.9 Grid independence study

Creating an accurate mesh structure for discretizing the fundamental governing equations is imperative. Therefore, the tetrahedral mesh simulates the fluid-structure and heat transfer in the pillow plate domain, allowing for precise and accurate resolution of the governing equations and post-processing to obtain all critical physical phenomena information. An appropriate external periodic boundary is selected. While excessive nodes increase computational effort, it provides a better and more accurate simulation than having too few or insufficient nodes and elements. Therefore, selecting an appropriate number of grid elements is necessary to balance accuracy, computational effort, and timing. The computational domain size in this work is determined by earlier research conducted by Shirzad et al. [34]. Nusselt number ( $Nu$ ) is compared across four different grids at a constant Reynolds number ( $Re$ ) of 1,200 for the presented computational simulation, as shown in Table 3.2, and a close grid view of the pillow-plate channel is shown in Fig. 3.4.

**Table. 3.2** Effect of different mesh sizes on  $Nu$  at  $Re = 1200$ .

Type	No. of elements	$Nu$	Improvement in $Nu$	% Improvement
'Grid-1'	1058756	62.95	-	-
'Grid-2'	1657852	64.20	1.25	1.98
'Grid-3'	2647823	65.10	0.90	1.40
'Grid-4'	3954578	65.45	0.35	0.53

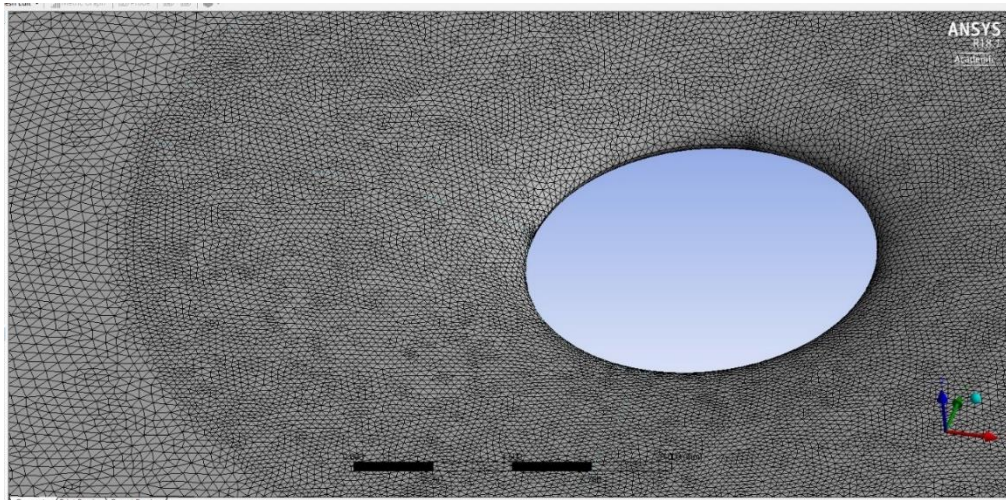


**Fig. 3.4** A fine grid view of Pillow-plate computational domain

### 3.10 Operating conditions and parameters

To validate the numerical simulation results with experimental data from Tran et al. [51,75,76], the same operating conditions and parameters were used for accuracy. The key geometrical parameters and operating conditions are listed in Table 3.3 and Table 3.4 [42].

**Table. 3.3** Parameters of the pillow plates investigated by Tran et al.[51,75,76] and Present study.

	In-line welding spots (XL = 42 mm/YT = 72mm, 3.4 mm expansion)	Staggered welding spots (XL = 72mm /YT = 42 mm, 3.0 mm expansion)	Staggered welding spots (XL = 72mm/YT = 42 mm, 7.0 mm expansion)	Staggered welding spots (XL = 72 mm/YT = 42 mm, 3.4 mm expansion)
Materials [35]	Experimental EN 1.4541 AISI 321	Experimental EN 1.4541 AISI 321	Experimental EN 1.4541 AISI 321	Present Numerical Study EN 1.4541 AISI 321
$h_i$	3.4	3.0	7.0	3.4
$\delta$	0.8	1	1	1
$X_L$	42	72	72	72
$Y_T$	72	42	42	42
$d_{cws}$	10	10	10	10
$d_h$	4.81	4.24	9.9	4.76
$A_{cs,i}$	685.19	604.58	1410.68	621.11
$A_{ht}$	0.6	0.6	0.6	0.58

For the current study, the pillow-plate channel maintains identical longitudinal ( $X_L$ ) and transverse ( $Y_T$ ) distances between the welding spots. Other critical parameters, such as the welding diameter ( $d_{cws}$ ) and inner channel expansion ( $h_i$ ), are also consistent with those used in Tran et al.'s experiments. These parameters ensure that the simulation setup closely replicates the experimental conditions for accurate validation.

**Table. 3.4** Operating conditions for the current computational study

Re	v	Mass flux	$T_i$ (K)	$T_w$	$T_o$ (K)	$\Delta p$
-	m/s	Kg/m <sup>2</sup> .s	(K)	(K)	(K)	Pa
1200	0.022	228.95	298.15	323.15	302.89	165.92
2800	0.052	534.21	298.15	323.15	301.49	576.45
4200	0.078	801.32	298.15	323.15	300.94	1123.03
6500	0.121	1240.14	298.15	323.15	300.54	2224.05
7800	0.146	1488.17	298.15	323.15	300.42	2946.89

### 3.11 Validation and results

This study utilized computational fluid dynamics (CFD) to analyze how different geometric factors, such as streamwise length, circular welding spot size ( $d_{cws}$ ), and inner hydraulic diameter ( $d_h$ ), affect fluid flow and thermal performance within a pillow plate. Turbulent single-phase flow at Reynolds number ( $Re$ ) = 1200 was considered. The simulation accurately predicted mean streamflow distribution, temperature gradient, pressure drop, convective heat transfer coefficient, and thermal performance. Operational parameters like Reynolds number ( $Re$ ), Nusselt number ( $Nu$ ), and pressure drop per length ( $\Delta p/L$ ) were also studied. Various pillow plate configurations were analyzed, and a grid test confirmed the computational results' reliability. The computational domain included specific dimensions, and a baseline model was used for grid reliability testing.

**Table. 3.5** Nusselt number and Pressure drop value obtained in numerical simulation.

	First order	Second order	First order	Second order	First order	Second order
$Re$	$Nu$	$Nu$	$\Delta p/L$	$\Delta p/L$	$f$	$f$
1200	22.2090	19.0713	17.4820256	11.52268	0.329612726	0.217253037
2800	32.2691	28.5165	50.7151215	40.03178	0.175628956	0.138632029
4200	39.8672	36.3363	87.5490111	77.98816	0.134749566	0.120034149
6500	52.2145	48.9361	159.153924	154.4482	0.102274025	0.099250077
7800	57.8396	54.3688	198.297917	204.6455	0.088491928	0.091324581

A pillow-plate channel section was utilized for validation, employing first- and second-order upwind schemes for discretizing the momentum and energy equations. Velocity and pressure were coupled using the SIMPLE algorithm, employing under-relaxation factors of 0.3 for pressure, 0.7 for momentum, and 0.9 for energy. This ensured that convergence criteria were met when residuals dropped below  $10^{-5}$  for all variables except the continuity equation. For continuity equation residuals, we obtained convergence of  $10^{-5}$  for the first-order upwind scheme and  $10^{-3}$  for the second-order upwind scheme. Comparison of CFD results with experimental data Tran et al. [76] revealed good agreement in  $Nu$  minimum and maximum values occurred  $\pm 27\%$  at  $Re = 1200$  and pressure drop per streamwise length ( $\Delta p/L$ ), with a discrepancy range from 0.3% at  $Re = 2800$  to 26% at  $Re = 7800$ , respectively (Table 3.2 and Figs. 3.5 and 3.6).

We used Root Mean Square Deviation (RMSD), a statistical measure that quantifies the differences between predicted and observed values within a dataset.

$$\text{RMSD} = \sqrt{\frac{1}{n} \sum_{i=1}^n (\Delta_i)^2} \quad (3.20)$$

Our results showed that the RMSD between the experimental and numerical values for the  $Nu$  using the first-order upwind scheme ranges from 0.04% to 3.39%. For the pressure drop per unit length ( $\Delta p/L$ ), the error with the first-order upwind scheme varies between 0.26% and 14.61%. However, for the second order upwind scheme, the RMSD for  $Nu$  and  $\Delta p/L$  are respectively ranging between 0.02% – 4.94% and 1.84% – 11.78%. This study highlights the effectiveness and accuracy of the numerical model in predicting flow and heat transfer characteristics in pillow-plate heat exchangers, validated against experimental data.

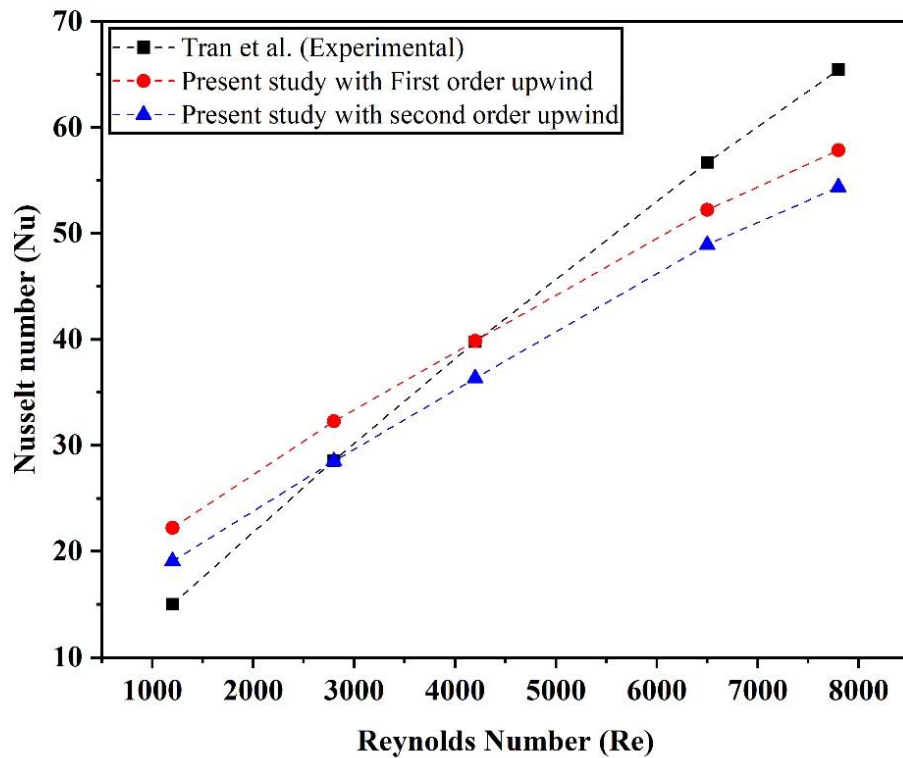


**Fig. 3.5** Validation of Nusselt number ( $Nu$ ) of numerical results against experimental results

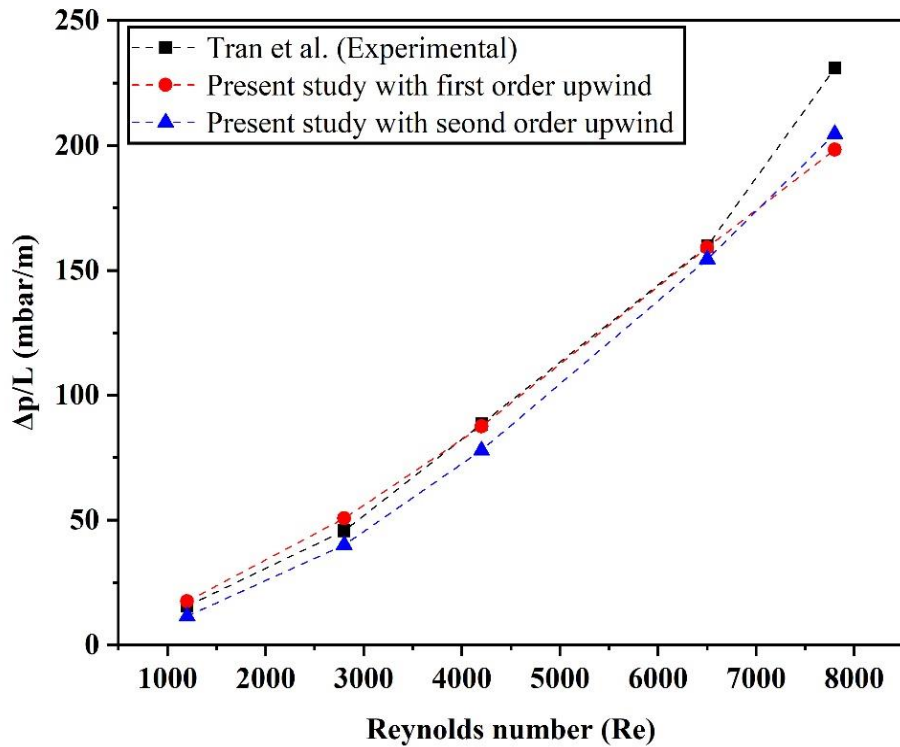


**Fig. 3.6** Validation of pressure drop ( $\Delta p/L$ ) of numerical results against experimental results

### 3.12 Comparison of different pillow-plate section/channel unit

The study compared fluid flow and temperature profiles across four different configurations (A), (B), (C) and (D) for  $X_L = 72$  mm, 144 mm, 216 mm and 288 mm respectively, (see Fig. 3.7 and Fig. 3.8) at varying Reynolds numbers: 1200, 2800, 4200, 6500, and 7800 for one, two, three, and four channel unit sections, respectively. The circular welding spots (SCWSP) position remained consistent within the pillow plate channel (PPC) across all cases. The SCWSP were set at a uniform staggered circular welding diameter ( $d_{cws} = 10$  mm) for all configurations.

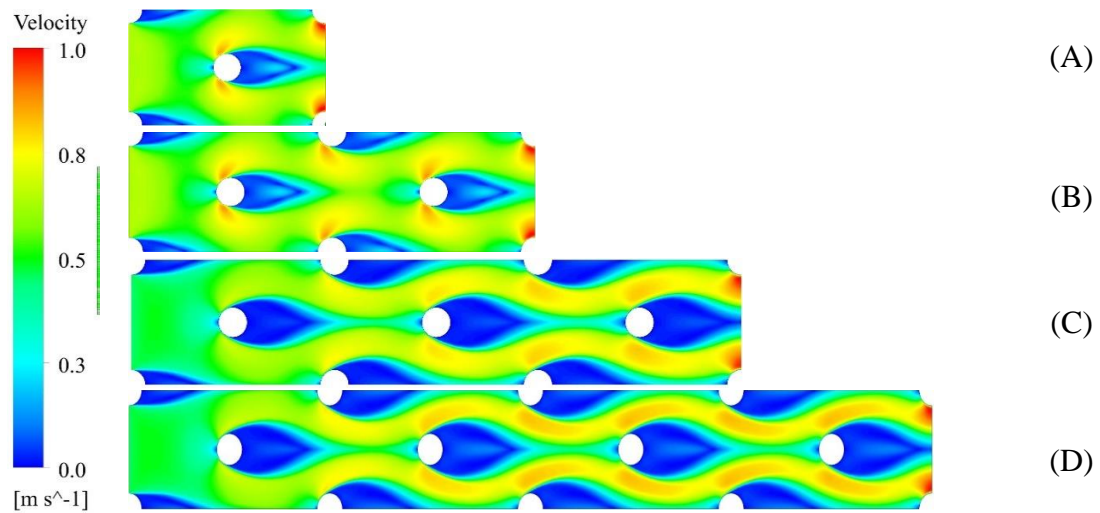


**Fig. 3.7** Comparison of velocity profile in different pillow-plate channel unit/section.

In addition, for the Pillow-plate heat exchanger (PPHE) model with more periodic unit sections as shown in Fig. 3.7 and Fig. 3.8, vortex shading has been observed for typical geometry for a Reynolds number ( $Re$ ) close to 7,800. Therefore, extending this pillow-plate channel model to a higher Reynolds number ( $Re$ ) may be subjected to errors of significant magnitude, which can only be assessed with experimental results or transient simulations, which is computationally costly. So, assuming this error is smaller, we extended our simulations up to 16,000.

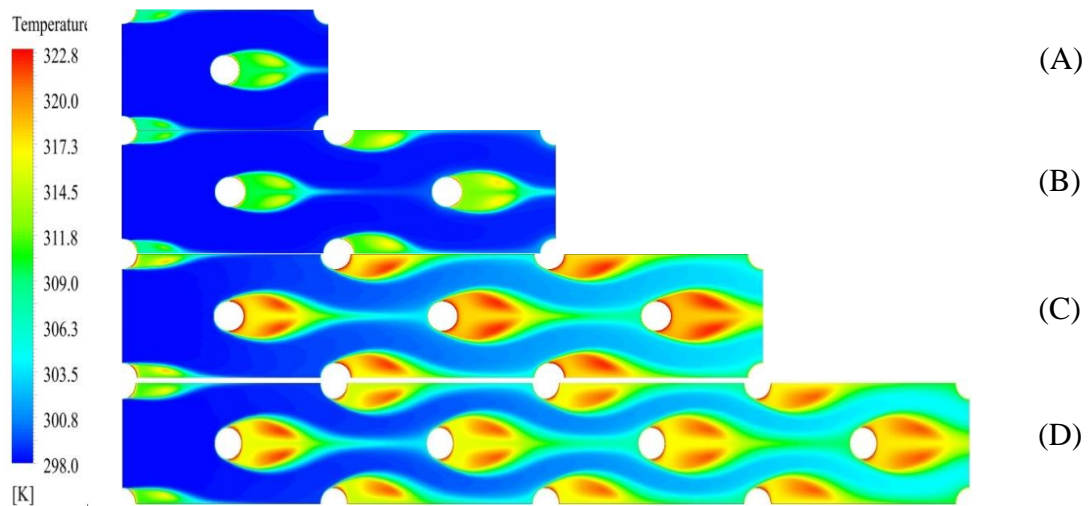


**Fig. 3.8** Comparison of temperature distribution profile in different pillow-plate channel unit/section.

### 3.13 Summary of chapter

In chapter 3, the utilization of the validated computational fluid dynamics (CFD) model for pillow-plate heat exchangers (PPHEs) presents promising avenues for advancing thermal engineering applications. Firstly, we can leverage the validated model to conduct geometry optimization studies tailored to pillow-plate heat exchangers (PPHEs). By systematically varying parameters such as streamwise length ( $X_L$ ), staggered circular welding spot pattern (SCWSP), and geometric arrangements, optimization methods can be employed in conjunction with the CFD model to identify optimal designs that maximize heat transfer efficiency, minimize pressure drop, or achieve other performance objectives. Through this approach, insights gained from the optimized geometry can lead to the development of more efficient and compact pillow-plate heat exchangers (PPHEs), with potential applications in industries ranging from refrigeration and HVAC systems to food processing and pharmaceutical manufacturing.

Secondly, the validated CFD model of the pillow-plate heat exchanger can be utilized to explore the effectiveness of various heat transfer enhancement techniques. These techniques may include the introduction of turbulence promoters, surface modifications, or the incorporation of secondary fluid flow patterns to enhance convective heat transfer rates. By systematically investigating these enhancement strategies through simulations, we can quantitatively assess their impact on heat transfer performance, thermal uniformity, and overall system efficiency. Insights gained from these studies can inform the development of innovative heat transfer enhancement methods tailored specifically to pillow-plate heat exchangers, with the potential to improve their heat transfer capabilities across a wide range of operating conditions.



# Chapter - 4: Heat Transfer Enhancement in Pillow-Plate Type Heat Exchangers (PPHE) with SCWSCs: An Entropy and Exergy Generation Optimization Approach

---

The design and development of the Pillow-plate heat exchanger (PPHE) have attracted more interest in the research and scientific communities in recent years. In this chapter, a new investigation is performed to examine the heat transfers and fluid flow characteristics for different streamwise lengths with Staggered Circular Welding Spot Configurations (SCWSCs). To analyze the heat transfer and friction factor parameters, a total of 25 different designs of  $d_h/X_L$  is considered,  $1000 \leq Re \leq 16,000$ . In addition to optimizing the exergy efficiency and thermal evaluation factor, some dimensional and non-dimensional thermodynamic and thermal-hydraulic, including thermal and frictional entropy generation, thermal and frictional exergy destruction, Nusselt number, friction factor, Bejan, entropy generation number are calculated by considering the second law efficiency approach based on thermo-dynamics for turbulent single-phase water flow in PPHE as wavy surface using transition SST  $k - \omega$  method and entropy-exergy generation optimization approach.

## 4.1 Introduction

In the field of engineering, heat transfer and the flow of fluid within ducts are frequently studied. The first law of thermodynamics is always applied to examine the energy flow in a thermal system. However, the second law analysis—which has to do with the formation of entropy—must be performed to examine the exergy or irreversibility of a thermal system. The total entropy generation in the fluid flow and heat transfer procedures is generated by the fluid's viscous friction against the wall and the two conditions—constant wall temperature and constant wall heat flux—that result from heat transfer across the internal flow. These are frequently examined in studies on entropy generation.

This chapter examines a contemporary shift in energy engineering research and application: the increasing significance of thermodynamics, particularly the second law, in problem-solving, modeling, and design optimization. This approach, known as thermodynamics optimization or entropy generation minimization (EGM), was initially introduced in a 1982 publication [77]. A recent review [78] indicates a rapid expansion in

adopting this methodology, which has also been referred to as finite time or endo-reversible thermodynamics.

This chapter illustrates the implementation of this method through examples drawn from refrigeration. It integrates heat and mass transfer principles, fluid mechanics, and engineering thermodynamics to develop realistic processes, devices, and systems models. By "realistic models," we mean models that accurately represent the inherent designs and configurations where entropy generation is minimized.

The methodology involves partitioning the system into subsystems that are in local thermodynamic equilibrium. The properties of these subsystems are governed by classical thermodynamics. Entropy is generated at the boundaries between subsystems, following rate equations derived from heat and mass transfer and fluid mechanics.

Consequently, the total rate of entropy generation is expressed as a function of the entire system's overall physical characteristics, such as finite size. Minimizing total entropy generation requires adjusting the physical characteristics of the system appropriately. These subsystems can range from macroscopic (comprising two or more subsystems within a system) to infinitesimally small (an infinite number). Thus, system modeling and entropy generation analysis can be conducted at macroscopic and differential levels, as exemplified in [77,78].

Conventional HEs are extensively used in thermal power industries, chemical engineering, petroleum refineries, and food processing industries, as well as in heat engines, automobiles, tractors, and ships, as well as in aviation and space satellite: refrigerant, micro-channel, and cryogenic engineering [79,80]. Therefore, heat exchangers are regularly exposed to thermodynamic optimization (or entropy generation minimization) in separation, separated from the larger installation that utilizes them [81]. Examples include counter, cross-flow, parallel, and phase-change HEs optimization diagrams [82]. Considering only the capital cost aspect of a heat exchanger's design would be misleading because high maintenance costs raise the total cost of the heat exchanger's service life. As a result, exergy study and energy conservation are critical entities in HEs design [83].

The thermodynamics optimization approach, also known as the EGM approach, has developed itself as a unique area of interest at the intersection of heat transfer, engineering thermodynamics, and fluid mechanism. Recently, Vargas et al. [84] presented a technique for examining a tube bank's internal geometric arrangement by optimizing the overall performance of the cross-flow HE installation. Ogulatu et al. [85] performed an

optimization design for a cross-flow rate in the HE based on the EGM, examining the best result using experimental data.

Exergy analysis and energy saving with thermodynamics optimization have received much attention over the last two decades and are now a well-traditional subfield in heat exchangers and engineering thermodynamics [86,87]. It is now recognized as the mechanism for research generation and community flow systems everywhere, in engineering and practical uses. Limitations in thermodynamics are caused by currents (fluid, heat) that must overcome resistance [88]. When the resistances are reduced together, the global performance improves. That is when the limitation is distributed optimally in space. Flow construction design in heat transfer equipment is the optimal distribution of defects [89].

## 4.2 Objectives

In this chapter, we conduct a computational numerical investigation of a heated wavy-shaped channel with a new geometry. Then we supplement it with SCWSCs to improve its thermal performance factor. It generates a sinusoidal velocity profile for a variety of PPC lengths. The current study is unique and distinct from previous studies. In this manuscript, a computer study (CFD simulation) is performed to analyze the influence of varied streamwise lengths ( $L_{A-E}$ ) = 256-384 mm of PPCs with a non-dimensional number  $d_h/X_L$  values ranging mentioned in Table 1. In each streamwise length, there are five different CWS ( $d_{CWS}$ ) changing from 8-12 mm (Case  $L_{A,1-E,25}$  (1-25)). Moreover, data is also presented to illustrate the influence of some thermos-hydrodynamic parameters, including Nusselt number, friction factor, heat transfer rate  $\dot{S}_{g,T}$  (Thermal entropy generation),  $\dot{S}_{g,F}$  (Thermal frictional generation),  $\dot{E}x_{dest,T}$  (Thermal exergy destruction),  $\dot{E}x_{dest,F}$  (Frictional exergy generation), Be (Bejan number),  $N_S$  (Entropy generation number),  $\eta_{ex}$  (exergy efficiency) and  $\eta$  (thermal Performance Factor) with different  $Re$  (Reynolds number) to optimize the efficiency of the PPHE. From the perspective of improving thermal performance, the primary goal is to identify the optimal set of physical and geometrical requirements for the heat exchanger channel's symmetric curve wavy geometry. The study also provides optimal heat transmission and pressure drop setup data. Finally, using an efficiency index, we examine the behavior of successive generations of re-circulating vortices formation and the temperature distribution in the wavy channel. The pillow plate's symmetrically wavy surface geometry has not been considered or studied.

Furthermore, the PPHX above curve with SCWSCs as vortex generators has not yet been seen in the literature. Other similar documents by different authors fail to address essential details like the impact of SCWSCs on the channel, the range of velocities and wide range of  $Re$  parameters considered, the channel's height, the flow rate, the velocity profile's shape, and the temperature distribution. Because of this, we looked at how to improve heat transmission and flow characteristics in a Pillow-plate by using a wavy shape strategically developed on the channel to create vortices.

In this chapter, we conduct a computational numerical investigation of a heated wavy-shaped channel with a new geometry. Then we supplement it with SCWSCs to improve its thermal performance factor. It generates a sinusoidal velocity profile for a variety of PPC lengths. The current study is unique and distinct from previous studies. In this manuscript, a computer study (CFD simulation) is performed to analyze the influence of varied streamwise lengths ( $L_{A-E}$ ) = 256-384 mm of PPCs with a non-dimensional number welding spot pitch ( $S_r$ ) values ranging mentioned in Table 1. In each streamwise length, there are five different CWS ( $d_{cws}$ ) changing from 8-12 mm (Case  $L_{A,1-E,25}$  (1-25)). Moreover, data is also presented to illustrate the influence of some thermos-hydrodynamic parameters, including Nusselt number, friction factor, heat transfer rate  $\dot{S}_{g,T}$  (Thermal entropy generation),  $\dot{S}_{g,F}$  (Thermal frictional generation),  $\dot{E}x_{dest,T}$  (Thermal exergy destruction),  $\dot{E}x_{dest,F}$  (Frictional exergy generation), Be (Bejan number),  $N_S$  (Entropy generation number),  $\eta_{ex}$  (exergy efficiency) and  $\eta$  (thermal Performance Factor) with different  $Re$  (Reynolds number) to optimize the efficiency of the PPHE. From the perspective of improving thermal performance, the primary goal is to identify the optimal set of physical and geometrical requirements for the heat exchanger channel's symmetric curve wavy geometry. The study also provides optimal heat transmission and pressure drop setup data. Finally, using an efficiency index, we examine the behavior of successive generations of re-circulating vortices formation and the temperature distribution in the wavy channel. The pillow plate's symmetrically wavy surface geometry has not been considered or studied. Furthermore, the PPHX above curve with SCWSCs as vortex generators has not yet been seen in the literature. Other similar documents by different authors fail to address essential details like the impact of SCWSCs on the channel, the range of velocities and wide range of  $Re$  parameters considered, the channel's height, the flow rate, the velocity profile's shape, and the temperature distribution. Because of this, we

looked at how to improve heat transmission and flow characteristics in a pillow plate by using a wavy shape strategically developed on the channel to create vortices.

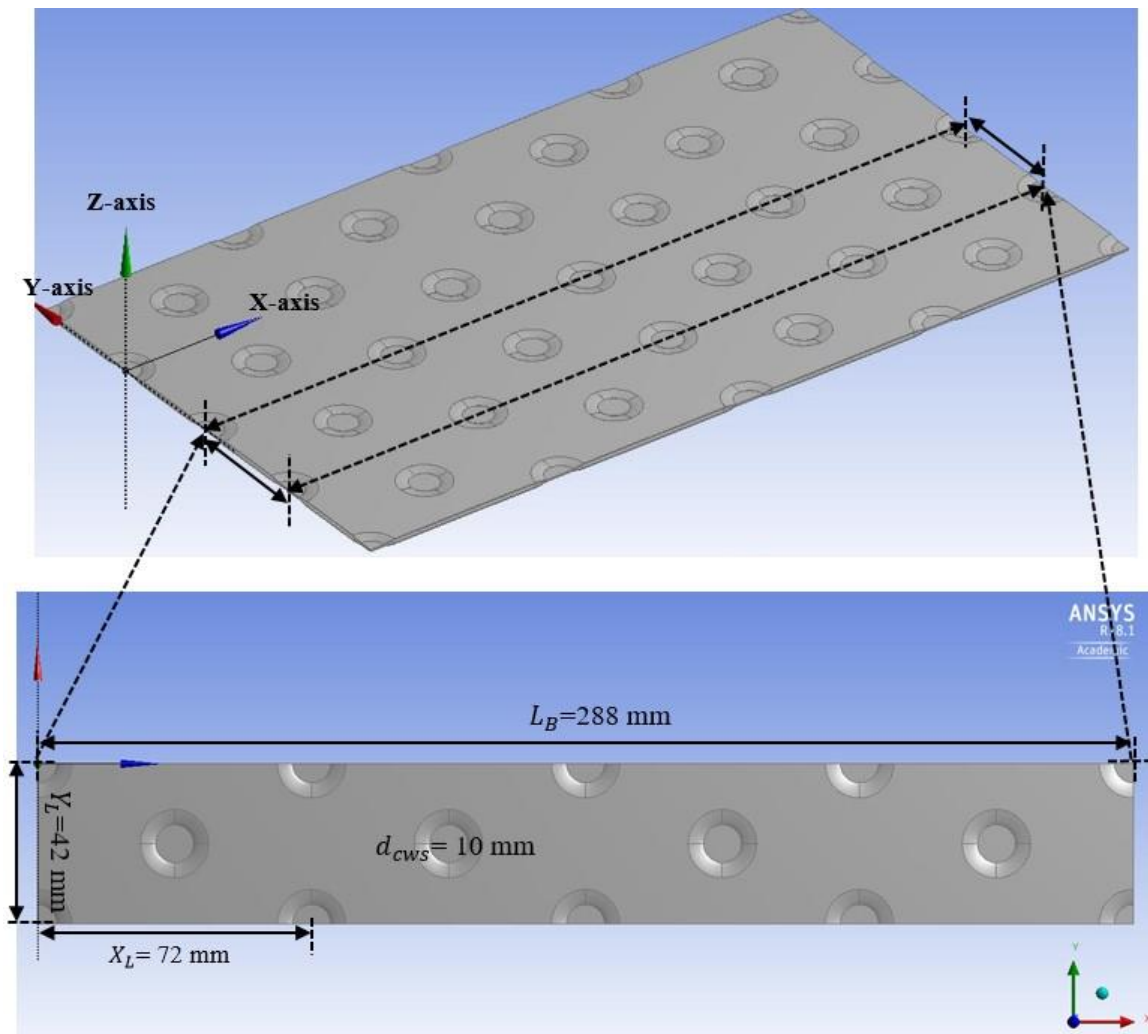


**Fig. 4.1** Schematic diagram of the pillow plate heat exchanger with SCWSPs.

### 4.3 Problem formulation

This section covers the fundamental and essential governing equations, assumptions, and boundary conditions. The problem is solved using the 3D Navier-Stokes, energy equations, and turbulent flow transition SST ( $k - \omega$ ) model. The governing equations are simplified further under the assumptions listed below.

### 4.3.1 The assumptions

- The flow is considered steady and turbulent—3D incompressible flow and heat transfer.
- The single-phase working fluid (water).
- The fluid flow is considered fully turbulent in all cases ( $L_{A,1-E,25}$ ).
- The thermo-physical properties of the fluids are constant, and the channel enclosure is insulated (no heat loss in the environment).

### 4.3.2 Boundary conditions

Three necessary external periodicity boundary conditions can be applied when considering a general three-dimensional heat transfer PPC in the computational simulation similar to [65].

- The boundary condition for momentum and energy equation at faces *A* (inlet) and *B* (outlet) of the computational domain. Furthermore, the external boundary condition is used in the transverse direction [90].
- At faces *C* and *D*, symmetry boundary conditions are applied.
- At faces *E* (top) and *F* (bottom), no-slip boundary conditions are applied on the channel [31].
- At the channel top and bottom is set a constant temperature of 323 K, and the inlet temperature of the computational domain is 298 K.

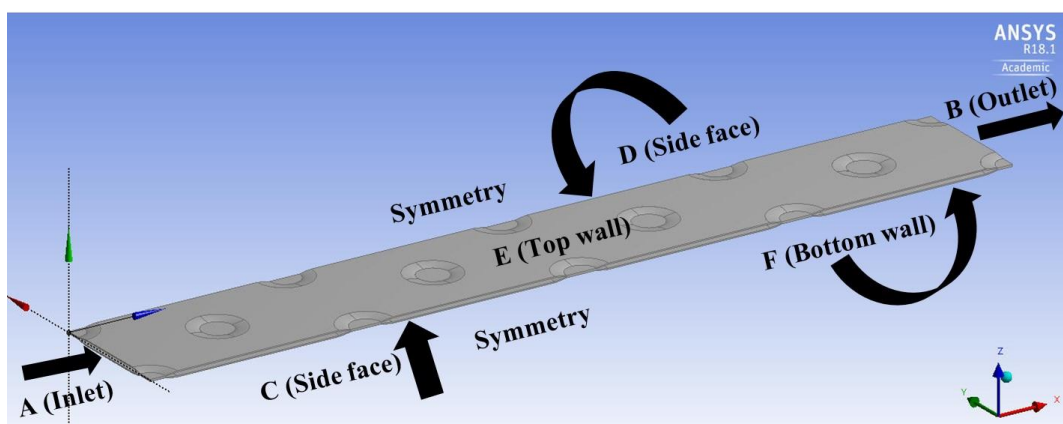


**Fig. 4.2** A schematic representation of a pillow plate heat exchanger with SCWSPs and fluid flow condition.

**Table. 4.1** Geometrical parameters considered in the present computational work (all dimensions in mm).

Case S.No.	Parameters						
	$L_{A-E}$	$X_L$	$Y_L$	$h_i$	$d_h$	$d_{CWS}$	$s_r$
1.	256	64	42	3.4	4.99	8	1.65
2.	288	72	42	3.4	4.92	8	1.88
3.	320	80	42	3.4	4.70	8	2.11
4.	352	88	42	3.4	4.47	8	2.35
5.	384	96	42	3.4	4.31	8	2.58
6.	256	64	42	3.4	4.93	9	1.67
7.	288	72	42	3.4	4.82	9	1.91
8.	320	80	42	3.4	4.64	9	2.15
9.	352	88	42	3.4	4.42	9	2.39
10.	384	96	42	3.4	4.20	9	2.63
11.	256	64	42	3.4	4.89	10	1.69
12.	288	72	42	3.4	4.76	10	1.94
13.	320	80	42	3.4	4.58	10	2.19
14.	352	88	42	3.4	4.36	10	2.44
15.	384	96	42	3.4	4.11	10	2.69
16.	256	64	42	3.4	4.80	11	1.71
17.	288	72	42	3.4	4.68	11	1.97
18.	320	80	42	3.4	4.51	11	2.23
19.	352	88	42	3.4	4.31	11	2.48
20.	384	96	42	3.4	4.02	11	2.74
21.	256	64	42	3.4	4.74	12	1.73
22.	288	72	42	3.4	4.60	12	2.00
23.	320	80	42	3.4	4.45	12	2.27
24.	352	88	42	3.4	4.26	12	2.53
25.	384	96	42	3.4	3.96	12	2.80

#### 4.4 Grid independence test and validation of numerical models

Creating an accurate mesh structure for discretizing the fundamental governing equations is imperative. Therefore, the tetrahedral mesh simulates the fluid-structure and heat transfer for the pillow plate domain to solve the governing equations, post-processing, and get all critical physical phenomena information precisely and accurately in the computational solution. It selects an appropriate imposed external periodic boundary. An excessive number of nodes increases computation effort and provides a better and more accurate computational simulation value than fewer or insufficient nodes and elements. Therefore, selecting an appropriate number of grid elements is necessary to simultaneously satisfy the requirements of accuracy, computational effort, and timing. The

size of the computational domain in this work is determined by earlier research conducted by Shirzad et al. [34].



**Fig. 4.3** Close grid view of Pillow plate domain

$Nu$  is compared in four different grids at constant  $Re = 7,800$  for the presented computational simulation as shown in Table 4.2. The current work's compared to Tran et al. [76] experimental findings for the pillow plate configuration Case  $L_{A,11}$ . To validate the present numerical model, the Reynolds numbers ( $Re$ ) 1200, 2800, 4200, 6500, and 7800 were used [76] as mentioned in Fig. 4.4 and 4.5. Differences in validation outcomes between Chapter 4 and Chapter 3 can be explored through the pillow-plate channel section unit ( $X_L = 72$  mm) selected for validation against experimental data.

**Table. 4.2.** Effect of different mesh sizes on  $Nu$  at  $Re = 7,800$ .

Type	No. of elements	Nu	Improvement in Nu	% Improvement
'Grid-1'	1198373	63.19	-	-
'Grid-2'	1937893	64.56	1.37	2.12
'Grid-3'	2776679	65.25	0.69	1.05
'Grid-4'	4285678	65.78	0.53	0.81
Comparison and validation of Case $L_{B,12}$ with experimental results [76]				
$Nu$ , Tran et al. [76]				
	66.04		0.26	0.4%



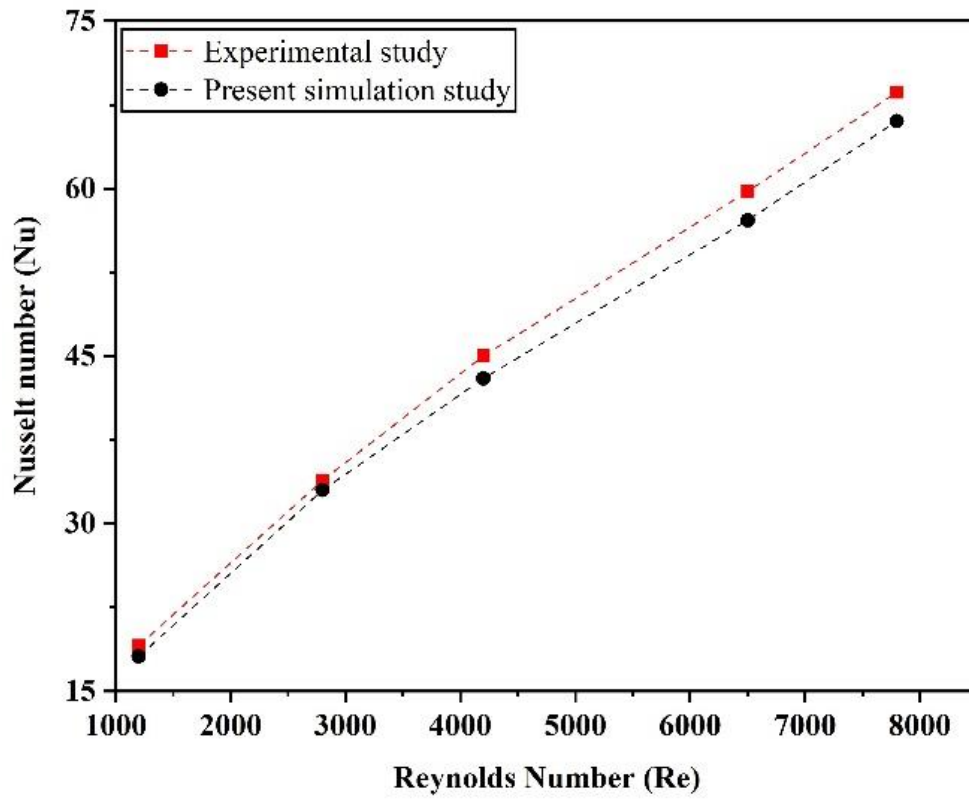


**Fig. 4.4.** Comparison of  $Nu$  obtained in the numerical simulation with experimental results [76] for  $Re = 1200, 2800, 4200, 6500,$  and  $7800$ .

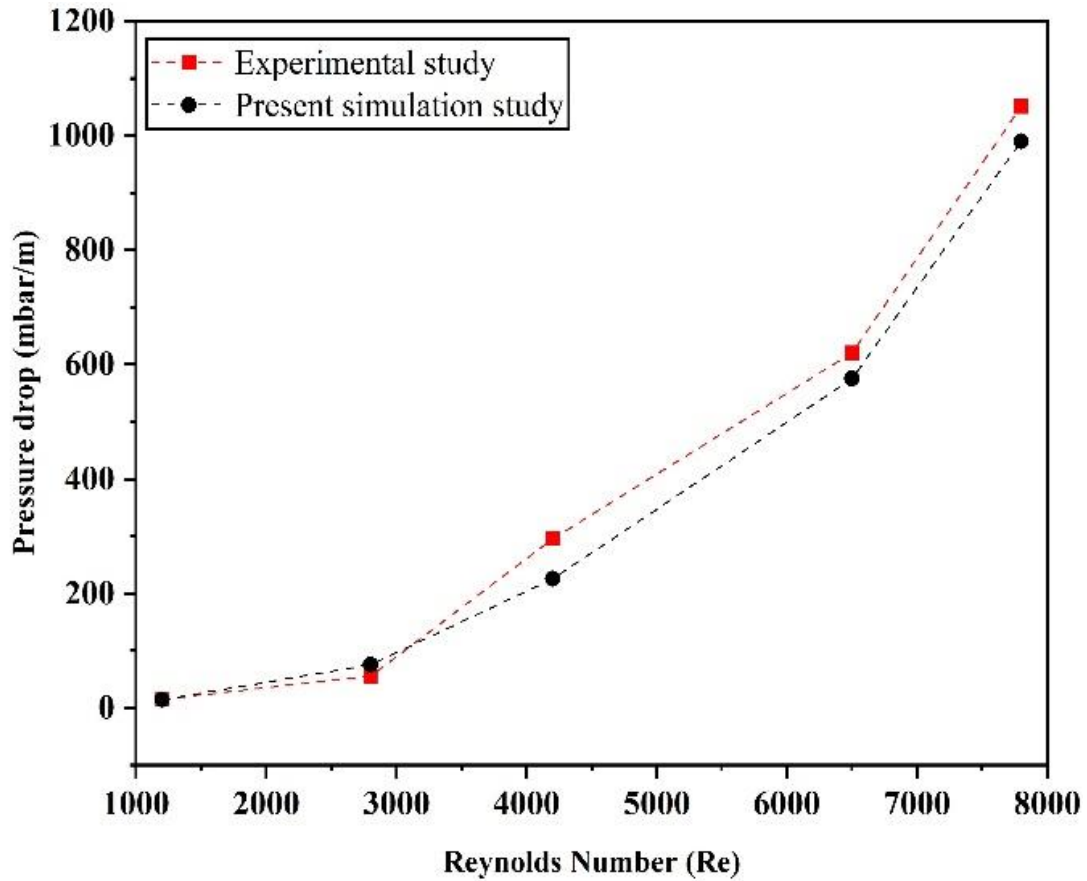


**Fig. 4.5.** Comparison of pressure drop obtained in the numerical simulation with experimental results of [76] for  $Re = 1200, 2800, 4200, 6500,$  and  $7800$ .

## 4.5 Thermodynamic analysis

### 4.5.1 Entropy analysis

Two types of losses occur in a heat exchanger: those caused by heat exchange across a finite temperature difference and those caused by fluid friction. The total entropy generation ( $\dot{S}_g$ ) of water in the PPC can be expressed/determined with  $\dot{S}_{g,T}$  (Thermal entropy generation), and  $\dot{S}_{g,F}$  (Frictional entropy generation) [91].

$$\dot{S}_g = \dot{S}_{g,T} + \dot{S}_{g,F} \quad (4.1)$$

$$\dot{S}_{g,T} = \frac{Q^2}{Nu\pi k T_{in} T_{out}} \quad (4.2)$$

$$\dot{S}_{g,F} = \frac{8fm^3 X_L}{\rho^2 \pi^2 d_h^5 (T_{out} - T_{in})} \ln\left(\frac{T_{out}}{T_{in}}\right) \quad (4.3)$$

The Bejan number ( $Be$ ), named after the distinguished thermodynamicist Adrian Bejan, is a dimensionless parameter in heat transfer and fluid mechanics. It represents the ratio of heat transfer irreversibility to convective heat transfer within a system. Mathematically, it is expressed as the entropy generation ratio due to irreversibility to the convective heat transfer rate.

The significance of the Bejan number ( $Be$ ) lies in its ability to provide insights into the thermodynamic efficiency of a system. The Bejan number helps engineers and researchers understand where energy losses occur within a system by quantifying the relative importance of irreversibility compared to convective heat transfer. This understanding is crucial for optimizing the design and operation of heat transfer equipment, such as heat exchangers, by identifying areas of inefficiency and guiding efforts to minimize energy losses.

Furthermore, the Bejan number ( $Be$ ) is a valuable formula for comparing different heat transfer systems and assessing the impact of various design modifications or operating conditions on system performance. It allows engineers to prioritize optimization efforts and make informed decisions to enhance the efficiency and effectiveness of heat transfer processes.

The Bejan number is determined using Eq. (4.4) [91].

$$(Be) = \frac{S_{g,T}}{S_{g,T} + S_{g,F}} \quad (4.4)$$

#### 4.5.2 Exergy efficiency ( $\eta_{ex}$ ) and entropy generation number ( $N_S$ )

The ratio of the valuable exergy output to the total exergy is called ‘exergy efficiency’ ( $\eta_{ex}\%$ ) expressed as [91]. In thermal engineering, exergy efficiency, also referred to as second-law efficiency or rational efficiency, evaluates a system's effectiveness concerning its performance under reversible conditions. This metric provides insight into how efficiently a system utilizes energy by comparing its performance to the theoretical maximum achievable under ideal, reversible conditions. By quantifying the quality of energy and accounting for irreversible losses, exergy efficiency offers a more comprehensive assessment of system performance beyond traditional energy efficiency measures. It serves as a valuable tool for optimizing thermal systems, identifying areas for improvement, and guiding sustainable energy practices.

$$\eta_{ex} = 1 - \frac{T_a S_{g,T}}{\left[1 - \left(\frac{T_a}{T_s}\right)\right] Q_h} \quad (4.5)$$

The thermal ( $\dot{E}x_{dest}$ ) and frictional ( $\dot{E}x_{dest,F}$ ) exergy destruction is expressed as the following equations [91].

$$\dot{E}x_{dest,T} = T_a \dot{S}_{g,T} \quad (4.6)$$

$$\dot{E}x_{dest,F} = T_a \dot{S}_{g,F} \quad (4.7)$$

Entropy generation number, often denoted as ( $N_s$ ), is a dimensionless parameter used in thermodynamics to quantify the irreversibility or entropy production within a system or a process. It provides insight into the efficiency and performance of a thermodynamic system by assessing the degree of departure from ideal, reversible conditions. The entropy generation number is typically the ratio of actual entropy generation to the maximum possible generation in a reversible process between the same initial and final states. A value greater than 1 indicates that the actual entropy generation exceeds the maximum possible entropy generation in a reversible process, signifying significant irreversibility and inefficiency within the system. Conversely, a value of equal to 1 suggests that the system operates at maximum efficiency with minimal entropy generation. Entropy generation number is a crucial parameter in thermodynamic analysis as it helps engineers and researchers identify sources of irreversibility within a system, assess the impact of inefficiencies, and guide the design and optimization of processes to minimize entropy generation and improve overall efficiency.

The entropy generation number ( $N_s$ ) is estimated from Eq. (4.8) [91].

$$N_s = \frac{T_a \dot{S}_{g,T}}{Q_h} \quad (4.8)$$

## 4.6 Results and discussion

In this section, the influence of different dimensional and non-dimensional parameters, such as  $\dot{S}_{g,T}$ ,  $\dot{S}_{g,F}$ ,  $\dot{E}x_{dest,T}$ ,  $\dot{E}x_{dest,F}$ , Bejan number ( $Be$ ),  $N_s$ ,  $\eta_{ex}$  and  $\eta$  ( $TPF$ ) are examined and described the thermo-hydraulic behavior of fluid flow inside the various pillow-plate channel lengths varies from 256-384 mm at different  $1000 \leq Re \leq 16,000$ . Note

that for  $Re = 1,000$ ,  $v = 0.1875$  m/s and for  $Re = 1,000-16,000$ ,  $v$  varies from  $0.1875 - 3$  m/s.

#### 4.6.1 Velocity and temperature field distribution

This section discusses the principal phenomena and mechanism of the flow and heat transfer characteristics around the SCWSCs in the pillow-plate channel. The primary objective is to examine the thermal-hydraulic performance of the different enhanced configurations  $L_{A,1-E,25} = 256-384$ . The thermal performance of the longitudinal configuration is superior to the transversal type, as discussed in the previous articles and publications [32,92]. Therefore, in this manuscript, we have discussed only the streamwise length of the SCWSPs. Discussing the dominant flow structures relevant to static pressure resistance and heat transfer in the PPC is essential for designing the heat exchanger for practical applications. Fig. 4.6 and Fig 4.7 shows the streamline associated with an elliptical recirculation pair for visualization and capturing the fluid flow behavior near the SCWSCs at  $Re = 2000$ , identical to [93]. The flow field (velocity contour) (Cases A, B, C, D, and E) and temperature distribution (Cases A, B, C, D, and E) along the five different streamwise channels with SCWSCs and near the CWS, respectively, at  $Re = 2000$  while,  $h_i$  and  $Y_L$ , are considered as a fixed value. Due to the SCWSPs' leadership, the inlet velocity is deflected towards the spanwise direction, and a complete 'elliptical vortex' region formation occurs behind the SCWSPs and near the inlet and outlet region of the channel. The nature and formation of the primary mainstream fluid flow forms inside the PPC is a 'sinusoidal wave'-like structure in the longitudinal type of pillow-plate channel configuration. This 'sinusoidal' wave formation associated with higher turbulence strength and intensity than the linear flow in a straight elliptical channel-type design. This is the main reason of the significant enhancement of the convective heat transfer and static pressure drop in the streamwise channel with SCWSPs compared to the straight elliptical channel duct (without SCWSPs).

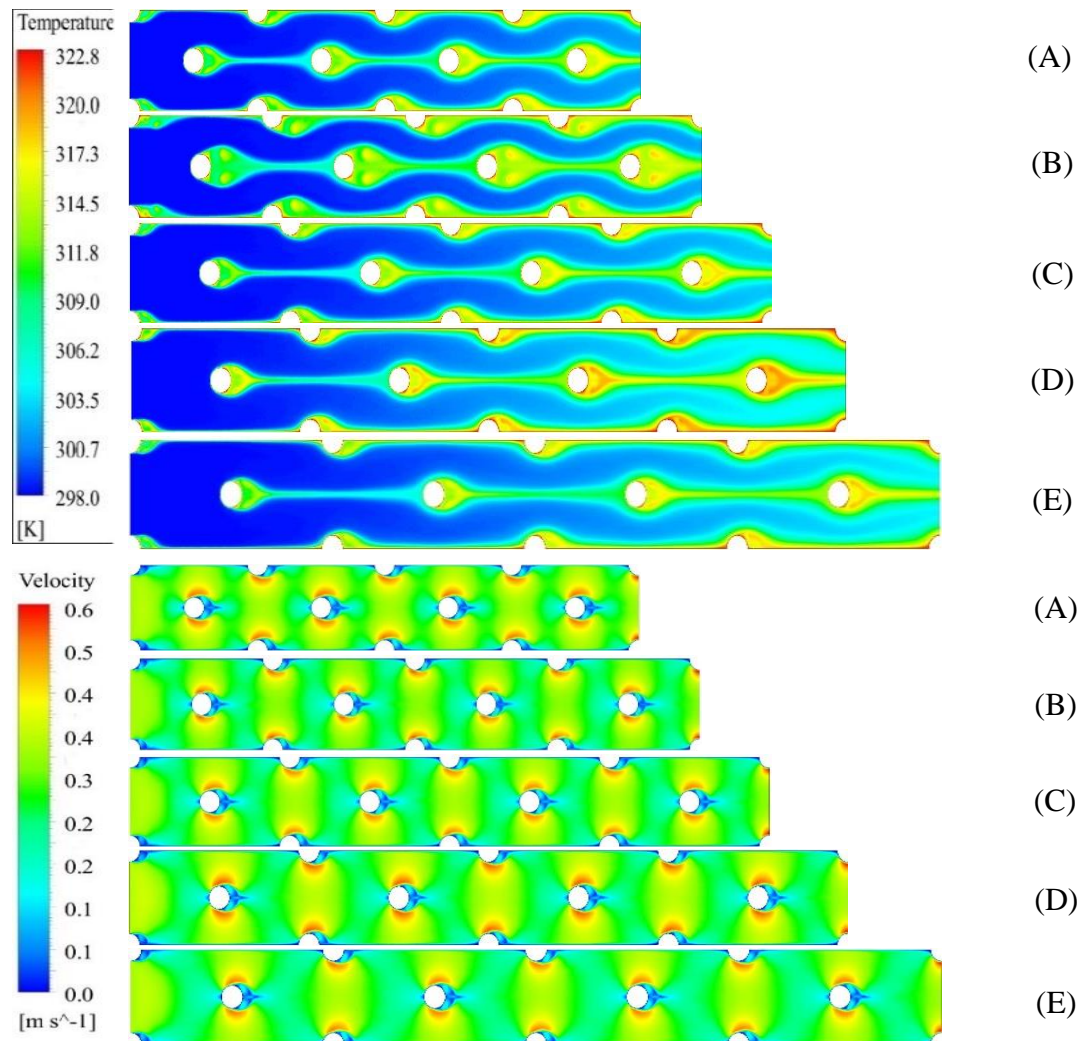


**Fig. 4.6** Representative domains used for thermal modeling, Case (A-E) temperature velocity and Case (A-E) velocity contour of five different streamwise arrangements  $L_{A,11-E,15} = (256-384 \text{ mm (Case 11 to 15)})$  of the PPC at  $Re = 2000$ .

Conversely, In the velocity profile contour and temperature distribution contour, as shown in Fig. 4.6 (A-E), an ‘elliptical recirculation vortex’ pair is developed behind the CWS and near the wall region inside the pillow-plate type channel. These ‘elliptical recirculation vortices’ induced spanwise velocity and improved heat transport from the fluid in the channel wake to the mainstream regions and vice versa. As seen, in the longitudinal (streamwise) channel, the primary core flow forms a linear pass, and the symmetrical recirculation zone (‘elliptical vortex’) is separated from the mainstream flow. On the contrary, the temperature gradient in the ‘elliptical vortex’ zone is higher than in the main flow, and these areas represent low convective heat transfer than the smooth type

channel. It is attributed that the enhanced mixing between the cold and hot fluid by ‘elliptical vortex’ flow is one of the essential mechanisms of heat transfer enhancement.

The pressure profile contours of different PPHE configuration ( $L_{A,11-E,15}$ ) at  $Re = 2000$  are examined separately in Fig. 4.7. Based on the computational contour information the SCWSPs behave as a vortex generator to generate reversing flows and secondary flow and ERV. Due to these secondary flows more fluid mixing and heat transfer occurs inside the PPC. Note that due to this flow separation behind the SCWSPs, the secondary flow and reverse flows and ERV are developed.

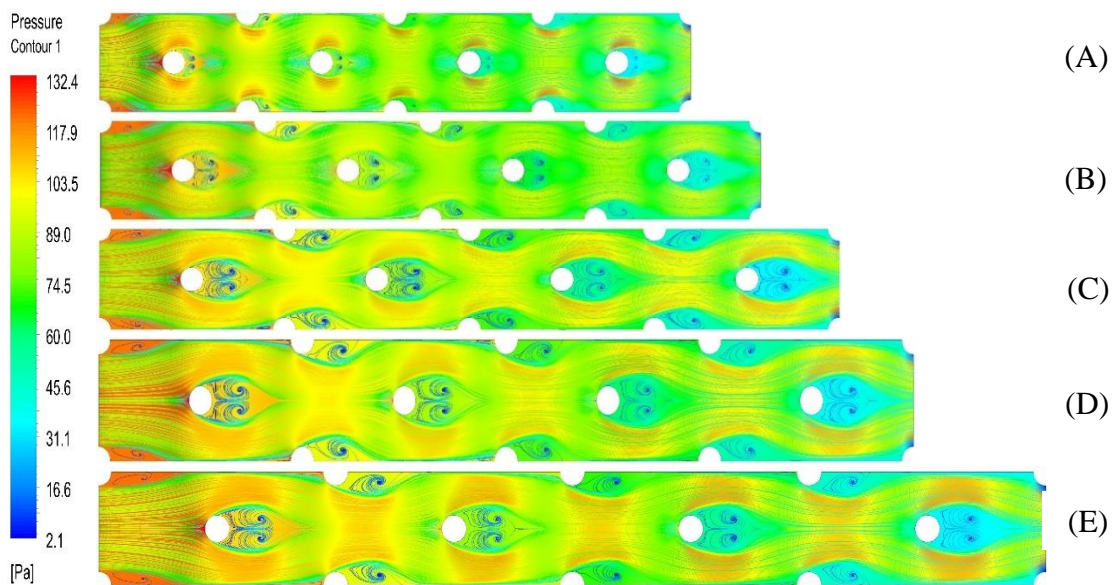


**Fig. 4.7** Static Pressure contour of different pillow-plate channel configuration  $L_{A,11-E,15} = 256-384$  mm (Case 11 to 15)) of the PPC at  $Re = 2000$ .

#### 4.6.2 The energy balance analysis

Changing the wavy PPCC significantly changes the computational simulation results of the  $Nu$  and  $h_{conv}$ . A channel with SCWSPs offers a  $h_{conv}$  higher than a smooth channel (without SCWSPs). Increasing the streamwise length further results in a higher value of the convective heat transfer coefficient, which can be attributed to increased turbulence through the disruption of the boundary layer. The  $Nu$  is higher with the longitudinal length of the channel due to the SCWSPs, as shown in Fig. 4.6. The OERV created by SCWSPs are responsible for this. In addition to increasing fluid mixing, decreasing the boundary layer thickness, and increasing the heat transfer rate, these SCWSPs can generate secondary flows and vortices pair. It's important to note that as the  $Re$  enhanced, the magnitude of the  $Nu$ , which increases due to SCWSPs (vortex generators), also increases

much more. For  $4,000 \leq Re \leq 16,000$ , the average  $Nu$  increases by around 25.34% with increasing  $Re$ .

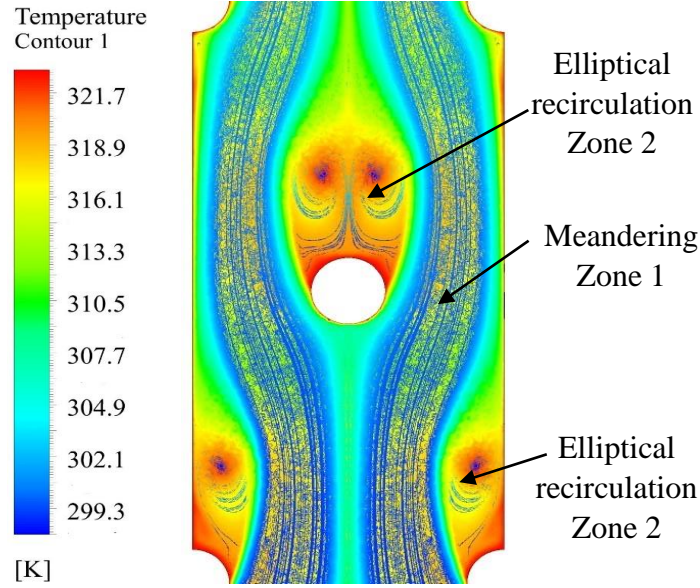


**Fig. 4.8** Representative domain of fluid flow inside the pillow-plate channel with two distinct zone at  $d_h/X_L = 0.076$  & Case (A) at  $Re = 2000$ .

The fluid flow distribution in the PPC can be classified into two distinct characteristics zones, as shown in the previous article [11]. From CFD simulation Fig. 4.8. Heat transfer and ERV (Elliptical Recirculation Vortex) zones (zone 2) are dominated by a meandering core flow (zone 1), which is generated by SCWSPs. In a meandering channel, the center region can have double the average speed of the remaining channel sections. Zone 1 boundary layers are highly turbulent and fully developed hydro-dynamically and thermally as shown in Fig. 4.8. Numerous previous works (e.g., Petukhov and Popov [94], Colburn [95], and Dittus and Boelter [96] have proposed a Nusselt number connection for this particular boundary layer.

$$Nu_{z1} = \frac{(f_{z1}/8)Re_{z1}Pr}{1.07 + 12.7\sqrt{(f_{z1}/8)(Pr^{2/3}-1)}} \quad (4.9)$$

Both zone 1 and the entire PPC must be modeled in the 'elliptical recirculation vortices' zone to complete the 2-zone model. This relationship was developed due to an energy balance analysis along the channel's surface as mentioned in the Fig. 4.8 and Fig. 4.9.

$$\dot{Q}_{tot} = \dot{Q}_{z1} + \dot{Q}_{z2} \quad (4.10)$$



According to Equation (4.10), the sum of the heat flow rates in each zone of 'elliptical recirculation vortices'  $\dot{Q}_{z2}$  is equals the overall heat flow rate  $\dot{Q}_{tot}$  transfer to the total channel surface. In addition, we can rearrange Eq. (4.11) to get the following equation.

$$\dot{Q}_{tot} (1-\varphi_Q) = \dot{Q}_{z1} \text{ with } \varphi_Q = \frac{\dot{Q}_{z2}}{\dot{Q}_{tot}} \quad (4.11)$$

The ratio of heat transfer in the recirculation zones to the total heat flow rate is represented by the dimensionless factor  $\varphi_Q$ . Using Newton's law of cooling, we can also calculate the heat flow rates  $\dot{Q}_{tot}$  and  $\dot{Q}_{z1}$ .

$$\dot{Q}_{tot} = h_{tot} A_{w,tot} \Delta T_{tot} \quad (4.12)$$

$$\dot{Q}_{z1} = h_{z1} A_{w,z1} \Delta T_{z1} \quad (4.13)$$

The mean variation between the bulk and wall temperatures is denoted by the term  $\Delta T_{tot}$  in Eq. (4.12). In contrast, the average difference between the bulk and wall temperatures in zone 1 is denoted by  $\Delta T_{z1}$ . Since the meandering zone in the PPC is the main contributor to the overall heat transfer. The following relationship was considered as given:

$$\Delta T_{tot} \cong \Delta T_{z1} \quad (4.14)$$

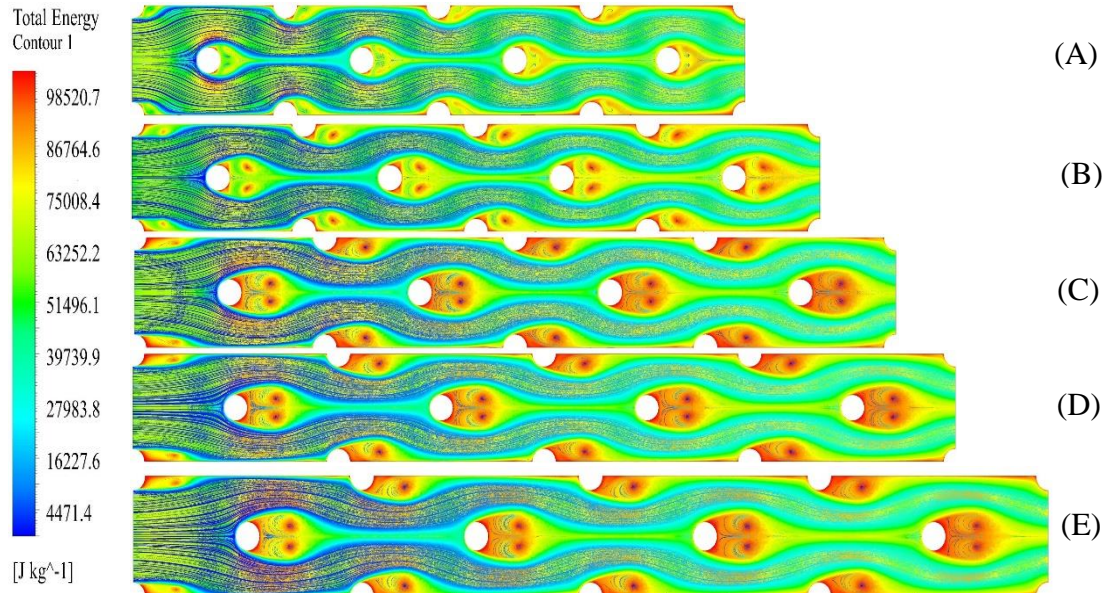


**Fig. 4.9** Energy contour of different pillow-plate channel arrangement  $L_{A,11-E,15}$  (256-384 mm (Case 11 to 15)) of the PPC at  $Re = 2000$ .

### 4.6.3 Nusselt number and friction factor

Fig. 4.10 depicted ‘periodic wave’-like structure of surface Nusselt Number ( $Nu$ ) in various PPCCs ( $L_{A,11-E,15}$ ) at  $Re = 2,000$  while, the variation of  $Nu$  value for all the Cases A-E ( $L_{A,1-E,25}$ ) is reported in Fig. 4.11 at various  $Re$ . As can be seen, the  $h_{conv}$  (in terms of  $Nu$ ) increases with  $1,000 \leq Re \leq 16,000$  while decreasing with the channel length increment from  $L_{A,1-E,25}=256-384$  mm. SCWSCs is the main reason for enhancing the heat transfer rate in the PPC. The PPC with larger SCWSPs  $d_{cws} = 10-12$  mm provides a more significant value in the  $Nu$  and static  $\Delta p$  compared to the smaller value of  $d_{cws} = 8-9$  mm. It is noted that the variation in the  $Nu$  and pressure drop is mainly due to pillow channel length configuration and diameter of CWS patterns/arrays. From the Fig. 4.11 it is found that the SCWSCs can boost the heat transfer (in terms of  $Nu$ ) at  $Re = 16,000$  is 51.92%, 58.07%, 66.93%, 35.32%, 44.00%, and at  $Re = 1000$ , 11.89%, 10.34%, 8.97%, 12.15%, 17.65% for Cases ( $L_{A,11-E,15}$ ) ( $d_h/X_L = 0.076, 0.066, 0.057, 0.05, \text{ and } 0.043$ ), respectively, compared to the without SCWSPs channel.

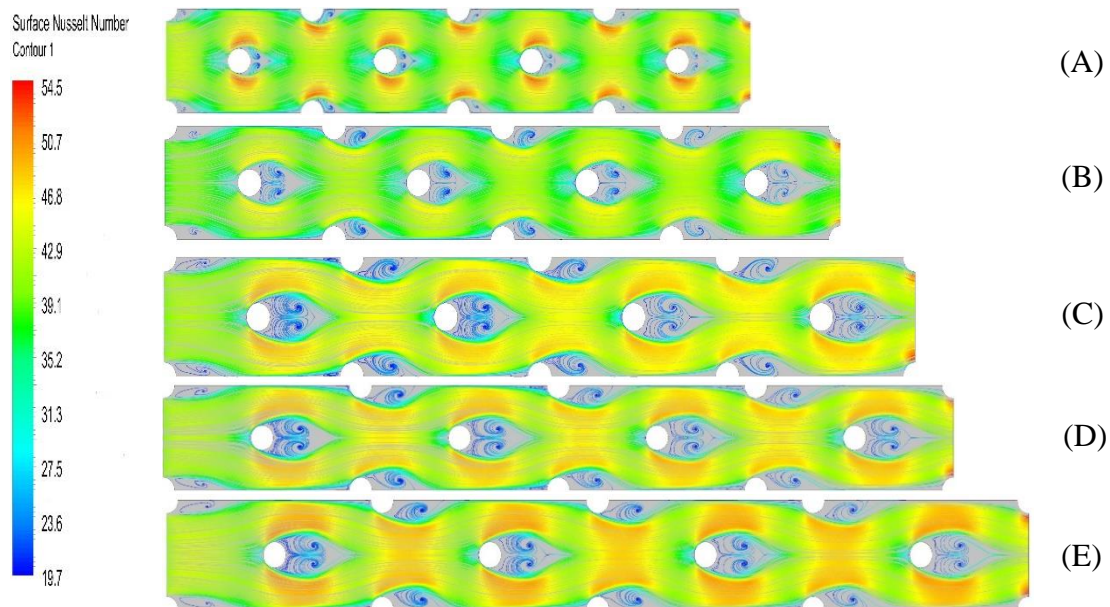


**Fig. 4.10** Surface Nusselt number contour of different pillow-plate channel configuration  $L_{A,11-E,15} = (256-384$  mm (Case 11 to 15)) of the PPC at  $Re = 2000$ .

The  $X_L = 64$  and  $72$ -mm channels with SCWSCs possess the highest values of  $Nu$ . It can be explained that these configurations generated higher ‘‘elliptical vortex’’ pairs. At the same time, if we have discussed the  $d_{cws}$  from  $8$  to  $12$  mm in each case  $d_{cws} = 9$  mm and  $d_{cws} = 10$  mm welding spot diameter developed higher  $Nu$  than other  $d_{cws}$  i.e.,  $8$  mm,  $11$ , and  $12$  mm. The overall conclusion is that the higher flow acceleration and more

intensified “elliptical vortex” configuration in the channel  $X_L = 64$  and  $72$  mm produced higher thermal performance than other channels (including the straight elliptical channel). Moreover, the variation of  $Nu$  with  $Re$  is very close in all cases of  $L_A$  and  $L_B$ . Therefore, according to the author’s opinion, it is very challenging to say which channel length either  $L_A$  and  $L_B$  provides better heat transfer performance because the value of  $Nu$  with  $Re$  from  $1000$ - $16,000$  is almost identical. Therefore, it should be optimized with the help of different multi-objective optimization techniques in the next step.

Fig. 4.12. depicts the variation of friction factor ( $f$ ) with the various  $Re$  for the case Cases A-E ( $L_{A,1-E,25}$ ), i.e.,  $d_h/X_L = 0.078$ - $0.041$ . Due to the SCWSPs, the  $f$  increases inside the PPHE. It's important to consider that the pressure decrease occurs precisely where the CWS is situated. Addollahi and Shams [97] demonstrated that the pressure coefficient varies similarly in a straight elliptical channel and a channel with vortex generators through the location of the vortex generators but subsequently drops sharply at the vortex generators. The  $f$  again appears to rise as the  $Re$  rises. Between  $4000$  and  $16,000$ , the  $Re, f$  increases by around  $3.29\%$  to  $16.91\%$ . The lowest and highest  $f$  is found in the higher and lower  $L_{A-B}$  respectively, than the straight elliptical channel arrangement. It is argued that the ‘elliptical vortex’ and the secondary flow on the convective heat transfer coefficient in higher streamwise channel length are not much more significant, as Shirzad et al. [24] mentioned. As the results increase the channel’s streamwise size, the flow becomes more linear, reducing the velocity and pressure resistance across the channel, as mentioned in Fig. 4.6 and Fig. 4.7 (A-E). Therefore, based on the numerical simulation results, the maximum  $f$  at  $Re = 1000$  is  $24.31\%$ ,  $21.10\%$ ,  $19.68\%$ ,  $17.61\%$ , and  $15.10\%$ , while the minimum  $f$  at  $Re 16,000$  is  $7.12\%$ ,  $5.84\%$ ,  $4.38\%$ ,  $3.21\%$ , and  $2.06\%$  occurred for Case A-E, respectively, compared to the without SCWSPs channel.

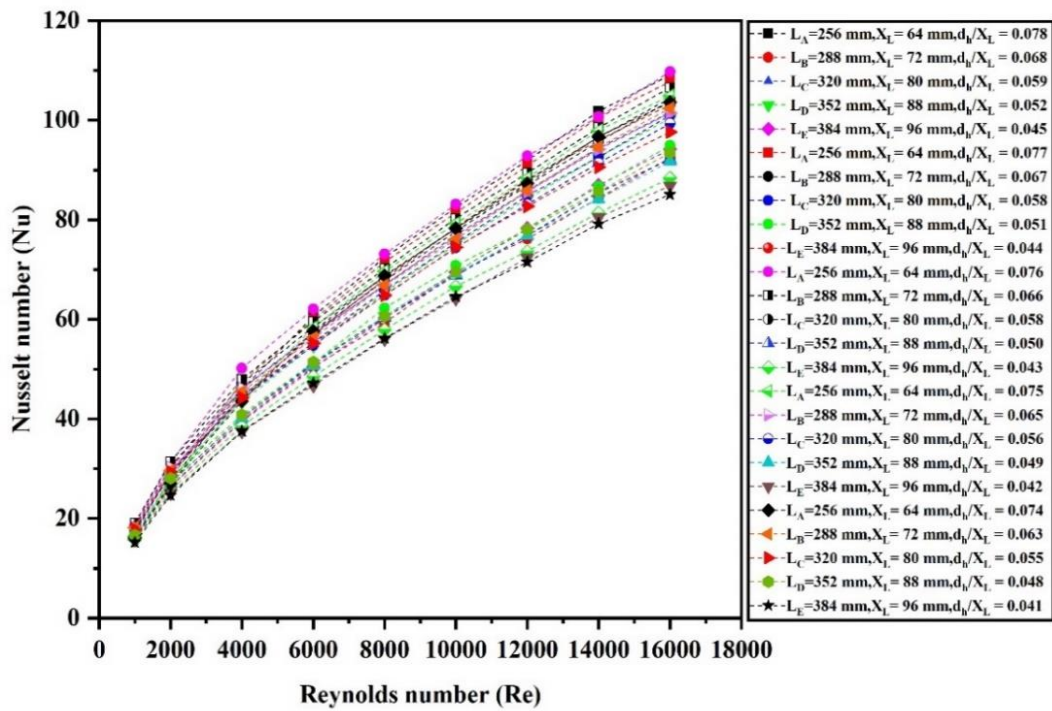


Fig. 4.11 Variation of Nusselt number ( $Nu$ ) vs. Reynolds number ( $Re$ ).

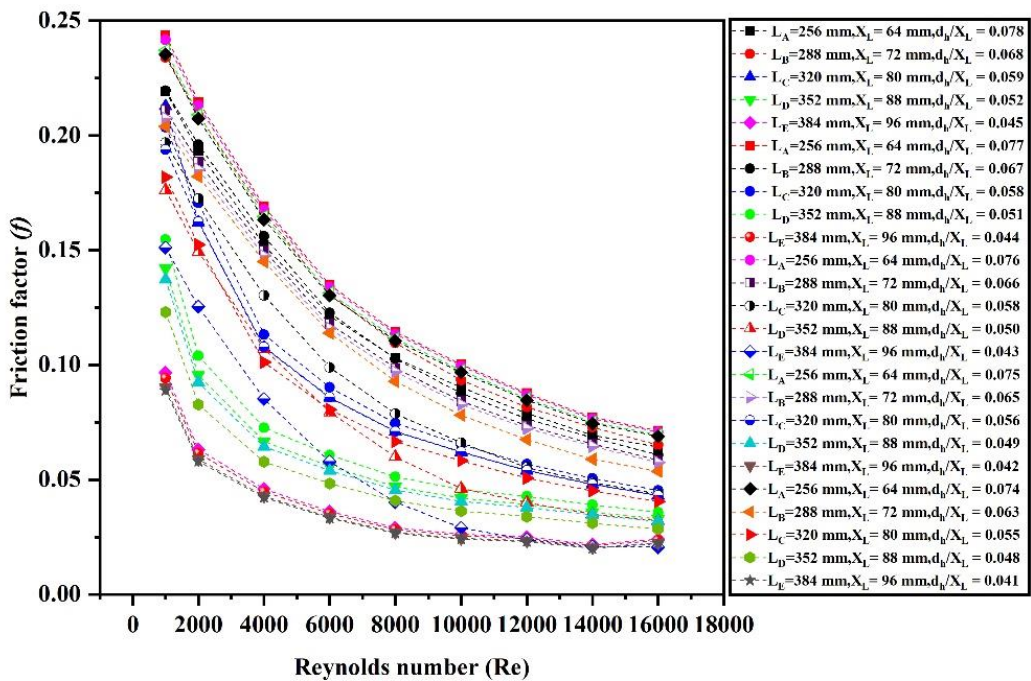
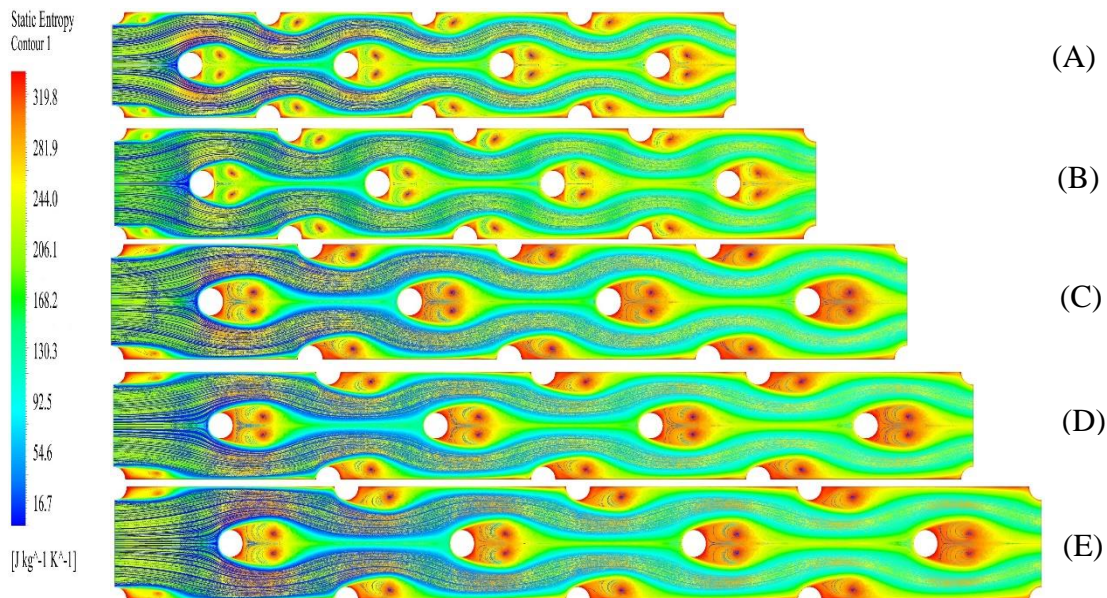


Fig. 4.12 Variation of Friction factor ( $f$ ) vs. Reynolds number ( $Re$ ).

#### 4.6.4 Thermal and frictional entropy generation

The relationship between the change in the  $Re$  and the fluctuation in the overall EG (Thermal and frictional entropy generation) is depicted in Fig. 4.12. For examining the PPHE's exergy efficiency ( $\eta_{ex}\%$ ), it is required to calculate the entropy generation value. Because for the exergetic performance enhancement of the PPC, the low entropy generation or optimum exergy efficiency is the essential factor. It has been noticed that there is an opposite correlation between increases in the  $Re$  and decreases in the overall EG. It is important to note that at low, i.e.,  $Re < 2000$ , the EG is mainly influenced by the heat transfer comparison with  $f$  in the PPHE. An increase in the  $Re$  causes a rise in the heat transfer rate while simultaneously reducing the irreversibility of the heat transfer. When the  $Re$  is increased, the temperature of the surface of the heat source drops. This results in a minor temperature difference between the fluid and the heat source, reducing the amount of entropy generated during the heat transfer process. Because heat transfer entropy production is the primary factor in the total EG, the total EG similarly decreases as the  $Re$  increases.



**Fig. 4.13** Entropy generation contour of different pillow-plate channel configuration  $L_{A,11-E,15} = (256-384 \text{ mm (Case 11 to 15)})$  of the PPC at  $Re = 2,000$ .

Using the Eq. (4.2) the  $\dot{S}_{g,T}$  of all the Cases  $d_h/X_L = 0.041-0.078$  is calculated, and all values are mentioned in Fig. 4.13 at the different  $1000 \leq Re \leq 16,000$ . The graph of  $\dot{S}_{g,T}$  (thermal entropy generation) is the dependent variable on the  $Re$  with various of  $X_L$

( $L_{A,1-E,25}$ ) and  $d_{cws} = 8-12$  mm. In Fig. 4.14, It is observed that, the  $S_{g,T}$  continuously enhancing with  $Re$  for all the cases of PPHE with SCWSCs than the straight elliptical channel (without SCWSCs). It is attributed that for all the inlet velocities the  $S_{g,T}$  increases and the  $h_{conv}$  decreases with  $Re$ , while the temperature gradient scattering through the channel is higher with an increase in the longitudinal length and surface of the medium. This phenomenon and mechanism may be interrelated to an increment in the entropy generation of the hot water (fluid flow), as thermal entropy generation is known to be a directly dependent linear function of the temperature gradient [83]. At the smaller channel length, higher velocities are achieved due to this higher turbulence will be developed so that the value of  $Nu$  increases in Case A, B  $X_L = 64$  and  $72$  mm than other Cases C to E while in  $d_{cws}$  case from 8-12 mm, the maximum  $S_{g,T}$  occurred in the  $d_{cws} = 12$  mm CWS compared to other cases, i.e., 8-11 mm in every channel length. The highest results of thermal entropy generation occur in the smallest values of  $d_h/X_L = 0.041$  for Case E ( $L_{E,25}$ ) and the lowest at the highest value of  $d_h/X_L = 0.078$ , Case A ( $L_{A,1}$ ). The maximum value of  $S_{g,T}$  is 5.41%, 0.80%, 11.91%, 15.76%, and 22.38% for Case A-E ( $L_{A,11-E,15}$ ) respectively, at  $Re = 16,000$ .

Besides the  $S_{g,T}$ , the contour of the velocity profile demonstrates that the generation of a high majority of  $S_{g,F}$  is associated with two specific distinct sections: the interaction region between the fluid and solid surface of the channel and the place where the slow flow faces higher velocity. According to Eq. (3.19), in the contact region of the fluid flow and channel surface, the velocity gradient is strong due to the influence of the channel wall, resulting in a high rate of  $S_{g,F}$  is generated. In some parts of the contact regions with backflow and ‘elliptical recirculation vortex’, the  $S_{g,F}$  values are minimum. The FEG (Friction Entropy Generation) variations against the  $Re$  for the PPHE are seen in Fig. 4.15. (b). Clearly, the FEG increases with an increase in the  $Re$ . Note that the fluid friction increases as the  $Re$  becomes more extensive, which increases the friction irreversibility. Besides this, the strength of the ERV increases with an increase in the  $Re$  due to the fluid’s viscosity diffusion. Moreover, the FEG is higher for the SCWSPs in the channel, especially at higher values of the  $Re$ . The FEG increases by installing the SCWSPs inside the PPC. Note that the elliptical recirculation flow occurs in the channel by the SWCSPs. This recirculating flow leads to more friction and subsequently increases the FEG.

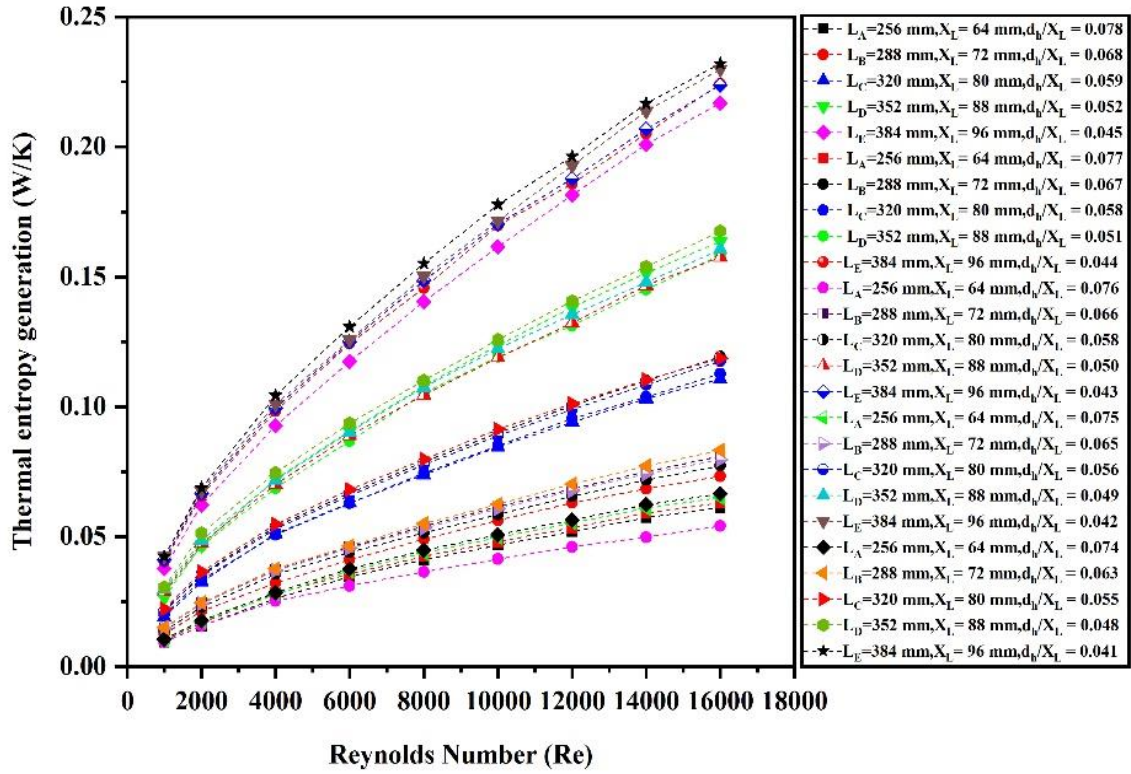


**Fig. 4.14** Thermal entropy generation vs. Reynolds number.

Based on this computational numerical simulation, as mentioned in Fig. 4.6, Fig. 4.8 and Fig. 4.9, it is attributed that in the ‘elliptical recirculation vortex’ formation region, the velocity distribution is more uniform or linear inside the Pillow-plate type channel, and the velocity gradient is not much significant as compared with the straight elliptical channel duct without SCWSPs, which diminishes the establishment rate of  $\dot{S}_{g,F}$ . Since the velocity distribution in the ‘elliptical vortex’ region near the SCWSCs and the wall is uniform, the fluid flow's velocity gradient is minimal. Consequently, small  $\dot{S}_{g,F}$  is developed inside the pillow plate in this region. While at the inlet and outlet boundary wall between the vortex pair and central zone of the channel, due to the low and high-velocity flow, a significant high-velocity gradient is generated because the size and shape of the ‘elliptical vortex’ pair change with SCWSCs, sometimes the ‘elliptical vortex’ pair is equal to the diameter CWS. Therefore, the velocity gradients behind the SCWSCs are also greater, causing high friction entropy generated. The overall conclusion of the section is that the influence and involvement of the  $\dot{S}_{g,F}$  to the total entropy generation is much more significant than the

$\dot{S}_{g,T}$ . The maximum value of the friction entropy generation ( $\dot{S}_{g,F}$ ) is 28.75%, 28.18%, 21.00%, 18.74 and 15.77% occurred at  $Re = 16,000$ .

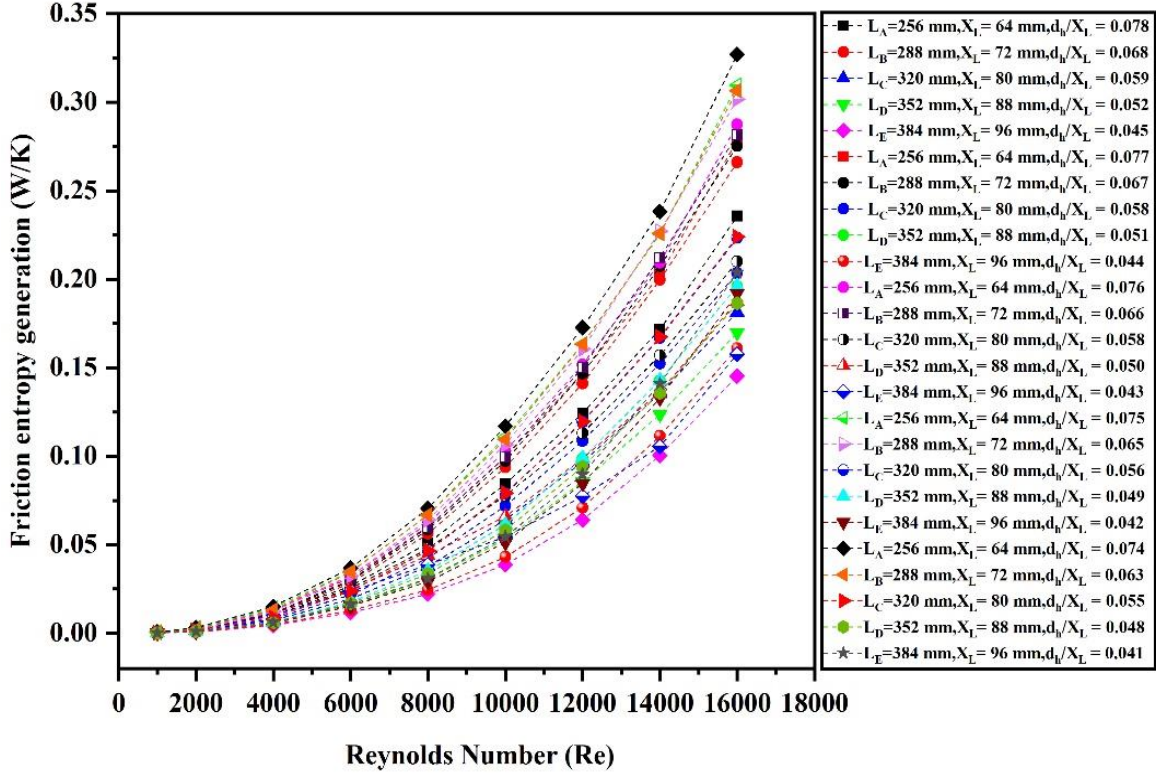


Fig. 4.15 Frictional entropy generation vs. Reynolds number.

#### 4.6.5 Thermal and frictional exergy destruction

In the second low thermodynamic, there is excess destruction in essential parameters to measure resource degradation. Exergy destruction assesses the degraded resources and specifies the elements in the resources where degradation occurs. Due to the irreversibilities of the system (In this study, we have discussed about the PPHE), the exergy degradation decreases. Using the Eqs. (4.6) and (4.7) the  $\dot{E}x_{dest,T}$  and  $\dot{E}x_{dest,F}$  is calculated and plotted these values against the  $1000 \leq Re \leq 16,000$  in Fig. 4.16. The maximum  $\dot{E}x_{dest,T}$  is 16.13, 24.11, 35.31, 46.96, and 66.69 W for water flowing through the PPC at  $Re = 16,000$  for Case A-E ( $L_{A,11-E,15}$ ), respectively.

In Fig. 4.17 it is observed that  $\dot{E}x_{dest,F}$  continuous increases with decreases in the channel length configurations while increases with SCWS diameter in all the cases from ( $L_{A,1-E,25}$ ) with  $Re$  because the velocity gradient of fluid is more significant. Another



reason is the higher velocity gradient between the fluid and channel surface domain. Another essential enhancement factor of the  $\dot{E}x_{dest,F}$  is friction factor ( $f$ ) higher in the channel with SCWSPs than in a medium without SCWSPs. The  $\dot{E}x_{dest,F}$  of the PPC against the influence of  $Re$  is shown in Fig. 4.17. The  $\dot{E}x_{dest,F}$  increment for ( $L_{A,11-E,15}$ ),  $d_{cws}=10$  mm is 0.18-85.67, 0.074-83.98, 0.069-62.58, 0.075-55.83, 0.096-46.98 W for the water through the Pillow-plate type heat exchanger  $Re$  varies from 1000-16,000.

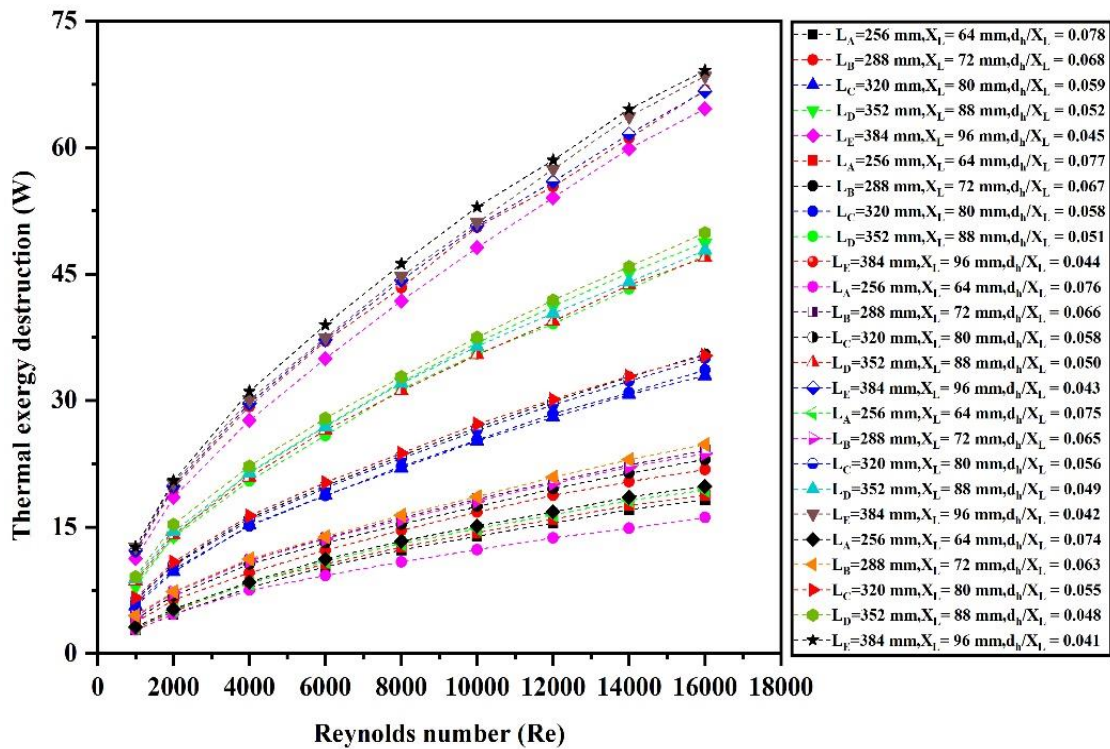


Fig. 4.16 Thermal exergy destruction vs. Reynolds number.

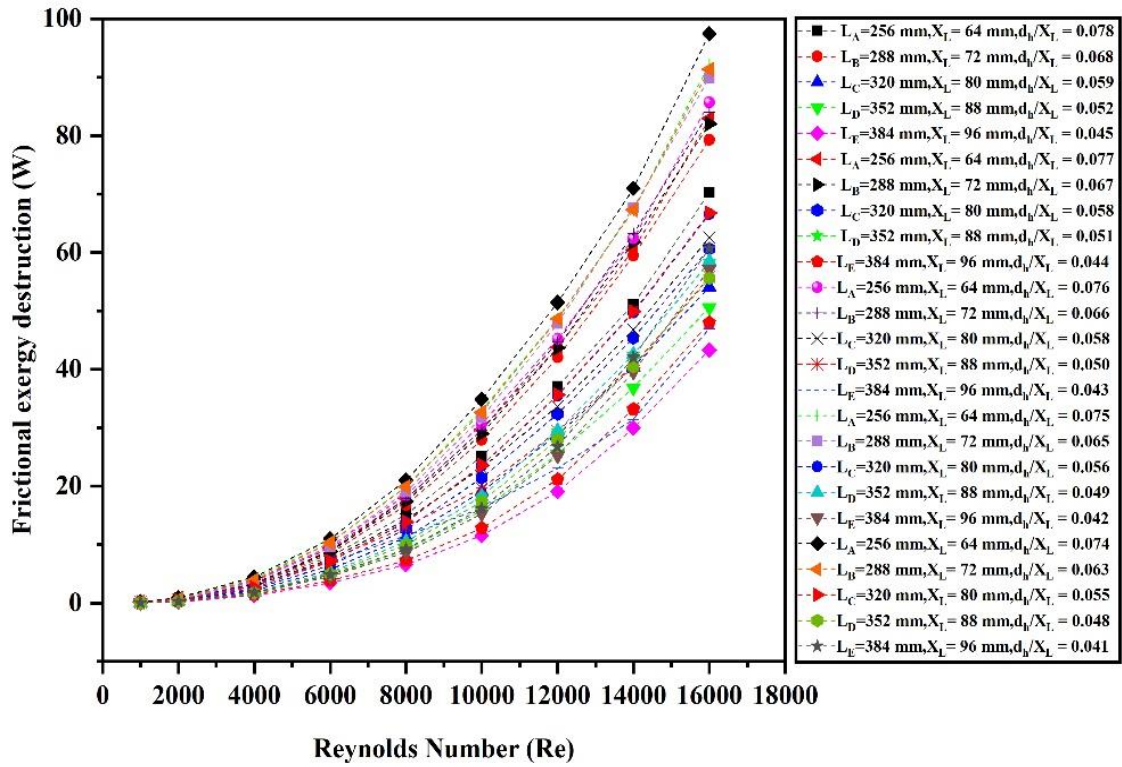
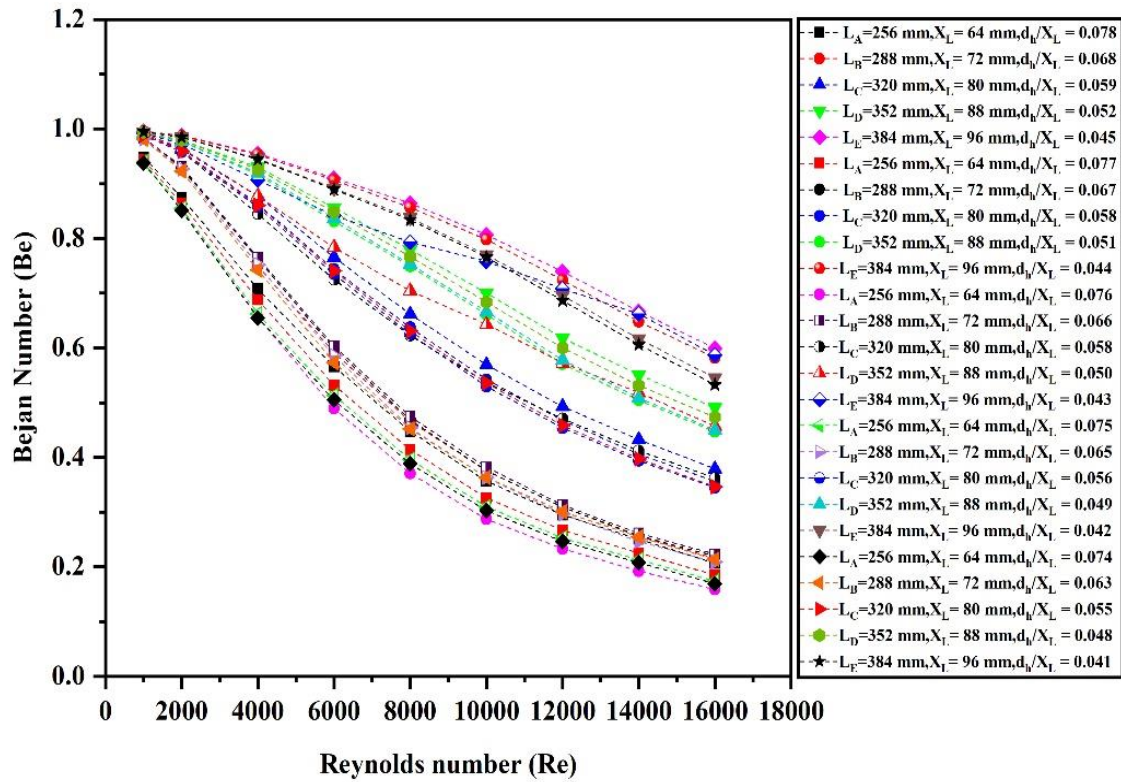


Fig. 4.17 Frictional exergy destruction vs. Reynolds number.

#### 4.6.6 Bejan number and entropy generation number

Fig. 4.18 depicts the Bejan number ( $Be$ ) of water passing through the closed pillow-plate enclosure channel at various  $Re$ . The ratio of thermal entropy generation to total irreversibility (due to frictional and heat transfer) is known as the Bejan factor (number). The Bejan number is a dimensionless or unitless parameter. The influence of  $\dot{E}x_{dest,F}$  of the Pillow-plate type heat exchanger with the effect of  $\Delta p$  is reduced as the Bejan number approaches one. The maximum number of the Bejan factor ( $Be$ ) specified that the entropy generation enhanced due to the convective heat transfer rate compared to the frictional entropy generation and internal irreversibility.



**Fig. 4.18** Bejan number vs. Reynolds number.

The Bejan number gradually decreases with  $Re$  from 1000-16,000 due to increases in the pressure resistance. The maximum increment of the Bejan number occurred at  $Re = 1000$ , and the value is 0.94, 0.98, 0.98, 0.99, and 0.99 from Cases A-E, respectively. The total extraction of internal irreversibility in the PPHE is unfeasible or unattainable; in all the case  $d_h/X_L = 0.041-0.078$  in that case; therefore, the Bejan factor (Be) does not approach 1. By increasing the longitudinal (streamwise) channel length with SCWSPs from  $LC-E = 80-96$  mm, the internal irreversibility decreased due to low turbulence enhancement compared with the  $L_{A-B} = 64-72$  mm. Hence, the heat transfer involvement of the fluid is insufficient due to the total irreversibility when the Reynolds number increased from 1,000-16,000.

Whereas Fig. 4.19. shows the influence of  $X_L$  and  $d_{cws}$  values on dimensionless  $N_s$  of Pillow-plate type heat exchanger configuration and the straight elliptical channel with SCWSPs as a function of  $Re$ . The fixed parameters value is taken as mentioned in section 3.2. From the Fig. 4.19. It can be concluded that the increasing rate of the  $N_s$  against the values of  $X_L$ , and  $Re$  continuously. This tradeoff behavior of the graph can be seen in

every Case A-E ( $L_{A,11-E,15}$ ). Based on the computational information, the results of  $N_s$  reduces with increases the  $d_h/X_L$  ratio, i.e., the values of  $N_s$  minimum for the  $d_h/X_L=0.076$  as compared to  $d_h/X_L=0.043$ . However, the values of  $N_s$  for the straight elliptical channel is not much higher than PPC with SCWSPs for all values of  $Re$ . In addition, Fig. 4.19. illustrates that a similar increasing trend is followed by  $N_s$  as a function of  $Re$  for all four values of  $d_{cws} = 8, 9, 10,$  and  $11$  mm compared with the straight elliptical channel without SCWSPs. The values of  $N_s$  is smaller for  $d_{cws} = 8$  mm compared to  $d_{cws} = 9$  mm,  $d_{cws} = 10$  mm and  $d_{cws} = 11$  mm. On the other hand, the straight elliptical channel has lower values of  $N_s$  as compared to all values of  $d_{cws}$  and  $Re$ .

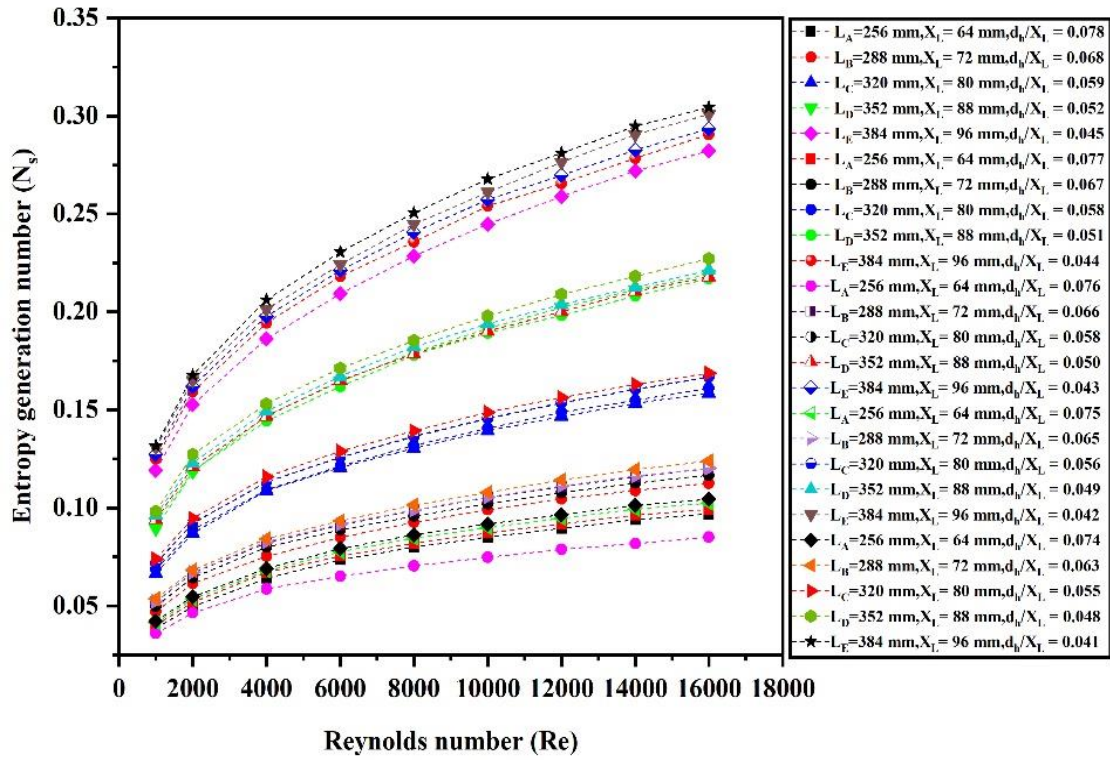
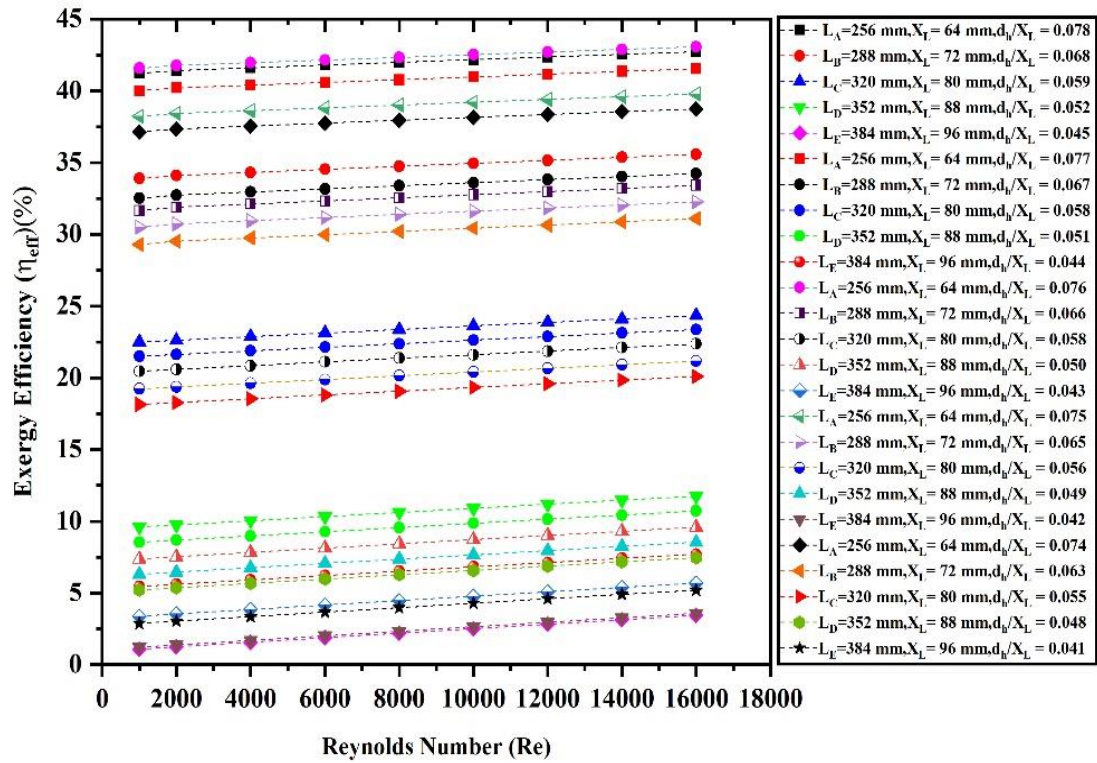


Fig. 4.19 Entropy generation number ( $N_s$ ) vs. Reynolds number ( $Re$ ).

#### 4.6.7 Exergy efficiency and thermal evaluation factor

Exergy efficiency evaluates the overall effectiveness of an energy system in converting available energy into useful work, considering the quality of energy. At the same time, thermal performance factor (TPF) specifically assesses the effectiveness of a heat transfer

system in transferring heat between media, without considering the quality of energy. Both metrics are important for evaluating and optimizing different energy systems, providing complementary insights into their performance. Higher exergy efficiency reflects higher energy quality used in the pillow plate channel, making the system more sustainable. In contrast, lower exergy efficiencies reflect energy losses and irreversible internal responses, resulting in low energy quality and a lower sustainable score. In other words, a reduction in the heat dissipation during the flow to the environment and higher heat transfer rate exchange between the cold and hot fluid resulting the higher turbulence is a crucial aspect of higher exergy efficiency and the thermal evaluation factor of the PPC. The Fig. 4.20 represent the maximum and minimum  $\eta_{ex}\%$  for all Cases ( $L_{A,1-E,25}$ ). The  $\eta_{ex}\%$  increasing with decreasing the streamwise length and the increasing  $Re$ . Due to the SCWSPs leadership, a ‘sinusoidal wave’ formation is developed inside the channel, creating an ‘elliptical vortex’ behind the CWS. This ‘elliptical vortex’ is more significant in the lower longitudinal length than the higher longitudinal length and straight elliptical channel; for all the Cases ( $L_{A,1-E,25}$ ). Due to this computational simulation visualization, it is attributed that the exergy loss is minimum in the lower streamwise length relative to other streamwise sizes and a straight elliptical channel without SCWSCs. In contrast, compared to lower  $d_{cws}$  i.e., 8, 11, and 12 mm, the higher exergy efficiency or lower exergy loss occurred in the  $d_{cws} = 9$  mm and 10 mm, from  $Re = 1,000-16,000$ . Identical phenomena and results to explain the increases or decreases of exergy efficiency for other cases  $L_{A,1-E,25}$ . This computational observation may be attributed to the fact that the ‘elliptical vortex formation’ is not much significant in the higher  $L_{C,E} = 320, 352, \text{ and } 384$  mm, hence low irreversibility and fluid separation occurred on the surface of pillow-plate type HEs. In addition, there might be another reason for heat transfer augmentation is better to contact between fluid flow and the pillow-plate channel surface.



**Fig. 4.20** Exergy efficiency vs. Reynolds number.

In other words, compared to the higher longitudinal length  $L_{C-E}$  and straight elliptical channel enclosure duct, the exergy loss is minimum in  $L_A$  and  $L_B$ . These results could be attributed to a low-temperature gradient distribution in the ‘elliptical vortex’ flow rate causing low turbulence strength and less irreversibility, which causes reduced exergy loss behind the SCWSPs because of the expansion of the length. At the lower  $Re = 1000-2000$ , the energy utilized by the lower longitudinal length is maximum compared to the higher channel length because of the surface area. The exergy efficiency is low in the case  $L_E$  compared to  $L_A$  because of the decreases in the flow rate resulting in the reduction in turbulence and less irreversibility, which are responsible for the low exergy efficiency. However, the decreased entropy generation of the fluid in the case  $L_A$ , while higher turbulence and the rate of irreversibilities in the PPC lead to enhanced exergistic efficiencies. A similar argument may be used to explain the increases or decreases in exergy efficiency for other cases.

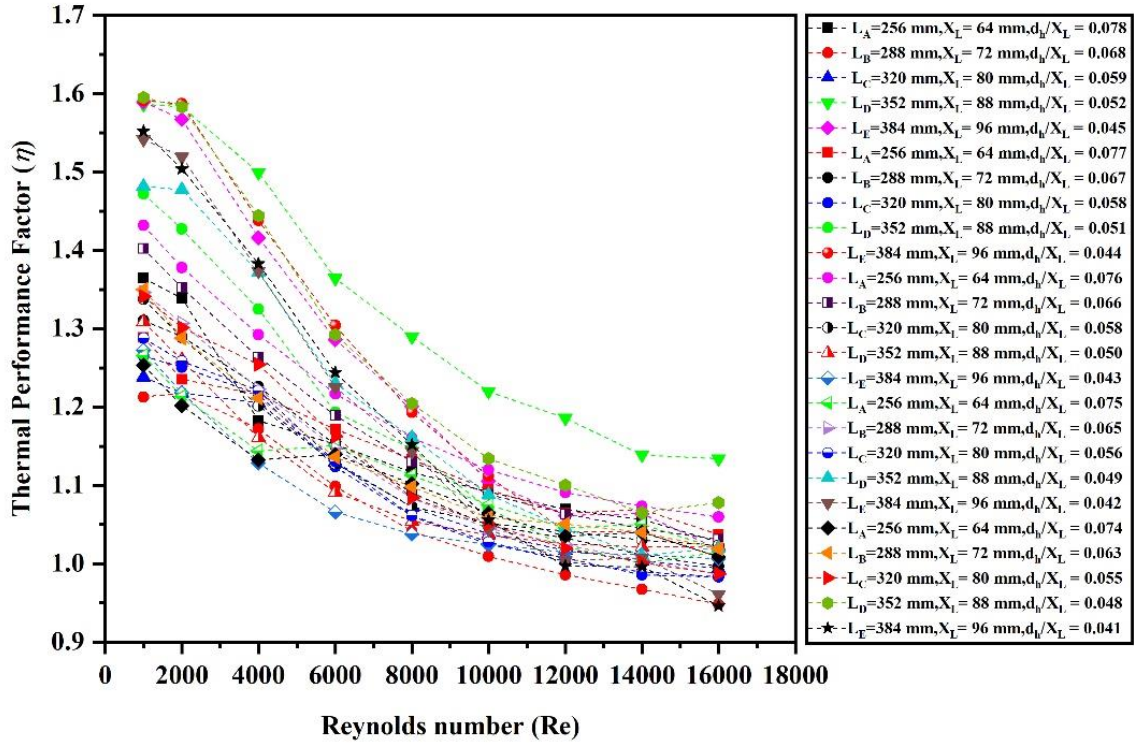


Fig. 4.21 Thermal evaluation factor ( $\eta_{eff}$ ) variation with Reynolds number ( $Re$ ).

The heat transfer and flow resistance must be considered together to calculate the overall performance of the PPHE. We can use thermodynamic performance or thermal evaluation factors to determine the heat exchanger's efficiency [98].

$$TEF = (Nu/Nu_0)/(f/f_0)^{0.33} \quad (4.15)$$

Fig. 4.21. illustrates the variation of  $TEF$  ( $\eta_{eff}$ ) with  $Re$  for the various PPC ( $L_{A-E} = 256-384$  mm). It can be distinguished that the  $TEF$  is directly dependent on  $Nu$  and  $f$ , which means the  $Nu$  and  $f$  affect the thermal evaluation factor of the channel. In all cases  $L_{A-E}$ , the  $TPF$  is more than unity for  $Re = 1000-16,000$ . The maximum  $TPF$  occurs at  $Re$  1000-2000. But when  $Re$  increases further (4,000-16,000) for all Cases of  $L_{A-E} = 256-384$  mm, the  $TPF$  starts decreasing. The thermal performance evaluation is enhanced by a factor of approximately 1.25-1.43 ( $r = 0.074-0.078$ ), 1.21-1.35 ( $r = 0.063-0.068$ ), 1.14-1.34 ( $r = 0.055-0.059$ ), 1.30-1.49 ( $r = 0.048-0.052$ ) and 1.27-1.52 ( $r = 0.041-0.045$ ) at  $Re = 1000-2000$ . Justifying which pillow-plate type channel is better at lower  $Re$  is challenging. Whereas, with increasing the value of  $Re = 4000-16,000$ . The case  $L_A$  and  $L_B$  with  $d_{cws} =$

9 and 10 mm provide much more significant results than other cases  $L_{C-E}$ , and straight elliptical channel. The overall conclusion is that the decrement in  $TEF$  with increasing  $X_L$  is inefficient at higher  $Re = 4000-16,000$ . Note that, it is possible for a particular streamwise length of a PPHE to have different values for exergy efficiency and thermal performance factor. This discrepancy arises because exergy efficiency and thermal performance factor measure different aspects of the PPHE's performance. Exergy efficiency evaluates the overall effectiveness of the PPHE in converting available energy into useful work or energy output while considering the quality of energy and accounting for irreversibility in the process. This measure considers factors such as fluid friction, heat transfer across finite temperature differences, and mixing, which can impact the exergy efficiency of the PPHE.

On the other hand, the thermal performance factor  $(Nu/Nu_0)/(f/f_0)^{0.33}$  specifically assesses the effectiveness of the PPHE in transferring heat between media, without considering the quality of energy (work). It evaluates the ratio of actual heat transfer achieved by the PPHE to the input energy or work required for that heat transfer, focusing solely on the thermal aspects of the system.

Therefore, different operational conditions, design parameters, or system configurations may lead to variations in exergy efficiency and thermal performance factor for the same length of the pillow-plate heat exchanger. For example, changes in fluid flow rates, temperatures, or materials may affect the exergy efficiency differently than their impact on the thermal performance factor (TPF). As such, it is essential to consider both metrics independently when evaluating the performance of the heat exchanger and optimizing its design or operation.



# Chapter - 5: Effect of SCWSP-VGs on Thermal-Hydraulic Performance of Pillow-Plate Heat Exchanger (PPHE)

---

Vortex Generators (VGs) are an innovative heat transfer enhancement in traditional heat exchangers. With this technique, the study investigates the combined impact of upper-lower Staggered Circular Welding Spot Patterns (SCWSP) and VGs, termed SCWSP-VGs, in a periodic enhanced Pillow-plate type heat exchanger (PPHX) using ANSYS Fluent 18.1. Numerical results reveal SCWSP-VGs induce a periodic velocity profile and opposite elliptical recirculation vortex (OERV) turbulence, significantly improving thermo-hydrodynamics compared to straight elliptical channels.

## 5.1 Introduction

The rapid development of technology for heat transmission within heat exchangers (HXs) is evidence of the widespread interest of the research community in potential applications. The evolution of thermal devices, combined with enhanced computational simulation capabilities, has transformed channel surfaces to optimize heat transmission and meet stringent efficiency and performance criteria. Despite these advancements, the inherent challenge of efficient heat transfer in HXs persists, primarily because of lower surface-to-volume ratios.

Several types of conventional heat exchangers, such as Compact heat exchangers (CHXs) [99], Triple tube heat exchangers (TTHXs) [100], Helical coil heat exchangers (HCHXs) [101], Twisted double-pipe heat exchangers (TDPHXs) [102], Fin and tube heat exchangers (FTHXs) [103], a Spiral wound heat exchanger (SWHXs) [104], Concentric heat exchanger (CHXs) [105] and Plate heat exchangers (PHXs) [106], have found extensive applications in diverse fields, including HVAC&R, manufacturing processes, electronics cooling, aerospace, defense, solar, and automobile engineering [107].

Enhancing the thermal performance of the above traditional HXs often involves various augmentation techniques, focusing on artificially roughened surface modifications. Strategies such as disrupting boundary layer formation, increasing turbulence intensity, utilizing high thermal conductivity working fluids, and inducing secondary flows are commonly employed. Notably, vortex generators (VGs) are pivotal in improving heat transfer efficiency in certain conventional HXs. Extensive research in published literature

investigates the heat transfer performance of traditional HXs incorporating different VGs, employing experimental and numerical methods. Common geometric forms of VGs include multiple V-shaped ribs and grooves [98,108] (used in solar heaters), triangular winglets, rectangular winglets, trapezoid winglets, and wavy grooves [109].

In this regard, Ahmed et al. [110] and Biswas et al. [111] have thoroughly examined active approaches for improving VG performance, including rectangular winglet pairs, delta wings, and delta winglets. The generation of longitudinal vortices by VGs and/or tubes enhances heat transfer without imposing a substantial heat penalty. Furthermore, VGs are adept at directing upstream fluid flow effectively, thereby impeding reflux and reducing the area of the wake region. Habchi et al. [112] numerical investigations reveal that counter-rotating vortices, induced by VGs, significantly contribute to the heightened heat transfer coefficients observed in multifunctional heat exchangers. Lei et al. [113] employ Computational Fluid Dynamics (CFD) methods to examine heat transfer characteristics using delta-winglet VGs in parallel studies. Their findings indicate that VG configurations in a common-flow-up arrangement accelerate fluid flow, postpone separation, and augment heat transfer. Moreover, as Reynolds numbers increase, heat transfer coefficients also rise. The strategic combination of circular tubes and winglet pairs demonstrates noteworthy enhancements in the overall performance of the heat exchanger.

The investigation into techniques for enhancing heat transfer, particularly through the application of vortex generators (VGs), remains a central focus in the heat exchanger (HX) research [113]. The literature review emphasizes the crucial role of VGs in directing fluid flow, minimizing wake regions, and optimizing heat transfer across diverse heat exchanger configurations [114]. Continued progress in understanding the underlying mechanisms and key parameters influencing heat transfer will play a pivotal role in the ongoing development of heat exchanger technology.

The current literature explores diverse methods to enhance heat transfer, encompassing artificial roughness, turbulators, and various types of winglets on heat exchanger surfaces. In other words, existing research on PPHX predominantly concentrates on performance analysis involving different working fluids, structural parameters, and turbulence techniques as shown in Table 5.1. Against this background, a substantial research gap exists in understanding the role played by vortex generators (VGs), particularly the concept, mechanism, and phenomena associated with PPHXs. This manuscript introduces a unique approach by proposing and implementing Staggered

Circular Welding Spot Patterns-Vortex Generators (SCWSP-VGs), strategically punched onto pillow-plate surfaces.

Conventional heat transfer techniques utilized in various thermal industry applications are inadequate to meet the escalating demands placed on HXs. While Pillow-plate type heat exchangers (PPHX) have gained popularity owing to their design flexibility, structural integrity, and cost-effective production process, there is a pressing need for further enhancements in their energy saving, heat transfer capabilities, and overall thermal performance.

The PPHX is a distinctive type of HX characterized by an intricate wavy structure [64], whose fabrication design and performance similarities to Plate Heat Exchangers (PHXs). The PPHX consists of a singular sealed component with entry and exit points. The two plates are seam-welded at the ends and sides, while the central section is laser spot-welded in either an aligned or alternated (staggered) pattern. Hydroforming expands the two welded metal sheet plates, creating an internal flow channel with mainstream velocity. The inline or staggered arrangements of the spot-welding patterns influence the thermo-hydraulic performance of PPHXs. Due to its completely sealed channel, it finds ideal applications in the food, chemical, and pharmaceutical industries and in HVACR and scenarios involving toxic fluids. Material and manufacturing limitations play an important role, with the materials' thermal conductivity and corrosion resistance inducing the available shapes. In addition, the three-dimensional wavy profile promotes flow separation, enhancing mixing and the rate of heat transfer augmentation.

Piper et al. [8] recently proposed a reliable design method for PPHXs based on forming simulations, accurately replicating the automatic three-dimensional wavy PPCCs by modeling the industrial PP process. However, this method falls short of determining the optimal structural parameters for PPHXs. Another study by Vocciante et al. [30] utilized Open-FOAM simulation software to explore various turbulence techniques ( $3000 \leq Re \leq 8000$ ) in the PPC. Their research focused on pressure losses, revealing that DES (Detached Eddy Simulation) presented a beneficial arrangement, exhibiting lower computational costs and easier organization than LES (Large Eddy Simulation) simulation.

Enhancing heat transfer through VGs (vortex generators), turbulence promoters, or turbulators represents a passive method to generate streamwise vortices, inducing significant turbulence in fluid flow across heat transfer surfaces. VGs disrupt the flow field and boundary layer growth and induce fluid swirling, promoting a robust exchange of

core and wall fluid. This, in turn, leads to improved heat transfer between the flowing fluid and the channel walls [115].

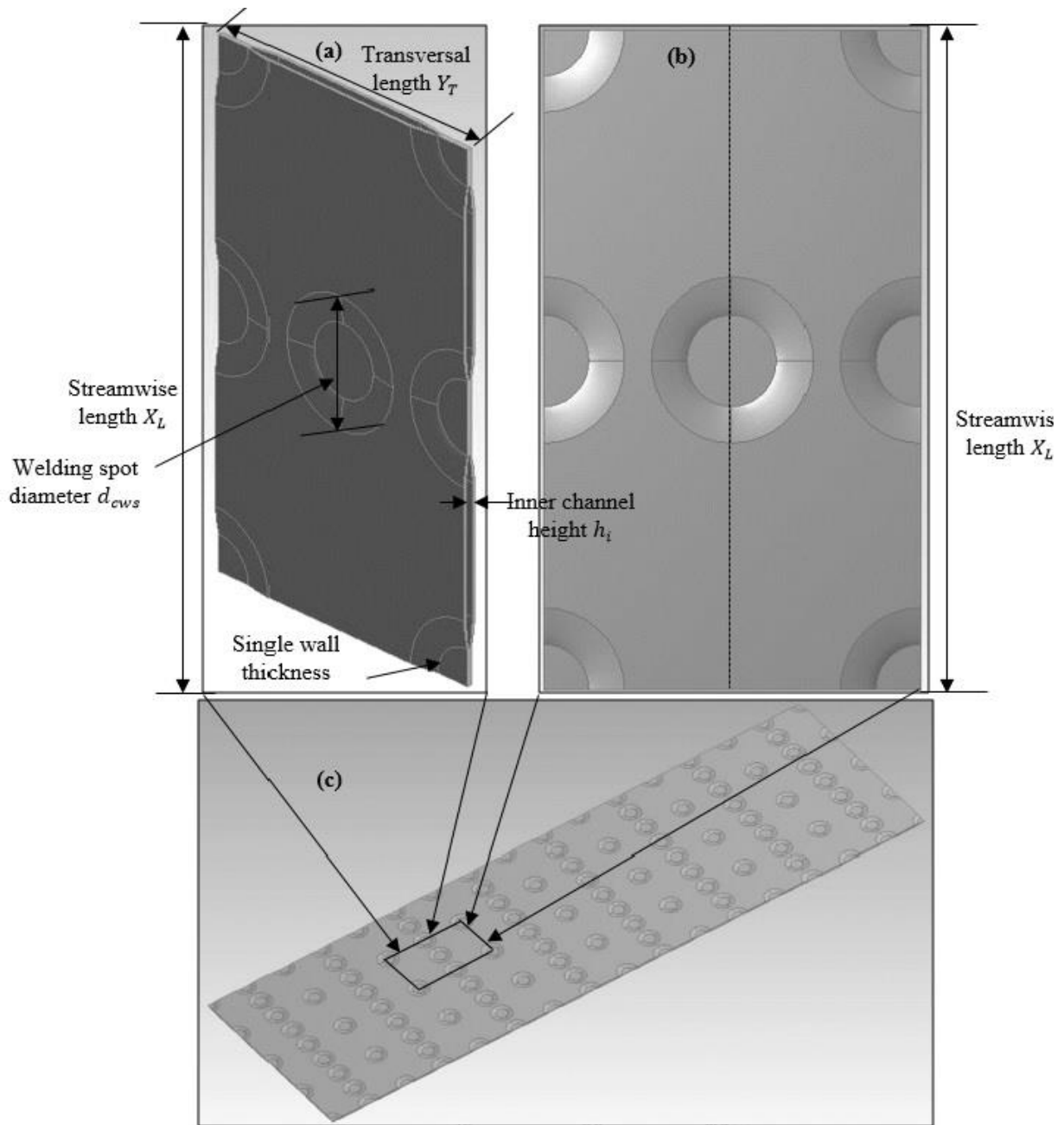


**Fig. 5.1** Schematic diagram of PP (a) Isometric view (b) Top view (vertical cut) (c) PPC

## 5.2 Objectives

The PPC with SCWSP-VGs can be characterized in non-dimensional form by the following parameter: -

$$s_r = X_L - d_{cws}/Y_L - d_{cws} \quad (5.1)$$

This entity is equal to one for an equidistant configuration ( $X_L - d_{cws} = Y_L - d_{cws}$ ), smaller than one for a spanwise configuration ( $X_L - d_{cws} < Y_L - d_{cws}$ ) and greater than one for a streamwise configuration  $X_L - d_{cws} > Y_L - d_{cws}$ . The hydraulic diameter ( $d_h$ ) is determined according to the technique proposed in [9]. Fig. 5.1 shows a schematic channel domain diagram for the PPC. The PPC system in the current work is a horizontal rectangular channel of five different configurations (four channel) with a total length (cases A-E)  $L_{A-E} = 256$  mm, 288 mm, 320 mm, 352 mm, and 384 mm as shown in Fig.5.1 (a, b, (single channel) and c) and Table 5.1. In the Fig. 5.1 (c) we have mentioned eight channels but due to computational effort reduce it up to fourth section/channel. The whole PPC categorized in four sections, i.e. entry section (first channel), working section (second and third channel), and exit section (fourth channel) for all the cases A-E. The entry and working section provide completely developed flow distribution condition while the exit section reduces the effects of downstream disturbance. In this simulation, it is assumed that the flow distribution inside the channel is uniform, and any potential effects of maldistribution, which may arise due to improper configuration and the complex geometry of the PPHX, are disregarded. Case B (Fig. 5.2) is reference geometry  $X_L = 72$  mm,  $Y_T = 42$  mm,  $h_i = 3.4$  mm and  $d_{c,ws} = 10$  mm are taken as the computational domain for the validation depicted in Fig. 2. Various values of  $X_L$ ,  $Y_L$ ,  $d_{cws}$ ,  $h_i$ ,  $d_h$  and  $s_r$  [21] are reported in Table 5.1.

**Table: 5.1** Currently used numerical parameters in computational investigations (all dimensions in mm).

Cases	$X_L$	$L_{A-E}$	$Y_L$	$d_h$	$r=d_h/X_L$	$h_i$	$d_{cws}$	$s_r$
A	64	256	42	4.86	0.076	3.4	10	1.69
B	72	288	42	4.76	0.066	3.4	10	1.94
C	80	320	42	4.58	0.057	3.4	10	2.19
D	88	352	42	4.36	0.049	3.4	10	2.44
E	96	384	42	4.11	0.043	3.4	10	2.96

## 5.3 Description of the numerical Method

### 5.3.1 Computational simulation

The transition SST ( $k-\omega$ ) model is used in the current computational study to represent the turbulence phenomena in Menter's Reynolds-averaged Navier-Stokes equations (RANS) [71]. In many computational tests, the transition SST ( $k-\omega$ ) model of turbulence is more effective at forecasting the boundary layer under strong pressure adverse gradients and at solving turbulence parameters close to the wall regions. The turbulence model's equations are shown below [71].

### 5.3.2 The assumptions for the solution domain

The study of fluid flow and heat transfer characteristics considers the following fundamental assumptions:

1. The flow is 3-D (three-dimensional), incompressible fluid, turbulent flow, in a steady state.
2. The influence of gravity and other body forces is considered negligible.
3. It is assumed that the PPC wall is hydro-dynamically smooth because the study concentrates on the effects of different structural characteristics in each situation.
4. No slip boundary is used in this simulation, and the velocity is fully developed at the inlet and outlet.
5. A single-phase model is considered for simulation.
6. Viscous dissipation is ignored.

### 5.3.3 Boundary conditions and solver setting

With the following properties: specific heat ( $C_p$ ) of 4.184 kJ/(kg. K), density ( $\rho$ ) of 998.2 kg/m<sup>3</sup>, viscosity ( $\mu$ ) of  $8.90 \times 10^{-4}$  Pa.s, thermal conductivity ( $k$ ) of 0.6 W/m.K, temperature inlet ( $T_{in}$ ) of 298.15 K, and wall temperature ( $T_w$ ) of 323.15 K, water is used as the working medium. At the inlet surface, a uniform velocity profile with a velocity magnitude of 0.1875 m/s in the face normal direction—which corresponds to  $Re = 1000$ —has been provided. At the outlet plane, the outflow boundary condition is applied. Conjugate heat transfer is simplified by the transfer between the fluid and walls; this is a crucial factor since it closely approximates the actual flow circumstance. Maintaining a

consistent temperature on these walls could lead to inaccurate performance indicator estimates.

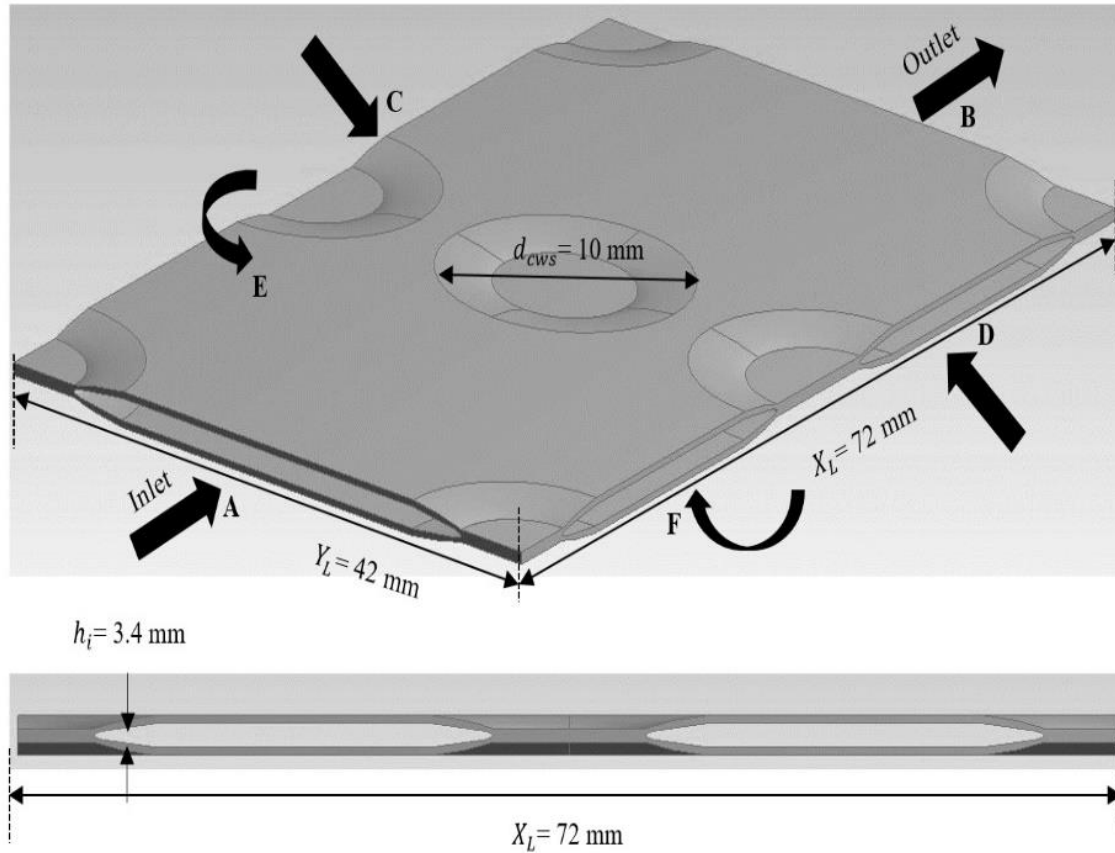


**Fig. 5.2** Schematic diagram of one PPC (a) Isometric view (b) Side view

Fig. 5.1 (a, b, and c) and Fig. 2 (one channel for reference) depict the symmetrical arrangement of PPHX geometry around the horizontal cutting lines. These two surfaces, C and D, are subjected to the symmetrical boundary condition. Because of the periodic geometry in the longitudinal direction, the flow pattern on either side of these two faces, C and D, or surface, is identical; thus, the flow can be repeated without losing simplification [76,116,117]. Therefore, PBC (Periodic boundary condition) is applied to these two faces, A and B. When both periodic and symmetrical boundary conditions are imposed, it becomes clear that the computational domain can be reduced while maintaining its essential features, as illustrated in Fig. 5.2. Because the CWS are also staggered, we only consider a longitudinal length compared to spanwise length because more effective results occur mentioned in the previous articles and journals [32,92].

The second-order upwind approach discretizes the dissipation rate and energy equations. All conservation equations have a solver tolerance of  $10^{-5}$  applied to

computations by monitoring the residues of continuity, velocity, and energy equations. To predict the values of  $Nu$ ,  $f$ , and the Colburn  $j$ -factor, steady-state simulations use the SST  $k$ - $\omega$  turbulent flow model for the entire flow field. The SIMPLEC (Semi-Implicit Method for Pressure Linked Equation Consistent) algorithm maintains pressure and velocity coupled (refer to section 3.4). The traditional scheme has been used for pressure discretization [118]. The kinetic energy and momentum of turbulent flows are discretized using the QUICK technique.

**Table. 5.2** The impact of various mesh sizes on  $Nu$ .

Type	No. of elements	Nu	Improvement in Nu	% Improvement
‘Grid-1’	1624578	61.15	-	-
‘Grid-2’	2145678	63.21	2.06	3.4
‘Grid-3’	2845712	65.96	2.75	4.4
‘Grid-4’	3512468	67.10	1.14	1.7
‘Grid-5’	4212475	67.50	0.4	0.5

### 5.3.4 Grid independence test

When discretizing the basic governing equations, creating an accurate mesh structure is important. Tetrahedral meshes are used to precisely and accurately solve the governing equations, post-processing, and obtain all necessary physical phenomenon information for the numerical simulation by simulating the fluid flow structure and heat transfer for the PP domain. To provide a consistent and precise solution independent of the grid domain at a reasonable computing cost, we verify the grid independence of five grids. Alignment in case B is considered for grid sizes between 1,624,578 (very coarse) to 4,212,475 (extremely fine). A mesh of five grids, totaling 4,212,475 grids, has been selected to carry out the computations, providing acceptable precision of the results, because the variation of the excellent grids is below 1%.

Simulation models simulate water flow inside a channel with a re-circular vortex, a longitudinal vortex, and a circular zone in the streamwise (longitudinal) direction, all with identical boundary conditions. Fig. 5.4 and Fig. 5 are taken from an experiment conducted by Tran et al. [51,76] and used to verify the accuracy of the numerical method. At  $Re =$



1200, 2800, 4200, 6500, and 7,800, the results of the current numerical model are in good agreement with the experimental data [51,76]. Numerical results based on the most up-to-date experimental data show that the maximum values for  $Nu$  and static pressure drop ( $\Delta p/L$ ) are smaller than 5.38% and 26%, respectively.

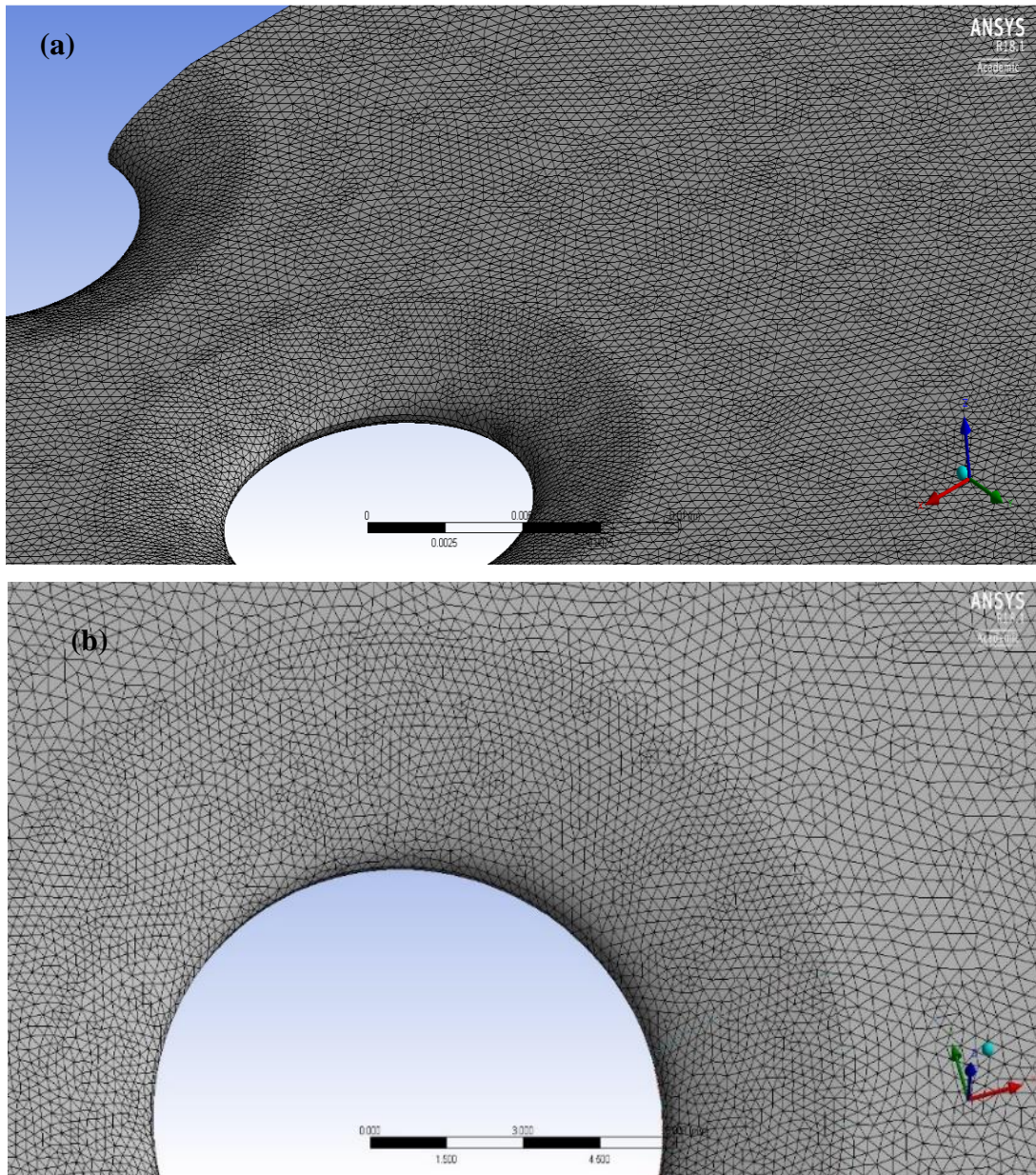


**Fig. 5.3** (a) Meshing and (b) close mesh view of PP domain

## 5.4 Computational results and discussion

In this study, computational simulation examines the combined impact of SCWSP-VGs on flow structure and hydro-thermal performance for five different configuration including case A, case B, case C, case D, and case E at the middle portion (surface) of the PPC at  $1000 \leq Re \leq 16000$ . The other parameters, including  $h_i$  or  $d_h$  and  $Y_L$ , are considered fixed values.

### 5.4.1 Effect of SCWSP-VGs and $X_L$ on velocity and temperature distribution

The X-Y plane streamlining of  $d_h/X_L = 0.076$  & case A at  $Re = 2000$ , identical to [93] is presented in Fig. 5.4. At lower  $Re$ , i.e.,  $Re = 1,000$  and  $2,000$ , low flow velocity profile occurred. Still, when the flow velocity encounters the center SCWSP-VGs and the convergent-divergent portion shaped by them, the fluid's intensity amplifies. It is diverted inward towards the center and outward towards the wall region. This redirection causes the flow to narrow, exhibiting both convergent and divergent behavior, primarily influenced by the SCWSP-VGs positioned in the channel's central area. Due to the upper-lower half and center full SCWSP-VGs, a periodic velocity profile developed inside the PP-type channel and relatively intense turbulent mixing between the surface wall and the core flow regions, significantly enhancing the convective heat transfer. This sinusoidal wave velocity profile forms an 'OERV' (Opposite elliptical recirculation vortices) region behind every SCWSP-VGs and near the wall, inlet, and outlet region.

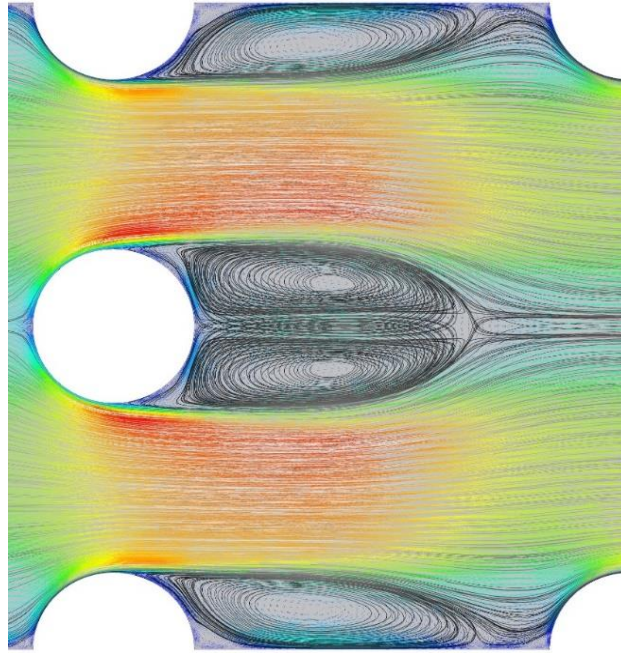


**Fig. 5.4** Streamline profile and longitudinal vortex formation at  $d_h/X_L = 0.076$  and  $Re = 2000$ .

Moreover, under the same diameter of SCWSP-VGs, a comparison of the periodic velocity distribution flow field along the longitudinal direction of different cases ( $L_{A-E}$ ) at  $Re = 2,000$  is presented in Fig. 5.5. Notably, in all the cases ( $L_{A-E}$ ), wake regions behind SCWSP-VGs are extensive. Strong opposite recirculation flow impedes fluid flow on downstream compared with straight elliptical channel (without SCWSP-VGs). In the straight elliptical channel case, no secondary flow is observed because SCWSP-VGs are absent. However, in all the cases ( $L_{A-E}$ ) of PPC, secondary flow is induced by SCWSP-VGs and the periodic enhanced surface. These observations indicate that the SCWSP-VGs generate secondary flow, which is crucial in enhancing fluid flow characteristics and heat transfer rate.

Furthermore, because of the SCWSP-VG's leadership, the continuous growth of high-speed 'OERV' in the channel, which has an impact on the vortices zone at the back side of the SCWSP-VGs at the center or near-wall region (the upper and lower portion in the channel), has significantly reduced backflow in this zone. Here it is noted that the center region of all the recirculation or vortices zones is bright compared to other areas in the channel (near the rear side of SCWSP-VGs) (cases A-E) in Fig. 5.5. The reason is that the rotation of 'OERVs' fluid (upward and downward) in this area is from inward to outward. These 'OERV', induced by the SCWSP-VGs, contribute significantly to the overall improvement in fluid flow patterns and heat transfer efficiency in the PPC. In addition,

compared to other cases B to E, in case A, i.e.,  $X_L = 64$  mm, the flow-separation and 'OERV' region are more effective because of the vortices zone. Thus, relatively high turbulence is developed that caused a high  $Nu$  increment in case-A at  $Re = 1000$ . Consequently, mixing the cold fluid in the center core flow and hot fluid in the near-wall region is improved. Therefore, the core flow rate inside the channel increases in Case A's outlet region. Similar phenomena also occur in other cases B-E, for all the  $Re = 1000-16000$ . Furthermore, due to this high mixing, more turbulence occurs behind the SCWSP-VGs that removes the stable/static fluid from the rear side of SCWSP-VGs, causing the relatively high heat transfer enhancement in case A compared to other cases B-E.

In addition, Fig. 5.5. (cases A, B, C, D, and E) illustrates the 'sinusoidal temperature contour field and scattering profile' inside the PPC at  $Re = 2000$ . The 'sinusoidal temperature distribution profile' significantly fluctuates at different  $Re = 1000-16000$ . From Fig. 5.5, it can be recognized that the temperature is reduced in the 'OERV' zone than in the wall section. In addition, compared to case A and case B, when  $X_L$ , of the channel extended, the surface area between the SCWSP-VGs is more; thus, more linear and uniform flow occurs in cases C, D, and E. Consequently, the velocity and pressure resistance reduced in cases C, D and E caused the influence of 'OERV' and 'SF' in the channel diminish. As a result, the  $h_{conv}$  slowed down, and pressure resistance, with an increase in the  $X_L$ , is reduced. Furthermore, the temperature scattering is decreased at the hot 'OERVs' pair zone than the wall section when the ratio of  $r = d_h/X_L$ , decreases with  $Re$  increases. That is another reason that indicates that the  $h_{conv}$  decreases with increases in the  $X_L$ , of the channel with more SCWSP-VGs. This can be attributed to the fluid velocity decreasing with the channel's length. Similar results are mentioned by Shirzad et al. [34], who elucidated that the heat transfer factor reduces with increases in the  $X_L$ .

Furthermore, the heat transfer rates are also lower in the upstream half of the channel wall in all PPCCs because of flow separation and recirculation. This is because the turbulent mixing in the near-wall flow region is significantly enhanced because of the 'OERV' flow shedding from the PP. However, in the downstream half of the PP wall, especially next to the SCWSP-VGs, the  $h_{conv}$  has significantly improved. In addition, the heat transfer reveals much higher values along the leading edge of the SCWSP-VGs due to the thermal entrance flow effects. It drops drastically after that. In other words, heat transmission appears to be considerably influenced by thermal entrance effects, as

depicted in Fig. 5.5, leading to almost complete development after the fourth SCWSP-VGs configuration.

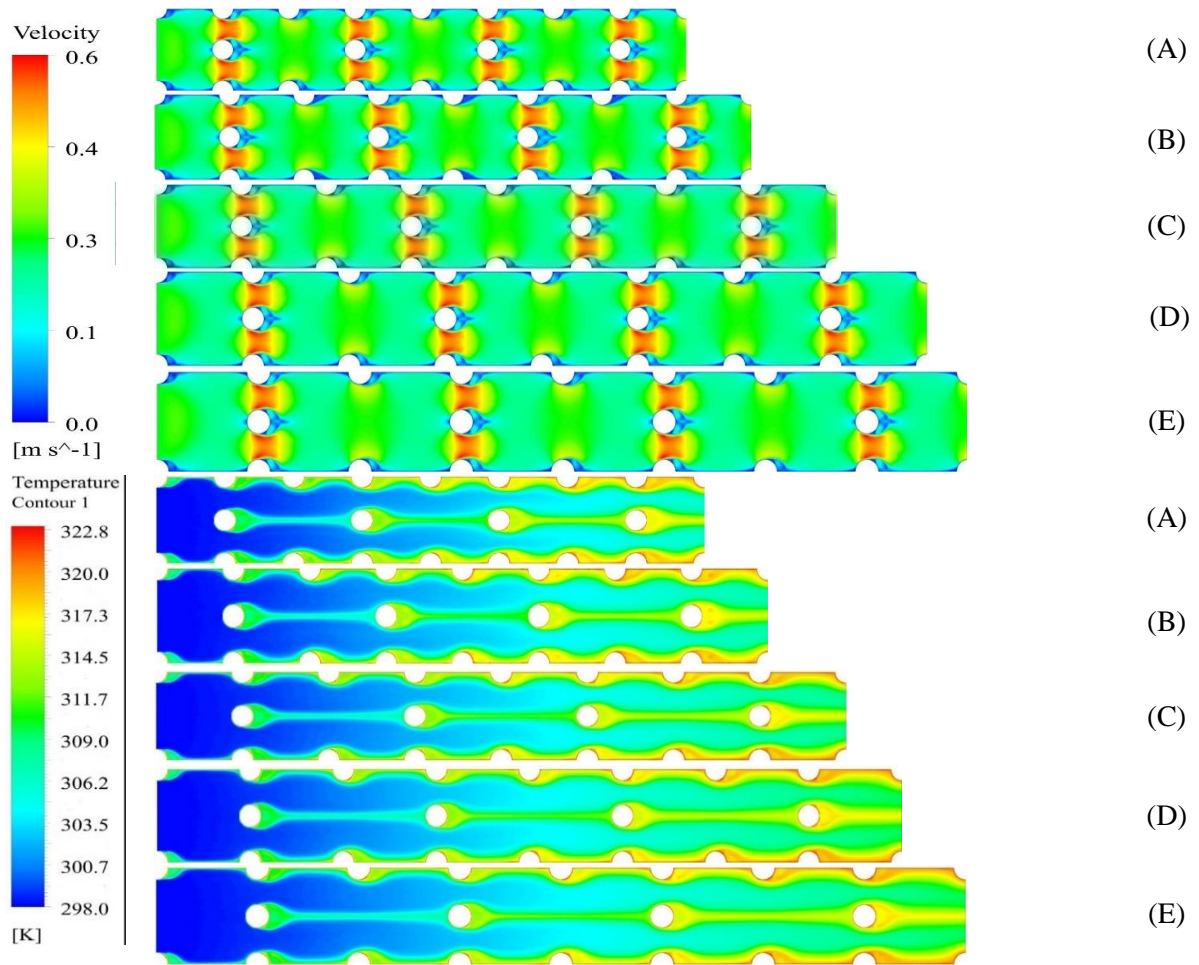


**Fig. 5.5** Velocity contour and Temperature contour case (A-E) inside the PPHX with a computational domain at  $Re = 2,000$ .

According to the simulation results, the convective heat transfer enhancement in the channel with SCWSP-VGs is much more significant than in the without SCWSP-VGs. Because of the straight slope of the upstream PP surface, the insufficient heat transfer in this area is concentrated there. More flow separation and recirculation occur in the upstream half of the channel at a lower  $Re = 2000$ , as shown in Fig. 5.5, creating the low heat transmission region more prominent than at a higher  $Re = 16000$ . Heat transfer enhancement of the PPC is thus significantly diminished at lower  $Re = 1000-2000$ .

### 5.4.2 Effect of SCWSP-VGs and $L_{A-E}$ on Nusselt number, and friction factor

As depicted in Figs. 5.6, 5.7, and 5.8, it is observed that with an increase in  $Re$ , the  $Nu$  also rises for all the cases (A-E) with SCWSP-VGs. Notably, the  $Nu$  value in the scenario with SCWSP-VGs is consistently more significant than that without VGs, i.e., straight elliptical channel. This observation underscores that SCWSP-VGs effectively generate longitudinal vortices and enhance the intensity of secondary flow, as shown in Fig. 5.6. Furthermore, the disparity between the  $Nu$  values in cases with and without SCWSP-VGs becomes more pronounced at higher Reynolds numbers, specifically  $Re \leq 4000$ . This significant difference emphasizes the crucial role played by SCWSP-VGs on the PP surfaces in inducing secondary flow, ultimately leading to heat transfer enhancement. The findings indicate that SCWSP-VGs contribute significantly to improving heat transfer on the surfaces of PPHX.

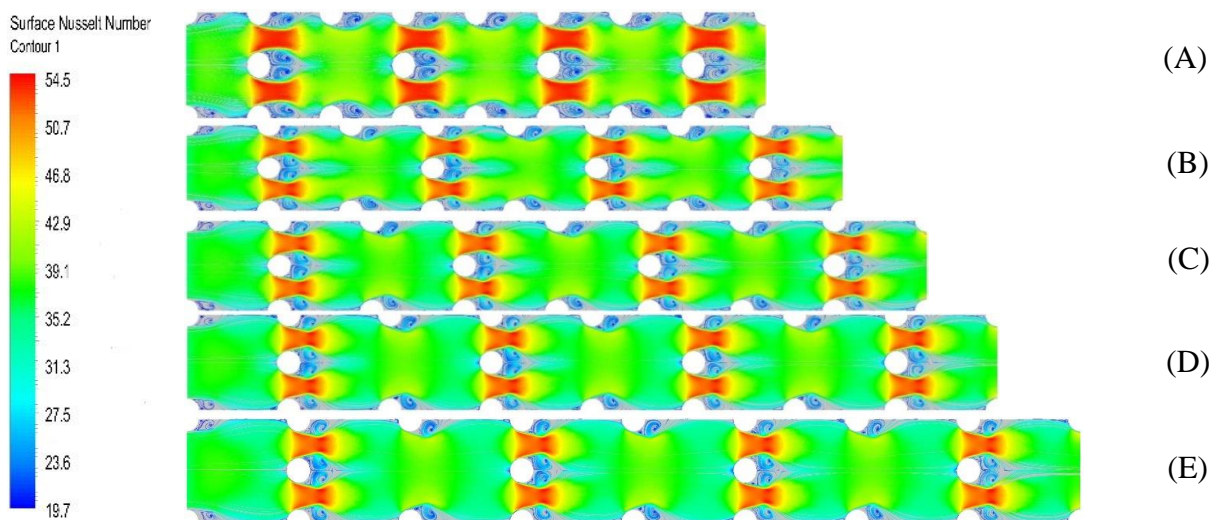


**Fig. 5.6** Surface Nusselt number variation inside PPC with SCWSP-VGs for case A-E at  $Re = 2000$ .

The  $Nu$  is presented along the mainstream direction in Fig. 5.6 and Fig. 5.7, depicting the cases with and straight elliptical channel (without SCWSP-VGs). A consistent trend is observed where  $Nu$  decreases along the streamwise direction for all the cases A-E. Notably, in most positions,  $Nu$  on all the PP surface cases with SCWSP-VGs exceeds the corresponding values in the straight elliptical channel duct. Significantly, the  $Nu$  values on the PPC surface with SCWSP-VGs case exhibit a substantial increase, particularly in the wake regions, compared to the case without SCWSP-VGs. These

findings affirm that SCWSP-VGs effectively guide fluid flow into the wake region, leading to a noteworthy improvement in heat transfer on the PP surface in contact with the wake region.

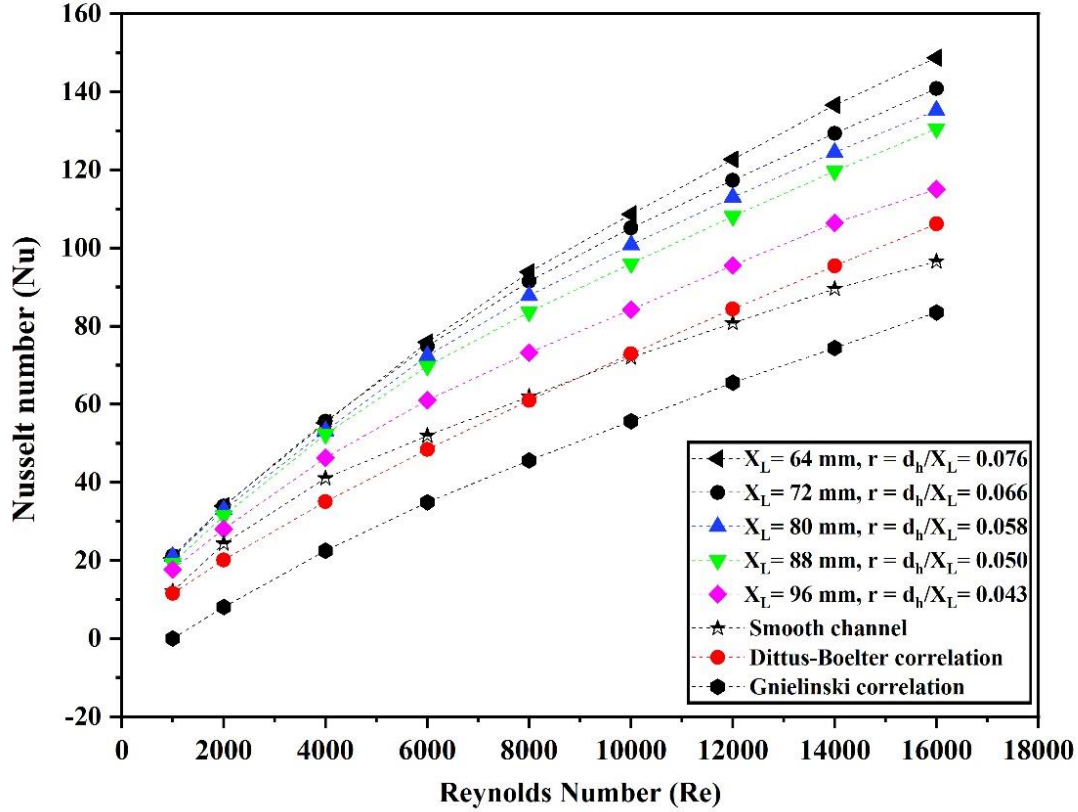


**Fig. 5.7** Nusselt number for different Reynolds numbers ( $Re$ ) through the PPC with SCWSP-VGs for  $d_h/X_L = 0.076-0.043$  and  $X_L = 64-96$  mm.

As shown in Fig. 5.7, the  $Nu$  grows with  $r = d_h/X_L$  for all  $d_h/X_L$  values, and with  $Re$  for all cases  $L_{A-E}$ . Because the  $Nu$  is a direct dependent function of the  $Re$ . The higher and lower value of  $Nu$  is obtained at  $Re = 1000$  and  $16,000$ , respectively, for  $X_L =$  case A (64 mm) (i.e.,  $r = 0.076$ ). Based on the computational results, the  $Nu$  increases linearly in cases A and B with  $Re$  but decreases individually with an increase in the  $X_L$ , of the channel cases = C-E. The smaller  $X_L$ , developed more turbulence and flow separation, which caused case A to provide maximum  $Nu$  compared to the other channel case B-E, and the straight elliptical channel duct (without SCWSP-VGs). It is attributed that the strength of the 'OERV' flow enhanced by periodic wavy structure on the channel increases with decreases in the  $X_L$ , i.e., in cases A and B, the possibility of the 'OERV' flow increases with increases in the streamwise length of PP type HXs. The computational data showed that the variation of  $Nu$  between cases A and B is not much more significant. The

value of convective heat transfer coefficient (in terms of  $Nu$ ) increment at  $Re = 1,000$  is 41.34% (Case A), 42.93% (Case B), 42.48% (Case C), 37.38% (Case D), 31.57% (Case E) and at  $Re = 16,000$ , 35.06% (Case A), 31.41% (Case B), 28.52% (Case C), 26.01% (Case D), 16.09% (Case E) for all  $d_h/X_L$ , compared to the straight elliptical channel.

According to Fig. 5.7, there is a more significant variation in  $Nu$  among all Cases A-E with different  $X_L$ ,  $d_h$  and  $h_i$ . Fig. 5.8 compares the  $Nu/Nu_0$  for all the cases A-E at  $1000 \leq Re \leq 16000$ , which rises with the increase in  $Re$  in each case except lower  $Re \leq 4000$ . All  $Nu/Nu_0$  values are more than 1. The dissimilarity is observed more instinctively via  $Nu/Nu_0$ , showing that using SCWSP-VGs significantly improves heat transfer. It is suggested that the value of  $Nu/Nu_0$  of all cases A-E exhibits a similar trend with increasing  $Re$ . It is also attributed that a contrary tendency is observed at a specific  $Re$ , between 8000-16000, relative to that at lower  $Re$ .

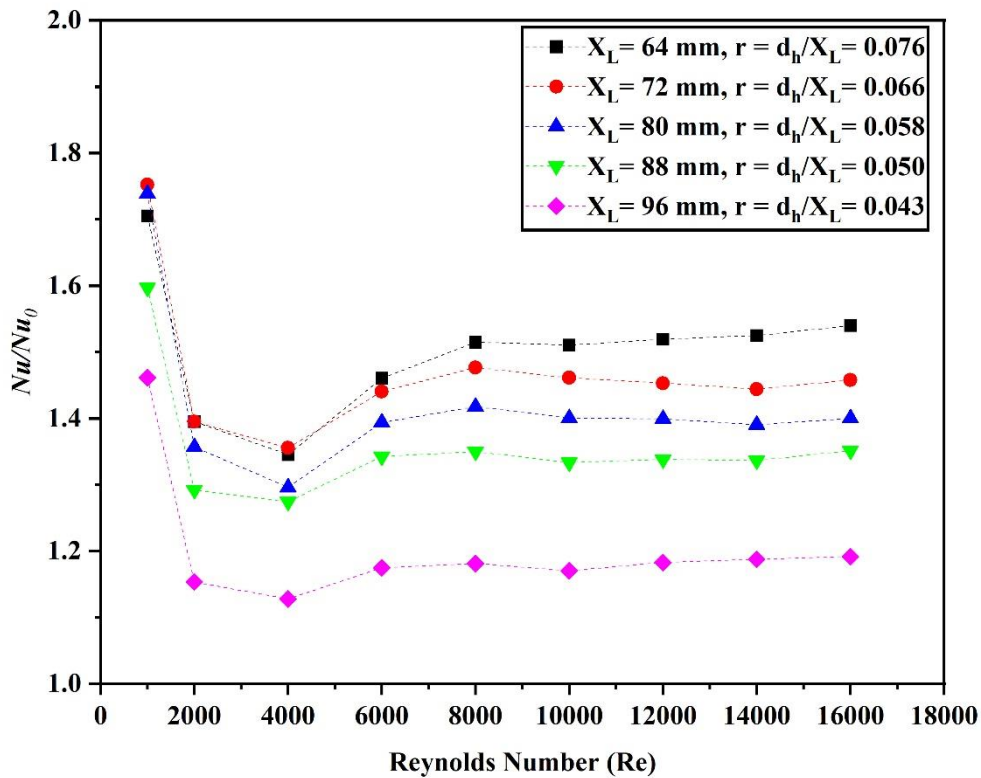


**Fig. 5.8** Nusselt number ratio for different Reynolds numbers ( $Re$ ) through the PPC with SCWSPs for  $d_h/X_L = 0.076-0.043$  and  $X_L = 64-96$  mm.

The maximum and minimum values of  $Nu/Nu_0$  are 1.74 ( $Re = 1000$ , Case C) and 1.19 ( $Re = 16000$ , Case D), respectively. In the case of A, the  $Nu/Nu_0$ , rises, falls, and



becomes constant from  $Re = 6000-16000$ . A similar trend can be seen in other cases were plotted against  $Re$ , resulting in higher data near the SCWSP-VGs and the wall area at  $Re = 1,000-2,000$ . Case A (64 mm) and case B (72 mm) provide the highest  $Nu/Nu_0$  values among the cases except including case C (80 mm), case D (88 mm), and case E (96 mm) at higher  $Re$ , while case B (72 mm) shows the highest sensitivity to  $Re$ . However, an opposite tendency is confirmed when  $Re$  is significantly larger than 1000–2000. Moreover, case D and case E's  $Nu/Nu_0$  values increase much slower with  $Re$  than in other cases. Such higher values in  $Nu/Nu_0$  are observed to be enhanced when the  $d_h/X_L$  is high and decreased in the lowest  $d_h/X_L$ . When  $d_h/X_L$  is reduced to lower, the maximum value of  $Nu/Nu_0$  becomes nearly linear or constant against the increase in  $Re$ . The PP with SCWSP-VGs offers the highest  $Nu/Nu_0$  value and more sensitivity than without SCWSP-VGs, according to a thorough computational data analysis. When the SCWSP-VGs are attached to the inner wall of the channel, heat transfer enhancement performance is better than when it is fixed on the outer wall. It's also important to recall that in cases A, B, and C with SCWSP-VGs, the  $Nu/Nu_0$  value does not significantly change when  $Re \leq 2000$ . Concerning  $d_h/X_L$ , it is indicated that the highest  $d_h/X_L$  provides the highest  $Nu/Nu_0$  at a given  $Re$ , indicating that a higher  $d_h$  achieves more significant heat transfer augmentation. Although an increment  $d_h/X_L$ , bring about a higher  $Nu$  in SCWSP-VGs cases. However, in straight elliptical channel cases, a higher  $Nu$  is also obtained with a higher  $d_h$ . As a result, SCWSP-VGs with a larger  $d_h/X_L$  have greater impact than SCWSP-VGs with a smaller  $d_h/X_L$ .

Therefore, the convective heat transfer performance is more sensitive to  $Re$  when fewer SCWSP-VGs are employed. However,  $Re$ 's effect on convective heat transfer rapidly decreases with increasing  $X_L$  and  $d_h$ . It is found that at low  $Re$ , additional 'OERV' zones, mostly behind the SCWSP-VGs, with low heat transfer behavior are formed when  $X_L$  is increased and  $d_h$  is decreased. As  $Re$  grows larger, the impact of the central core flow increases while the impact of SCWSP-VGs decreases. Under these circumstances, the channel with the highest  $d_h$  exhibits the most resistibility as  $Re$  develops. In contrast, the channel with the lowest  $X_L$  behaves most similarly to a straight elliptical channel due to the slightest geometry modification compared to other situations.

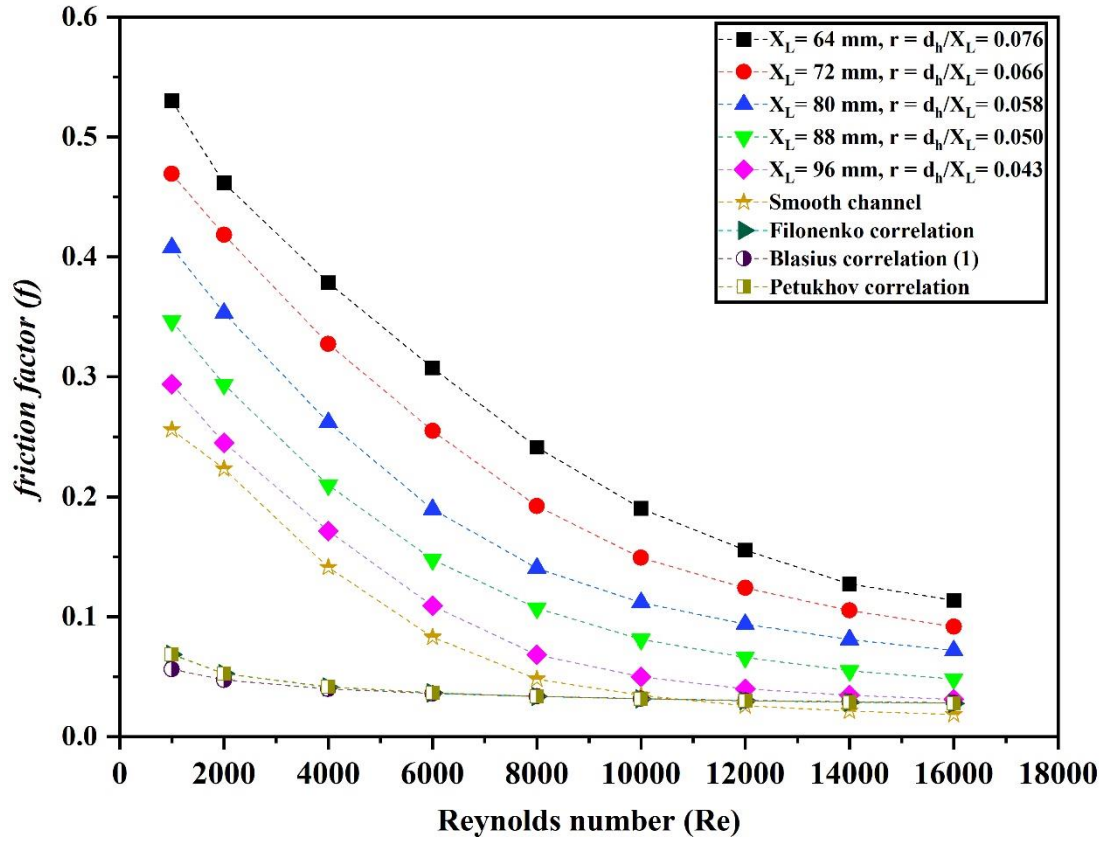


**Fig. 5.9** Variation of Friction factor against different  $Re$  through the PPC with SCWSPs for  $r = 0.076-0.043$  and  $X_L = 64-96$  mm.

The  $f$  and dimensionless resistance coefficients  $f/f_0^{0.33}$ , shown in Fig. 5.9 and Fig. 5.10, respectively, show that  $f$  decreases with increasing  $Re$  in all cases. The use of SCWSP-VGs increases  $f$  when compared to smooth cases/surfaces. Increasing  $d_h/X_L$  results in a greater  $f$  at a fixed  $Re$ , with or without SCWSP-VGs. The relationship between  $f$  and the other variables is given by Eq. (13), where  $f$  is proportional to  $d_h$  and  $\Delta p$  and inversely proportional to  $X_L$ , and  $U_m^2$ . As the  $Re$  improves, the  $f$  reduces while the  $\Delta p$  increases. As discussed in the previous sub-section 3.1, the velocity becomes linear because of channel length enlargement, and the wavy profile or  $\Delta p$  decreases. The average static  $\Delta p$  increases with decreased  $X_L$ , and maximum  $\Delta p$  near the SCWSP-VGs and the wall region presented in Fig. 5.11. Moreover, static  $\Delta p$  is also an essential factor in the periodic difference, and this phenomenon can improve or enhance the convective heat transfer rate. Fig. 5.9. shows the friction factor ( $f$ ) variation with the  $d_h/X_L = 0.076-0.043$ . The maximum and minimum  $f$  at  $Re = 16,000$  are 64.87%, 61.06%, 58.18%, 55.30%,

40.43%, and 10.80% occurred at  $Re = 8000$  and  $1000$ , respectively, for Case (A-E), compared to the straight elliptical channel.

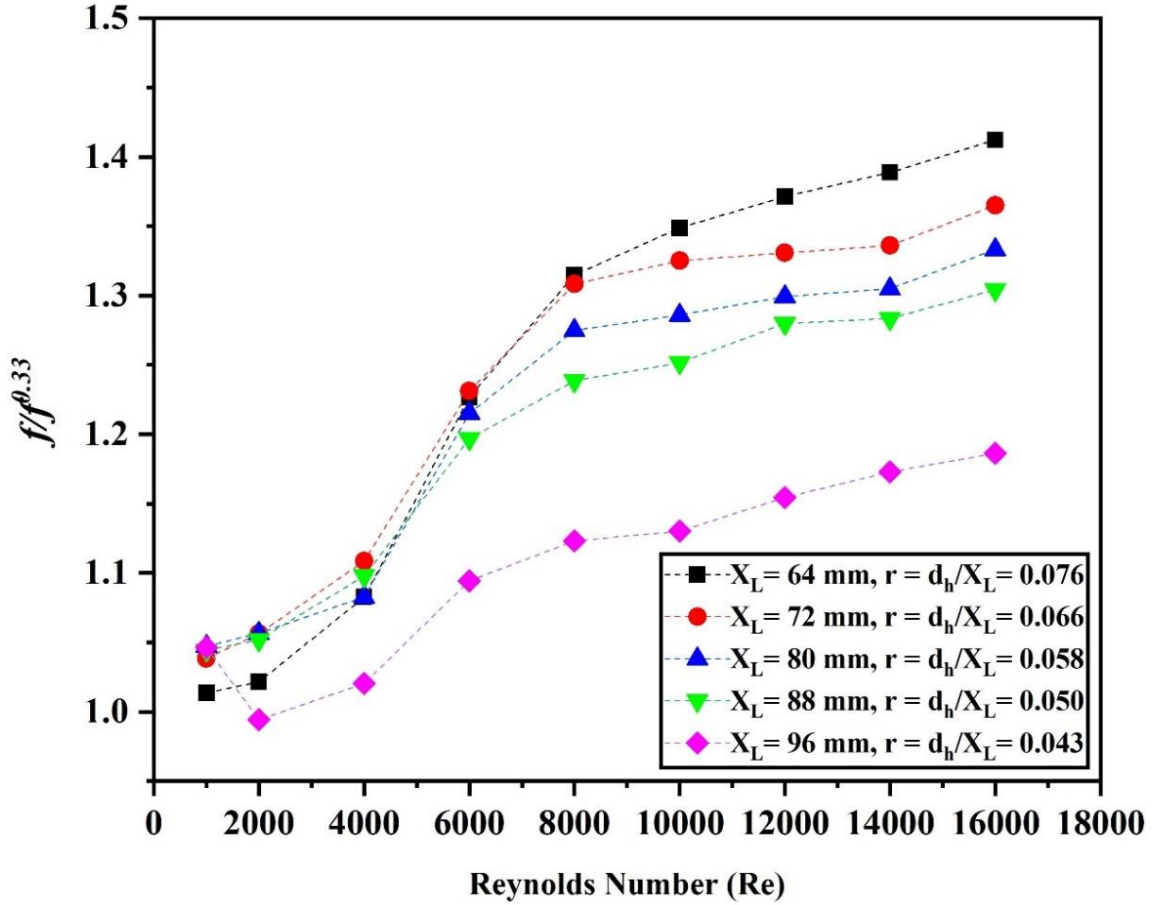


**Fig. 5.10** Friction factor ratio for different  $Re$  through the PPC with SCWSP-VGs for  $r = 0.076-0.043$  and  $X_L = 64-96$  mm.

Based on the findings shown in Fig. 5.10, it can be observed that all cases of  $f/f_0^{0.33}$  exhibit a slow and gentle development as the  $Re$  increases. No discernible difference between cases is observed at low  $Re$ , especially cases A to case D (except case E). With increasing  $Re$ , the disparity becomes more noticeable. It is shown that increasing  $d_h/X_L$ , increases  $f/f_0^{0.33}$ , implying that increasing  $d_h$  produces a higher friction penalty. Fig. 5.9 and Fig. 5.10 depict the tendency more intuitively with increasing  $Re$ , the difference between cases with other  $X_L$ , and  $d_h$  becomes noticeable. Due to a more prominent disruption to the main flow at high  $Re$  and intensified flow recirculation behaviors an increase in  $d_h$  or  $d_h/X_L$ , leads to an increase in  $f/f_0^{0.33}$  at a given  $Re$ .

The  $f/f_0^{0.33}$  for all examples of case A-E also increases when  $Re$  is greater than 1000-16000. An ineffective separation caused by an unfavorable pressure gradient and reattachment characteristics leads to a low  $f/f_0^{0.33}$ , suggesting that the SCWSP-VGs in the

channel behave such a smooth surface at low  $Re$ . Increases in  $Re$  cause a clear rise in  $f/f_0^{0.33}$  as the flow separates from and returns to itself more frequently. For a given value of  $Re$ , the intensity of the core streamflow flow decreases the SCWSP-VGs' impact.

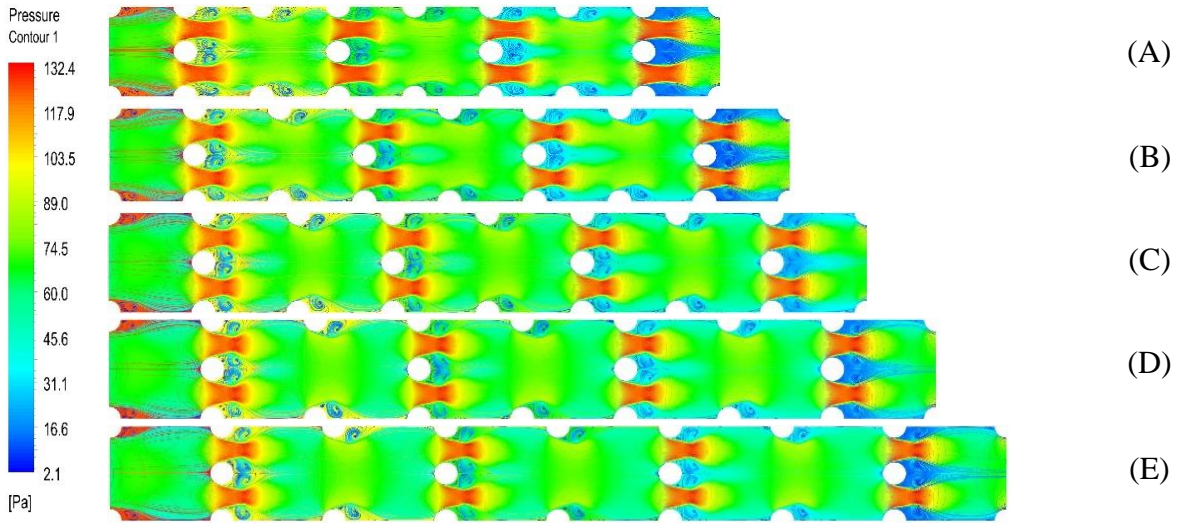


**Fig. 5.11** Static Pressure profile inside the PPC domain with SCWSP-VGs for case A-E at  $Re = 2000$ .

As a result, compared to the smooth duct/channel, the slope of resistance behavior  $f/f_0^{0.33}$  increases with  $Re$  in the PPC. Furthermore, as previously stated, the situation with the least or lowest SCWSP-VGs has the least resistance to developing  $Re$ . Due to the minor geometry change, situations D and E have the most in common with smooth duct, which causes  $f/f_0^{0.33}$  to drop with increasing  $Re$  for values of  $Re$  greater than 4000.

### 5.4.3 Standard correlation of Nusselt number and Friction factor

Numerical values for the PPHX's  $Nu$  and  $f$  are compared in Fig. 5.7 and Fig. 5.9 with those of the Dittus-Boelter [119], Gnielinski [120], Blasius correlations [121], Filonenko [121], Petukhov [121], and straight elliptical channel. It is typical to employ the Blasius equation Eq. (5.12) and Eq. (5.13) and the Filonenko equation Eq. (5.14) to determine turbulent flow in a straight elliptical channel. In this case, the experimental values are within the allowable range. Based on the computational information, it is seen that the trends of the  $Nu$  and  $f$  of the PPC with SCWSP-VGs are in good agreement with the experimental results of Tran et al. [76]. In contrast, the slope of  $Nu$  and  $f$  with Eq. (5.10)-Eq. (5.15) for transition SST  $k-\omega$  gives not significant results except at higher  $Re$ .

Dittus-Boelter correlation [119]:

$$Nu = 0.023Re^{0.8}Pr^{0.4} \quad (5.10)$$

Gnielinski correlation [120]:

$$Nu = \frac{(f/8)(Re-1000)Pr}{1+12.7(f/8)^{1/2}(Pr^{2/3}-1)} [0.5 \leq Pr \leq 2000, 3000 \leq Re \leq 5 \times 10^6] \quad (5.11)$$

Blasius correlation (1) [121]:

$$f = 0.3164Re^{-0.25} (Re \leq 2 \times 10^4) \quad (5.12)$$

Filonenko correlation [121]:

$$f = (1.82 \ln Re - 1.64)^{-2} (10^4 \leq Re \leq 10^8) \quad (5.14)$$

Petukhov correlation [121]:

$$f = (0.790 \ln Re - 1.64)^{-2} (3000 \leq Re \leq 5 \times 10^6) \quad (5.15)$$

#### 5.4.4 Influence of SCWSP-VGs and $X_L$ on Colburn $j$ -factor

$$\text{Colburn } j\text{-factor, } j = Sr/Pr^{2/3} \quad (5.16)$$

Fig. 5.12 and Fig. 5.13 showed the calculated and simulation results of the Colburn  $j$ -factor against the various  $Re$  values. It can be observed that the velocity flow reveals a 'periodic' behavior profile in the longitudinal trend. The flow is significantly improved between the upper-center-lower SCWSP-VGs. Due to the SCWSP-VGs obstruction, a high-velocity zone is developed between the center and upper- lower SCWSP-VGs in the direction of fluid flow. As computational results, a central relatively high-velocity region is generated in the fluid straight flow path. Moreover, a reverse in fluid flow originated near the SCWSP-VGs region because of back pressure flow. The back pressure is mostly

produced by the pressure downstream over the system pressure. Further, to recognize in detail the effect of velocity distribution on the thermal performance of PPHX with SCWSP-VGs, the Colburn  $j$ -factor, and the  $Re$  variation are shown in Fig. 5.12 and Fig. 5.13. The Colburn  $j$ -factor is calculated based on the  $St$  (Stanton number),  $Re$  (Reynolds number), and  $Pr$  (Prandtl number). The enhancement rate of Colburn  $j$ -factor at  $Re = 1,000$  and  $16,000$  is 15.49% (case A), 6.98% (case B), 3.26% (case C), 7.23% (case D) and 11.94% (case E) and 5.8% (case A), 6.98% (case B), 6.71% (case C), 7.23% (case D) and 13.68% (case E).

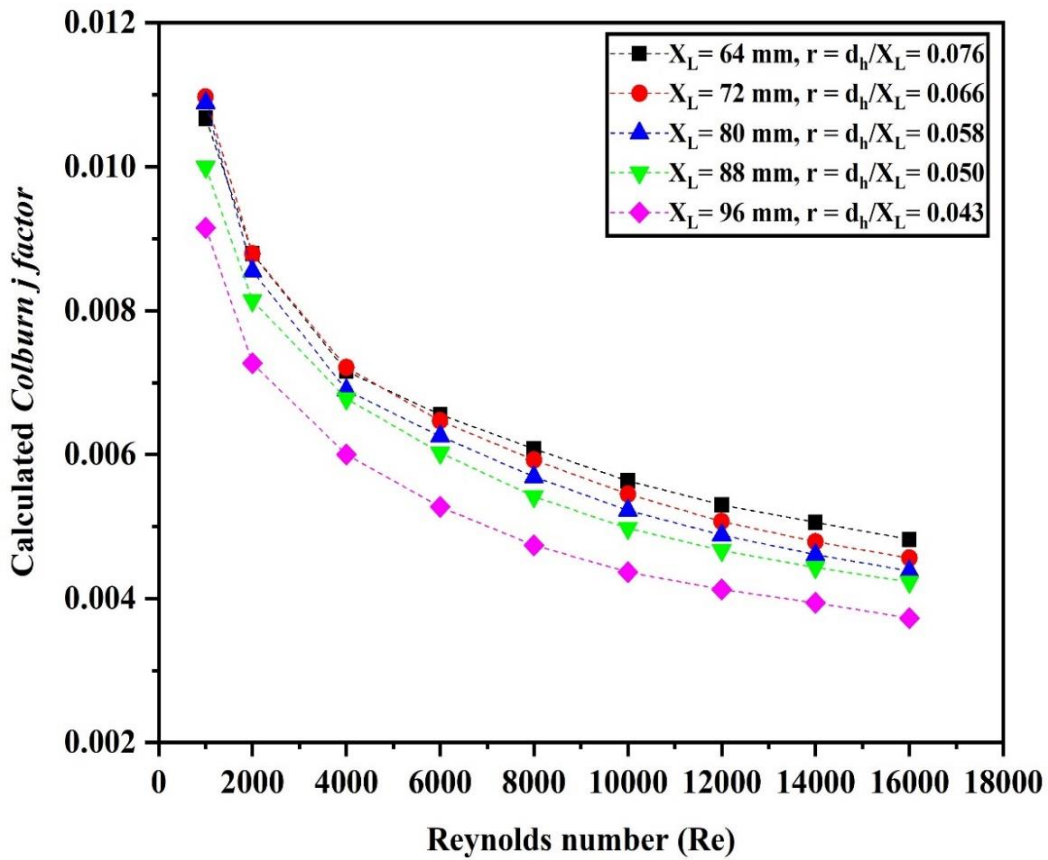


**Fig. 5.12** Variation of calculated Colburn  $j$ -factor against  $Re$  for  $r = 0.076-0.043$  and  $X_L = 64-96$  mm.

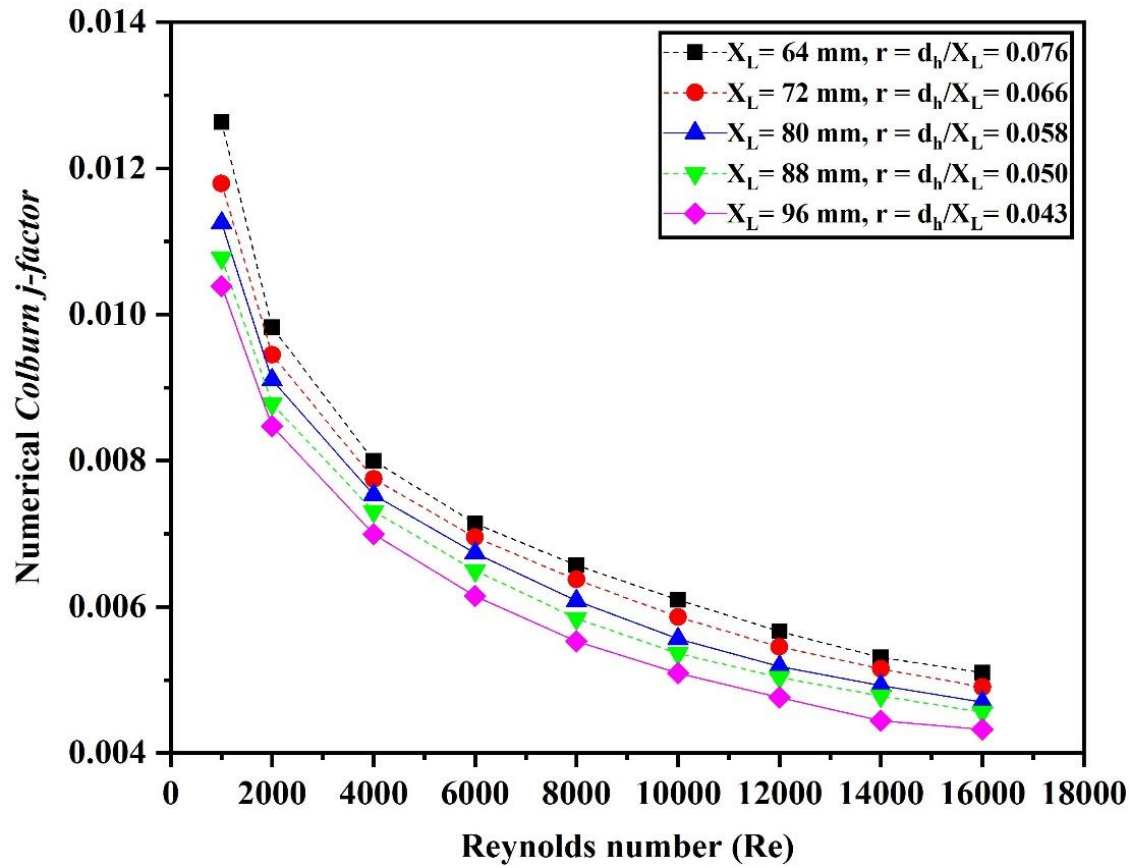
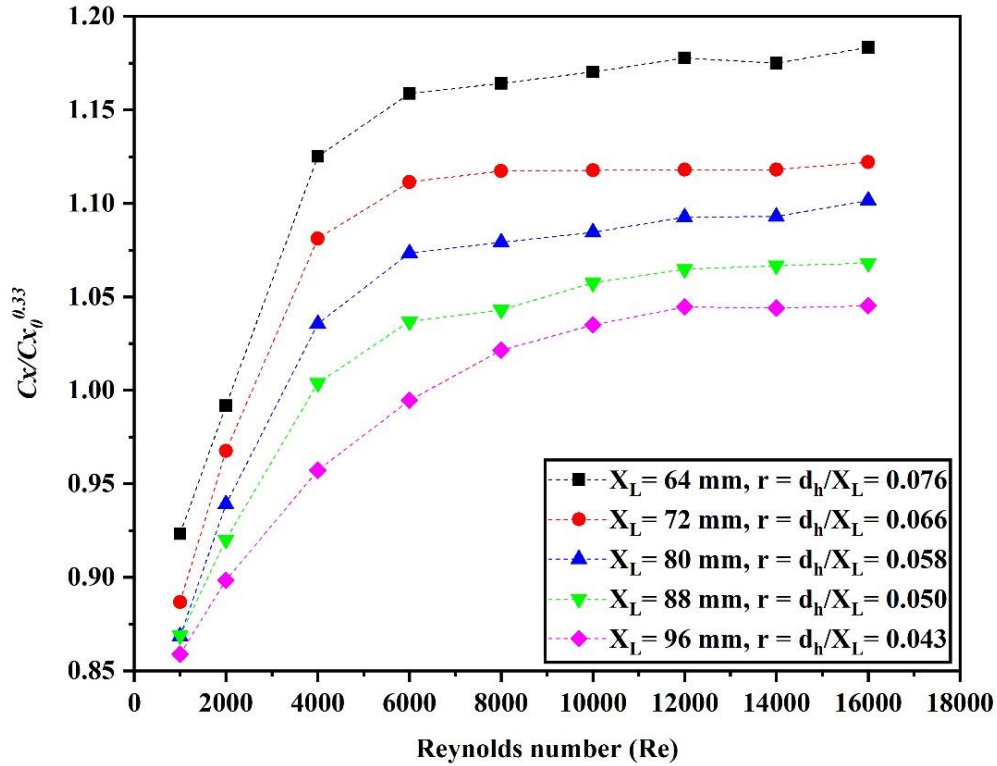


Fig. 5.13 Variation of Numerical Colburn  $j$ -factor against  $Re$  for  $r = 0.076-0.043$  and  $X_L = 64-96$  mm.

#### 5.4.5 Calculation of normalized drag coefficient and RAF (Reynolds analogy factor)

$$\text{Normalized Drag Coefficient (refer to Eq. 3.20)} = C_x/C_{x0}^{0.33} \quad (5.17)$$

Fig. 5.14 presents the dimensionless drag coefficient distribution  $C_x/C_{x0}^{0.33}$  in the PPHX. For all cases A-E, the ratio  $C_x/C_{x0}^{0.33}$  first increases (at  $Re = 4000$ ), and then fluctuations become a constant value when  $Re$  is more significant than 6000. It is shown that the highest form of drag is found in the  $d_h/X_L = 0.076$  for  $X_L = 64$  mm (case A), while the lowest form drag is found in the  $d_h/X_L = 0.043$  for  $X_L = 96$  mm (case E). It can be observed that the drag is higher in the PPC with a lower  $X_L$  than decreasing with a higher  $X_L$  with decreasing the diameter of SCWSP-VGs from  $d_{cws} = 8-10$  mm.



**Fig. 5.14** Variation of  $C_x/C_{x0}^{0.33}$  against different  $Re$  for  $r = 0.076-0.043$  and  $X_L = 64-96$  mm.

The maximum enhancement of the relative drag ratio  $C_x/C_{x0}^{0.33}$  is from 0.92-1.18 (case A), 0.89-1.12 (case B), 0.87-1.10 (case C), 0.87-1.07 (case D), 0.86-1.04 (case E) from  $1000 \leq Re \leq 16000$ . Based on the computational information, the relative drag increases with the  $X_L$ , of the SCWSP-VGs. In the authors' opinion, the increment in  $C_x/C_{x0}^{0.33}$  in the lowest and highest  $X_L$ , respectively, are also due to the interaction between the upper-center-lower staggered arrangement of the circular welding spot and the area captured by the SCWSP-VGs over the entire  $X_L$  in the PPC.

The pillow plate's thermo-hydraulic performance factor or heat-transfer efficiency can be described by its ratio of heat-transfer improvement to drag improvement. Most researchers and authors [86,122,123] employ one of the following criteria:  $(St/St_0/C_x/C_{x0})$ ,  $(St/St_0/C_x/C_{x0})^{0.5}$ , and  $(St/St_0/C_x/C_{x0})^{0.33}$  [124]. The condition of the computational simulation is associated with velocity and temperature gradients flowing through the internal PP with sufficient accuracy. As a result,  $(St/St_0/C_x/C_{x0})^{0.33}$  is selected as the thermo-hydraulic evaluation factor. The expression  $(St/St_0/C_x/C_{x0})^{0.33}$  is used in this computational simulation. The relationship between the heat-hydraulic efficiency



$(St/St_0/C_x/C_{x0})^{0.33}$  and the  $Re$  is shown in Fig. 5.17. In other words, we plotted the average quantity dependences and different heat transfer ratio criteria on the various PPC configurations in Fig. 5.15. For case A-E, this dependency is monotonic, approaching its higher at  $Re = 1000-2000$  while increasing with the  $Re$ . The heat transfer augmentation factor  $St/St_0$  is higher at  $Re = 2000$ . The separation and reattachment are less effective with low  $Re$ , causing low convective heat transfer.

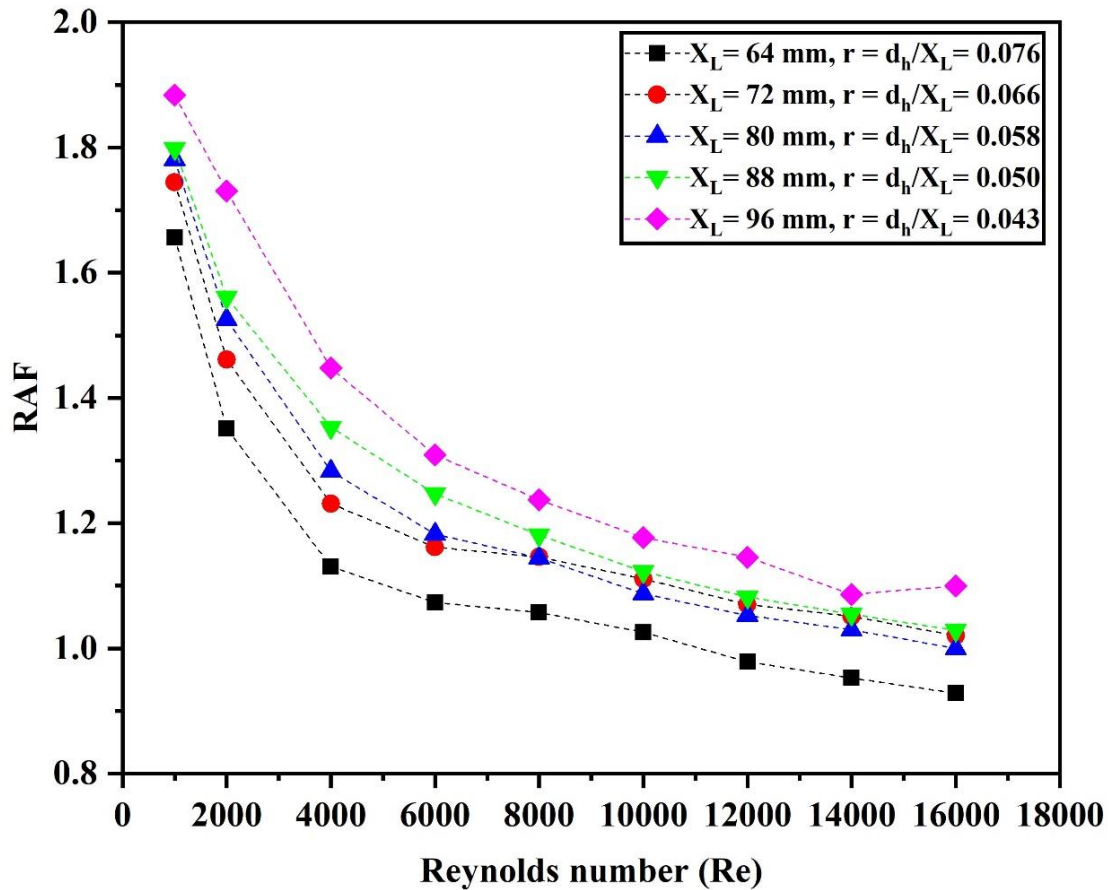


**Fig. 5.15** Variation of  $RAF$  against different  $Re$  for  $r = 0.076-0.043$  and  $X_L = 64-96$  mm.

From  $Re = 1000$  to  $Re = 6000$ ,  $St/St_0 > C_x/C_{x0}$  in every case. With an increase in the  $Re$ ,  $RAF$  rapidly grows towards unity or more significant than unity. A lower value in  $RAF$  is not substantial for cases D and E. Due to a minor increment in the drag for the PP surfaces with  $X_L = 80$  mm to 96 mm (cases C and E)  $RAF > 1$  on the  $Re$  range less than 4,000. Mean values of the drag development, the heat transfer development, and the  $RAF$  values of the relative drag and heat transfer coefficient for any cases, and the

corresponding  $Re$  shown in Fig. 5.15 are determined by the mean values of  $C_x/C_{x0}$ ,  $St/St_0$ , and  $RAF$  over the  $Re$  based on the boundary layer length.

Case A and B with SCWSP-VGs provide the lead values of the average heat transfer ratio due to the most excellent values of the relative drag coefficient being considered higher than the relative heat transfer coefficient. The relative transfer coefficient for cases B and C is on the surface with SCWSP-VGs due to uninterrupted mainstream flow regions between the upper and lower SCWSP-VGs. However, their relative drag coefficient is considerably more significant than the surface without SCWSP-VGs. Case A and B have greater heat-hydraulic efficiency values thanks to the lowest values of  $(C_x/C_{x0})^{0.33}$ . The drag created by SCWSP-VGs was significantly reduced due to the decrease in the streamlined curvature generated near the surface of the SCWSP-VGs and the wall of the channel. The heat transfer coefficient is highly stable here. It improves the surfaces' heat transfer and hydraulic efficiency.

The  $(St/St_0/C_x/C_{x0})^{0.33}$  is more significant than unity for all cases A-E against the  $Re$ . This quality is the greatest for case E,  $(St/St_0/C_x/C_{x0})^{0.33} = 1.88/1.09$ , and the least for case A  $(St/St_0/C_x/C_{x0})^{0.33} = 1.65/0.93$ . For cases B, C, and D, the expression  $(St/St_0/C_x/C_{x0})^{0.33}$  equals 1.74/1.02, 1.78/1.00, and 1.80/1.03, respectively, at  $Re = 1000/16000$ .

#### 5.4.6 Performance evaluation criteria of PPHE with SCWSP-VGs

Performance evaluation criteria [117],

$$(PEC) = (Nu/Nu_0)/(f/f_0)^{0.33} \quad (5.18)$$

The  $(Nu/Nu_0)/(f/f_0)^{1/3}$  of cases A-E is presented in Fig. 5.16 against  $Re$ . It can be distinguished that the  $PEC$  is directly dependent on  $Nu$  and  $f$ . The  $(Nu/Nu_0)/(f/f_0)^{1/3}$  values of most working points are higher than 1, indicating outstanding thermal efficiency compared with smooth cases against additional flow resistance.

The highest and lowest  $(Nu/Nu_0)/(f/f_0)^{1/3}$  are 1.68 and 1.39 for cases A and E, respectively, at  $Re = 1,000$ . The  $PEC$  of individual cases first increases and then descends with a growing  $Re$ , leaving the highest rate when  $Re$  varies from 1,000-2,000. These peak values occurred from cases A to E configuration when  $d_h/X_L$  and  $X_L$  drops. It is indicated that the  $(Nu/Nu_0)/(f/f_0)^{1/3}$  of all cases decreases with the increase in  $Re$ . It is also shown

that a lower  $d_h/X_L$ , offers a higher  $(Nu/Nu_0)/(ff_0)^{1/3}$  at a given  $Re$ . The maximum  $(Nu/Nu_0)/(ff_0)^{1/3}$  occurs at  $Re = 1000$  and  $2000$ . But when  $Re$  increases further (4000-16000) for all cases A-E of  $d_h/X_L = 0.076-0.043$ , the  $(Nu/Nu_0)/(ff_0)^{1/3}$  starts decreasing. The thermal performance is higher for case A = 64 mm while lower in case E = 96 mm. Because the  $d_h/X_L$ , higher in case A, while lower in case E. Results attributed that the lower the value of  $X_L$ , the higher the value of  $(Nu/Nu_0)/(ff_0)^{1/3}$  at low  $Re$ . The overall conclusion is that the decrement in thermal efficiency with increasing  $X_L$  is not efficient at higher  $Re = 4000-8000$ . As for the effects of  $X_L$ , unlike  $(Nu/Nu_0)/(ff_0)^{1/3}$ , it occurred in Fig. 5.16 that a lesser  $X_L$  brings about a greater  $(Nu/Nu_0)/(ff_0)^{1/3}$  at a given  $Re$  than a higher  $X_L$ , which might be affected a more leading role in  $(Nu/Nu_0)/(ff_0)^{1/3}$  compared to a straight elliptical channel one.

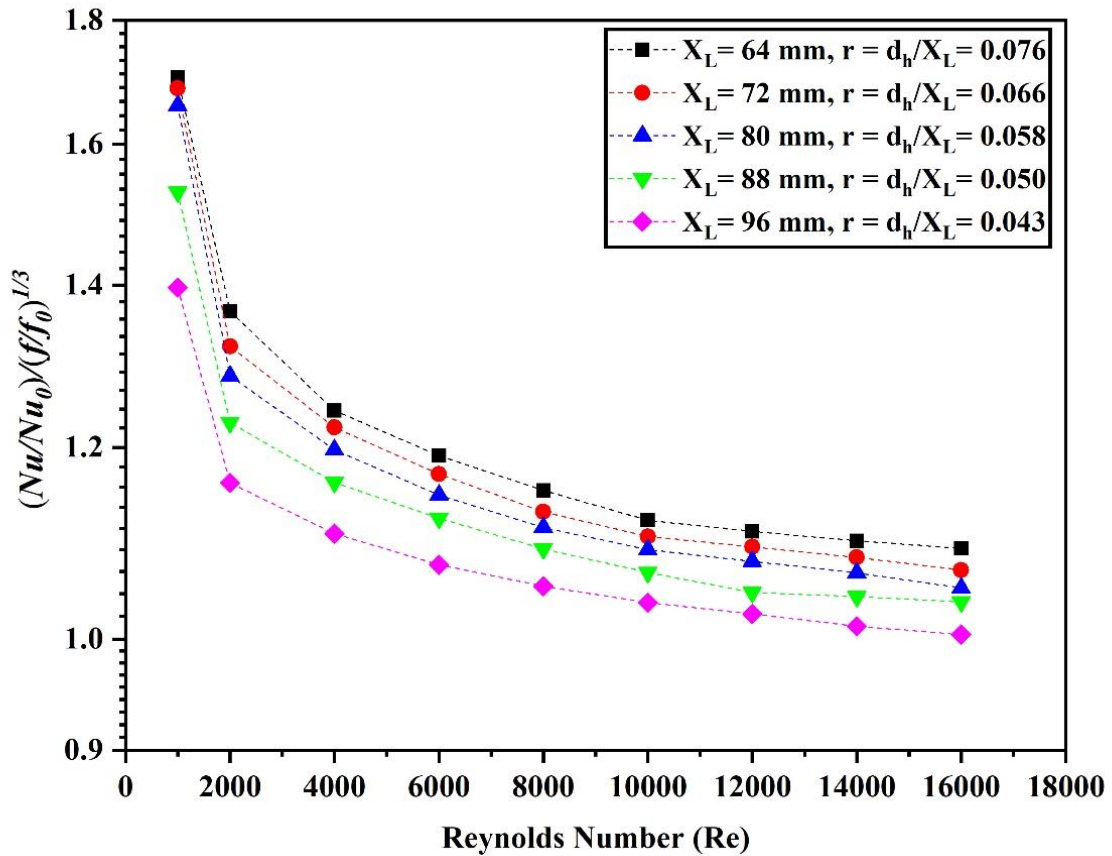


**Fig. 5.16** The variation of  $(Nu/Nu_0)/(ff_0)^{1/3}$  against different  $Re$  for  $r = 0.076-0.043$  and  $X_L = 64-96$  mm.

#### **5.4.7 Comparison of the effect of SCWSP-VGs with some previous VGs**

Based on the literature, several investigations study various types of VGs devices used in a solar receiver heat exchanger such as multiple V-baffle [125], groove and perforated-delta wing [126], winglet and wavy-groove [127], perforated winglet [128], V-baffle [129], V-shaped ribs and grooves [130], punched V-ribs and chamfer [131], multiple-ribs [132], delta winglet [133], turbulators [134].

Depending on their purpose, these distinct VGs devices have varied parameters. Specific criteria for one technology may not be relevant for another. It is challenging to compare VGs equally because of their diverse range of methodologies. Additionally, there is not enough information in the literature on these topics combined. In contrast to other conventional HXs with VGs, the thermal performance of PPHX with SCWSP-VGs is more significant and exciting for scientists and researchers to study.

Moreover, by referencing Fig. 5.9-5.15, the impact of SCWSP-VGs in guiding more fluid flow into the wake region. Examining these figures, it becomes apparent that  $Nu$  is increased downstream of the SCWSP-VGs on most areas of the PP surface. This suggests that the longitudinal vortices generated by SCWSP-VGs contribute to stronger fluid mixing, enhancing heat transfer on the channel surface. The changes observed in these figures underscore the role of SCWSP-VGs in influencing fluid flow patterns and, consequently, improving surface heat transfer characteristics.

# Chapter - 6: Summary, Conclusion, and Future scope

---

In essence, this thesis explores the realm of thermal engineering, focusing on the significant impact of Pillow-Plate Heat Exchangers across industries. Our work aims to enhance efficiency and sustainability through numerical analysis, paving the way for an eco-friendlier future. By combining analytical techniques with cutting-edge computational methods, we seek to innovate PPHE designs, driving energy savings and industrial progress. We strive to optimize PPHE performance through a comprehensive approach, addressing challenges such as pressure drops and production costs while maximizing heat transfer efficiency. Ultimately, our research contributes to improving heat exchanger technology, fostering environmental responsibility and industrial advancement.

## 6.1 Summary and conclusion

Heat exchangers are essential components across various industries, including HVAC&R, food processing, pharmaceuticals, and power generation. Among them, Pillow-Plate Heat Exchangers (PPHEs) represent a creative advancement in thermal engineering, known for their superior heat transfer efficiency, flexibility, and compact design. With their distinctive wavy surfaces and adaptability to different applications, PPHEs offer significant potential to replace or supplement traditional heat exchangers, enabling enhanced energy savings, lower environmental impact, and increased industrial productivity. However, achieving optimal performance requires a deeper understanding of their complex fluid dynamics and heat transfer mechanisms. This research aims to push the boundaries of heat exchanger efficiency and sustainability through innovative PPHE designs, employing advanced computational and experimental methods to maximize their potential.

Developing efficient, compact, and cost-effective heat exchangers is critical in an era where industries strive for both energy efficiency and environmental sustainability. Traditional heat exchangers often struggle to maintain a balance between high thermal performance, low pressure drop, and operational cost-effectiveness. PPHEs address many of these limitations with lightweight structures, customizability, and the ability to operate in extreme conditions. However, improving their performance requires overcoming several challenges, including the optimization of flow behavior and thermal efficiency.

This research is motivated by the need to develop high-performance PPHEs tailored for modern industrial needs, such as refrigeration, condensers, evaporators, and room heating applications.

Despite their advantages, PPHEs present several research challenges and knowledge gaps. One major challenge is managing fluid flow resistance and pressure loss without compromising heat transfer efficiency. Enhancing turbulence-induced mixing while minimizing pressure drops is critical to achieving this balance. Additionally, optimizing geometric parameters such as channel height, welding spot configuration, and plate design is crucial for improving overall performance, yet there is limited research exploring the interaction between these factors. Numerical and experimental limitations further complicate the development process, as current computational models often struggle to accurately predict the complex fluid flow and turbulence within the wavy channels, while experimental validations remain resource-intensive and difficult due to the intricate geometry and diverse operational conditions. Moreover, selecting appropriate materials and customizing PPHEs to meet specific industry requirements, such as in food processing or pharmaceutical manufacturing, add further complexity to the optimization process.

This research influences ANSYS Fluent to perform numerical simulations and optimize PPHE designs, providing new insights into their thermal and flow behavior. The study demonstrates that optimizing geometric parameters, such as channel dimensions and welding spot arrangements, enhances heat transfer through vortex formation and lateral mixing. The transition Shear Stress Transport (SST)  $k-\omega$  turbulence model accurately captures secondary flows and turbulence, which are crucial for improved thermal performance. Additionally, strategies for reducing pressure drop are developed through validated CFD models, which balance flow resistance and heat transfer efficiency. The use of tetrahedral mesh improves computational efficiency by capturing intricate geometry details, enabling parallel processing and solver compatibility.

The key findings from chapters 4 and 5 are listed below for quick reference.

1. As a result of SCWSPs, more turbulence is created, causing the continuous development of ‘elliptical vortices’ that affect flow from lower to higher streamwise length for Cases  $L_{A,1-E,25}$ .
2. The  $Nu$  increases in the individual  $L_{A-E}$  but decreases with increasing the  $L_{A-E} = 256-384$  mm, while friction factor ( $f$ ) decreases significantly with  $Re$

increases in both individual and overall Cases A-E. Compared to without SCWSPs channels, with increasing  $d_h/X_L = 0.041-0.078$ , and decreasing the  $L_{A-E} = 256-384$  mm, the thermal efficiency ( $\eta_{eff}$ ) of PPHE provides significant results at lower  $Re$  than at higher one.

3. The  $S_{g,T}$ , and  $S_{g,F}$  increases with the longitudinal length of SCWSPs and  $d_{cws} = 8-12$  mm with  $1000 \leq Re \leq 16,000$ . That means the temperature and velocity gradient dominates the thermal and frictional entropy generation in the lower and higher longitudinal streamwise length with SCWSPs than the straight elliptical channel. The  $S_{g,T}$  is increased from 5.41% to 22.38%, while  $S_{g,F}$  decreased from 28.92 % to 15.76% at  $Re = 16,000$  for Cases A-E, or vice-versa compared with the straight elliptical channel at  $Re = 16,000$ .
4. Thermal exergy and frictional exergy destruction increase with the streamwise length of the Pillow-plate type HEs, while a slight increment or variation occurs with the increasing the  $d_{cws} = 8-12$  mm.
5. The maximum peak of Bejan number ( $Be$ ) is occurred at  $Re = 1000$  for all the Cases  $L_{A,1-E,25} = 256-384$ , and then it decreases continuously with  $Re$  and the maximum and minimum  $N_S$  occurred is 0.29 and 0.12 at  $Re = 1000$  and 16,000, respectively, for case  $L_E$  compared to other cases  $L_{A-D}$ .
6. Based on computational numerical simulation, the exergy efficiency value is minimal in the case of a 'sinusoidal wavy surface' of the Pillow-plate type HEs relative to the straight elliptical channel (without SCWSPs). The maximum  $\eta_{ex}$  is found to be 43.07 % compared to the other Cases  $L_{B-E}$ . The range of maximum exergy ( $\eta_{ex}$  %), efficiency enhanced by 38.74 %-43.07 % for all the Cases  $L_A$  ( $d_{cws} = 8-12$  mm,  $r = 0.074-0.078$ ) at  $Re = 1000-16,000$  and thermal performance factor ( $\eta_{eff}$ ) is 1.54 in the  $r = d_h/X_L = 0.044$  at  $Re = 1000$ , respectively.
7. Further research is recommended on heat transport techniques, especially on vortex generation, thermal enhancement ratio, and drag coefficient, given the complexity of PPHE computational models.
8. Due to middle and central SCWSP-VGs, more turbulence flow created causes the continuous development of 'OERV', affecting the primary and secondary flow from lower to higher  $X_L$ .

9. Heat transfer is greatly improved due to the SCWSP-VGs-generated multiple longitudinal vortex arrangement in the PPC, which leads to a long path with a sinusoidal wavy profile and relatively intense turbulent mixing between the channel's surface and the mainstream core flow zone.
10. The  $Nu$  fluctuates by increasing the arrays of SCWSP-VGs. The  $Nu$  increases in the individual  $X_L$  for  $Re$  from 1000-16000 but decreases with increasing the  $X_L = 64-96$  mm, while  $\Delta p$  decreases with  $X_L$ . The  $f$  decreases significantly with  $Re$  increases in both individual and overall cases. In addition, the value of  $Nu$  is higher in case A = 64 mm compared to other cases B-E. Interestingly, the value of  $Nu\%$  in case A = 64 mm and case B= 72 mm is almost the same at lower  $Re = 1000-2000$ . The computational simulation provided good prediction results on the performance of a wavy surface in a PPC. Predicted results have shown good agreement with experimental results.
11. The highest and lower  $Nu/Nu_0$  are 1.74 and 1.19, respectively. The  $Nu/Nu_0$  first increases and then becomes constant against the  $Re$  rise, leaving the highest value with  $Re$  between 1,000 and 2,000. More significant heat transfer augmentation is reached when a higher  $d_h/X_L$ , is used. Increases  $X_L$  results in higher  $Nu/Nu_0$  at lower  $Re$  after that it decreases and becomes linear with higher  $Re$ . The  $f/f_0$  increases with the  $Re$ . Based on this computational study's non-dimensional parameters including  $Nu/Nu_0$ ,  $f/f_0$ , and Colburn  $j$ -factor provided more significant results for the cases.
12. Compared to straight elliptical channel, with increasing  $d_h/X_L = 0.043-0.076$  and decreasing the  $X_L = 96-64$  mm, the  $(Nu/Nu_0)/(f/f_0)^{1/3}$  of PPHX provides significant results at lower  $Re$  than higher one. The  $(Nu/Nu_0)/(f/f_0)^{1/3}$  values for PP-type HXs vary from 1.39-1.68. The  $(Nu/Nu_0)/(f/f_0)^{1/3}$  value increases with the  $d_h/X_L$ , ratio and decreases with increases in the  $X_L$ . Cases A and B yield the maximum  $(Nu/Nu_0)/(f/f_0)^{1/3}$  value. The  $d_h/X_L = 0.076, 0.066,$  and  $0.058$  are recommended for practical applications. The  $(Nu/Nu_0)/(f/f_0)^{1/3}$  values increase with  $d_h/X_L$ , and decrease with increasing  $d_h/X_L$ , ratio. The overall conclusion is that the enhanced wavy surface shows more significant potential than the smooth surface.

Overall, the utilization of enhanced wavy surfaces, facilitated by SCWSPs and SCWSP-VGs, presents promising potential for improving heat transfer efficiency in pillow-plate



Heat Exchangers (PPHE). These advancements could yield substantial benefits in waste heat recovery, energy conservation, and cost reduction in various industrial applications, including two-phase flow systems, HVAC, and cooling processes, demanding further exploration and application.

## **6.2 Future scope**

Further research on Pillow-Plate Heat Exchangers (PPHEs) is required, particularly focusing on exploring curved or curvature-based designs under various flow scenarios to enhance performance. Implementing multiple improvement strategies can further boost the efficiency of PPHEs, making them more effective for extracting high thermal flux in micro-power and micro-electronic cooling applications. Additionally, the combination of pillow-plate structures with dimpled features has shown promising results, indicating the need for further studies to optimize these configurations and better understand their potential benefits.

## References

- [1] Tran JM, Piper M, Kenig EY, Scholl S. Pillow-plate heat exchangers: Fundamental characteristics. *Innov Heat Exch* 2017;233–45. [https://doi.org/10.1007/978-3-319-71641-1\\_7](https://doi.org/10.1007/978-3-319-71641-1_7).
- [2] Zohuri B. Compact heat exchangers: Selection, application, design and evaluation. 2016. <https://doi.org/10.1007/978-3-319-29835-1>.
- [3] Mastani Joybari M, Selvnes H, Sevault A, Hafner A. Potentials and challenges for pillow-plate heat exchangers: State-of-the-art review. *Appl Therm Eng* 2022;214:118739. <https://doi.org/10.1016/j.applthermaleng.2022.118739>.
- [4] Tavallaei M, Farzaneh-Gord M, Moghadam AJ, Ebrahimi-Moghadam A. Parametric study and optimization of pillow-plate heat exchanger using multi-objective genetic algorithm and entropy generation minimization approaches. *Heat Mass Transf Und Stoffuebertragung* 2023;59:1687–706. <https://doi.org/10.1007/s00231-023-03363-x>.
- [5] Peze A. Welded plate fin heat exchanger and heat exchanger plate fin manufacturing process 1996.
- [6] Rosenblad AE. Method of forming dimpled plate heat exchanger elements by the use of hydrostatic pressure. In, Google Patents 1970.
- [7] Mitrovic J, Peterson R. Vapor condensation heat transfer in a thermoplate heat exchanger. *Chem Eng Technol* 2007;30:907–19. <https://doi.org/10.1002/ceat.200700082>.
- [8] Mitrovic J, Maletic B. Numerical simulation of fluid flow and heat transfer in thermoplates. *Chem Eng Technol* 2011;34:1439–48. <https://doi.org/10.1002/ceat.201100271>.
- [9] Piper M, Olenberg A, Tran JM, Kenig EY. Determination of the geometric design parameters of pillow-plate heat exchangers. *Appl Therm Eng* 2015;91:1168–75. <https://doi.org/10.1016/j.applthermaleng.2015.08.097>.
- [10] Arsenyeva O, Piper M, Zibart A, Olenberg A, Kenig EY. Investigation of heat transfer and hydraulic resistance in small-scale pillow-plate heat exchangers. *Energy* 2019;181:1213–24. <https://doi.org/10.1016/j.energy.2019.05.099>.
- [11] Piper M, Zibart A, Kenig EY. New design equations for turbulent forced convection heat transfer and pressure loss in pillow-plate channels. *Int J Therm Sci* 2017;120:459–68. <https://doi.org/10.1016/j.ijthermalsci.2017.06.012>.

- [12] Goedecke R, Scholl S. Enlarged operation ranges for thermosiphon reboilers using pillow plates. *Chem Eng Res Des* 2015. <https://doi.org/10.1016/j.cherd.2015.05.037>.
- [13] Piper M, Zibart A, Tran JM, Kenig EY. A numerical study on turbulent single-phase flow and heat transfer in pillow plates. *Proc 15th Int Heat Transf Conf IHTC 2014* 2014. <https://doi.org/10.1615/ihtc15.hex.008929>.
- [14] Dutka K. Laser welded pillow plate panels for austenitic steel tanks. *Weld Int* 2012;26:692–6. <https://doi.org/10.1080/09507116.2011.590697>.
- [15] Guo Y, Qiu C, Xu M, Zhang W, Yan X, Li L. Crack failure analysis of laser 316L stainless steel edge joints in pillow plate heat exchanger used in oil refinery. *Eng Fail Anal* 2021;122:105215. <https://doi.org/10.1016/j.engfailanal.2021.105215>.
- [16] Djakow E, Springer R, Homberg W, Piper M, Tran J, Zibart A, et al. Incremental electrohydraulic forming - A new approach for the manufacture of structured multifunctional sheet metal blanks. *AIP Conf Proc* 2017;1896. <https://doi.org/10.1063/1.5008083>.
- [17] Voccianta M, Kenig EY. Pillow-Plate Heat Exchangers: An Overview on Advances, Limitations and Prospects. *Chem Eng Trans* 2021;88:865–70. <https://doi.org/10.3303/CET2188144>.
- [18] LASER H. Pillow Plate Heat Exchangers Welded by Laser Weld System n.d. <https://doi.org/https://www.cthslaser.com/news/news-2.html>.
- [19] Sabourishirazi A, Ghodrati M, Liow JL, Behnia M. Recent advances in design and performance optimization of pillow-plate heat exchangers: a critical review. *J Therm Anal Calorim* 2023;148:13679–707. <https://doi.org/10.1007/s10973-023-12571-w>.
- [20] Selvnes H, Allouche Y, Sevault A, Hafner A. A CFD analysis for the performance assessment of a novel design of plates-in-tank latent storage unit for freezing applications. *Refriger Sci Technol* 2019;2019–April:303–10. <https://doi.org/10.18462/iir.nh3-co2.2019.0041>.
- [21] Piper M, Zibart A, Tran JM, Kenig EY. Numerical investigation of turbulent forced convection heat transfer in pillow plates. *Int J Heat Mass Transf* 2016;94:516–27. <https://doi.org/10.1016/j.ijheatmasstransfer.2015.11.014>.
- [22] Sundermeier S, Passmann M, aus der Wiesche S, Kenig EY. Flow in Pillow-Plate Channels for High-Speed Turbomachinery Heat Exchangers. *Int J Turbomachinery, Propuls Power* 2022;7. <https://doi.org/10.3390/ijtp7020012>.
- [23] Selvnes H, Allouche Y, Hafner A, Schlemminger C, Tolstorebrov I. Cold thermal energy storage for industrial CO<sub>2</sub> refrigeration systems using phase change material:

- An experimental study. *Appl Therm Eng* 2022;212:118543. <https://doi.org/10.1016/j.applthermaleng.2022.118543>.
- [24] Selvnes H, Allouche Y, Sevault A, Hafner A. CFD modeling of ice formation and melting in horizontally cooled and heated plates CFD modeling of ice formation and melting in horizontally cooled and heated plates. Eurotherm Semin #112 Adv Therm Energy Storage 2019.
- [25] Ayub ZH. Plate heat exchanger literature survey and new heat transfer and pressure drop correlations for refrigerant evaporators. *Heat Transf Eng* 2003;24:3–16. <https://doi.org/10.1080/01457630304056>.
- [26] Eldeeb R, Aute V, Radermacher R. A survey of correlations for heat transfer and pressure drop for evaporation and condensation in plate heat exchangers. *Int J Refrig* 2016;65:12–26. <https://doi.org/10.1016/j.ijrefrig.2015.11.013>.
- [27] Eldeeb R, Aute V. Investigation of Thermal-Hydraulic Characteristics of Pillow Plate Heat Exchangers Using CFD Department of Mechanical Engineering , University of Maryland. *Int Compress Eng Refrig Air Cond High Perform Build Conf* 2016:1–10.
- [28] Tran JM, Linnemann M, Piper M, Kenig EY. On the coupled condensation-evaporation in pillow-plate condensers: Investigation of cooling medium evaporation. *Appl Therm Eng* 2017;124:1471–80. <https://doi.org/10.1016/j.applthermaleng.2017.06.050>.
- [29] Piper M, Tran JM, Kenig EY. HT2016-7176 2017:1–7.
- [30] Vocciante M, Piper M, Zibart A, Kenig EY. Numerical Evaluation of Different Turbulence Models for Single-Phase Flow in the Outer Pillow-Plate Channel. vol. 43. Elsevier Masson SAS; 2018. <https://doi.org/10.1016/B978-0-444-64235-6.50072-3>.
- [31] Kumar S, Premachandran B, Subbarao PMV. Study on thermo–hydraulics in a Pillow Plate Channel. *Int J Therm Sci* 2019;145:106020. <https://doi.org/10.1016/j.ijthermalsci.2019.106020>.
- [32] Kumar S, Premachandran B, Subbarao PMV. Large eddy simulation of single-phase forced convection in pillow plate channel with periodic boundary conditions. *Int J Heat Mass Transf* 2020;149:119176. <https://doi.org/10.1016/j.ijheatmasstransfer.2019.119176>.
- [33] Zibart A, Kenig EY. Numerical investigation of conjugate heat transfer in a pillow-plate heat exchanger. *Int J Heat Mass Transf* 2021;165:120567. <https://doi.org/10.1016/j.ijheatmasstransfer.2020.120567>.
- [34] Shirzad M, Delavar MA, Ajarostaghi SSM, Sedighi K. Evaluation the effects of

- geometrical parameters on the performance of pillow plate heat exchanger. *Chem Eng Res Des* 2019;150:74–83. <https://doi.org/10.1016/j.cherd.2019.06.032>.
- [35] Arsenyeva O, Tran J, Piper M, Kenig E. An approach for pillow plate heat exchangers design for single-phase applications. *Appl Therm Eng* 2019;147:579–91. <https://doi.org/10.1016/j.applthermaleng.2018.08.083>.
- [36] Goedecke R, Scholl S. Modelling and simulation of a pillow plate thermosiphon reboiler. *Heat Mass Transf Und Stoffuebertragung* 2019;55:95–104. <https://doi.org/10.1007/s00231-018-02543-4>.
- [37] Tran JM, Piper M, Kenig EY. Experimentelle untersuchung des konvektiven wärmeübergangs und druckverlustes in einphasig durchströmten thermoblechen. *Chemie-Ingenieur-Technik* 2015;87:226–34. <https://doi.org/10.1002/cite.201400140>.
- [38] Pathan N, Mitkari S. Heat Transfer Enhancement by Using Dimple Surface. *Int J Trend Sci Res Dev* 2018;Volume-2:2267–70. <https://doi.org/10.31142/ijtsrd12739>.
- [39] Alizadeh A. Numerical investigation of nanofluid flow and heat transfer in a pillow plate heat exchanger using a two-phase model : Effects of the shape of the welding points used in the pillow plate 2021:1–28. <https://doi.org/10.1002/zamm.202000300>.
- [40] Zibart A, Kenig EY. International Journal of Heat and Mass Transfer Numerical investigation of conjugate heat transfer in a pillow-plate heat exchanger. *Int J Heat Mass Transf* 2021;165:120567. <https://doi.org/10.1016/j.ijheatmasstransfer.2020.120567>.
- [41] Zibart, Alexander EYK. Falling liquid film flow over the wavy surface of vertical pillow plates – A numerical investigation n.d.:6575–82.
- [42] Selvnes H, Hafner A, Kauko H. Design of a cold thermal energy storage unit for industrial applications using CO<sub>2</sub> as refrigerant. *Refrig Sci Technol* 2019;2019–Augus:1879–86. <https://doi.org/10.18462/iir.icr.2019.0139>.
- [43] Sevault A, Bohmer F, Næss E, Wang L. Latent heat storage for centralized heating system in a ZEB living laboratory: Integration and design. *IOP Conf Ser Earth Environ Sci* 2019;352:0–8. <https://doi.org/10.1088/1755-1315/352/1/012042>.
- [44] A. Sevault, F. Vullum-Bruer OLT. Active PCM-Based Thermal Energy Storage in Buildings. 14th Gustav Lorentzen Conf Japan, December –9, 2020 n.d.
- [45] Lin W, Zhang W, Ling Z, Fang X, Zhang Z. Experimental study of the thermal performance of a novel plate type heat exchanger with phase change material. *Appl Therm Eng* 2020;178. <https://doi.org/10.1016/j.applthermaleng.2020.115630>.
- [46] Al-Turki YA, Yarmohammadi A, Alizadeh A, Toghraie D. Numerical investigation of

- nanofluid flow and heat transfer in a pillow plate heat exchanger using a two-phase model: Effects of the shape of the welding points used in the pillow plate. *ZAMM Zeitschrift Fur Angew Math Und Mech* 2021;1–28. <https://doi.org/10.1002/zamm.202000300>.
- [47] Shirzad M, Ajarostaghi SSM, Delavar MA, Sedighi K. Improve the thermal performance of the pillow plate heat exchanger by using nanofluid: Numerical simulation. *Adv Powder Technol* 2019;30:1356–65. <https://doi.org/10.1016/j.apt.2019.04.011>.
- [48] Yao Y, Ding J, Zhang Y, Wang W, Lu J. Heat transfer performance of pillow plate heat exchanger with molten salt and supercritical carbon dioxide. *Int J Heat Mass Transf* 2022;183. <https://doi.org/10.1016/j.ijheatmasstransfer.2021.122211>.
- [49] Mechanics F, City S, Africa S, Mitrovic J, Peterson R, Engineering TP, et al. Study of single-phase convection and condensation in thermoplate heat exchanger (part ii) n.d.
- [50] Arsenyeva O, Tran J, Kenig EY. Thermal and hydraulic performance of pillow-plate heat exchangers. vol. 43. Elsevier Masson SAS; 2018. <https://doi.org/10.1016/B978-0-444-64235-6.50033-4>.
- [51] Tran JM, Sommerfeld S, Piper M, Kenig EY. Investigation of pillow-plate condensers for the application in distillation columns. *Chem Eng Res Des* 2015;99:67–74. <https://doi.org/10.1016/j.cherd.2015.03.031>.
- [52] Piper M, Wecker C, Olenberg A, Tran JM, Kenig EY. An experimental analysis of the topology and dynamics of a falling liquid film over the wavy surface of a vertical pillow plate. *Chem Eng Sci* 2015;130:129–34. <https://doi.org/10.1016/j.ces.2015.03.005>.
- [53] Selvnes H, Allouche Y, Hafner A. Experimental characterisation of a cold thermal energy storage unit with a pillow-plate heat exchanger design. *Appl Therm Eng* 2021;199:117507. <https://doi.org/10.1016/j.applthermaleng.2021.117507>.
- [54] Arsenyeva OP, Piper M, Zibart A, Olenberg A, Kenig EY. Heat transfer and pressure loss in small-scale pillow-plate heat exchangers. *Chem Eng Trans* 2018;70:799–804. <https://doi.org/10.3303/CET1870134>.
- [55] Scholl S. Pillow Plate Heat Exchangers as Falling Film Evaporator or Thermosiphon Reboiler 2018.
- [56] Siebeneck K, Popov W, Stefanak T, Scholl S. Pillow plate heat exchangers - Investigation of flow characteristics and wetting behavior at single-flow conditions. *Chemie-Ingenieur-Technik* 2015;87:235–43. <https://doi.org/10.1002/cite.201400055>.

- [57] Wang D, Zhang H, Wang G, Yuan H, Peng X. International Journal of Heat and Mass Transfer Experimental and numerical study on the heat transfer and flow characteristics of convex plate heat exchanger based on multi-objective optimization. *Int J Heat Mass Transf* 2023;202:123755. <https://doi.org/10.1016/j.ijheatmasstransfer.2022.123755>.
- [58] Deen KM, Virk MA, Haque CI, Ahmad R, Khan IH. Failure investigation of heat exchanger plates due to pitting corrosion. *Eng Fail Anal* 2010;17:886–93. <https://doi.org/10.1016/j.engfailanal.2009.10.023>.
- [59] Sedriks AJ, Dudt PJ. Corrosion Resistance, Coating, and Magnetic Property Issues of Nonmagnetic Austenitic Stainless Steels for Ship Hulls. *Corrosion* 2001;57:84–91. <https://doi.org/10.5006/1.3290334>.
- [60] SELVNES H., ALLOUCHE Y. HA. A cold thermal energy storage unit for CO<sub>2</sub> refrigeration using phase change material: First experimental results. 9th IIR Conf Ammon CO<sub>2</sub> Refrig Technol Proc Ohrid, North Maced 16-17 Sept 2021 n.d.
- [61] Yao Y, Ding J, Zhang Y, Wang W, Lu J. Thermal and hydraulic optimization of supercritical CO<sub>2</sub> pillow plate heat exchanger with ellipse weld spots in CSP system. *Int Commun Heat Mass Transf* 2023;143:106739. <https://doi.org/10.1016/j.icheatmasstransfer.2023.106739>.
- [62] Tong Z, Yang Q, Tong S, Chen X. Two-stage thermal-hydraulic optimization for Pillow Plate Heat Exchanger with recirculation zone parameterization. *Appl Therm Eng* 2022;215. <https://doi.org/10.1016/j.applthermaleng.2022.119033>.
- [63] Eldeeb R, Ling J, Aute V, Radermacher R. Weld Shape Optimization for Pillow Plate Heat Exchangers 2018:1–10.
- [64] Eldeeb R, Aute V, Radermacher R. Pillow plate heat exchanger weld shape optimization using approximation and parallel parameterized CFD and non-uniform rational B-splines. *Int J Refrig* 2020;110:121–31. <https://doi.org/10.1016/j.ijrefrig.2019.10.024>.
- [65] Kumar S, Premachandran B, Subbarao PMV. Performance analysis of the pillow plate channel using artificial neural network. *Int J Therm Sci* 2022;172:107275. <https://doi.org/10.1016/j.ijthermalsci.2021.107275>.
- [66] Piper M, Zibart A, Djakow E, Springer R, Homberg W, Kenig EY. Heat transfer enhancement in pillow-plate heat exchangers with dimpled surfaces: A numerical study. *Appl Therm Eng* 2019;153:142–6. <https://doi.org/10.1016/j.applthermaleng.2019.02.082>.

- [67] Kumar S, Premachandran B, Subbarao PMV. Study on thermo–hydraulics in a Pillow Plate Channel. *Int J Therm Sci* 2019;145:106020. <https://doi.org/10.1016/j.ijthermalsci.2019.106020>.
- [68] Ramesh Kumar MKS& SB. Single-phase convective heat transfer augmentation in pillow-plate heat exchanger: A review. *Lect Notes Mech Eng Springer, Singapore* 2021;3. [https://doi.org/https://doi.org/10.1007/978-981-19-6270-7\\_80](https://doi.org/https://doi.org/10.1007/978-981-19-6270-7_80).
- [69] Launder BE, Spalding DB. The numerical computation of turbulent flows. *Comput Methods Appl Mech Eng* 1974;3:269–89. [https://doi.org/10.1016/0045-7825\(74\)90029-2](https://doi.org/10.1016/0045-7825(74)90029-2).
- [70] Wilcox DC. Formulation of the k-w Turbulence Model Revisited. *AIAA J* n.d.;46. <https://doi.org/https://doi.org/10.2514/1.36541>.
- [71] Menter FR. Two-equation eddy-viscosity turbulence models for engineering applications. *AIAA J* 1994;32:1598–605. <https://doi.org/10.2514/3.12149>.
- [72] Patankar S. Numerical heat transfer and fluid flow: Computational methods in mechanics and thermal science. Hemisph Publ Corp DC 1980:1–197.
- [73] Versteeg H., Malalasekera W. An Introduction to Computational Fluid Dynamics. Longman Gr Ltd 1995:149–151.
- [74] Murmu SC, Bhattacharyya S, Chattopadhyay H, Biswas R. Analysis of heat transfer around bluff bodies with variable inlet turbulent intensity: A numerical simulation. *Int Commun Heat Mass Transf* 2020;117:104779. <https://doi.org/10.1016/j.icheatmasstransfer.2020.104779>.
- [75] Tran JM, Piper M, Kenig EY. Single-phase flow and condensation in pillow-plate condensers. *Innov Heat Exch* 2017;247–65. [https://doi.org/10.1007/978-3-319-71641-1\\_8](https://doi.org/10.1007/978-3-319-71641-1_8).
- [76] Tran JM, Piper M, Kenig EY. Experimental Investigation of Convective Heat Transfer and Pressure Drop in Pillow Plates under Single-Phase Through-Flow Conditions. *Chemie-Ingenieur-Technik* 2015;87:226–34. <https://doi.org/10.1002/cite.201400140>.
- [77] Bejan A, Kestin J. Entropy generation through heat and fluid flow 1983.
- [78] Bejan A. Entropy generation minimization: The new thermodynamics of finite-size devices and finite-time processes. *J Appl Phys* 1996;79:1191–218. <https://doi.org/10.1063/1.362674>.
- [79] Chennu R, Paturu P. Development of heat transfer coefficient and friction factor correlations for offset fins using CFD. *Int J Numer Methods Heat Fluid Flow* 2011;21:935–51. <https://doi.org/10.1108/09615531111177732>.



- [80] Kumar R, Garg H, Dhiman SK, Kumar B. Micro-electronics cooling devices for heat extracting using nano Ferro fluid. Proc - Int Conf Vis Towar Emerg Trends Commun Networking, ViTECoN 2019 2019. <https://doi.org/10.1109/ViTECoN.2019.8899578>.
- [81] Xu M, Guo J, Li X. Thermodynamic Analysis and Optimization Design of Heat Exchanger. 2014. <https://doi.org/10.1007/978-3-319-01793-8>.
- [82] Sheik Ismail L, Ranganayakulu C, Shah RK. Numerical study of flow patterns of compact plate-fin heat exchangers and generation of design data for offset and wavy fins. Int J Heat Mass Transf 2009;52:3972–83. <https://doi.org/10.1016/j.ijheatmasstransfer.2009.03.026>.
- [83] Pandey SD, Nema VK. An experimental investigation of exergy loss reduction in corrugated plate heat exchanger. Energy 2011;36:2997–3001. <https://doi.org/10.1016/j.energy.2011.02.043>.
- [84] Vargas JVC, Bejan A, Siems DL. Integrative thermodynamic optimization of the crossflow heat exchanger for an aircraft environmental control system. J Heat Transfer 2001;123:760–9. <https://doi.org/10.1115/1.1375811>.
- [85] Ogulata RT, Doba F, Yilmaz T. Irreversibility analysis of cross flow heat exchangers. Energy Convers Manag 2000;41:1585–99. [https://doi.org/10.1016/S0196-8904\(00\)00020-0](https://doi.org/10.1016/S0196-8904(00)00020-0).
- [86] Rashidi S, Hormozi F, Sundén B, Mahian O. Energy saving in thermal energy systems using dimpled surface technology – A review on mechanisms and applications. Appl Energy 2019;250:1491–547. <https://doi.org/10.1016/j.apenergy.2019.04.168>.
- [87] Jin D, Zuo J, Quan S, Xu S, Gao H. Thermohydraulic performance of solar air heater with staggered multiple V-shaped ribs on the absorber plate. Energy 2017;127:68–77. <https://doi.org/10.1016/j.energy.2017.03.101>.
- [88] Rongchai K, Tundee S. Development, testing and design optimisation of a water and R134a based thermosyphon heat exchanger for air-water heat recovery systems. Case Stud Therm Eng 2022;39:102453. <https://doi.org/10.1016/j.csite.2022.102453>.
- [89] Grazzini G, Gori F. Entropy parameters for heat exchanger design. Int J Heat Mass Transf 1988;31:2547–54. [https://doi.org/10.1016/0017-9310\(88\)90180-9](https://doi.org/10.1016/0017-9310(88)90180-9).
- [90] Jiansheng W, Yan Z, Xueling L. The flow and heat transfer characteristics in a rectangular channel with miniature cuboid dimples. Int Commun Heat Mass Transf 2021;126:105474. <https://doi.org/10.1016/j.icheatmasstransfer.2021.105474>.
- [91] Syam Sundar L, Mesfin S, Venkata Ramana E, Said Z, Sousa ACM. Experimental investigation of thermo-physical properties, heat transfer, pumping power, entropy

- generation, and exergy efficiency of nanodiamond + Fe<sub>3</sub>O<sub>4</sub>/60:40% water-ethylene glycol hybrid nanofluid flow in a tube. *Therm Sci Eng Prog* 2021;21. <https://doi.org/10.1016/j.tsep.2020.100799>.
- [92] Norouzi A, Sodagar-Abardeh J, Arabkoohsar A, Ismail KAR. Investigating thermo-hydraulic behavior of pillow plate heat exchangers using entropy generation approach. *Chem Eng Process - Process Intensif* 2022;174:108887. <https://doi.org/10.1016/j.cep.2022.108887>.
- [93] Goel V, Kumar R, Bhattacharyya S, Tyagi V V., Abusorrah AM. A comprehensive parametric investigation of hemispherical cavities on thermal performance and flow-dynamics in the triangular-duct solar-assisted air-heater. *Renew Energy* 2021;173:896–912. <https://doi.org/10.1016/j.renene.2021.04.006>.
- [94] Petukhov B. S. Popov VN. Theoretical calculation of heat exchange in turbulent flow in tubes of an incompressible fluid with variable physical properties. *High Temp n.d.*;1(1):69–83.
- [95] Colburn AP. A method for correlating forced convection heat transfer data and a comparison with fluid friction. *Int J Heat Mass Transf* 1964;84. [https://doi.org/http://dx.doi.org/10.1016/0017-9310\(64\)](https://doi.org/http://dx.doi.org/10.1016/0017-9310(64)).
- [96] Dittus FW, Boelter LMK. Heat transfer in automobile radiators of the tubular type. *Int Commun Heat Mass Transf* 1985. [https://doi.org/10.1016/0735-1933\(85\)90003-X](https://doi.org/10.1016/0735-1933(85)90003-X).
- [97] Abdollahi A, Shams M. Optimization of shape and angle of attack of winglet vortex generator in a rectangular channel for heat transfer enhancement. *Appl Therm Eng* 2015;81:376–87. <https://doi.org/10.1016/j.applthermaleng.2015.01.044>.
- [98] Jin D, Zhang M, Wang P, Xu S. Numerical investigation of heat transfer and fluid flow in a solar air heater duct with multi V-shaped ribs on the absorber plate. *Energy* 2015;89:178–90. <https://doi.org/10.1016/j.energy.2015.07.069>.
- [99] Hein LL, Mortean MVV. Theoretical and experimental thermal performance analysis of an additively manufactured polymer compact heat exchanger. *Int Commun Heat Mass Transf* 2021;124:105237. <https://doi.org/10.1016/j.icheatmasstransfer.2021.105237>.
- [100] Yadav D, Kushwaha A, Trivedee D, Upadhyay Z. A comprehensive experimental analysis for optimal flow configurations in a triple tube heat exchanger (TTHXr). *Int Commun Heat Mass Transf* 2022;138:106385. <https://doi.org/10.1016/j.icheatmasstransfer.2022.106385>.
- [101] Hormozi F, ZareNezhad B, Allahyar HR. An experimental investigation on the effects

- of surfactants on the thermal performance of hybrid nanofluids in helical coil heat exchangers. *Int Commun Heat Mass Transf* 2016;78:271–6. <https://doi.org/10.1016/j.icheatmasstransfer.2016.09.022>.
- [102] Fallah Najafabadi M, Talebi Rostami H, Farhadi M. Analysis of a twisted double-pipe heat exchanger with lobed cross-section as a novel heat storage unit for solar collectors using phase-change material. *Int Commun Heat Mass Transf* 2021;128:105598. <https://doi.org/10.1016/j.icheatmasstransfer.2021.105598>.
- [103] Erdinc MT. Computational thermal-hydraulic analysis and geometric optimization of elliptic and circular wavy fin and tube heat exchangers. *Int Commun Heat Mass Transf* 2023;140:106518. <https://doi.org/10.1016/j.icheatmasstransfer.2022.106518>.
- [104] Wang S, Jian G, Xiao J, Wen J, Zhang Z, Tu J. Fluid-thermal-structural analysis and structural optimization of spiral-wound heat exchanger. *Int Commun Heat Mass Transf* 2018;95:42–52. <https://doi.org/10.1016/j.icheatmasstransfer.2018.03.027>.
- [105] Çakmak G, Yildiz C. The influence of the injectors with swirling flow generating on the heat transfer in the concentric heat exchanger. *Int Commun Heat Mass Transf* 2007;34:728–39. <https://doi.org/10.1016/j.icheatmasstransfer.2007.03.007>.
- [106] Nilpueng K, Keawkamrop T, Ahn HS, Wongwiset S. Effect of chevron angle and surface roughness on thermal performance of single-phase water flow inside a plate heat exchanger. *Int Commun Heat Mass Transf* 2018;91:201–9. <https://doi.org/10.1016/j.icheatmasstransfer.2017.12.009>.
- [107] Özenbiner Ö, Yurddaş A. Numerical analysis of heat transfer of a nanofluid counter-flow heat exchanger. *Int Commun Heat Mass Transf* 2022;137. <https://doi.org/10.1016/j.icheatmasstransfer.2022.106306>.
- [108] Jin D, Quan S, Zuo J, Xu S. Numerical investigation of heat transfer enhancement in a solar air heater roughened by multiple V-shaped ribs. *Renew Energy* 2019;134:78–88. <https://doi.org/10.1016/j.renene.2018.11.016>.
- [109] Promvong P, Promthaisong P, Skullong S. Experimental and numerical thermal performance in solar receiver heat exchanger with trapezoidal louvered winglet and wavy groove. *Sol Energy* 2022;236:153–74. <https://doi.org/10.1016/j.solener.2022.02.052>.
- [110] Ahmed HE, Mohammed HA, Yusoff MZ. An overview on heat transfer augmentation using vortex generators and nanofluids: Approaches and applications. *Renew Sustain Energy Rev* 2012;16:5951–93. <https://doi.org/10.1016/j.rser.2012.06.003>.
- [111] Biswas G, Chattopadhyay H, Sinha A. Augmentation of Heat Transfer by Creation of

- Streamwise Longitudinal Vortices Using Vortex Generators. *Heat Transf Eng* 2012;33:406–24. <https://doi.org/10.1080/01457632.2012.614150>.
- [112] Habchi C, Russeil S, Bougeard D, Harion JL, Lemenand T, Della Valle D, et al. Enhancing heat transfer in vortex generator-type multifunctional heat exchangers. *Appl Therm Eng* 2012;38:14–25. <https://doi.org/10.1016/j.applthermaleng.2012.01.020>.
- [113] Li MJ, Zhou WJ, Zhang JF, Fan JF, He YL, Tao WQ. Heat transfer and pressure performance of a plain fin with radiantly arranged winglets around each tube in fin-and-tube heat transfer surface. *Int J Heat Mass Transf* 2014;70:734–44. <https://doi.org/10.1016/j.ijheatmasstransfer.2013.11.024>.
- [114] Hatami M, Ganji DD, Gorji-Bandpy M. Experimental investigations of diesel exhaust exergy recovery using delta winglet vortex generator heat exchanger. *Int J Therm Sci* 2015;93:52–63. <https://doi.org/10.1016/j.ijthermalsci.2015.02.004>.
- [115] Promvong P, Suwannapan S, Pimsarn M, Thianpong C. Experimental study on heat transfer in square duct with combined twisted-tape and winglet vortex generators. *Int Commun Heat Mass Transf* 2014;59:158–65. <https://doi.org/10.1016/j.icheatmasstransfer.2014.10.005>.
- [116] Choudhury D, Karki KC. Calculation of fully developed flow and heat transfer in streamwise-periodic dimpled channels. *J Thermophys Heat Transf* 1991;5:81–8. <https://doi.org/10.2514/3.230>.
- [117] Kumar R, Bhattacharyya S. Heat transfer enhancement in pillow-plate type heat exchanger with SCWSCs using an entropy and exergy generation approximation technique. *Int Commun Heat Mass Transf* 2023;147:106994. <https://doi.org/10.1016/j.icheatmasstransfer.2023.106994>.
- [118] Rao Y, Li B, Feng Y. Heat transfer of turbulent flow over surfaces with spherical dimples and teardrop dimples. *Exp Therm Fluid Sci* 2015;61:201–9. <https://doi.org/10.1016/j.expthermflusci.2014.10.030>.
- [119] Huang Z, Li ZY, Yu GL, Tao WQ. Numerical investigations on fully-developed mixed turbulent convection in dimpled parabolic trough receiver tubes. *Appl Therm Eng* 2017;114:1287–99. <https://doi.org/10.1016/j.applthermaleng.2016.10.012>.
- [120] Singh SK, Kacker R, Chaurasiya PK, Gautam SS. Correlations on heat transfer rate and friction factor of a rectangular toothed v-cut twisted tape exhibiting the combined effects of primary and secondary vortex flows. *Int Commun Heat Mass Transf* 2022;139:106503. <https://doi.org/10.1016/j.icheatmasstransfer.2022.106503>.

- [121] Fang X, Xu Y, Zhou Z. New correlations of single-phase friction factor for turbulent pipe flow and evaluation of existing single-phase friction factor correlations. *Nucl Eng Des* 2011;241:897–902. <https://doi.org/10.1016/j.nucengdes.2010.12.019>.
- [122] Webb RL. Performance evaluation criteria for use of enhanced heat transfer surfaces in heat exchanger design. *Int J Heat Mass Transf* 1981;24:715–26. [https://doi.org/10.1016/0017-9310\(81\)90015-6](https://doi.org/10.1016/0017-9310(81)90015-6).
- [123] Ligrani P. Heat transfer augmentation technologies for internal cooling of turbine components of gas turbine engines. *Int J Rotating Mach* 2013;2013. <https://doi.org/10.1155/2013/275653>.
- [124] Leontiev AI, Kiselev NA, Vinogradov YA, Strongin MM, Zditovets AG, Burtsev SA. Experimental investigation of heat transfer and drag on surfaces coated with dimples of different shape. *Int J Therm Sci* 2017;118:152–67. <https://doi.org/10.1016/j.ijthermalsci.2017.04.027>.
- [125] Tamna S, Skullong S, Thianpong C, Promvong P. Heat transfer behaviors in a solar air heater channel with multiple V-baffle vortex generators. *Sol Energy* 2014;110:720–35. <https://doi.org/10.1016/j.solener.2014.10.020>.
- [126] Skullong S, Promvong P, Thianpong C, Pimsarn M. Thermal performance in solar air heater channel with combined wavy-groove and perforated-delta wing vortex generators. *Appl Therm Eng* 2016;100:611–20. <https://doi.org/10.1016/j.applthermaleng.2016.01.107>.
- [127] Skullong S, Promvong P, Thianpong C, Jayranaiwachira N, Pimsarn M. Heat transfer augmentation in a solar air heater channel with combined winglets and wavy grooves on absorber plate. *Appl Therm Eng* 2017;122:268–84. <https://doi.org/10.1016/j.applthermaleng.2017.04.158>.
- [128] Skullong S, Promthaisong P, Promvong P, Thianpong C, Pimsarn M. Thermal performance in solar air heater with perforated-winglet-type vortex generator. *Sol Energy* 2018;170:1101–17. <https://doi.org/10.1016/j.solener.2018.05.093>.
- [129] Hoonpong P SS. Performance improvement of solar air heater with v-baffles on absorber plate. *J Res Appl Mech Eng* 2018;6:29–39. <https://doi.org/10.14456/jrame.2018.4>.
- [130] Promvong P, Tongyote P, Skullong S. Thermal behaviors in heat exchanger channel with V-shaped ribs and grooves. *Chem Eng Res Des* 2019;150:263–73. <https://doi.org/10.1016/j.cherd.2019.07.025>.
- [131] Promvong P, Skullong S. Heat transfer in solar receiver heat exchanger with

- combined punched-V-ribs and chamfer-V-grooves. *Int J Heat Mass Transf* 2019;143:118486. <https://doi.org/10.1016/j.ijheatmasstransfer.2019.118486>.
- [132] Promvong P, Skullong S. Thermal characteristics in solar air duct with V-shaped flapped-baffles and chamfered-grooves. *Int J Heat Mass Transf* 2021;172:121220. <https://doi.org/10.1016/j.ijheatmasstransfer.2021.121220>.
- [133] Joardar A, Jacobi AM. A numerical study of flow and heat transfer enhancement using an array of delta-winglet vortex generators in a fin-and-tube heat exchanger. *J Heat Transfer* 2007;129:1156–67. <https://doi.org/10.1115/1.2740308>.
- [134] Amirahmadi S, Rashidi S, Abolfazli Esfahani J. Minimization of exergy losses in a trapezoidal duct with turbulator, roughness and beveled corners. *Appl Therm Eng* 2016;107:533–43. <https://doi.org/10.1016/j.applthermaleng.2016.06.182>.
- [135] Mastani Joybari M, Selvnes H, Vingelsgård E, Sevault A, Hafner A. Parametric study of low-temperature thermal energy storage using carbon dioxide as the phase change material in pillow plate heat exchangers. *Appl Therm Eng* 2023;221:119796. <https://doi.org/10.1016/j.applthermaleng.2022.119796>.

# Appendix 1

---

## The cost estimation and analysis of PPHE

The preliminary efforts to estimate the cost of various Pillow-Plate Heat Exchangers (PPHEs) involved determining a parameter that relates the heat transfer rate ( $Q$ ) within the thermo-plate channels to the required pumping power ( $W_{\text{pump}}$ ) [20]. This parameter, defined as the ratio  $Q/W_{\text{pump}}$ , serves as a metric to evaluate the operating cost efficiency of different heat exchanger geometries. It enables comparison of various thermo-plate designs, especially across a range of fluid Reynolds numbers with flat channels. However, this ratio alone provides only a partial picture and is insufficient for a comprehensive cost assessment. The total cost of PPHEs consists of two primary components [48]: capital cost (CC) and operating cost (OC).

The capital cost accounts for material procurement and manufacturing expenses, while the operating cost reflects the energy consumed by the electric motor throughout the equipment's lifecycle. Pillow Plates offer a cost advantage over traditional shell-and-tube heat exchangers (STHX) due to their relatively low production costs. Their construction involves welding two metal sheets, typically using resistance or laser welding techniques. The exact price of PPHEs varies based on several factors, including the size, material, and customization requirements. Common materials include AISI 304, AISI 321, AISI 316L, and AISI 316Ti, with pricing for specific configurations as follows: AISI 304 material in dimensions of 100 ft  $\times$  1/16 mm  $\times$  1.59 mm, 50 ft  $\times$  3.18 mm  $\times$  0.085 mm, and 50 ft  $\times$  6.35 mm  $\times$  5.3 mm (L  $\times$  O.D  $\times$  I.D) costs Rs. 48,000, Rs. 24,000, and Rs. 27,000, respectively.

When it comes to welding, the choice between resistance and laser welding significantly affects both capital and operating costs. Laser welding is generally more energy-efficient, requiring only 35 kW of power compared to the 350kW needed for resistance welding, of which 180 kW is absorbed by the process. Although laser welding requires a higher initial investment for the plant setup, it offers a lower life cycle cost, with operational savings that offset the initial expense over time. Additionally, laser welding enhances the mechanical and corrosion resistance of the welded materials, particularly in thermally affected zones, which improves the heat exchanger's durability and long-term performance. Compared to conventional heat exchangers such as shell-and-tube or plate-

and-frame designs, PPHEs have not been extensively studied in terms of capital cost breakdowns. Available literature highlights several factors that influence the capital cost of PPHEs, including PPHE type, material selection, the number of thermoplates, heat transfer area, and welding method [31,48,53,143,144]. Among these, the geometry and orientation of thermoplate channels play a crucial role in determining performance and cost. For example, longitudinal channel designs offer higher heat transfer rates than other configurations, which allows for a smaller heat transfer area and subsequently lowers material and manufacturing costs [37].

The adoption of CNC-assisted laser welding technology has further improved the cost-efficiency of PPHEs by accelerating the welding process, enhancing quality, and reducing the expenses associated with quality testing [48]. Another effective strategy to reduce costs is to minimize welding length by using larger thermoplate dimensions, which decreases the need for multiple smaller plates. Additionally, replacing austenitic stainless steel with alternative materials such as aluminum alloys has shown promising results in cost reduction. Aluminum offers superior thermal conductivity, lower density, and reduced material costs, making it an attractive option for low-pressure applications. However, aluminum's lower mechanical strength limits its use in high-pressure environments [26,53,143].

Despite these advancements, the development of a standardized or definitive method for estimating the capital cost of PPHEs remains a challenge. Most cost approximations rely on the price of thermoplate materials, but these estimates often involve significant uncertainty [48]. Research continues to explore correlations between PPHE material, geometry, and manufacturing processes to improve the accuracy of capital cost predictions.

$$W_{pump} = \frac{m_{I-channel} \left( \frac{\Delta P_{I-channel}}{\rho_{I-channel}} \right) + m_{O-channel} \left( \frac{\Delta P_{O-channel}}{\rho_{O-channel}} \right)}{\eta_{pump}} \quad (1)$$

$$OC = \sum_n^{n-year} \frac{(EC)(WH_{pump})(W_{pump})}{(1+i)^n} \quad (2)$$

Where,  $\eta_{pump}$  is the pump efficiency, EC is the energy cost per hour,  $WH_{pump}$  is the annual pump working hours,  $i$  is the annual interest rate, and n-year is the lifetime of the PPHE.



Geometric characteristics of PPHEs play a crucial role in minimizing operational costs by reducing pressure drops in both channels. For example, transversal PPCs generally have lower pressure losses than longitudinal ones under similar operating conditions [21,67]. Widening the gaps between adjacent I-channels can also reduce pressure loss in the O-channel, thereby lowering operating costs [35,135]. However, larger gaps in the O-channel can negatively impact the thermal performance of PPHEs, so finding an optimal balance between channel spacing and performance is critical [135].

# List of Publication

---

## SCI Journal

**Ramesh Kumar**, Suvanjan Bhattacharyya, “Heat transfer enhancement in pillow-plate type heat exchanger with SCWSCs using an entropy and exergy generation approximation technique,” *International Communications in Heat and Mass Transfer*, vol. 147, pages 106994, October 2023. <https://doi.org/10.1016/j.icheatmasstransfer.2023.106994>.

**Ramesh Kumar** “Effect of SCWSP-VGs and thermal performance investigation of pillow-plate type heat exchanger (PPHX),” *International Journal of Thermal Sciences*, vol. 201, 108994, July 2024. <https://doi.org/10.1016/j.ijthermalsci.2024.108994>

**Ramesh Kumar** “Investigating the impact of different SCWSVGs arrangements on thermo-hydrodynamic flow within pillow-plate type heat exchanger” *Thermal Science and Engineering Progress*, vol. 50, 102572, May 2024. <https://doi.org/10.1016/j.tsep.2024.102572>

## International and National conference proceedings

**Ramesh Kumar**, Manoj Kumar Soni and Suvanjan Bhattacharyya, Numerical Analysis of CWSPs on different Streamwise lengths of Pillow-plate Heat Exchanger, *9th International and 49th National Conference on Fluid Mechanics and Fluid Power (FMFP)*, Indian Institute of Technology Roorkee, December 14-16, 2022.

**Ramesh Kumar**, Manoj Kumar Soni and Suvanjan Bhattacharyya, Single-Phase Fluid Flow and Heat Transfer Characteristics in Pillow-Plate Heat Exchanger: A Numerical Study, *Proceedings of the 48th National Conference on Fluid Mechanics and Fluid Power (FMFP)*, Vol. 3, BITS Pilani, Pilani Campus, Rajasthan, December 27-29, 2021. [https://doi.org/10.1007/978-981-19-6270-7\\_81](https://doi.org/10.1007/978-981-19-6270-7_81)

**Ramesh Kumar**, Manoj Kumar Soni and Suvanjan Bhattacharyya, Influence of material on heat transfer and fluid flow in the pillow-plate heat exchanger, *Proceedings of the 48th National Conference on Fluid Mechanics and Fluid Power (FMFP)*, Vol. 3, BITS Pilani, Pilani Campus, Rajasthan, December 27-29, 2021. [https://doi.org/10.1007/978-981-19-6270-7\\_95](https://doi.org/10.1007/978-981-19-6270-7_95)

**Ramesh Kumar**, Manoj Kumar Soni and Suvanjan Bhattacharyya, Single-phase convective heat transfer augmentation in pillow-plate heat exchanger: A review, *Proceedings of the 48<sup>th</sup> National Conference on Fluid Mechanics and Fluid Power (FMFP)*, Vol. 3, BITS Pilani, Pilani Campus, Rajasthan, December 27-29, 2021. [https://doi.org/10.1007/978-981-19-6270-7\\_80](https://doi.org/10.1007/978-981-19-6270-7_80)

**Ramesh Kumar**, Shivam Raj and S.K. Dhiman, Experimental and numerical analysis of Ferrofluid in partially heated closed rectangular micro-channel tube under non-uniform magnetic field, *9th International and 49th National Conference on Fluid Mechanics and Fluid Power (FMFP)*, Indian Institute of Technology Roorkee, December 14-16, 2022. [https://doi.org/10.1007/978-981-99-7177-0\\_49](https://doi.org/10.1007/978-981-99-7177-0_49)

**Ramesh Kumar** and S.K. Dhiman, Experimental and Numerical Analysis of ferrofluid in partially heated transparent enclosure microchannel under a non-uniform magnetic field generated by single, double, and circular ring permanent magnet, *ISHMT-ASTFE, IHMTC-2023*, Indian Institute of Technology Patna, 14-16 December 2023. [10.1615/IHMTC-2023.1280](https://doi.org/10.1615/IHMTC-2023.1280)

## Biography

---



**Mr. Ramesh Kumar** is a Ph.D. Research Scholar in Mechanical Engineering at BITS Pilani, Pilani campus, Rajasthan, India since August 2019, focusing on impactful research and contributions to the academic community. With recognition, awards, and publications, he demonstrates a commitment to advancing knowledge. Previously, he served as an Engineer in a 26 MW Thermal Power Plant, Raipur, Chhattisgarh, gaining valuable insights into practical mechanical engineering and power plant operations.

Having earned a specialization M.E. degree in Thermal Engineering from BIT Mesra in May 2019. His master's thesis delved into “Analysis and Evaluation of Thermo-Magnetic Convection of Ferro-fluid cooling system”. He worked as a research assistant at CSIR-CSIO Lab, Chandigarh, from June 2018 to July 2019, specializing in Computational Fluid Dynamics (CFD) under Dr. Harry Garg.

His academic journey includes a first-class honors B.E. in Mechanical Engineering from Chhattisgarh Swami Vivekananda Technical University, Bilai, Chhattisgarh in 2014. His interests in Pillow-plate heat exchangers, heat transfer in micro and minichannels, CFD, multiphase flows, and both laminar and turbulent flow. Proficient in ANSYS Fluent and COMSOL Multiphysics software, he brings a comprehensive skill set to his research endeavors.



**Dr. Aneesh A.M.** is a distinguished academician and researcher currently serving as an Assistant Professor in the Department of Mechanical Engineering at Birla Institute of Technology and Science (BITS) Pilani, Pilani campus, Rajasthan, India. His journey in the field of mechanical engineering and heat transfer has been marked by significant contributions and academic achievements.

Dr. Aneesh embarked on his academic career as an Adhoc Faculty at NIT Calicut, refining teaching skills from July to December 2018. He earned his Ph.D. from IIT Bombay, showcasing expertise in thermo-hydraulic analysis of printed circuit heat

exchangers. His M.Tech thesis on mixed convection earned first-class from the University of Kerala in 2011.

Starting with a first-class B.E. in Mechanical Engineering from the University of Calicut in 2009, Dr. Aneesh's research spans compact heat exchangers, micro and minichannels, rarefied gas dynamics, physiological fluid dynamics, and fluid-structure interaction. As an Assistant Professor at BITS Pilani, he imparts knowledge and passion, shaping the future of mechanical engineering. His journey from student to professor highlights consistent excellence and dedication to diverse research interests with a significant impact on academia and industry.



**Dr. Anirudh Singh Rana** is an accomplished academician and researcher currently serving as an Associate Professor in the Department of Mathematics at Birla Institute of Technology and Science (BITS) Pilani, located in Rajasthan, India. His academic journey has been marked by diverse experiences, both nationally and internationally, contributing significantly to the fields of fluid dynamics, computational fluid dynamics, kinetic theory, non-equilibrium thermodynamics, computational and mathematical rheology, and more. His professional journey at BITS Pilani began in June 2019 when he assumed the role of Assistant Professor in the Department of Mathematics. Recognized for his exceptional contributions and academic prowess, he was subsequently promoted to the position of Associate Professor in July 2023, where he continues to shape the academic landscape of the institution.

Dr. Rana's global exposure and collaborative engagements are noteworthy. Prior to joining BITS Pilani, he held the prestigious Marie Skłodowska Curie WIRL COFUND fellowship at the Institute of Advanced Study, University of Warwick, UK, from September 2016 to May 2019. During this period, he also served as a Postdoctoral Researcher at the Mathematics Institute, University of Warwick, UK, further enriching his research portfolio. His international experience extends to a prior role as a Postdoctoral Researcher at the Aerospace Computational Modeling Laboratory, Gyeongsang National University, South Korea, from July 2014 to February 2016.

Dr. Rana's educational background is impressive, with a Ph.D. earned from the Department of Mechanical Engineering at the University of Victoria in Canada.

Additionally, he completed an Advanced Diploma Programme in Modelling and Simulation (ADPMS) from the Centre for Modelling and Simulation, University of Pune, India, in collaboration with the Seminar for Applied Mathematics, ETH Zurich, Switzerland. His foundation in mathematics is rooted in a Master's degree (M.Sc.) from C.C.S. University, Meerut, India.

A prolific researcher, Dr. Rana has made significant contributions to various scientific publications, including the Journal of Heat Transfer, Physics of Fluids, and the Journal of Fluid Mechanics. His research interests span a wide array of topics, including fluid dynamics, computational fluid dynamics, kinetic theory, non-equilibrium thermodynamics, computational and mathematical rheology, finite-volume methods for hyperbolic-parabolic equations, Monte-Carlo methods, and molecular dynamics.

In addition to his research endeavors, Dr. Rana has actively contributed to the academic community by organizing conferences and workshops. Notable events include the International Conference on Advances in Mechanics, Modelling, Computing, and Statistics at BITS Pilani in March 2022 and the 48th National Conference on Fluid Mechanics and Fluid Powers in December 2021. These events provided platforms for scholars and researchers to exchange knowledge and ideas.

Dr. Rana's commitment to academic advancement is further reflected in the seminars he has organized, such as the one on the Multiscale Modeling Approach to Fluid Flows Involving Phase Change at the University of Warwick in July 2018 and another on Recent Developments in the Kinetic Theory of Gases at the same institution in July 2017. These seminars showcase his dedication to fostering intellectual discussions and staying at the forefront of emerging research trends.